Progress Report

"Determination of Stability and Control Derivatives for the NASA F/A-18 HARV from Flight Data Using the Maximum Likelihood Method"

NASA Grant NCC 2-759

submitted by
Marcello R. Napolitano, Assistant Professor
Department of Mechanical and Aerospace Engineering
West Virginia University
Morgantown, WV 26506/6106
Tel. (304) 293-4111 Ext. 346
FAX (304) 293-6689
E-mail : napolit@faculty.coe.wvu.edu
January 1995

Technical Monitor :
Albion H. Bowers, F/A-18 HARV Program Manager
Tel. (805) 258-3716
NASA Dryden Flight Research Facility

F/A-18 HARV PID REPORT

INTRODUCTION

The following is a compilation of PID results for both longitudinal and lateral directional analysis that was completed at West Virginia University during the Fall 1994 semester.

During Summer 94 it was established that the maneuvers available for PID containing independent control surface inputs from OBES were not well suited for extracting the cross-coupling static (ie. $C_{N\beta}$) or dynamic (ie. C_{Npf}) derivatives. This was due to the fact that these maneuvers were designed with the goal of minimizing any lateral directional motion during longitudinal maneuvers and vice-versa. This allows for greater simplification in the aerodynamic model as far as coupling between longitudinal and lateral directions is concerned. As a result, efforts were made to reanalyze this data and extract static and dynamic derivatives for the F/A-18 HARV without the inclusion of the cross-coupling terms such that more accurate estimates of classical model terms could be acquired.

FLIGHT DATA ANALYZED

The following listings show the flight numbers, maneuver types and angle of attack ranges examined in this analysis.

Longitudinal:

Flight	Maneuver Type	Angle of Attack (deg)
166	SSI MD	25,30,40,50,60
226	SSI MD	20,30,40,50
250	OLON $\delta_E=7.5^o$	20,40
	3211 $\delta_E=7.5^o$	20
	1" STICK PITCH STEPS	20,30
253	SSI MD	20,30,40,50,60

Lateral:

Flight	Maneuver Type	Angle of Attack (deg)
226	SSI MD	10,20,30
248	SSI MD	10,20,30,50
250	SSI MD	50,60
	OLAT $\delta_A=5^o,\delta_R=10^o$	20,40

*SSI MD - Single Surface Input Multiple Doublet maneuvers (OBES ON, RFCS ON)
*OLON $\delta_E=7.5^o$ - Optimal Longitudinal Input, elevator deflected 7.5^o (OBES ON, RFCS ON)
*3211 $\delta_E=7.5^o$ - 3211 Frequency Sweep, elevator deflected 7.5^o (OBES ON, RFCS ON)
*1" STICK PITCH STEPS - Pilot applied 1" control stick pitch steps (OBES OFF, RFCS OFF)
*OLAT $\delta_A=5^o,\delta_R=10^o$ - Optimal Lateral Input, aileron deflected 5^o, rudder deflected 10^o (OBES ON, RFCS ON)

Note that each flight often has more than one run at each angle of attack tested. The proper time cuts, maneuver descriptions and average values of all required mass characteristics (Ix, Iy, etc.) for each time cut have been placed in a textfile database available upon request.

LONGITUDINAL SETUP

Four longitudinal flights containing static PID maneuvers were examined. Time histories of leading-edge and trailing-edge flap deflections clearly indicated high correlations between themselves, as well as angle of attack, due to their scheduled deflections based on α. In order to avoid encountering any unwanted biases in the estimated derivatives all leading-edge flap derivatives ($C_{N\delta lef}$, $C_{m\delta lef}$ & $C_{A\delta lef}$) were held constant at the appropriate wind tunnel values. All trailing-edge flap derivatives ($C_{N\delta tef}$, $C_{m\delta tef}$ & $C_{A\delta tef}$) were also held constant at appropriate wind tunnel data ONLY if the trailing-edge flaps were NOT PULSED by OBES. If the trailing-edge flaps were independently pulsed by OBES then these coefficients were also estimated. All wind tunnel values were based upon angle of attack and Mach for the maneuver. Also note that all wind tunnel data was presented in terms of C_L, C_D and C_m. The lift and drag terms were easily converted to normal and axial force coefficients by using:

$$C_N = C_L \cos(\alpha) + C_D \sin(\alpha)$$

$$C_A = C_D \cos(\alpha) - C_L \sin(\alpha)$$

All mass properties (x_{cg}, y_{cg}, z_{cg}, I_x, I_y, I_z, I_{xz} and mass) were considered to be unique values for each individual maneuver. These values were also cut using getFdas and an average value of each property over the maneuver time was used in pEst for the model.

The only dynamic derivatives estimated here were C_{Nqf}, C_{mqf} and C_{Aqf} due to the lack of excitation in the lateral direction during the maneuvers. The classical static derivatives estimated were: C_{No}, $C_{N\alpha}$, $C_{N\delta e}$, $C_{N\delta tef}$, $C_{N\delta pv}$, $C_{N\delta yv}$, $C_{N\delta as}$, C_{mo}, $C_{m\alpha}$, $C_{m\delta e}$, $C_{m\delta tef}$, $C_{m\delta pv}$, $C_{m\delta yv}$, $C_{m\delta as}$, C_{Ao}, $C_{A\alpha}$, $C_{A\delta e}$, $C_{A\delta tef}$, $C_{A\delta pv}$, $C_{A\delta yv}$, $C_{A\delta as}$

Two additional parameters anBias and axBias were estimated to model the measurement biases for the normal and axial linear accelerometers. The goal with respect to the longitudinal cost function (J) was to minimize the difference between measured and computed values of: α, q, θ, a_n, a_x and climb angle γ. Note that although q_{mod} was computed no weighting was applied in the cost function for it. This was done because q and q_{mod} are nearly identical responses where:

$$q_{mod} = q - \omega \sin(\beta)$$

In these longitudinal directional OBES maneuvers ω and β are near zero. Consequently, if q measured and q computed match properly then naturally q_{mod} will follow by definition.

LONGITUDINAL MODEL

The classical state equations already available in pEst for alphadot, qdot and thetadot were used. Note that the new state equation gammadot describing directional change in the

velocity vector (climb angle) was added. It is a function of the total coefficients C_N, C_A and C_Y.

$$\dot{\gamma}=\frac{g}{V_T}[n_x(\sin\alpha\cos\mu+\cos\alpha\sin\beta\sin\mu)-n_y(\cos\beta\sin\mu)+n_z(\cos\alpha\cos\mu-\sin\alpha\sin\beta\sin\mu)-\cos\gamma]$$

where:

$$n_x=-\frac{\bar{q}S}{mg}C_A+\frac{T}{mg} \qquad n_y=\frac{\bar{q}S}{mg}C_Y \qquad n_z=\frac{\bar{q}S}{mg}C_N$$

While decoupling longitudinal and lateral, as was the goal with these maneuvers, it was found that the C_Y term could be safely set to zero and thus its subcomponents not estimated. This approximation holds since μ, the bank angle about the velocity vector, is often small during such maneuvers. The total coefficient buildup for the longitudinal model can be found in [2,3] while the added state equation for γ developed by Kalviste using spherical mapping, may be seen in [1,3].

Also recall that the model being used breaks aircraft rotation down into three of the four components possible at each discrete time point (p_{mod}, q_{mod}, r_{mod} and ω) allowing for the estimation of coefficients in the buildup equivalent to rotary balance (ie. $C_{l\omega}$, etc.) and forced oscillation derivatives (ie.C_{Nqf}, etc.). Details on this modeling technique can be found in [2,3].

LATERAL SETUP

Three lateral directional flights of PID static maneuvers were also examined. In this case it was found necessary to hold the differential horizontal stabilizer derivatives constant to wind tunnel data if this control surface was NOT pulsed independently by OBES. This was found to be the case in the "optimal lateral input" runs made using OBES where some correlation, although small, was still present between aileron pulses (made using OBES) and differential stabilizer. As before, the wind tunnel data was based on Mach and angle-of-attack for the considered run.

All mass properties were again taken to be unique values for each individual maneuver. These values were also cut using getFdas and an average value of each property over the maneuver time was used in pEst for the model.

The dynamic derivatives estimated were C_{Ypf}, C_{Yrf}, C_{Yw}, C_{lpf}, C_{lrf}, C_{lw}, C_{npf}, C_{nrf} and C_{nw} due to the lack of deliberate longitudinal excitation in the lateral maneuvers. The classical lateral static derivatives estimated were: C_{Yo}, $C_{Y\beta}$, $C_{Y\delta A}$, $C_{Y\delta dH}$, $C_{Y\delta R}$, $C_{Y\delta pv}$, $C_{Y\delta yv}$, C_{lo}, $C_{l\beta}$, $C_{l\delta A}$, $C_{l\delta dH}$, $C_{l\delta R}$, $C_{l\delta pv}$, $C_{l\delta yv}$, C_{no}, $C_{n\beta}$, $C_{n\delta A}$, $C_{n\delta dH}$, $C_{n\delta R}$, $C_{n\delta pv}$, $C_{n\delta yv}$.

The additional parameter ayBias was estimated to model the measurement bias for the lateral directional accelerometer.

The goal regarding the lateral cost function (J) was to minimize the difference between measured and computed values of: β, p, r, ϕ, a_y, p_{mod}, r_{mod}, ω and μ. As opposed to the longitudinal case, the time history for p is not similar to p_{mod} and r is not similar to r_{mod}. Thus, each of these responses had to be included in the cost function.

LATERAL MODEL

The classical state equations already available in pEst for betadot, pdot, rdot and phidot were used. The new state equation mudot describing bank angle (μ) of the aircraft about the velocity vector was added. It is a function of the total coefficients C_A and C_N, body axis roll rate (P), body axis yaw rate (R) and the rate change of heading for the velocity vector (sigmadot). Due to the design of the available lateral directional maneuvers any deviation from the longitudinal steady state trim is minimized. Since this proposes a decoupling of longitudinal and lateral motion the C_A and C_N terms are approximated as zero (their subcomponents are not estimated). Examination of the relation for mudot shows that the contribution due to these two terms are small compared to those of P and R.

$$\dot{\mu} = (P\cos\alpha + R\sin\alpha)\sec\beta + \dot{\sigma}\sin\gamma + \frac{g}{V_T}(n_x\sin\alpha + n_z\cos\alpha - \cos\mu\cos\gamma)\tan\beta$$

In this analysis sigmadot was set in pEst with the option to be computed as a response. Sigmadot is a function of the total force coefficients C_A, C_Y and C_N. Note that sigmadot was not integrated with the goal of matching σ measured and σ computed because it is equivalent to a compass heading. This would be an awkward response to match. Consequently, it made more sense to try matching sigmadot measured and sigmadot computed (or the rate change of the velocity vector heading). However, here it turns out that C_A and C_N have a strong contribution in the model for sigmadot as seen below.

$$\dot{\sigma} = \frac{g}{V_T\cos\gamma}\left[n_x(\sin\alpha\sin\mu - \cos\alpha\sin\beta\cos\mu) + n_y(\cos\beta\cos\mu) + n_z(\cos\alpha\sin\mu + \sin\alpha\sin\beta\cos\mu)\right]$$

As a result, the assumption of a decoupled model where C_A and C_N have negligible contribution is not appropriate. Consequently, the measured time history for sigmadot was used in the model throughout the analysis. Recall the previous expressions shown for n_x, n_y and n_z and again note that the lateral directional aerodynamic buildup expressions can be seen in [2,3] while the two new state equations developed by Kalviste can be seen in [1,3].

CONCLUSIONS

A more detailed evaluation of the results are planned to be incorporated into a proposed journal paper during Spring 95. Overall, with the data analyzed it was found that less scatter, as well as smaller Cramer-Rao bounds, were achieved for the classical parameters over the previous attempt at modeling the cross-coupling derivatives in strictly longitudinal and lateral maneuvers. In addition, the majority of the control surface coefficients were well estimated especially with the use of the SSI MD inputs. One problem encountered with the independent longitudinal pitch vane pulse at the end of the appropriate time cuts was that the system experienced difficulties returning the computed model back to trim after recovery from the pulse. As a result, the longitudinal SSI MD time histories were adjusted to include elevator, trailing-edge flap and symmetric aileron only. Perhaps a pitch vane doublet would prove better than a single pulse since the yaw vane doublets did not encounter this problem.

Enclosed with this document are the full set of longitudinal and lateral-directional parameter estimate plots showing coefficient estimates along with Cramer-Rao bounds. All bounds were multiplied by a factor of three to account for any modeling errors. In addition, a representative time history match for each type of maneuver tested at each angle of attack is also

enclosed. Additional plots of time histories are available upon request.

REFERENCES

[1] Kalviste, Juri, "Spherical Mapping and Analysis of Aircraft Angles for Maneuvering Flight", AIAA Journal of Aircraft, August 1987.

[2] Kalviste, Juri, "Use of Rotary Balance and Forced Oscillation Test Data in a Six Degrees of Freedom Simulation", AIAA paper 82-1364, August 1982.

[3] Napolitano, M. R., et. al., "Parameter Estimation for the NASA F/A-18 HARV at High Angles of Attack", AIAA paper 94-3504, Atmospheric Flight Mechanics Conference, Scottsdale, AZ, August 1994.

Appendix A

Reference [3]

Appendix B

Plots of estimates and time histories

Appendix A

Reference [3]

Napolitano, M. R., et. al., "Parameter Estimation for the NASA F/A-18 HARV at High Angles of Attack", AIAA paper 94-3504, Atmospheric Flight Mechanics Conference, Scottsdale, AZ, August 1994.

AIAA ATMOSPHERIC FLIGHT MECHANICS CONFERENCE

AUGUST 1-3, 1994
SCOTTSDALE, ARIZONA

Parameter Estimation for the NASA F/A-18 HARV at High Angles of Attack

Marcello R. Napolitano
Alfonso C. Paris
Joelle Spagnuolo

Department of Mechanical and Aerospace Engineering
West Virginia University, Morgantown WV 26506/6101

Albion H. Bowers
NASA Dryden Flight Research Facility
Edwards, CA 93523/0273

AIAA Paper 94-3504

PARAMETER ESTIMATION FOR THE NASA F/A-18 HARV AT HIGH ANGLES OF ATTACK

Marcello R. Napolitano#, Alfonso C. Paris* and Joelle Spagnuolo*
Department of Mechanical and Aerospace Engineering
West Virginia University, Morgantown WV 26506/6101

Albion H. Bowers+
NASA Dryden Flight Research Facility
Edwards, CA 93523-0273

Abstract

The subject of this paper is the determination of the aerodynamic stability and control derivatives from flight data using the Maximum Likelihood method for the NASA F/A-18 HARV at high angles of attack. The parameter identification (PID) code pEst, developed at NASA Dryden, was provided by NASA and modified for an alternative modeling approach for high angle of attack conditions. Estimates were obtained for longitudinal dynamics parameters.

Symbols

a_n = normal acceleration, g
a_x = longitudinal acceleration, g
a_y = lateral acceleration, g
b = wing span, ft
$\overline{c}$ = mean aerodynamic chord
C_i = aerodynamic coefficient where i=(L,N,D,A,m,Y,l,n,δ), rad^{-1} or deg^{-1}
E = expected value
g = gravity acceleration, ft/sec^2
J = quadratic cost functional
k_α = upwash correction factor
k_β = sidewash correction factor
m = aircraft mass, slugs
n_t = number of discrete time points in a maneuver
n_z = number of responses in the cost function J
n_ξ = number of parameters estimated
P(z) = maximum likelihood probability
p = roll rate, deg/sec
q = pitch rate, deg/sec
$\overline{q}$ = dynamic pressure, lbs/ft^2
r = yaw rate, deg/sec
S = wing planform area, ft^2
V = velocity, ft/sec
var = variance
W_1 = response error weighting matrix
W_2 = "a priori" weighting matrix
x = X-axis position, ft
y = computed aircraft response vector, or Y-axis position, ft
z = measured aircraft response vector, or Z-axis position, ft

Greek

α = angle-of-attack, deg
β = sideslip angle , deg
Δ = increment
δ = deflection, deg
θ = pitch attitude, deg
ξ = parameter vector to be estimated
ξ_o = "a priori" parameter estimates
ξ_{xy} = correlation coefficient
Σ = summation
ϕ = roll attitude, deg
ψ = yaw attitude, deg
ω = angular rate vector, deg/sec
ω_n = natural frequency, rad/sec
∇ = gradient

Subscripts

1 = steady state trim flight conditions
A = axial force
A = aileron
cg = center of gravity
D = drag force
E = elevator
IH = stabilizer
L = lift force
l = rolling moment
m = pitching moment
mod = modified angular rate
N = normal force
n = yawing moment

Assistant Professor, AIAA member
* Graduate Research Assistant, AIAA member
+ Chief Research Engineer, AIAA member

R = rudder
Y = side force

Superscripts

T = transpose
-1 = inverse
. = first derivative with respect to time
— = vector quantity

Introduction

Today's high performance military aircraft are required to be able to fly at high angles of attack, often at high angular velocity.

The National Aeronautics and Space Administration (NASA) is currently involved in a high alpha technology program using different aircraft which has the following objectives:

-to provide flight validated prediction methods including experimental and computational methods that accurately simulate high angle of attack aerodynamics, flight dynamics and flying qualities
-to improve aircraft agility at high angles of attack

Part of the overall program for each test aircraft involves a parameter identification (PID) analysis in which a complete set of stability and control parameters is extracted from flight data at high angles of attack. A first purpose for this analysis is to evaluate the correlation of the flight data estimated from aerodynamic characteristics with the correspondent wind tunnel and/or numerically predicted characteristics. An additional purpose of this analysis is to extend the data base of the aircraft aerodynamics which, in turn, allows to update the simulation codes in flight simulators and provide the control engineers with a better understanding of the aircraft non-linear behavior for a more efficient design of non-linear control laws.

The use of flight data to estimate aircraft stability and control derivatives has been implemented for many years. The most efficient parameter identification (PID) method to date is the Maximum Likelihood (ML) approach used in conjunction with a Newton-Raphson (NR) algorithm for the minimization of a cost function related to the estimation process.[7,8] This method has been used at NASA Dryden since the late 1960's and several codes have been developed for the purpose.

This paper is relative to the determination of the stability and control derivatives for the NASA F/A-18 HARV at high angles of attack using the ML method with NR algorithm. The NASA F/A-18 High Alpha Research Vehicle (HARV) is a special research aircraft equipped with a thrust vectoring system consisting of axisymmetric nozzles and six post exit vanes that allow vectoring capability in both pitch and yaw. An additional feature of the aircraft which makes it very attractive for PID investigation is the onboard excitation system (OBES) in the flight control computer which allows independent control surface motions. The PID process has been performed using the pEst software, which is the more recent and sophisticated estimation code developed at NASA Dryden. Among the capabilities of the pEst code there are efficient user interaction and the handling of non-linearitites in the dynamic equations of motion.

It is clear that at high angle of attack conditions the concept of evaluating the stability derivatives about a steady state flight condition can no longer be applied. This is due to the inherent aerodynamic non-linearities as well as the potential coupling between the longitudinal and lateral dynamics. The main contribution of this paper is to implement a particular aerodynamic and dynamic modeling procedure for these non-linear conditions[3,4,6] used in conjunction with the ML method for PID purposes.

This investigation has evolved from a previous PID analysis using a more conventional modeling procedure.[13]

Overview of the Maximum Likelihood Method with the Newton-Raphson Algorithm

The most successful parameter identification approach to date has been the ML method with a NR technique to minimize a quadratic cost functional containing differences between the aircraft measured and computed responses. This implies the maximization of the probability that the aircraft model computed responses, using a given set of estimates for the unknown aerodynamic coefficients, are representative of the true system dynamics. The relations forming a basis for this technique are shown in Figure 1.[7] Define $P(z/\xi)$ as the probability that the actual system response z occurs for a given value of the unknown parameters placed in a vector ξ. Define $P(\xi)$ as the probability that the unknown derivatives in the parameter vector match some "a priori" values. It is assumed that $P(z/\xi)$ and $P(\xi)$ are independent and follow Gaussian distributions.

It is clear that, as the accuracy of the estimates increases, the differences between the values of the components of z and y, at the same

discrete time index, decrease. Using the independence assumption for the two probabilities yields the ML cost functional P(z). The cost function $J(\xi)$ must therefore be minimized in order to maximize the ML cost functional. A modified NR algorithm is used to solve the associated system of equations by using the first and second gradients of the cost function with respect to the vector ξ.[1,7,10] The relations governing the NR algorithm are listed in Figure 2. The process is iterative with updating of the vector ξ until some user defined convergence criteria is met. Using a Taylor Series expansion an expression is generated for $J(\xi)$. Using the Newton-Raphson method, this cost functional is minimized by setting its gradient with respect to ξ equal to zero. This allows for the determination of an iterative expression for ξ with the first and second gradients of $J(\xi)$. An overview of the aircraft parameter estimation process is shown in Figure 3.

Aerodynamic and Dynamic Modeling at Non-linear Conditions

One of the main purposes of this paper is to introduce a particular modeling procedure for the non-linear dynamic and aerodynamic conditions of the F/A-18 HARV at high angles-of-attack. The modeling starts from the classic non-linear longitudinal and lateral-directional equations of motion along the stability axes as seen in [6,12]. They are shown in Figure 4. A particular innovation described in [3,4] consists of the introduction of a new set of dynamic axes called the dynamic stability axes. A key characteristic of this new dynamic frame is that the axes are not orthogonal. By definition, the equations of the rotation of the aircraft around these dynamic stability axes are given by:

-Equation of the time rate of change of the flight path bank angle ($\dot{\mu}$)
-Equation of the time rate of change of the flight path elevation ($\dot{\gamma}$)
-Equation of the time rate of change of the flight path heading angle ($\dot{\sigma}$)

These equations are shown in Figure 5. These relations make use of the body axis angular rates to obtain the transformation to the dynamic stability axis rates.

Having defined the new system of aircraft dynamic equations new aerodynamic coefficients describing this motion must be introduced. The classical stability parameters (C_N,C_A,C_m,C_l,C_n and C_y) can be separated into two components. Each of the total non-dimensional stability derivatives can be partitioned into static and dynamic terms:[3]

$$P(z/\xi)=\frac{1}{2\pi^{n_t\left(\frac{n_z}{2}\right)}\left(\frac{1}{W_1}\right)^{\frac{n_t}{2}}}\, e^{-\frac{1}{2}\left(\frac{1}{n_t n_z}\sum_{k=1}^{n_t}([z(t_k)-y(t_k)]^T W_1[z(t_k)-y(t_k)]\right)} \tag{1}$$

$$P(\xi)=\frac{1}{2\pi^{\left(\frac{n_\xi}{2}\right)}\left(\frac{1}{W_2}\right)^{\frac{1}{2}}}\, e^{-\frac{1}{2}[(\xi-\hat{\xi}_o)^T W_2(\xi-\hat{\xi}_o)]} \tag{2}$$

$$P(z)=P(z/\xi)\;P(\xi)=\frac{1}{2\pi^{\left(\frac{n_t n_z+n_\xi}{2}\right)}\left(\frac{1}{W_1}\right)^{\frac{n_t}{2}}\left(\frac{1}{W_2}\right)^{\frac{1}{2}}}\, e^{-\frac{1}{2}J(\xi)} \tag{3}$$

$$J(\xi)=\frac{1}{n_t n_z}\sum_{k=1}^{n_t}([z(t_k)-y(t_k)]^T W_1[z(t_k)-y(t_k)]) + (\xi-\hat{\xi}_o)^T W_2(\xi-\hat{\xi}_o) \tag{4}$$

Figure 1: Relations forming a basis for the Maximum Likelihood method

$$J(\xi)=J(\xi_i)+(\xi-\xi_i)^T\ [\nabla_\xi J(\xi_i)]^T+\frac{1}{2}(\xi-\xi_i)^T\ \nabla^2_\xi J(\xi_i)\ (\xi-\xi_i) \tag{5}$$

$$\nabla_\xi J(\xi)\ =\ \nabla_\xi J(\xi_i)+(\xi-\xi_i)^T\ \nabla^2_\xi J(\xi_i)\ =\ 0 \tag{6}$$

$$\xi_{i+1}=\ \xi_i\ -\ [(\nabla^2_\xi J(\xi_i))^T]^{-1}\ \nabla^T_\xi J(\xi_i) \tag{7}$$

$$\nabla_\xi J(\xi)=\frac{-2}{n_t\ n_z}\sum_{k=1}^{n_t}\left[(z(t_k)-y(t_k))^T\ W_1\ \nabla_\xi y(t_k)\right]+2(\xi-\hat{\xi}_o)^T\ W_2 \tag{8}$$

$$\nabla^2_\xi J(\xi)=\frac{2}{n_t\ n_z}\sum_{k=1}^{n_t}\left[[\nabla_\xi y(t_k)]^T\ W_1\ \nabla_\xi y(t_k)\right]+2W_2 \tag{9}$$

Figure 2: Relations governing the parameter update process using the Newton-Raphson algorithm.

$$C_i=C_{i_{static}}(\alpha,\beta,V,h,\delta)\ +$$

$$C_{i_{dyn}}(\alpha,\beta,V,h,\delta,P,Q,R,\dot{\alpha},\dot{\beta}) \tag{23}$$

where i=(N,A,m,l,n and Y). The static terms are made up of non-rotational motion while the dynamic terms contain all aircraft motion parameters. The static terms are the known conventional derivatives often based on aircraft geometry which may be represented as follows in their body axis forms:[3]

$$C_{N_{static}}=C_{N_o}+C_{N_\alpha}\alpha+C_{N_\beta}\beta+C_{N_\delta}\delta \tag{24}$$

$$C_{A_{static}}=C_{A_o}+C_{A_\alpha}\alpha+C_{A_\beta}\beta+C_{A_\delta}\delta \tag{25}$$

$$C_{m_{static}}=C_{m_o}+C_{m_\alpha}\alpha+C_{m_\beta}\beta+C_{m_\delta}\delta \tag{26}$$

$$C_{l_{static}}=C_{l_o}+C_{l_\beta}\beta+C_{l_\alpha}\alpha+C_{l_\delta}\delta \tag{27}$$

$$C_{n_{static}}=C_{n_o}+C_{n_\beta}\beta+C_{n_\alpha}\alpha+C_{n_\delta}\delta \tag{28}$$

$$C_{Y_{static}}=C_{Y_o}+C_{Y_\beta}\beta+C_{Y_\alpha}\alpha+C_{Y_\delta}\delta \tag{29}$$

Note the cross-coupling stability derivatives in these relations. These are required due to the presence of dynamic coupling between the longitudinal and lateral directions of motion at high angles-of-attack. The dynamic terms are new and warrant further examination.

The dynamic derivatives may be built up from components due to each rotational term as shown in Figure 6.[3] Estimates for these terms are found during conventional wind tunnel tests utilizing the rotary balance and forced oscillation methods in addition to translational acceleration terms. The total contribution of these dynamic terms are also shown in the component build-up of Figure 6. The first term in the equation is obtained from rotary balance wind tunnel tests. The next three terms are measured in the oscillation wind tunnel test. The last two terms are the acceleration derivatives. The P_{mod}, Q_{mod} and R_{mod} terms are the components of total rotation vector about the x, y and z axes. The total rotation vector of the aircraft has been divided into only three components. The reason for this is that division into

$$\dot{\alpha} = Q - \tan\beta(P\cos\alpha + R\sin\alpha) - \frac{\bar{q}\,s}{mV\cos\beta}C_L + \frac{g}{V\cos\beta}(\cos\theta\cos\phi\cos\alpha + \sin\theta\sin\alpha) \tag{10}$$

$$I_y\dot{Q} - I_{yz}\dot{R} - I_{xy}\dot{P} = \bar{q}s\bar{c}C_m + [PR(I_z - I_x) + (R^2 - P^2)I_{xz} + QRI_{xy} - PQI_{yz}] \tag{11}$$

$$\dot{\theta} = Q\cos\phi - R\sin\phi \tag{12}$$

$$\dot{V} = -\frac{\bar{q}s}{m}C_D + g(\cos\phi\cos\theta\sin\alpha\cos\beta + \sin\phi\cos\theta\sin\beta - \sin\theta\cos\alpha\cos\beta) \tag{13}$$

$$\dot{\beta} = P\sin\alpha - R\cos\alpha + \frac{\bar{q}s}{mV}C_Y + \frac{g}{V}(\cos\beta\cos\theta\sin\phi) + \frac{g}{V}(-\sin\beta(\cos\theta\cos\phi\sin\alpha - \sin\theta\cos\alpha)) \tag{14}$$

$$I_x\dot{P} - I_{xy}\dot{Q} - I_{xz}\dot{R} = \bar{q}sbC_l + [QR(I_y - I_z) + (Q^2 - R^2)I_{yz} + PQI_{xz} - PRI_{xy}] \tag{15}$$

$$I_z\dot{R} - I_{xz}\dot{P} - I_{yz}\dot{Q} = \bar{q}sbC_n + [PQ(I_x - I_y) + (P^2 - Q^2)I_{xy} + PRI_{yz} - QRI_{xz}] \tag{16}$$

$$\dot{\phi} = P + \tan\theta(R\cos\phi + Q\sin\phi) \tag{17}$$

Where:

$$C_L = C_N\cos(\alpha) - C_A\sin(\alpha) \tag{18}$$

$$C_D = C_A\cos(\alpha) + C_N\sin(\alpha) \tag{19}$$

Figure 4: The classical non-linear longitudinal and lateral equations of motion about the stability axis.

$$\dot{\sigma} = \frac{g}{V_T\cos\gamma}[a_x(\sin\alpha\sin\mu - \cos\alpha\sin\beta\cos\mu) + a_y(\cos\beta\cos\mu) + a_z(\cos\alpha\sin\mu + \sin\alpha\sin\beta\cos\mu)] \tag{20}$$

$$\dot{\gamma} = \frac{g}{V_T}[a_x(\sin\alpha\cos\mu + \cos\alpha\sin\beta\sin\mu) - a_y(\cos\beta\sin\mu) + a_z(\cos\alpha\cos\mu - \sin\alpha\sin\beta\sin\mu) - \cos\gamma] \tag{21}$$

$$\dot{\mu} = (P\cos\alpha + R\sin\alpha)\sec\beta + \dot{\sigma}\sin\gamma + \frac{g}{V_T}(a_x\sin\alpha + a_z\cos\alpha - \cos\mu\cos\gamma)\tan\beta \tag{22}$$

Figure 5: Relations transforming body axis angular rates to dynamic stability axis rates.

$$C_{i_{DYN}} = C_i(\alpha,\beta,V,h,\delta,P) + C_i(\alpha,\beta,V,h,\delta,Q) + C_i(\alpha,\beta,V,h,\delta,R) + C_i(\alpha,\beta,V,h,\delta,\dot{\alpha}) + C_i(\alpha,\beta,V,h,\delta,\dot{\beta}) \tag{30}$$

$$C_i = C_{i_\omega}\left(\frac{b}{2V_T}\right)\omega + C_{i_P}{}^F\left(\frac{b}{2V_T}\right)P_{\text{mod}} + C_{i_Q}{}^F\left(\frac{\bar{c}}{2V_T}\right)Q_{\text{mod}} + C_{i_R}{}^F\left(\frac{b}{2V_T}\right)R_{\text{mod}} + C_{i_{\dot{\alpha}}}\left(\frac{\bar{c}}{2V_T}\right)\dot{\alpha}_T + C_{i_{\dot{\beta}}}\left(\frac{b}{2V_T}\right)\dot{\beta}_T \tag{31}$$

Figure 6: Relations showing the dynamic axis stability derivative build-up.

four components along the X, Y, Z and velocity vector often results in a modified rotational rate that may be greater in magnitude and opposite in sign than the measured body axis data. Entering roll rates into the equations of motion with the wrong sign would cause misinterpretation of the actual aircraft dynamics. The method for breaking the total rotational vector into only three of the four available components result in the following modified roll-rate equations:

$$P_{\text{mod}} = P - \omega\cos\alpha\cos\beta \tag{32}$$

$$Q_{\text{mod}} = Q - \omega\sin\beta \tag{33}$$

$$R_{\text{mod}} = R - \omega\sin\alpha\cos\beta \tag{34}$$

The procedure begins by setting the modified roll-rate to zero and solving for ω. The corresponding values of Q_{mod} and R_{mod} are then calculated. If they are less in magnitude compared to the total body axis values for Q and R, and of the same sign, then the rotation vector is broken into Q_{mod}, R_{mod} and ω. If this test fails then the same procedure is performed with the Q_{mod} and R_{mod} relations. Should all three methods fail then the rotation vector is broken up into the body axis P, Q and R values. The result of these tests at each time point are placed into the dynamic parameter model previously shown where it affects the overall aircraft response. The translational acceleration terms found in the dynamic build-up are defined as:

$$\dot{\alpha}_T = \dot{\alpha} - Q + (P\cos\alpha + R\sin\alpha)\tan\beta \tag{35}$$

$$\dot{\beta}_T = \dot{\beta} - P\sin\alpha + R\cos\alpha \tag{36}$$

where the first term in each relation contains effects due to aircraft velocity vector translation and body axis rotational motion. The trailing terms represent effects due to aircraft rotational motion alone. Again, the total non-dimensional stability derivatives are the sum of the static and dynamic components. The total components for C_l, C_m and C_n affect the aircraft motion through the body axis equations for $\dot{P}$, $\dot{Q}$ and $\dot{R}$. The terms for C_y and C_D are located in the expression for $\dot{V}$ while C_N, C_A and C_y affect the body axis response equations for a_z, a_x and a_y respectively.

Modifications to the pEst code to include these coupling static and dynamic terms, as well as the general equations allowing for aircraft flight path angle translation, have been implemented for integration with the parameter estimation process.

Results From the Parameter Estimation Process

One flight was performed with the NASA F/A-18 HARV at six different angle of attack trim conditions (10°, 25°, 30°, 40°, 50°, 60°) for use in extracting the longitudinal aircraft stability derivatives. The longitudinal derivative components of normal force (C_N), aircraft pitching moment (C_m) and axial force (C_A) were chosen to be estimated in the PID process. The data relative to the longitudinal flights were run through the pEst code to produce parameter estimates along with measured and computed response curve-fits. The quadratic cost functional was set to include differences between measured and computed α, q, θ, a_n, a_x, $\dot{q}$, γ and q_{mod}. The response error weighting matrix W_1 was an 8x8 diagonal matrix. Response errors for measurements with higher measurement noise such as α, a_n and a_x were given much lower weightings than for those responses recorded with a lower noise level. The "a priori" weighting W_2 was not implemented in the PID process.

A very useful feature in pEst is the capability to generate the Cramer-Rao bound. This

is an experimental variance, presented to the pEst user in standard deviation form, which can be used as a measure of accuracy for the estimates for the given data. For each parameter this bound gives the minimum variance of the estimate using:

$$var(\hat{\xi}) \geq \frac{1}{E\left[\left(\frac{\partial}{\partial \xi}\ln(f_{\xi}(\hat{\xi}))\right)^2\right]} \qquad (37)$$

where, for a normal distribution:

$$\frac{\partial}{\partial \xi}\ln(f_{\xi}(\hat{\xi})) = \frac{(\hat{\xi}-\xi)}{\sigma_{\xi}^2} \qquad (38)$$

To account for modeling discrepancies the Cramer-Rao bounds are multiplied by a factor of 10. Their most practical use is as a measure of the scatter of the final estimates for the given set of flight data.

The results of the PID have shown a remarkable agreement between the actual time histories and the ones generated with the mathematical model using the estimates. A comparison of the actual and computed α, θ and q time histories at α = 10°, 25°, 30°, 50° are shown in Figures 7-10. The matching between the actual and computed time histories for θ is excellent, due to the accurate and noise-free θ measurements. The matching is acceptable for the α and q measurements, which show the presence of a substantial level of noise.

The main target derivatives in this investigation included $C_{N\alpha}$, $C_{N\delta E}$, $C_{m\alpha}$ and $C_{m\delta E}$. The results are shown in Figures 11-14. The outcome of this investigation has been compared with previous results[13] obtained with convential modeling procedures using the same flight data. Some reservations exist on the goodness of this flight data at α = 25°. It is believed that at that particular condition the aircraft longitudinal dynamics had not been properly excited due to some deflection of the trailing and leading edge flaps not coordinated with the elevator deflections. The results of the PID process for $C_{N\alpha}$ shown in Figure 11 indicate that the introduction of this modeling procedure provide estimates which are somewhat higher than conventional modeling[13] at higher angles of attack (α = 50°, 60°) and slightly lower at lower angles of attack (α = 10°, 25°, 30°). For $C_{N\delta E}$, whose results are shown in Figure 12, it was noticed that the results of this investigation are consistently lower than the previous analysis.[13] On the other side the results for $C_{N\delta E}$ in [13] were higher then expected. Some reservations about the goodness of the results in [13] also existed for $C_{m\alpha}$ and $C_{m\delta E}$ at lower angles of attack (α = 10°, 25°). The results of this investigation for $C_{m\alpha}$ and $C_{m\delta E}$, shown in Figures 13 and 14, reveal more predictable values at these angles of attack.

Conclusions

Flight data provided by NASA Dryden for the longitudinal maneuvers at varying angles of attack were used in this preliminary study to determine the aerodynamic stability and control derivatives using the Maximum Likelihood method for the NASA F/A-18 HARV at high angles of attack. The parameter identification (PID) code pEst, developed at NASA Dryden, was provided by NASA and modified for an alternative modeling approach for high angle of attack conditions. Preliminary results for key longitudinal derivatives using this method were obtained using a single set of flight data. A partial proof of the suitability of this alternative method for modeling high angle of attack conditions is given by more meaningful estimates for $C_{m\alpha}$ with respect to classic modeling procedures. Additional investigations are scheduled using additional flight data. The PID process will be extended to the other longitudinal derivatives and to the lateral-directional derivatives.

Acknowledgements

This research has been sponsored by the NASA Grant NCC 2-759. Partial support for graduate student Alfonso Paris was provided by the West Virginia/NASA Consortium Grant NGT-40047.

References

1- Iliff, K.W., Taylor, L.W., "Determination of Stability Derivatives From Flight Data Using A Newton-Raphson Minimization Technique", NASA TN D-6579, 1972

2- Iliff, K.W., Maine, R.E., "Practical Aspects of Using A Maximum Likelihood Estimation Method to Extract Stability and Control Derivatives From Flight Data", NASA TN D-8209, 1976

3- Kalviste, Juri, "Use of Rotary Balance and Forced Oscillation Test Data in a Six Degrees of Freedom Simulation", AIAA paper 82-1364, August 1982.

4- Kalviste, Juri, "Spherical Mapping and Analysis of Aircraft Angle for Maneuvering Flight", AIAA Journal of Aircraft, August 1987, Vol. 24, Num. 8, pg 523.
5- Maine, Richard, E., and Murray, James, E., "pEst Version 2.1 User's Manual", NASA-TM 88280, Sept 1987
6- Maine, Richard, E., Iliff, Kenneth, W., "Application of Parameter Estimation to Aircraft Stability and Control, The Output-Error Approach", NASA-RP 1168, June 1986
7- Maine, R.E., Iliff, K.W. "Identification of Dynamic Systems ; Theory and Formulation, NASA RP-1138, 1985
8- Maine, R.E., Iliff, K.W. "User's Manual for MMLE3, A General FORTRAN Program for Maximum Likelihood Parameter Estimation, NASA TP-1563, 1980
9- Maine, R.E., Iliff, K.W. "Identification of Dynamic Systems ; Theory and Formulation", NASA RP-1138, 1985
10- Maine, Richard, E., Iliff, Kenneth, W., "Application of Parameter Estimation to Aircraft Stability and Control, The Output-Error Approach", NASA-RP 1168, June 1986
11- Maine, Richard E., Iliff, K.W., "The Theory and Practice of Estimating the Accuracy of Dynamic Flight-Determined Coefficients", NASA RP-1077, 1981
12- Roskam, Jan, Airplane Flight Dynamics and Automatic Flight Controls, Roskam Aviation and Engineering Corporation, Ottawa, Kansas, 1982
13- Spagnuolo, Joelle, "Determination of the Stability and Control Derivatives for the F/A-18 HARV", Thesis West Virginia University Mechanical and Aerospace Dept., Morgantown, WV, 1993

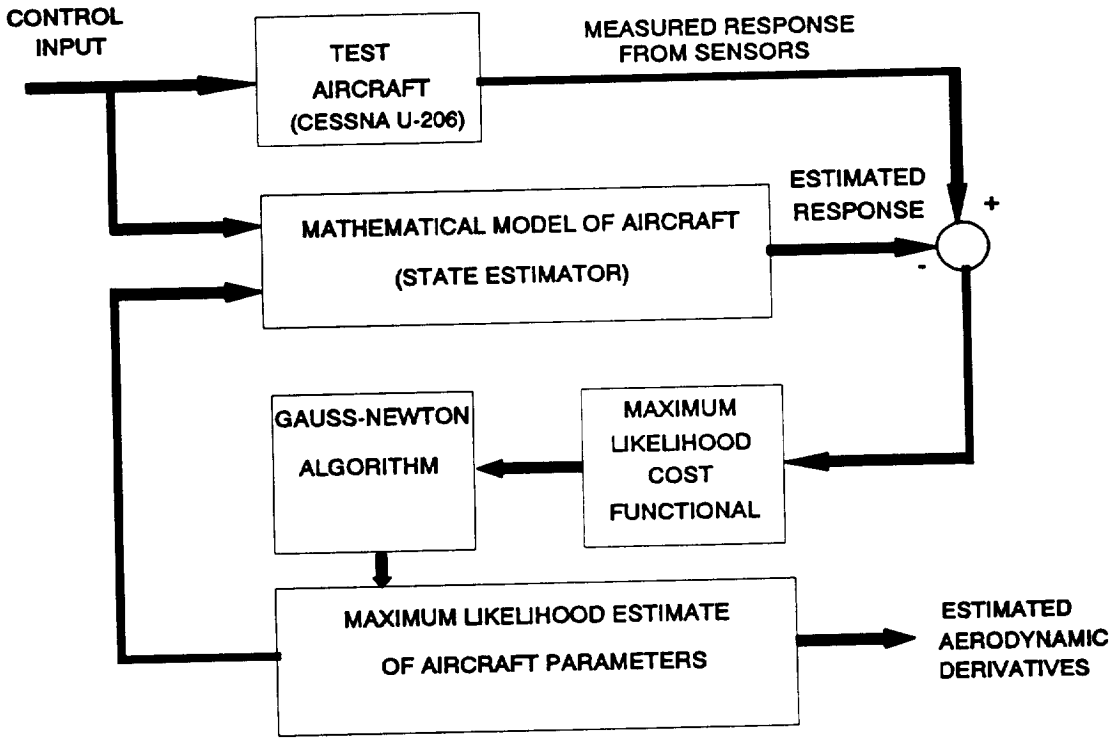

Figure 3: Block diagram of the parameter estimation process.

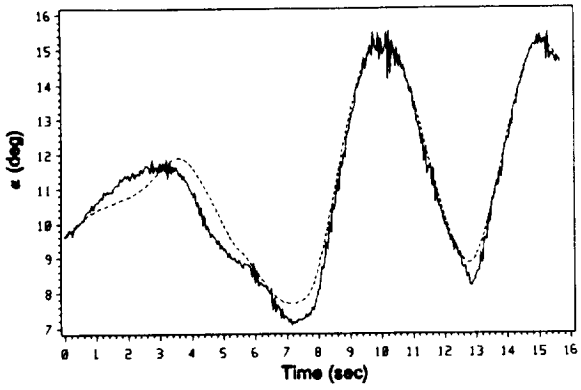

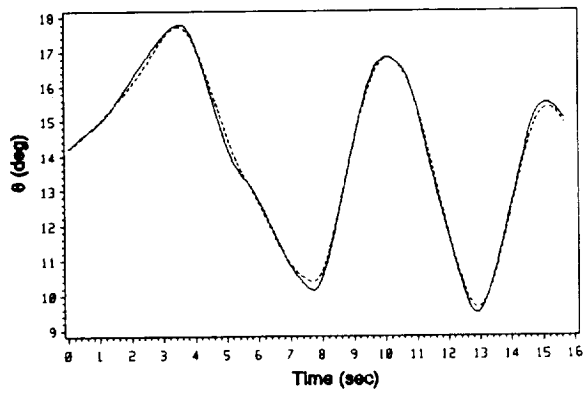

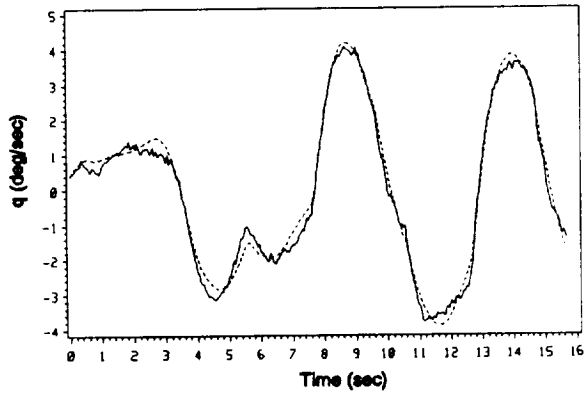

Figure 7: Comparison of time histories for $\alpha = 10^{\circ}$.

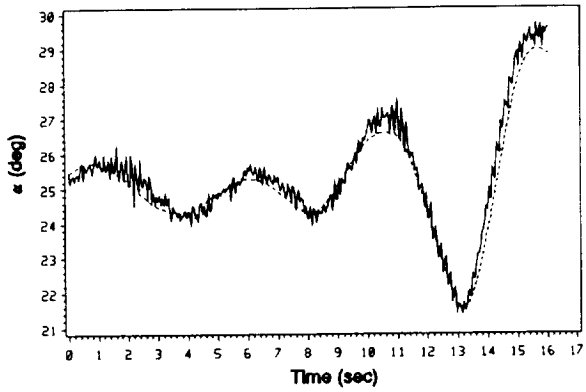

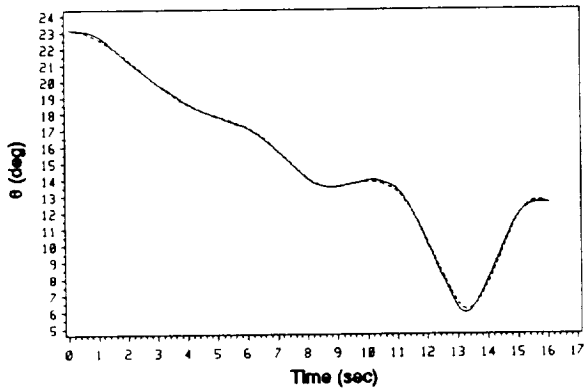

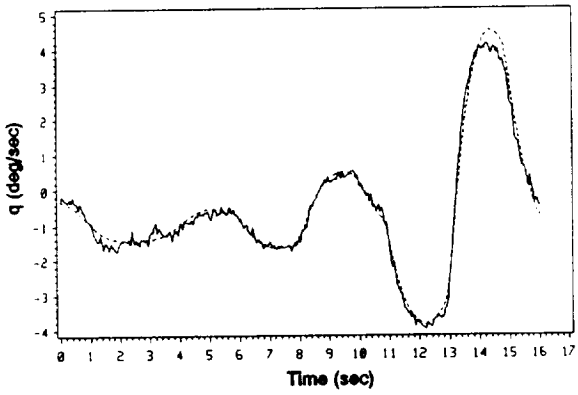

Figure 8: Comparison of time histories for $\alpha = 25^{\circ}$.

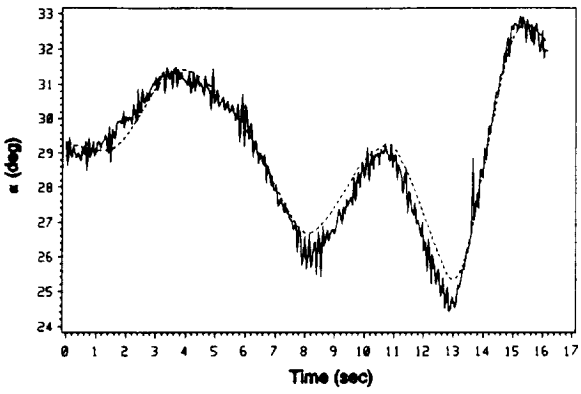

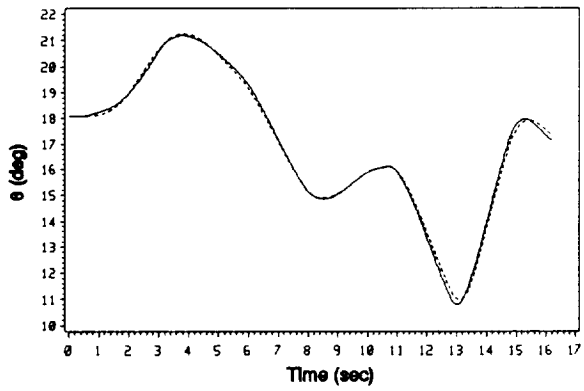

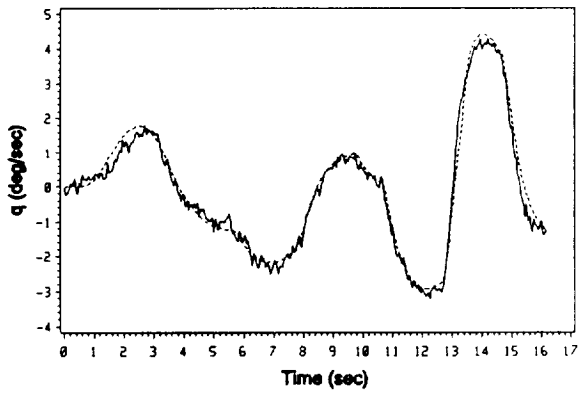

Figure 9: Comparison of time histories for $\alpha=30°$.

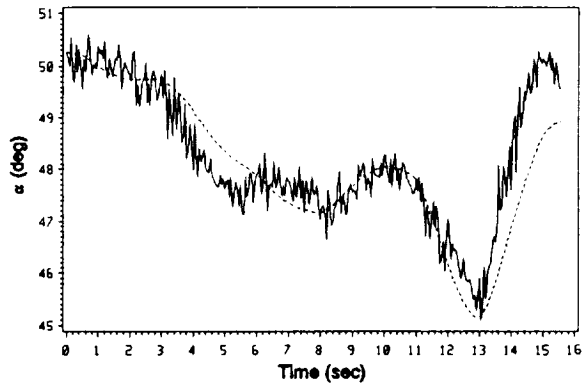

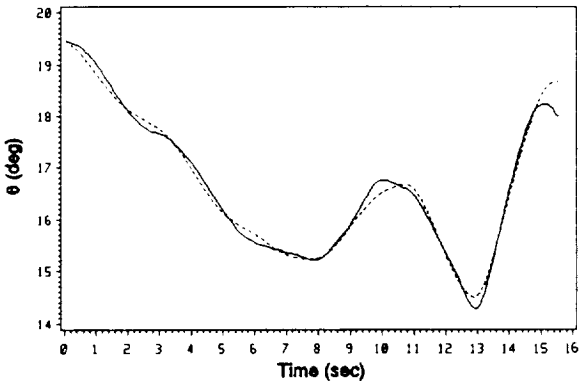

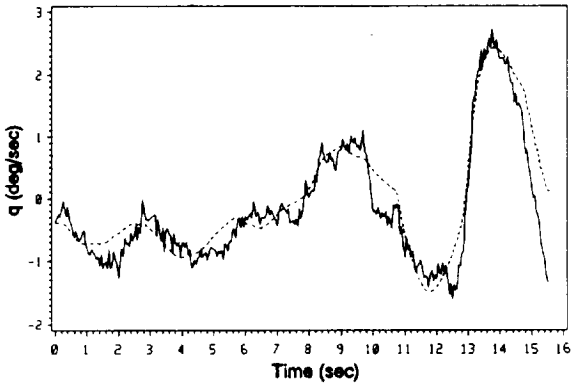

Figure 10: Comparison of time histories for $\alpha=50°$.

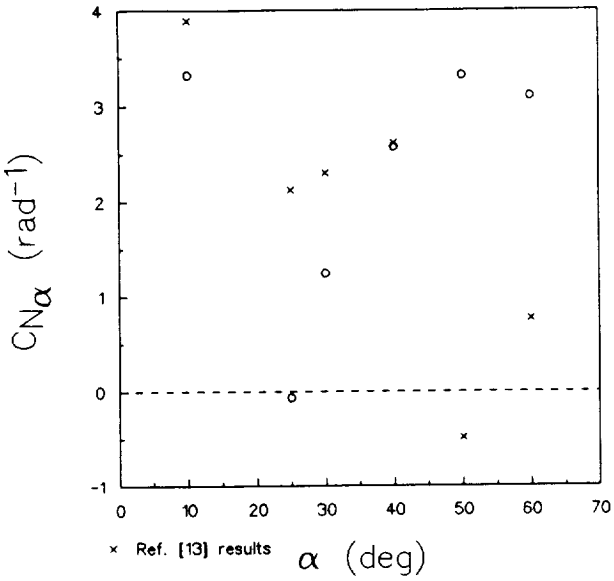

Figure 11: Estimation results for the longitudinal stability derivatives of the F/A-18 HARV.

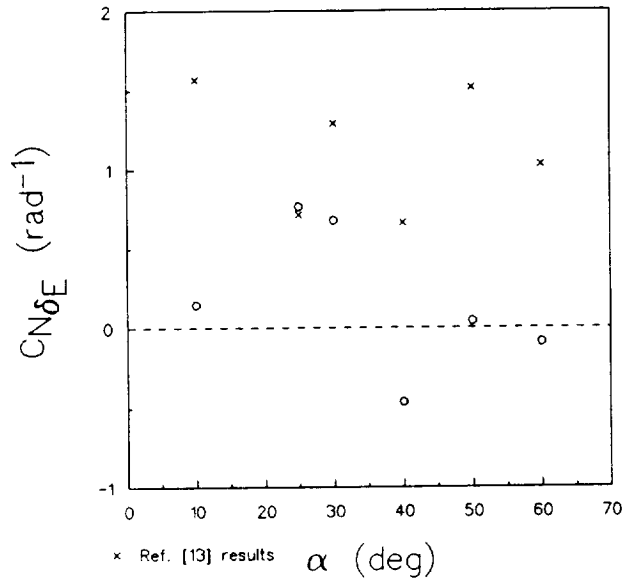

Figure 12: Estimation results for the longitudinal stability derivatives of the F/A-18 HARV.

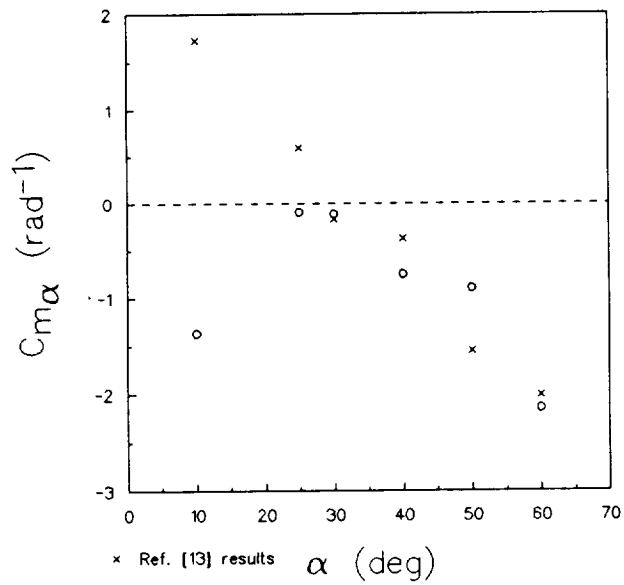

Figure 13: Estimation results for the longitudinal stability derivatives of the F/A-18 HARV.

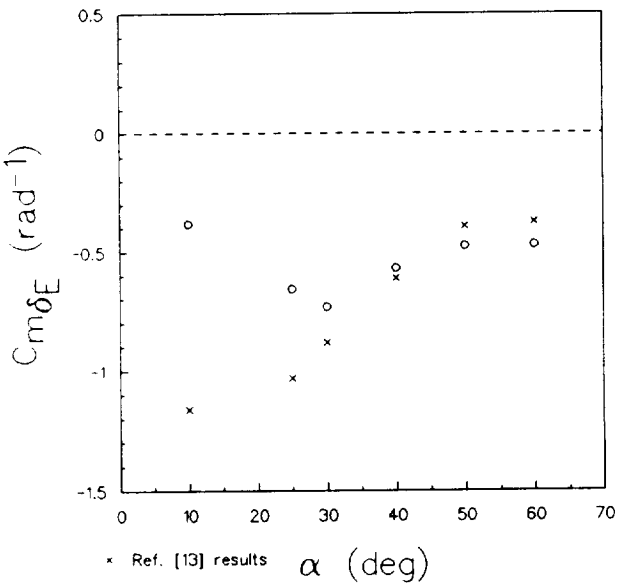

Figure 14: Estimation results for the longitudinal stability derivatives of the F/A-18 HARV.

Appendix B

Plots of estimates and time histories

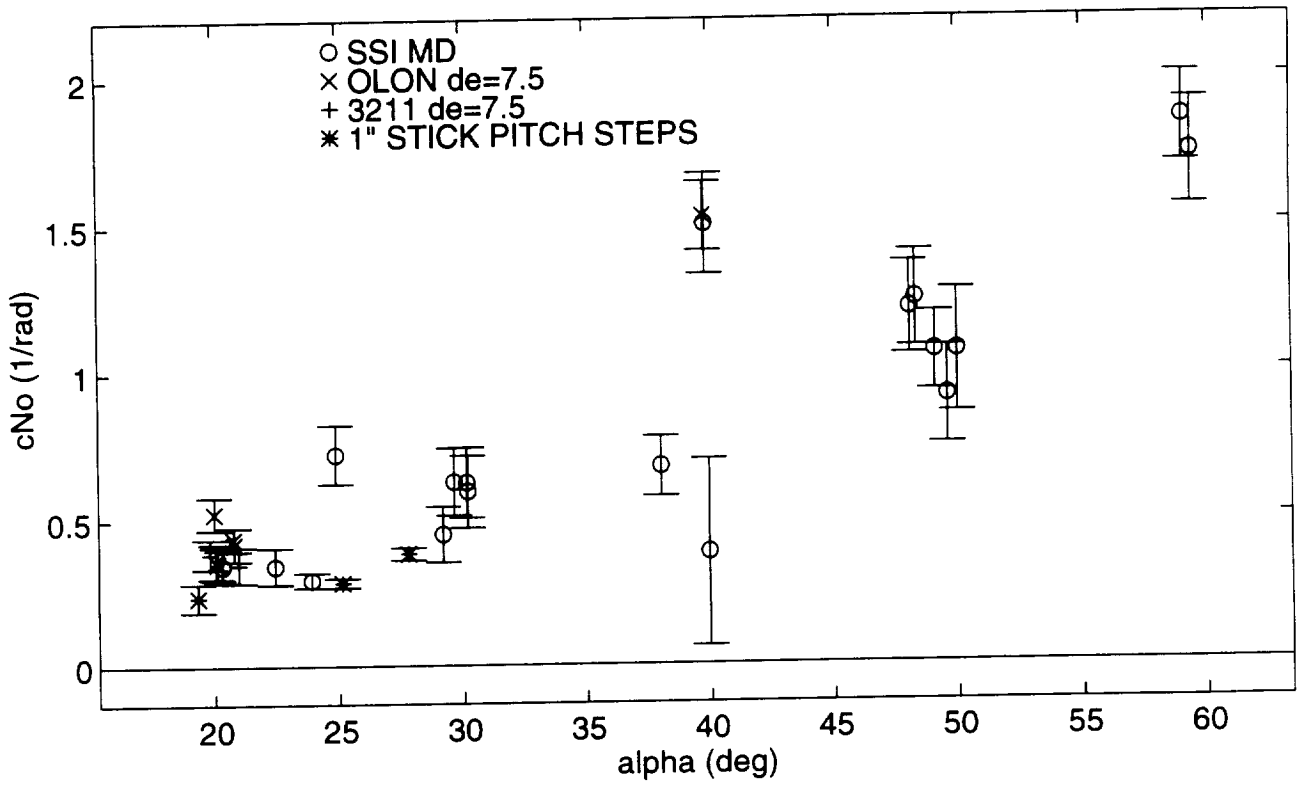
o SSI MD
× OLON de=7.5
+ 3211 de=7.5
✳ 1" STICK PITCH STEPS
cNo (1/rad)
alpha (deg)
2
1.5
1
0.5
0
20
25
30
35
40
45
50
55
60

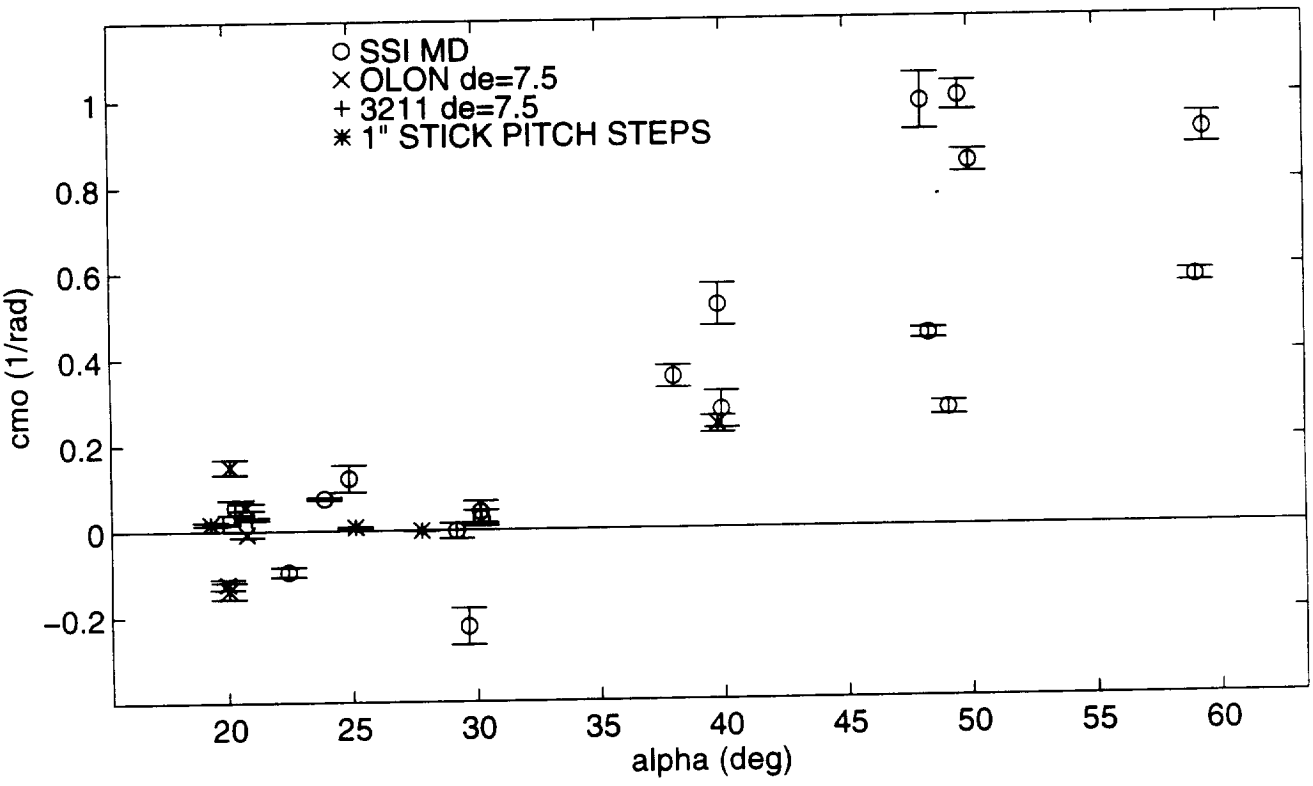
o SSI MD
× OLON de=7.5
+ 3211 de=7.5
✳ 1" STICK PITCH STEPS
cmo (1/rad)
alpha (deg)
1
0.8
0.6
0.4
0.2
0
-0.2
20
25
30
35
40
45
50
55
60

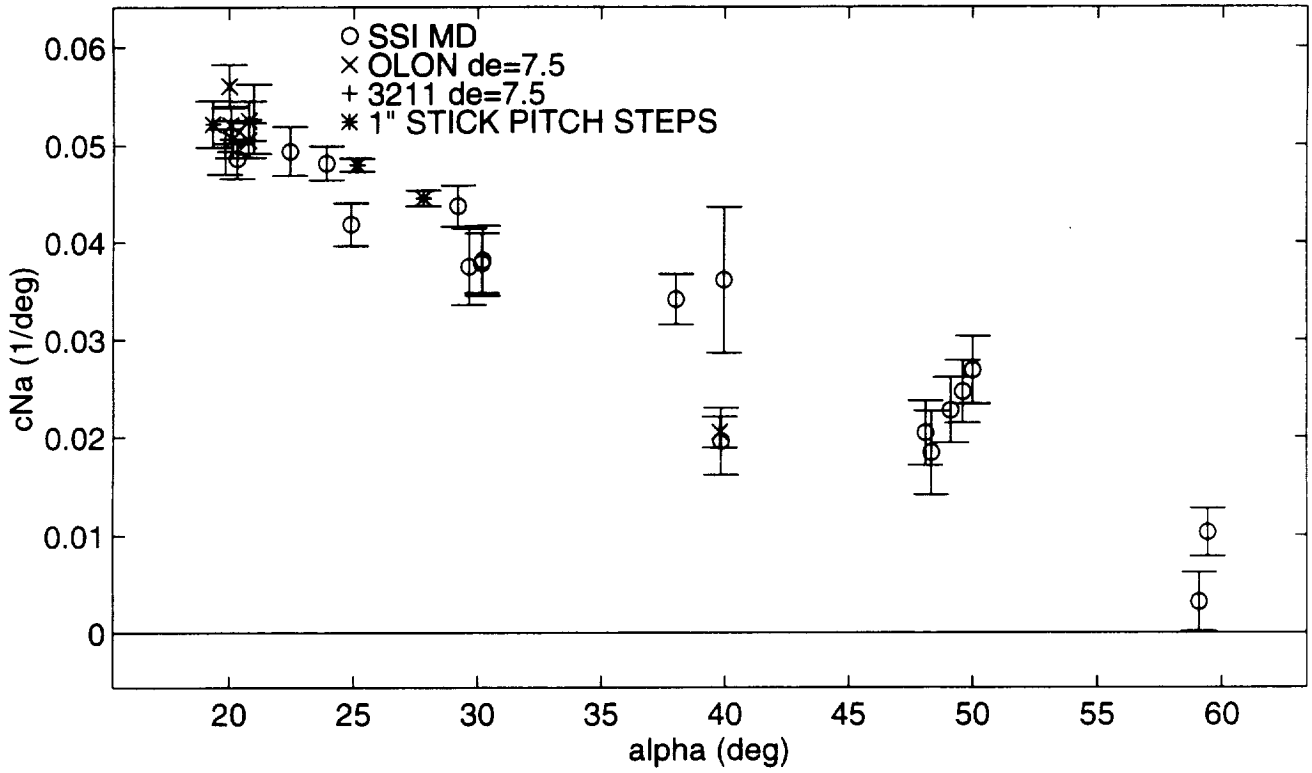
SSI MD
OLON de=7.5
3211 de=7.5
1" STICK PITCH STEPS
cNa (1/deg)
alpha (deg)
0.06
0.05
0.04
0.03
0.02
0.01
0
20
25
30
35
40
45
50
55
60

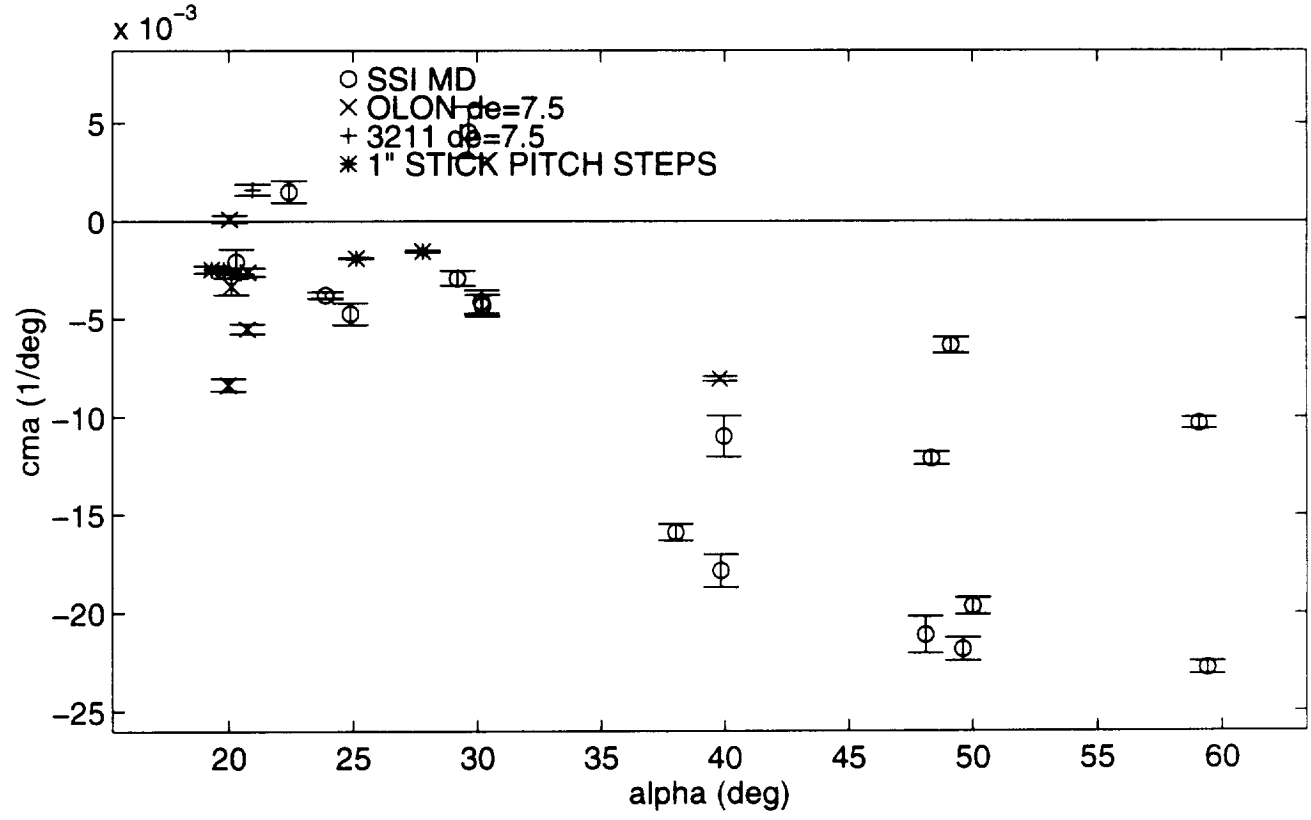
x 10^-3
SSI MD
OLON de=7.5
3211 de=7.5
1" STICK PITCH STEPS
cma (1/deg)
alpha (deg)
5
0
-5
-10
-15
-20
-25
20
25
30
35
40
45
50
55
60

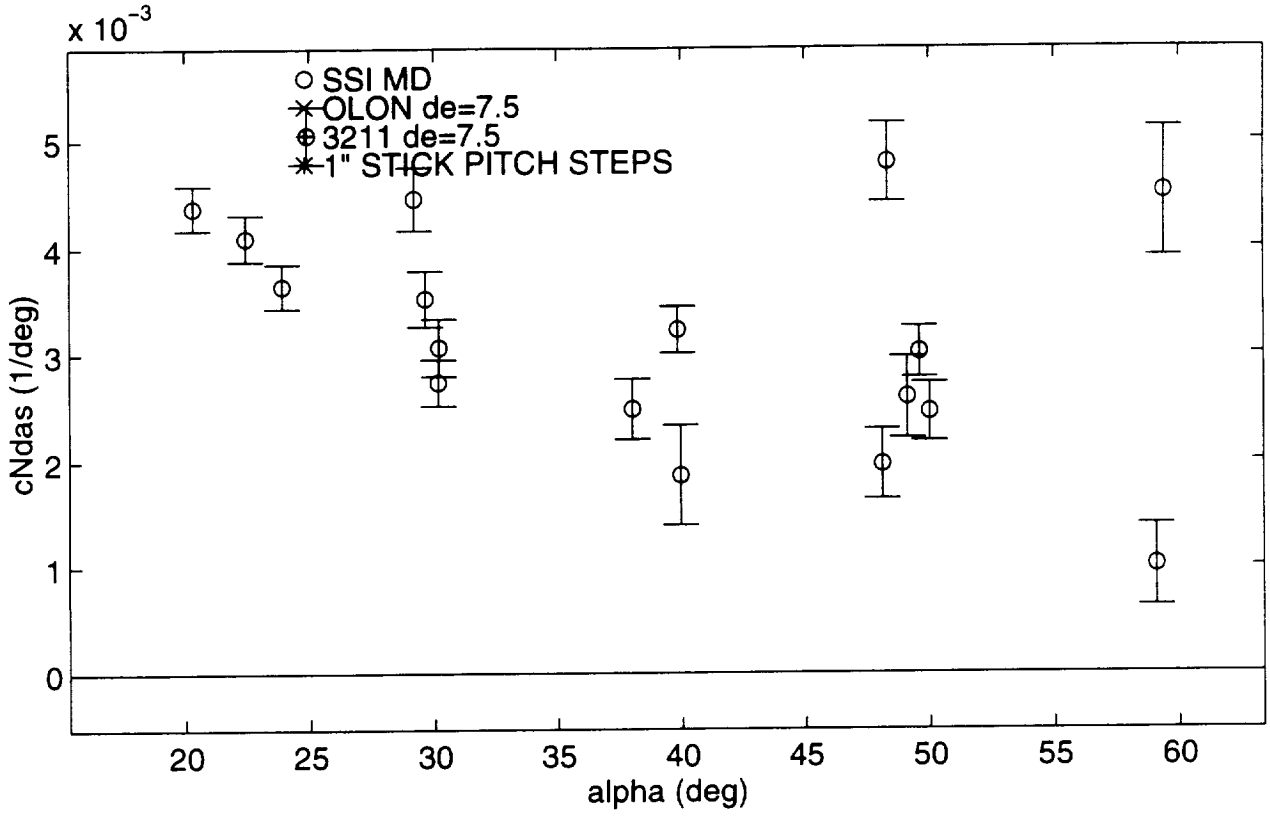
x 10^-3
SSI MD
OLON de=7.5
3211 de=7.5
1" STICK PITCH STEPS
cNdas (1/deg)
alpha (deg)

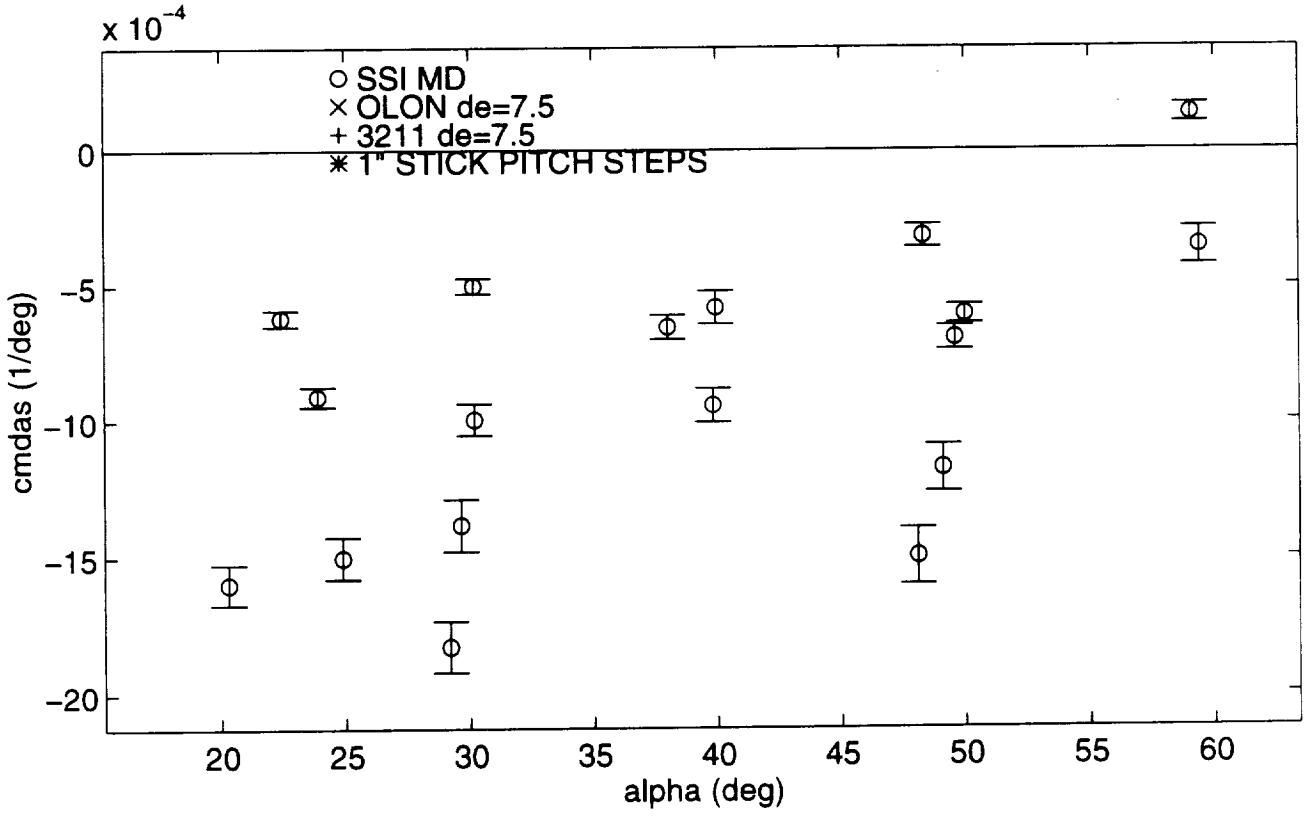
x 10^-4
SSI MD
OLON de=7.5
3211 de=7.5
1" STICK PITCH STEPS
cmdas (1/deg)
alpha (deg)

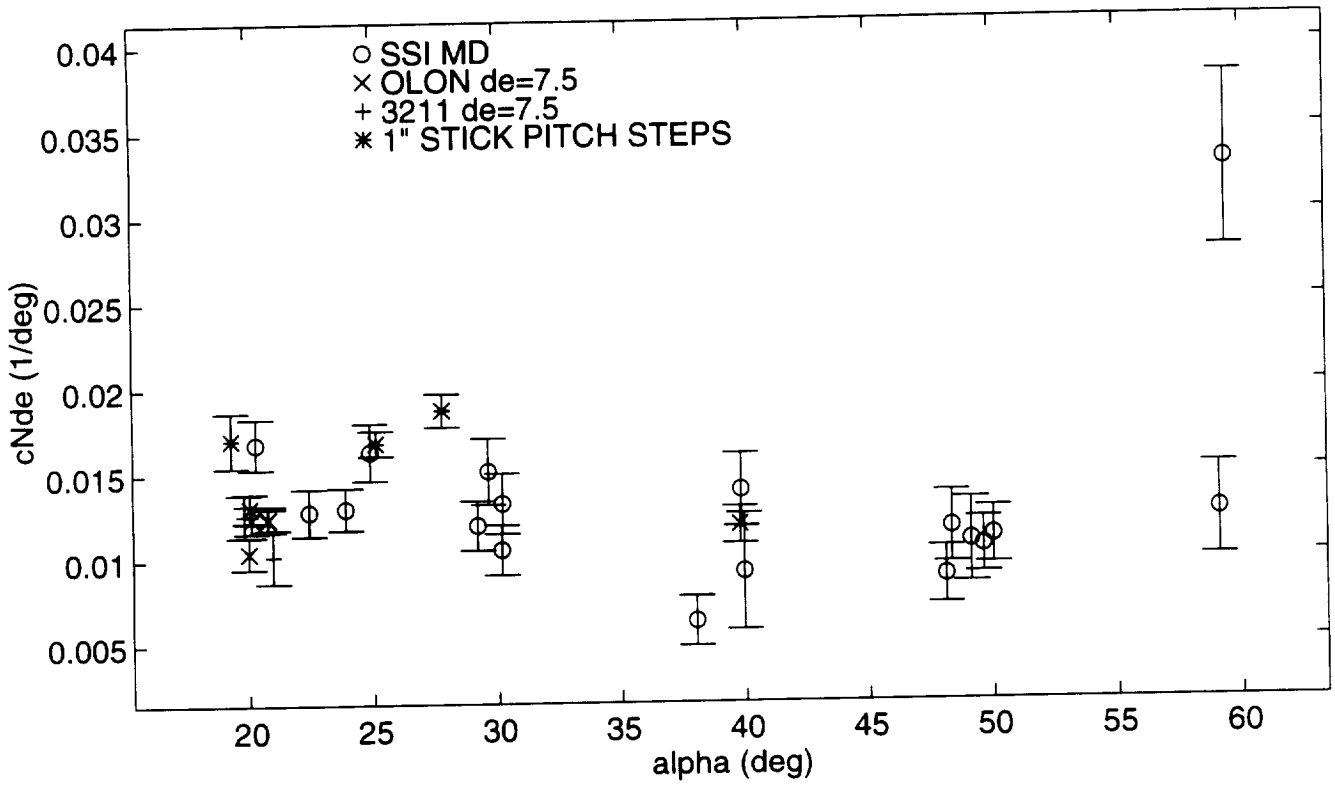
o SSI MD
× OLON de=7.5
+ 3211 de=7.5
* 1" STICK PITCH STEPS
cNde (1/deg)
alpha (deg)
0.04
0.035
0.03
0.025
0.02
0.015
0.01
0.005
20
25
30
35
40
45
50
55
60

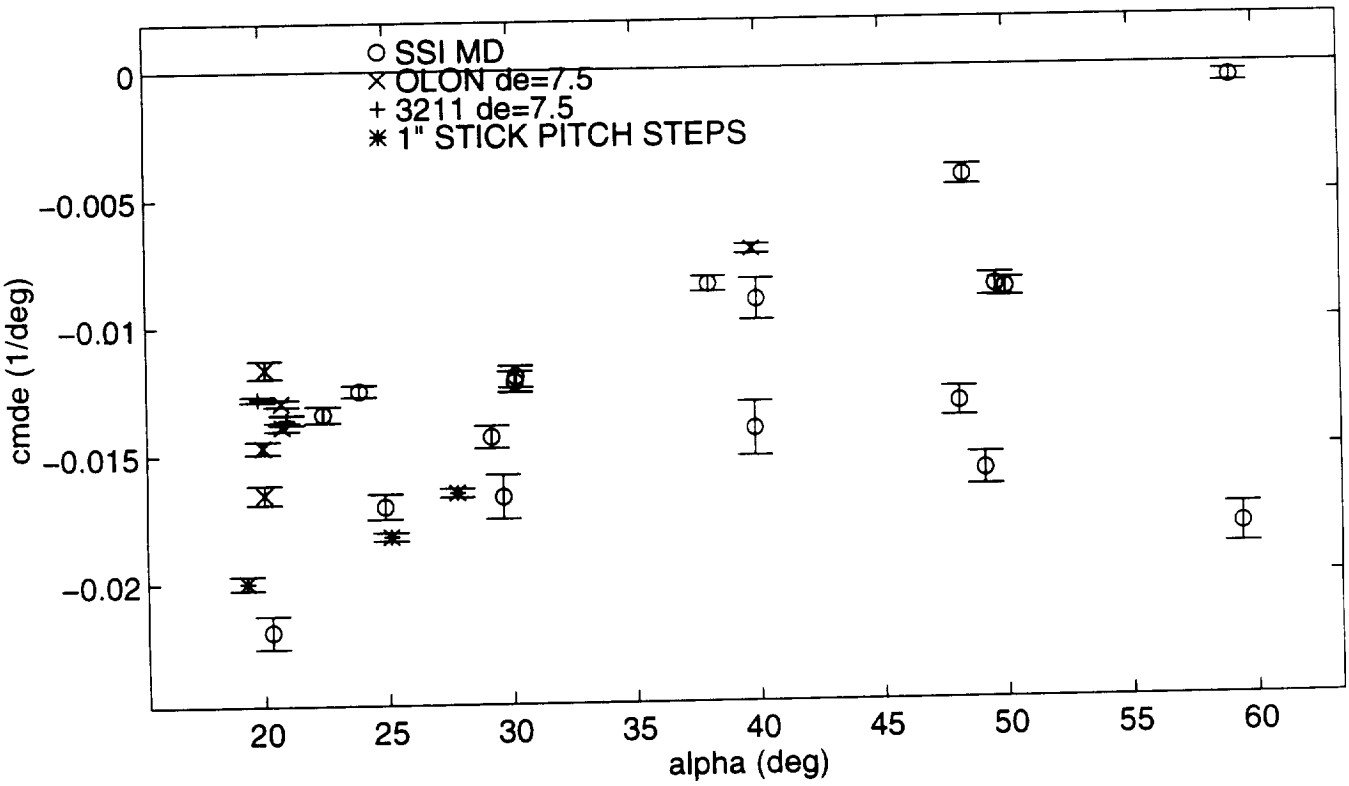
o SSI MD
× OLON de=7.5
+ 3211 de=7.5
* 1" STICK PITCH STEPS
cmde (1/deg)
alpha (deg)
0
-0.005
-0.01
-0.015
-0.02
20
25
30
35
40
45
50
55
60

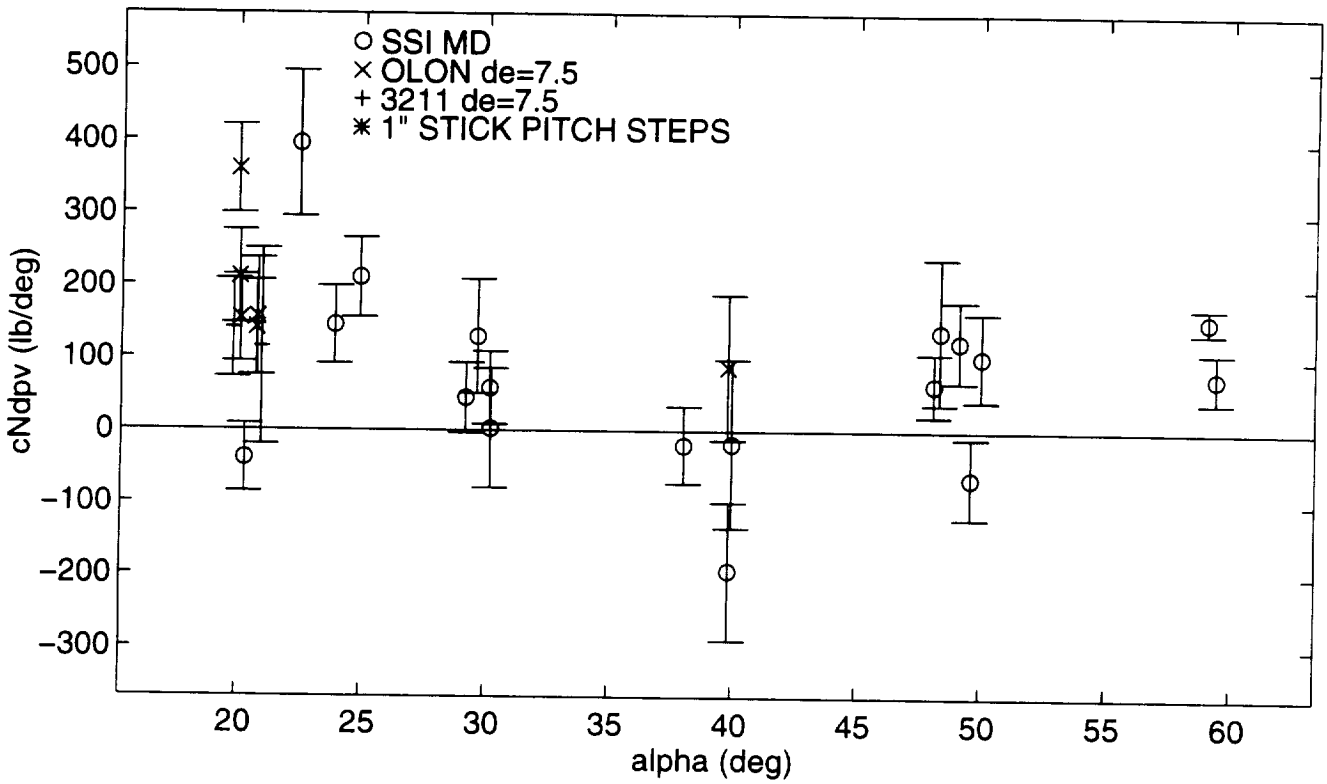
SSI MD
OLON de=7.5
3211 de=7.5
1" STICK PITCH STEPS
cNdpv (lb/deg)
alpha (deg)

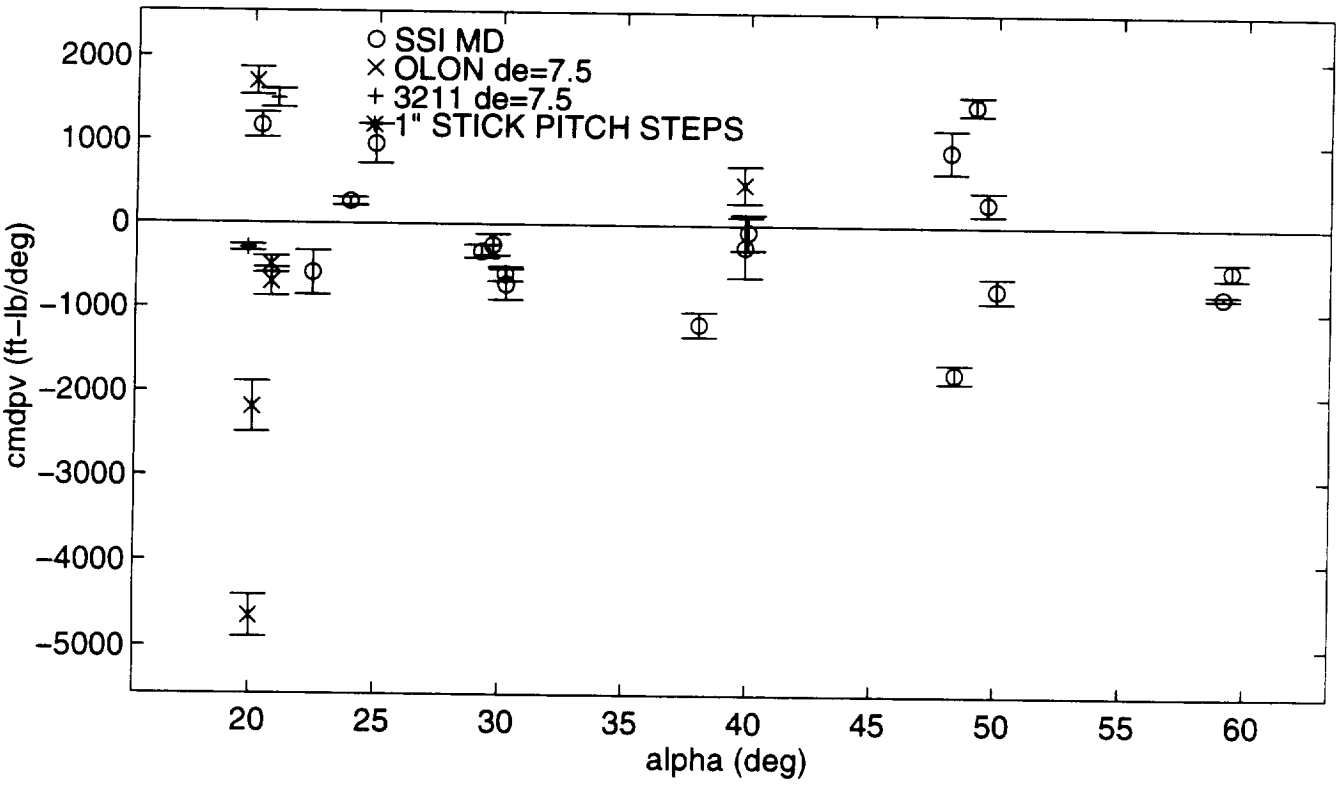
SSI MD
OLON de=7.5
3211 de=7.5
1" STICK PITCH STEPS
cmdpv (ft-lb/deg)
alpha (deg)

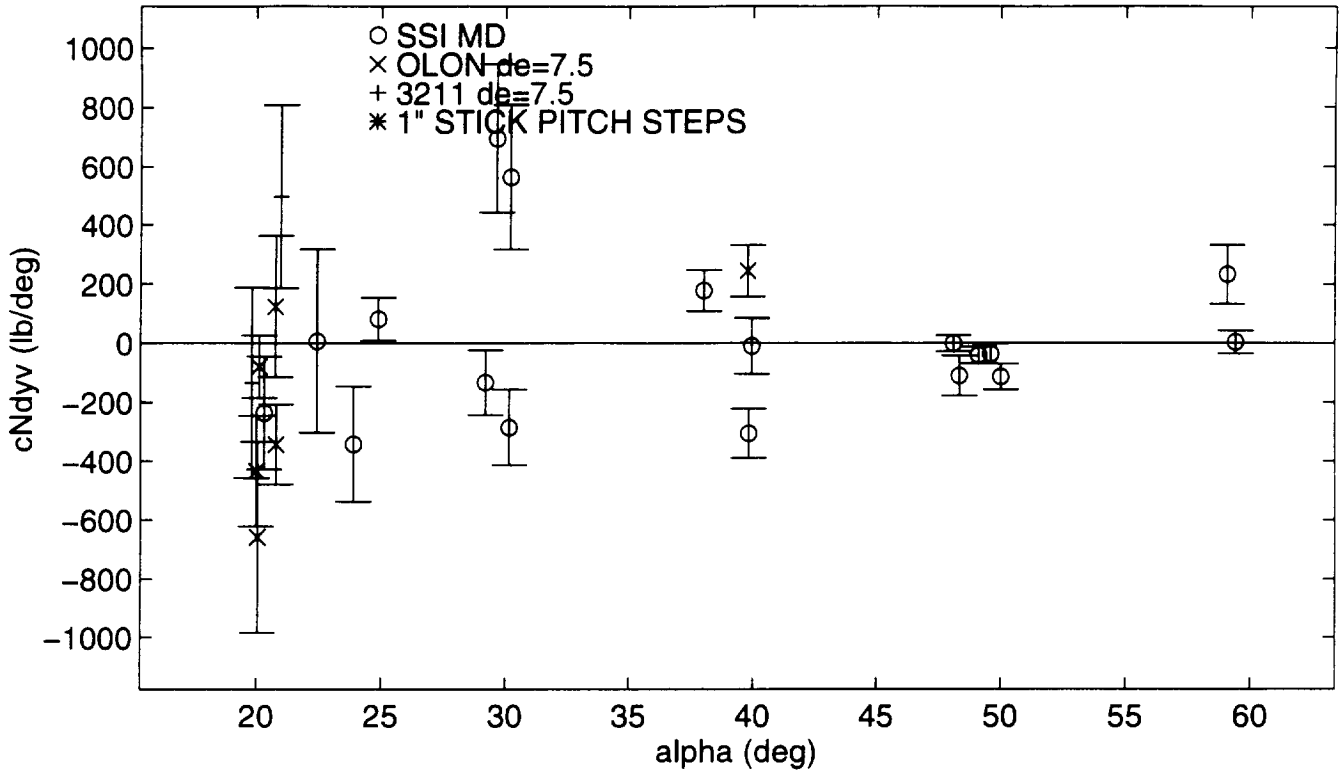
SSI MD
OLON de=7.5
3211 de=7.5
1" STICK PITCH STEPS
cNdyv (lb/deg)
alpha (deg)

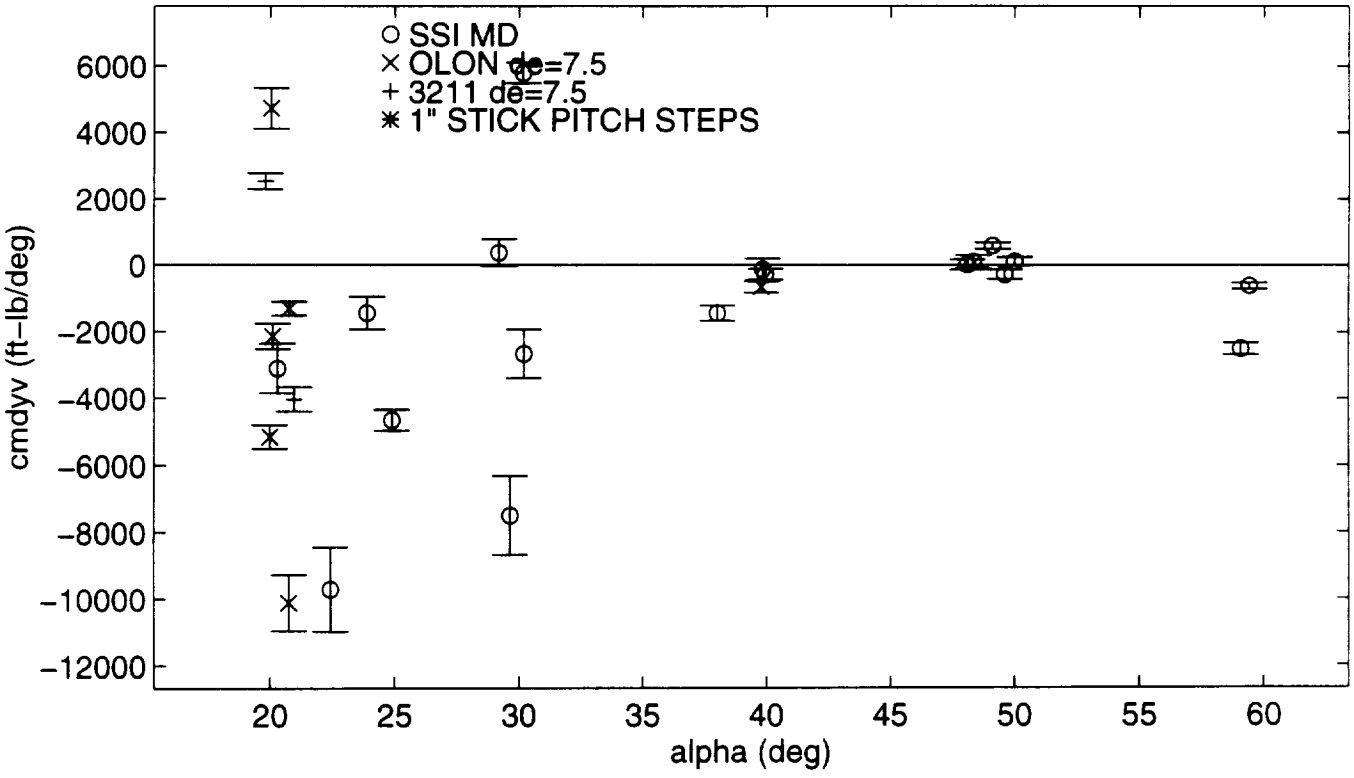
SSI MD
OLON de=7.5
3211 de=7.5
1" STICK PITCH STEPS
cmdyv (ft-lb/deg)
alpha (deg)

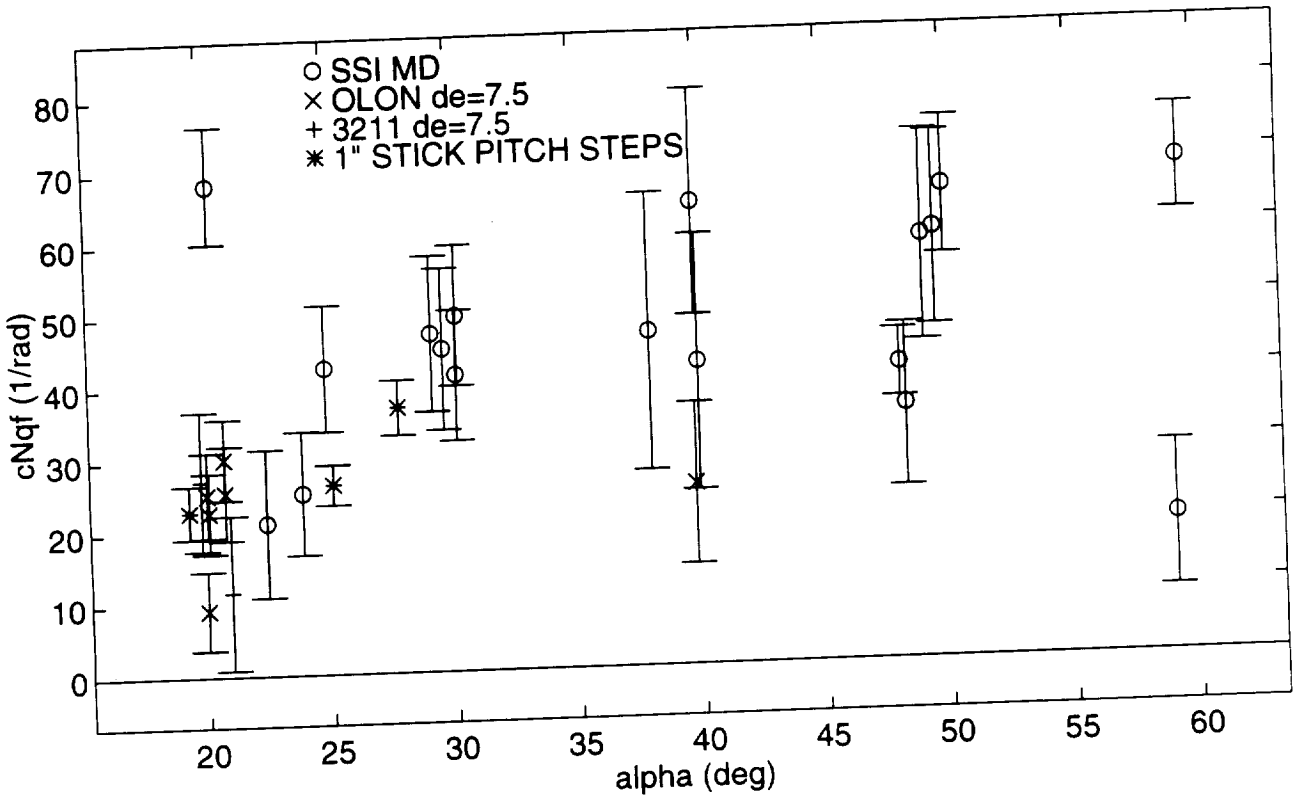
o SSI MD
× OLON de=7.5
+ 3211 de=7.5
✱ 1" STICK PITCH STEPS
cNqf (1/rad)
alpha (deg)

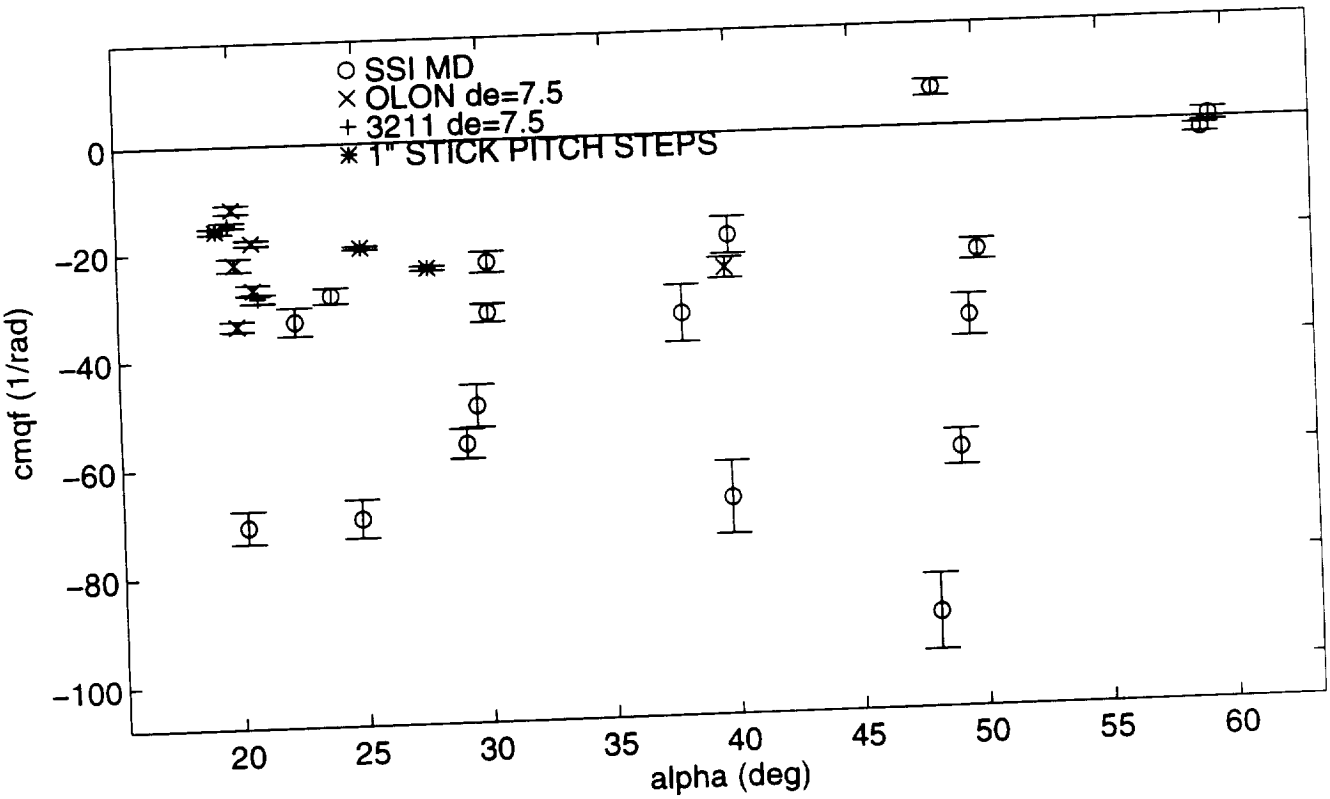
o SSI MD
× OLON de=7.5
+ 3211 de=7.5
✱ 1" STICK PITCH STEPS
cmqf (1/rad)
alpha (deg)

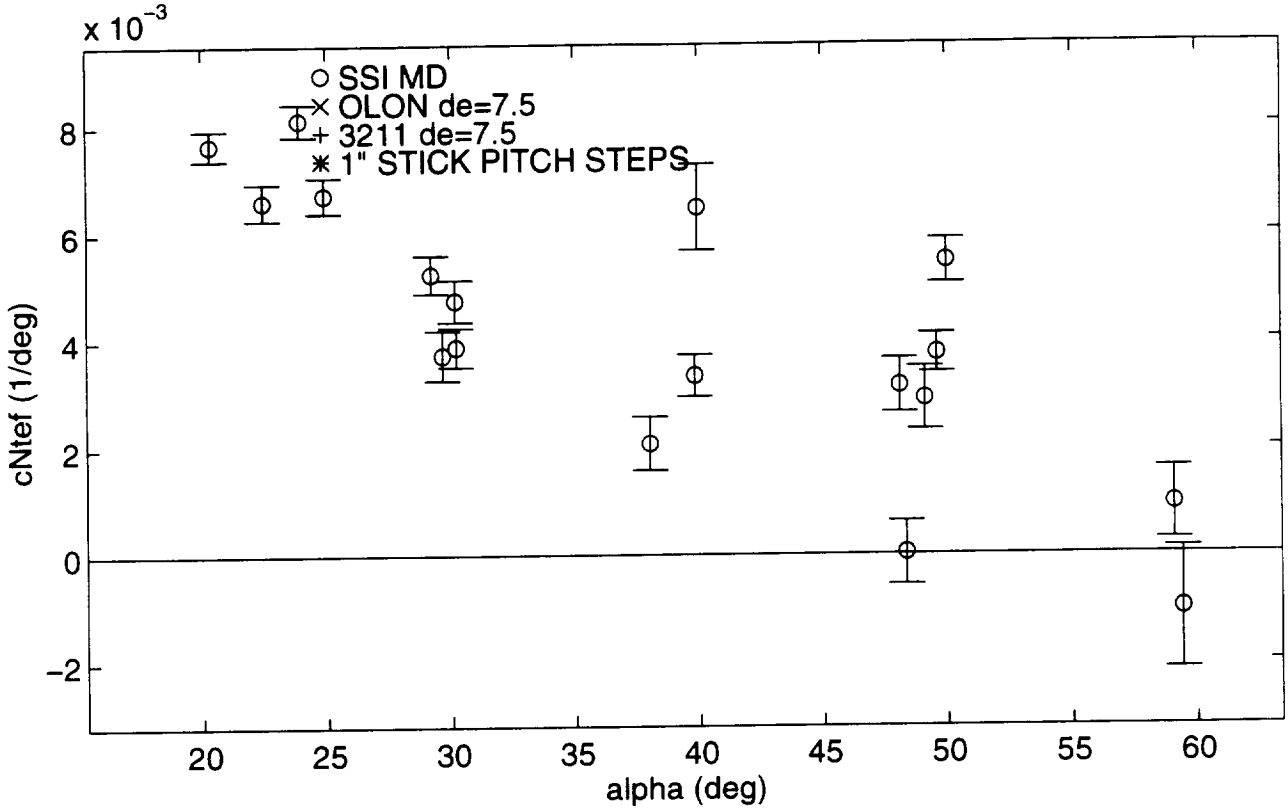
x 10^-3
SSI MD
OLON de=7.5
3211 de=7.5
1" STICK PITCH STEPS
cNtef (1/deg)
alpha (deg)

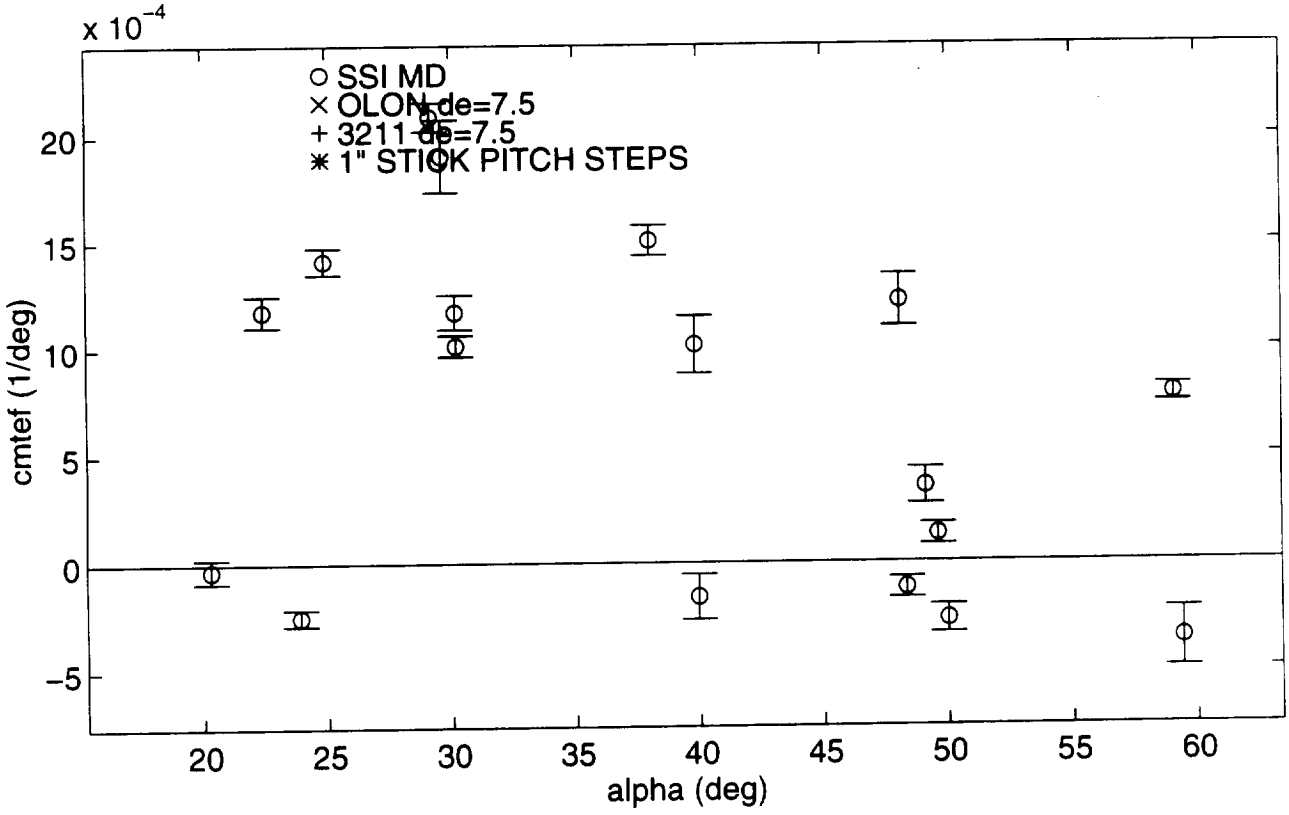
x 10^-4
SSI MD
OLON de=7.5
3211 de=7.5
1" STICK PITCH STEPS
cmtef (1/deg)
alpha (deg)

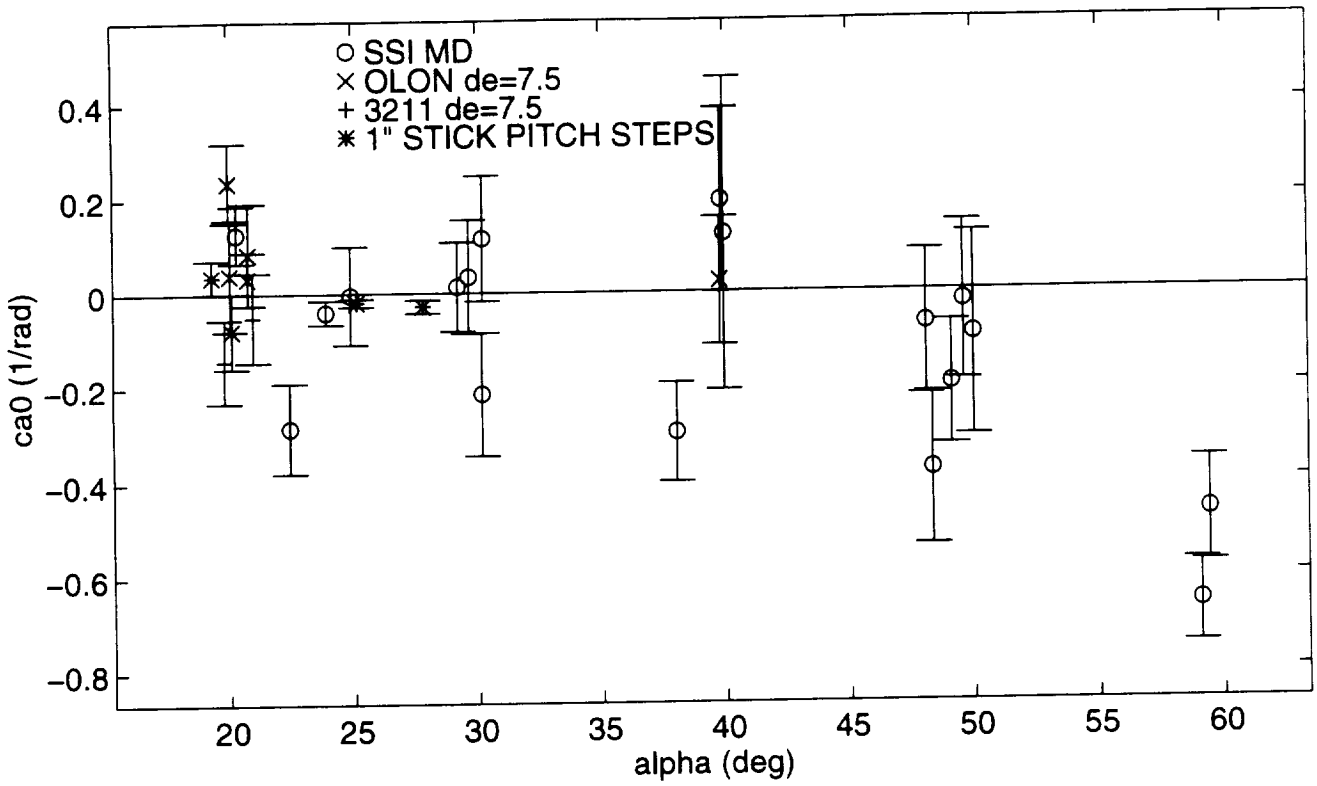
SSI MD
OLON de=7.5
3211 de=7.5
1" STICK PITCH STEPS
ca0 (1/rad)
alpha (deg)
0.4
0.2
0
−0.2
−0.4
−0.6
−0.8
20
25
30
35
40
45
50
55
60

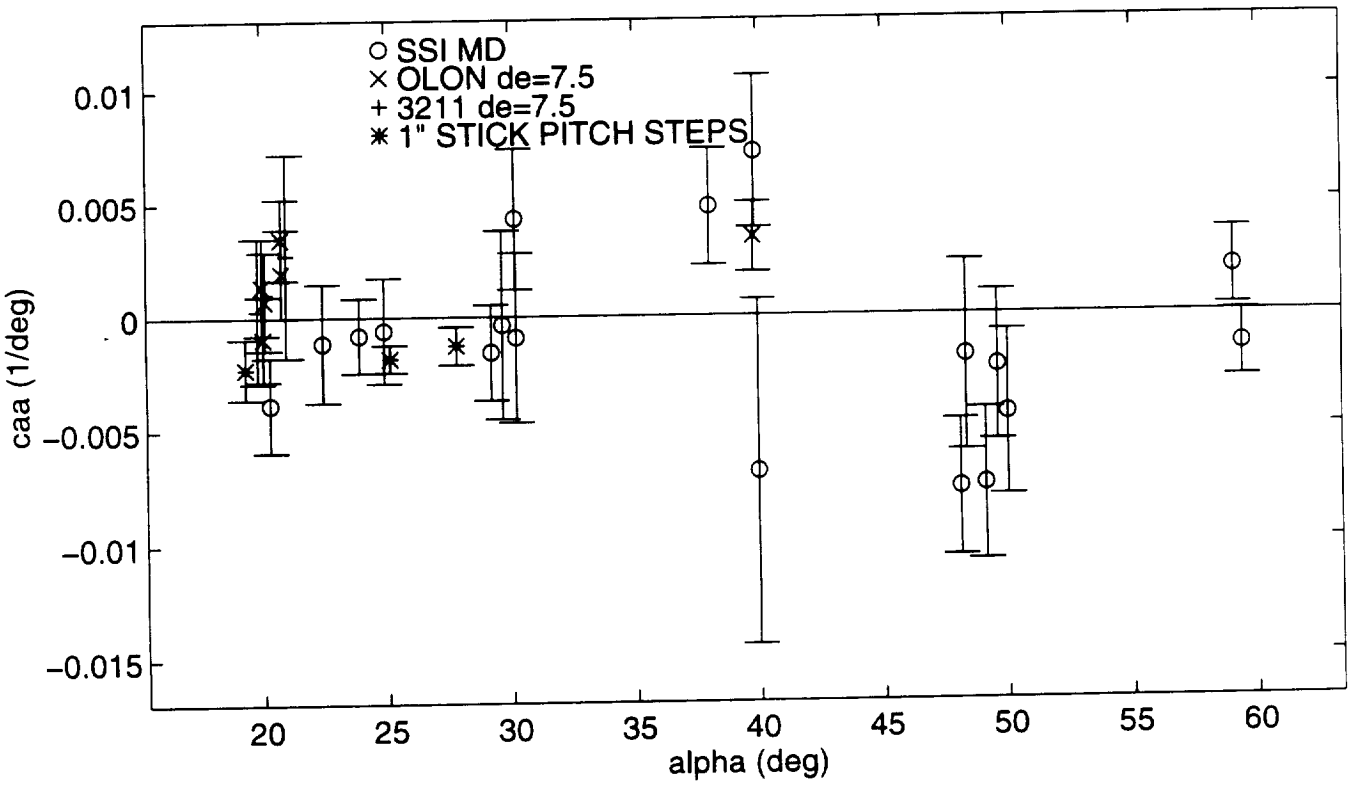
SSI MD
OLON de=7.5
3211 de=7.5
1" STICK PITCH STEPS
caa (1/deg)
alpha (deg)
0.01
0.005
0
−0.005
−0.01
−0.015
20
25
30
35
40
45
50
55
60

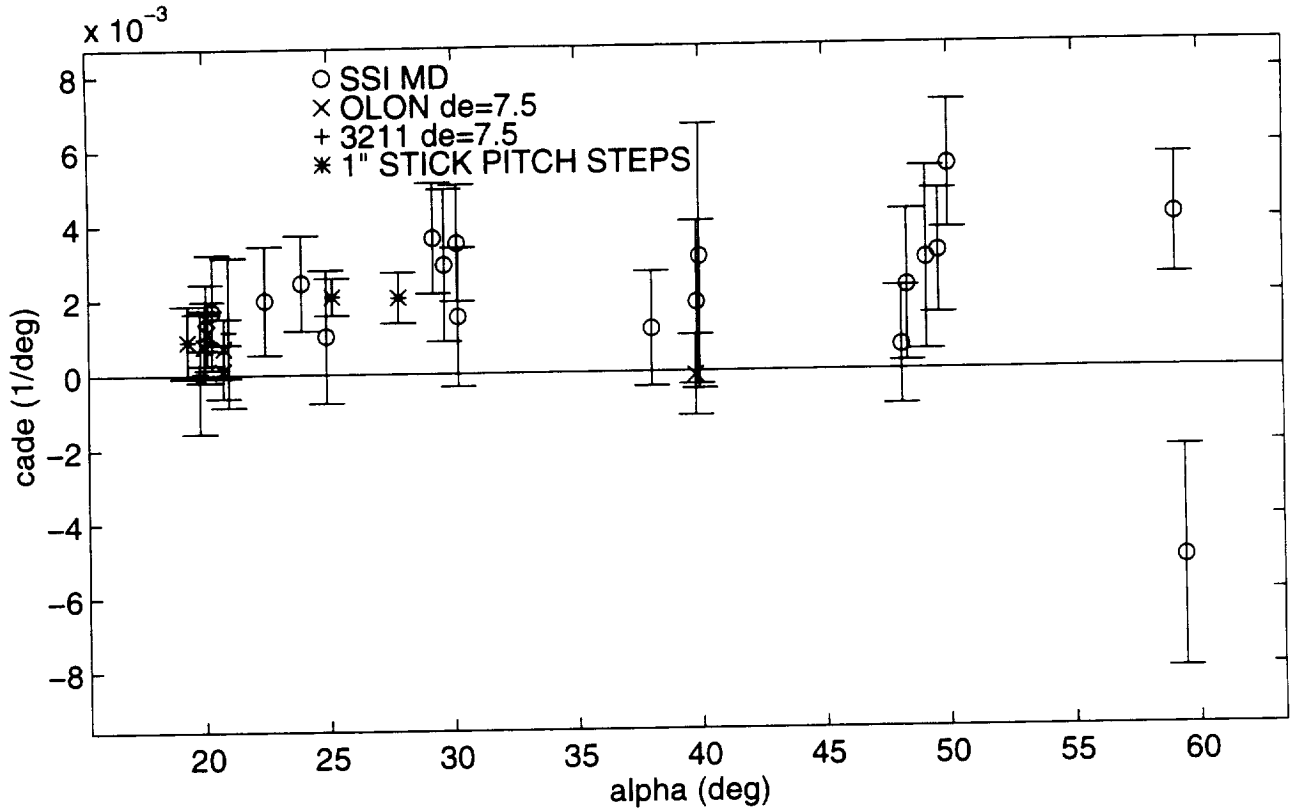
x 10^-3
SSI MD
OLON de=7.5
3211 de=7.5
1" STICK PITCH STEPS
cade (1/deg)
alpha (deg)

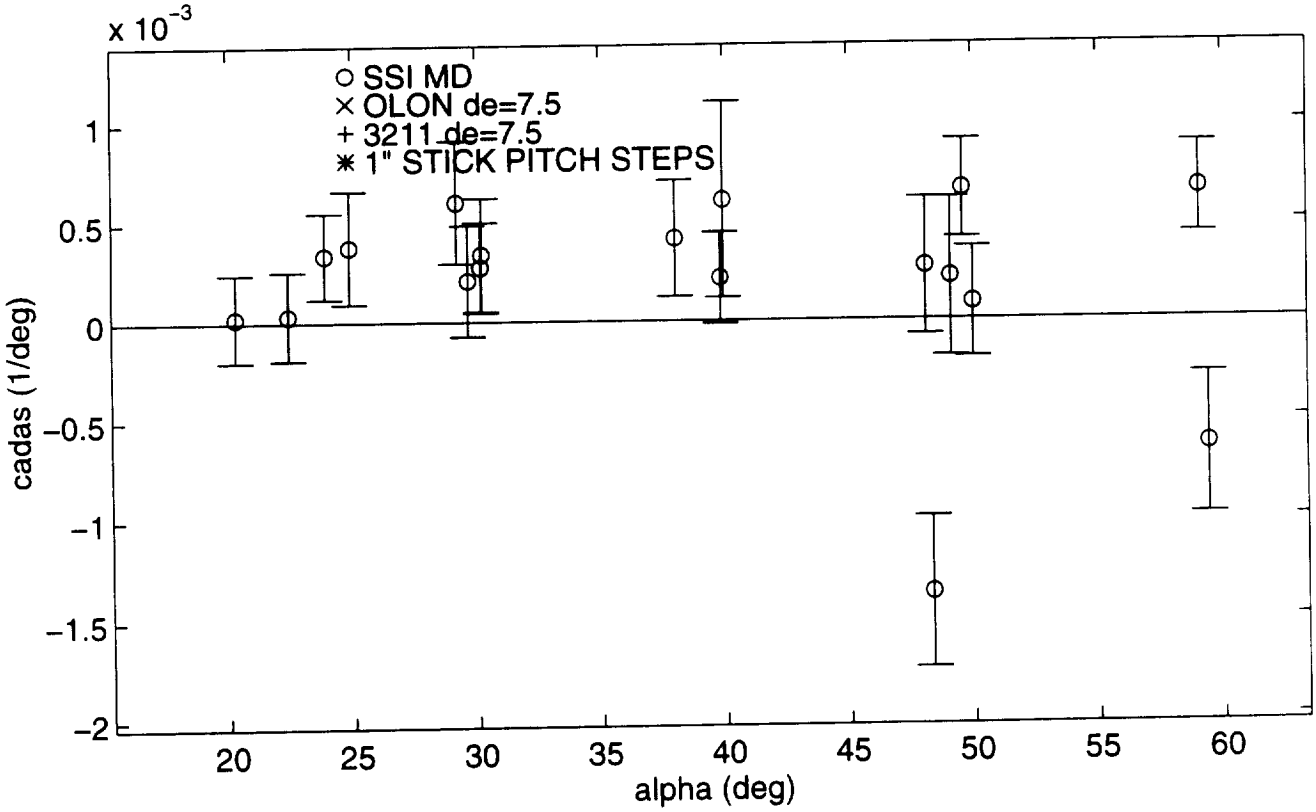
x 10^-3
SSI MD
OLON de=7.5
3211 de=7.5
1" STICK PITCH STEPS
cadas (1/deg)
alpha (deg)

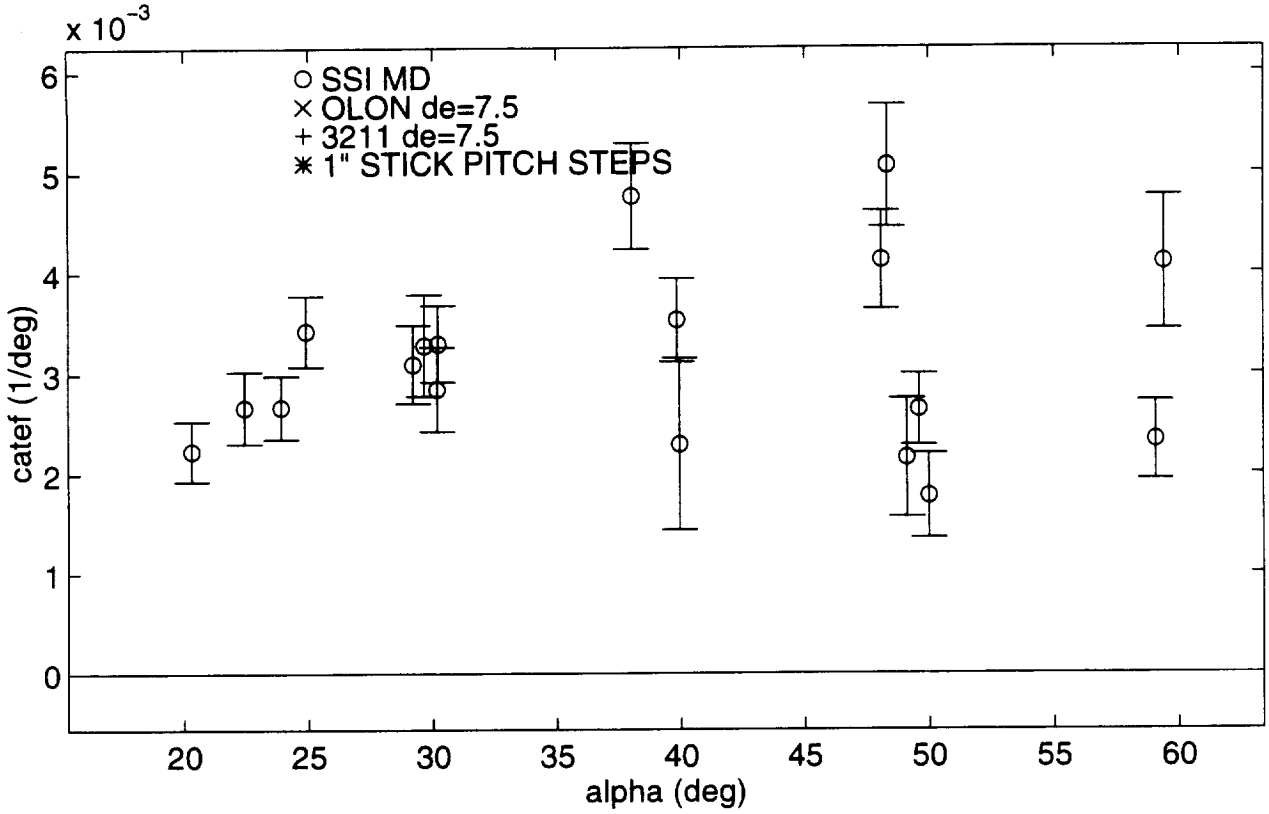
x 10^-3
SSI MD
OLON de=7.5
3211 de=7.5
1" STICK PITCH STEPS
catef (1/deg)
alpha (deg)

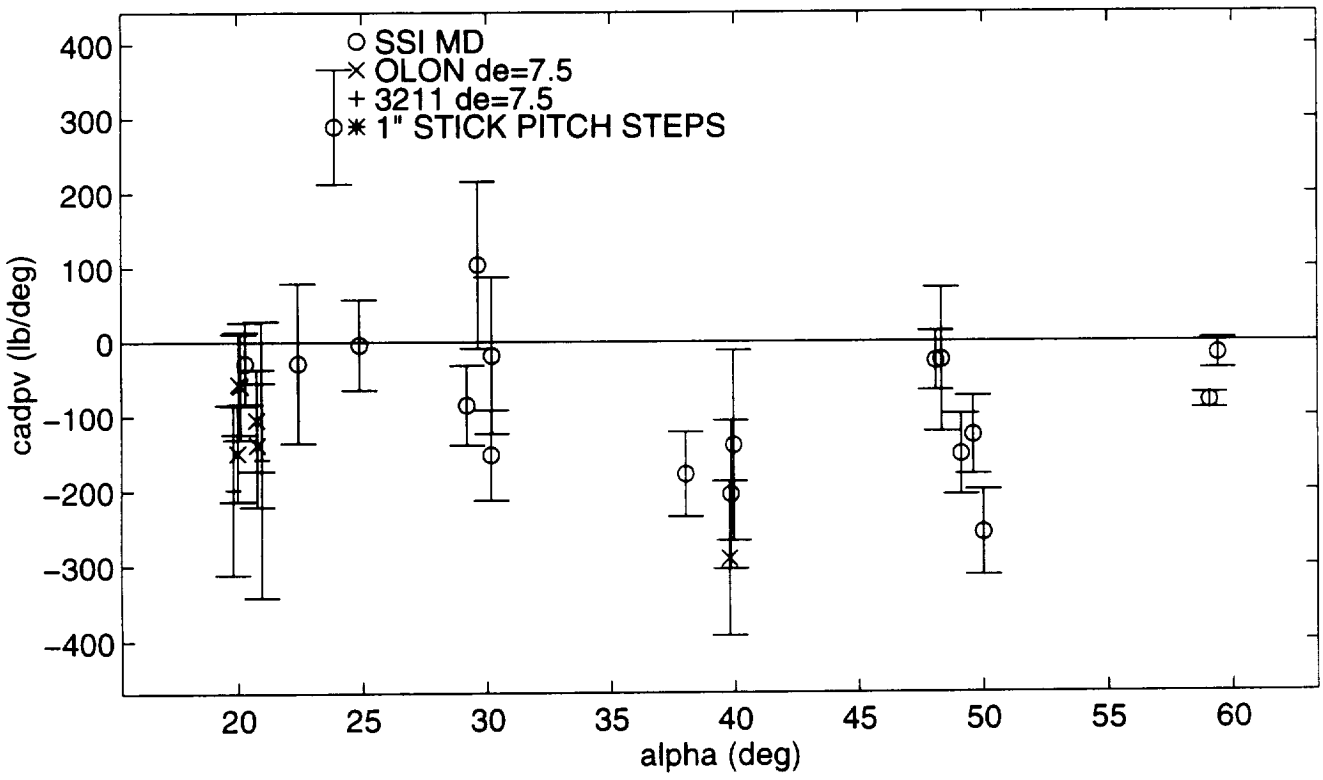
SSI MD
OLON de=7.5
3211 de=7.5
1" STICK PITCH STEPS
cadpv (lb/deg)
alpha (deg)

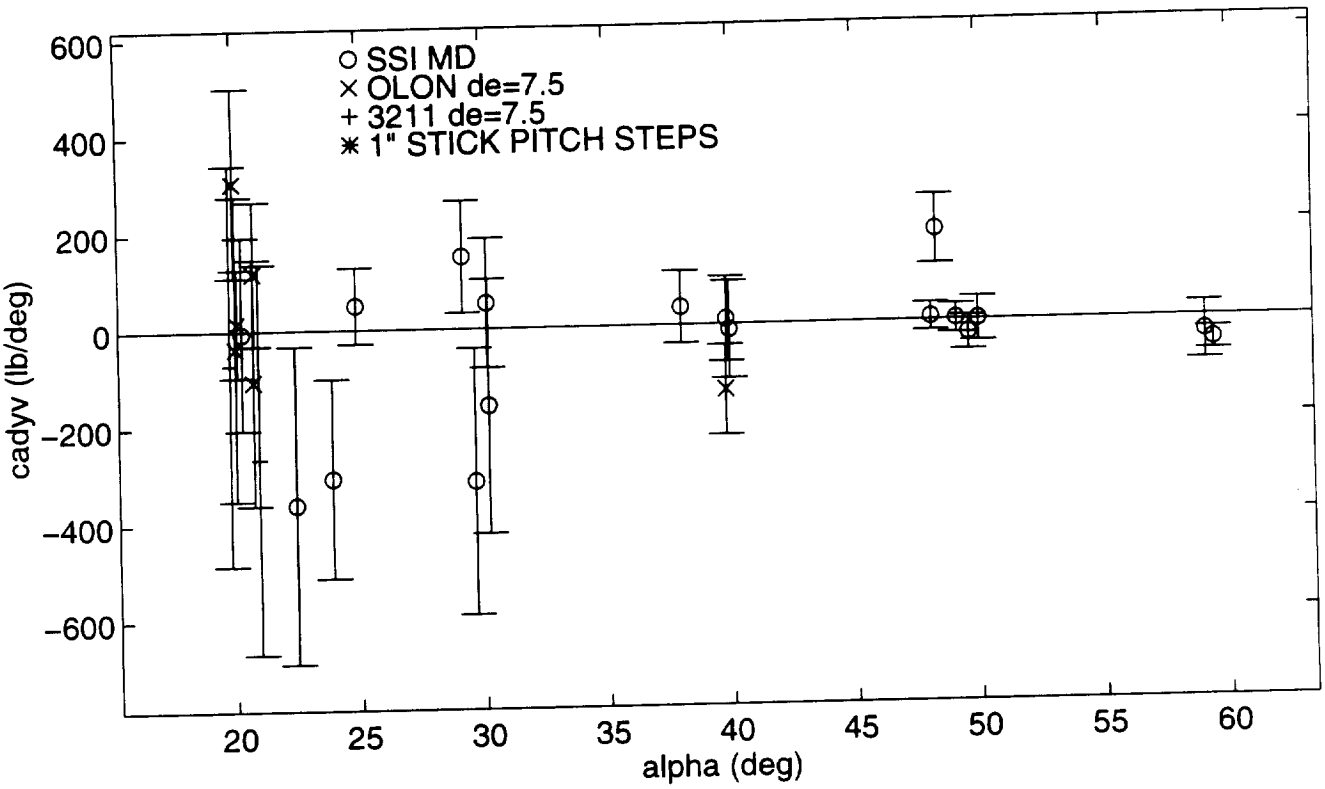
SSI MD
OLON de=7.5
3211 de=7.5
1" STICK PITCH STEPS
cadyv (lb/deg)
alpha (deg)
600
400
200
0
-200
-400
-600
20
25
30
35
40
45
50
55
60

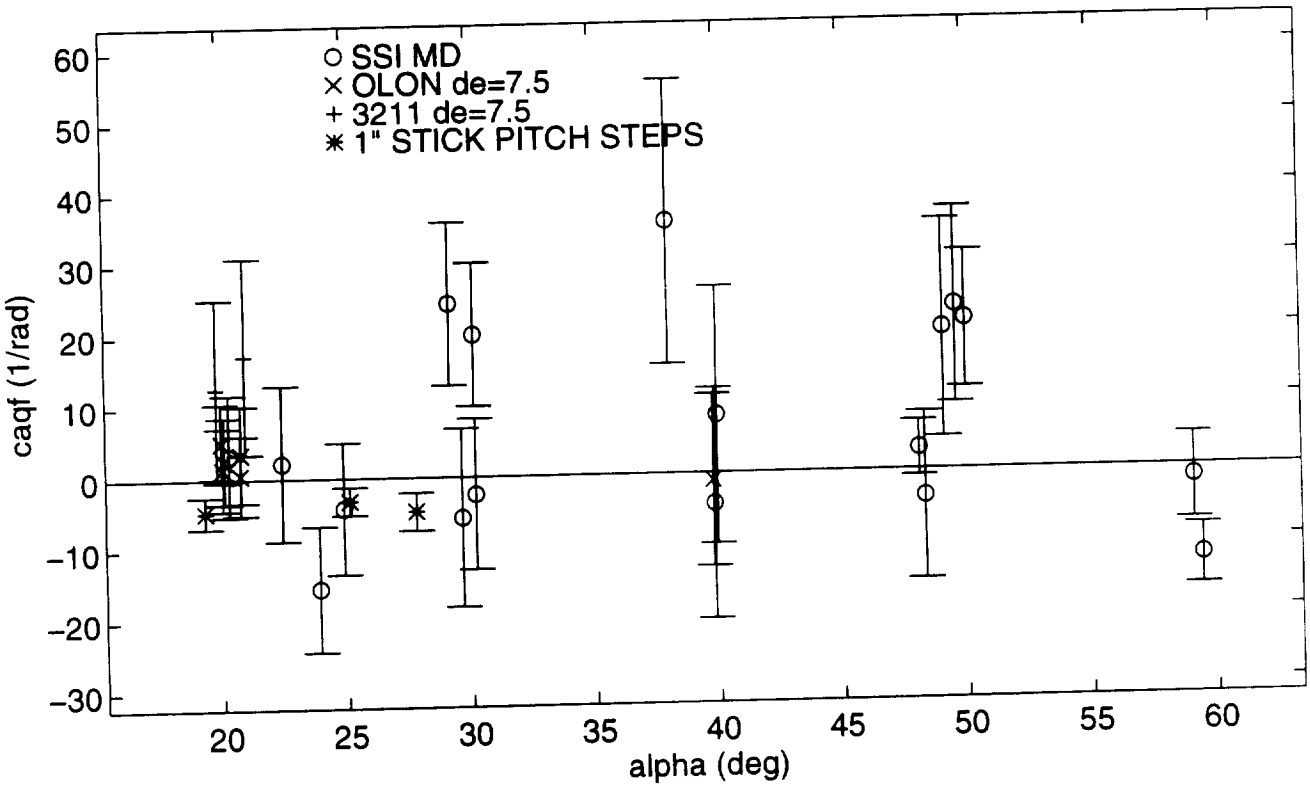
SSI MD
OLON de=7.5
3211 de=7.5
1" STICK PITCH STEPS
caqf (1/rad)
alpha (deg)
60
50
40
30
20
10
0
-10
-20
-30
20
25
30
35
40
45
50
55
60

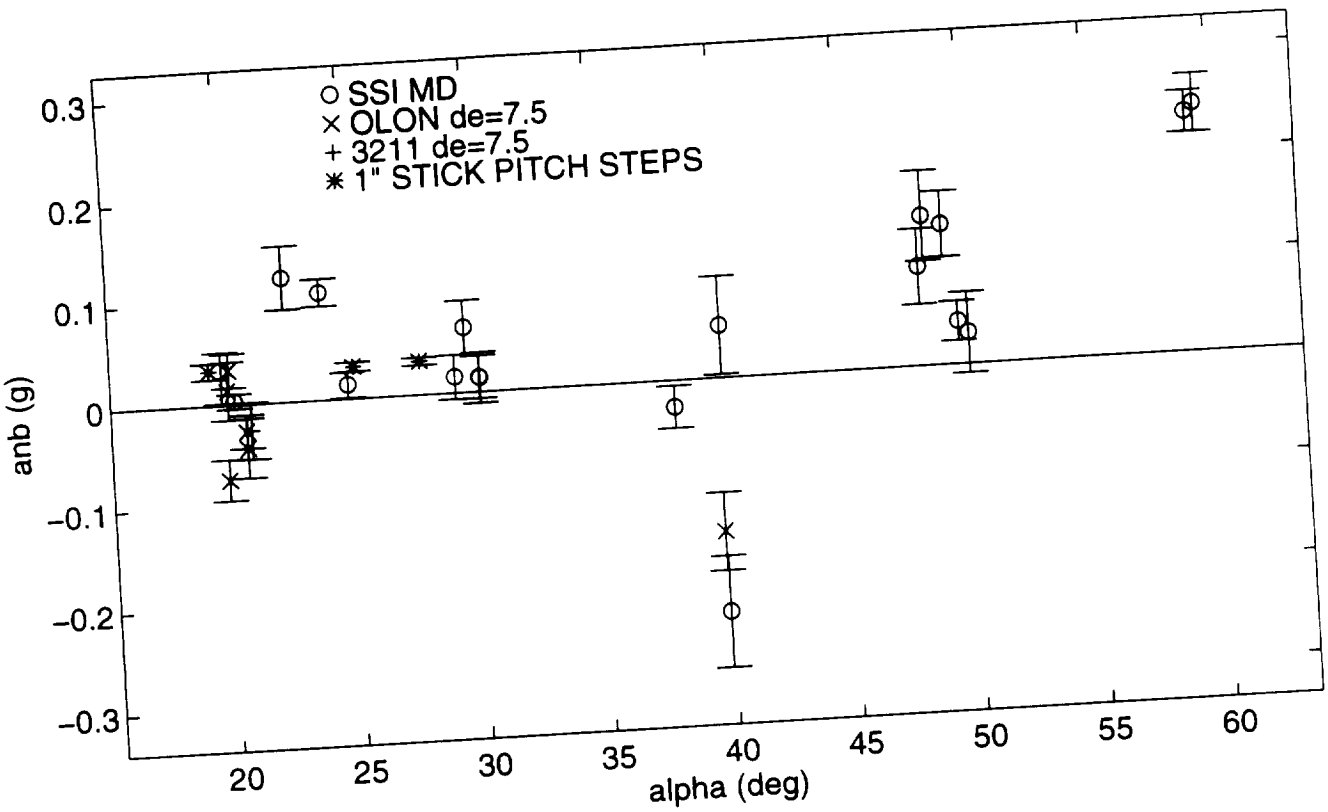
SSI MD
OLON de=7.5
3211 de=7.5
1" STICK PITCH STEPS
anb (g)
alpha (deg)
0.3
0.2
0.1
0
−0.1
−0.2
−0.3
20
25
30
35
40
45
50
55
60

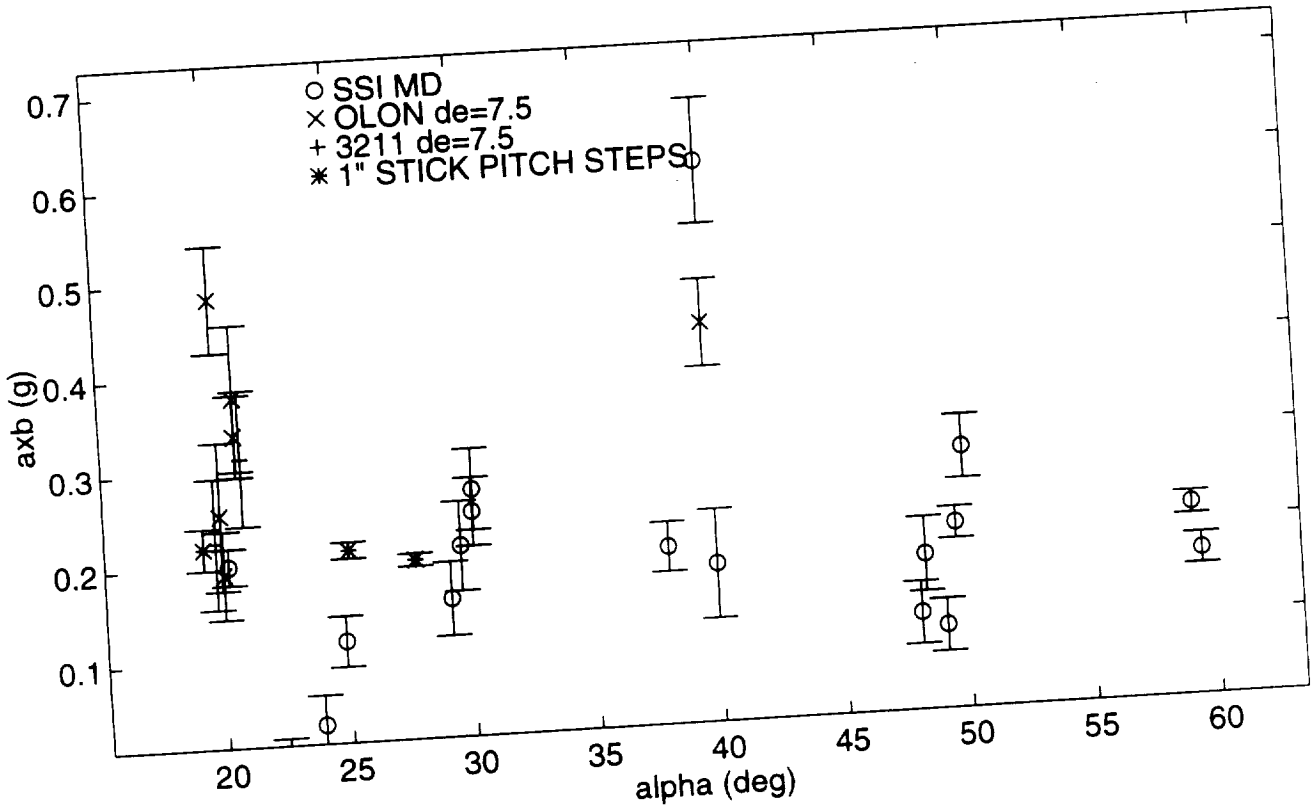
SSI MD
OLON de=7.5
3211 de=7.5
1" STICK PITCH STEPS
axb (g)
alpha (deg)
0.7
0.6
0.5
0.4
0.3
0.2
0.1
20
25
30
35
40
45
50
55
60

LONGITUDINAL SINGLE SURFACE MULTIPLE DOUBLET FOR ALPHA OF 20 DEGREES

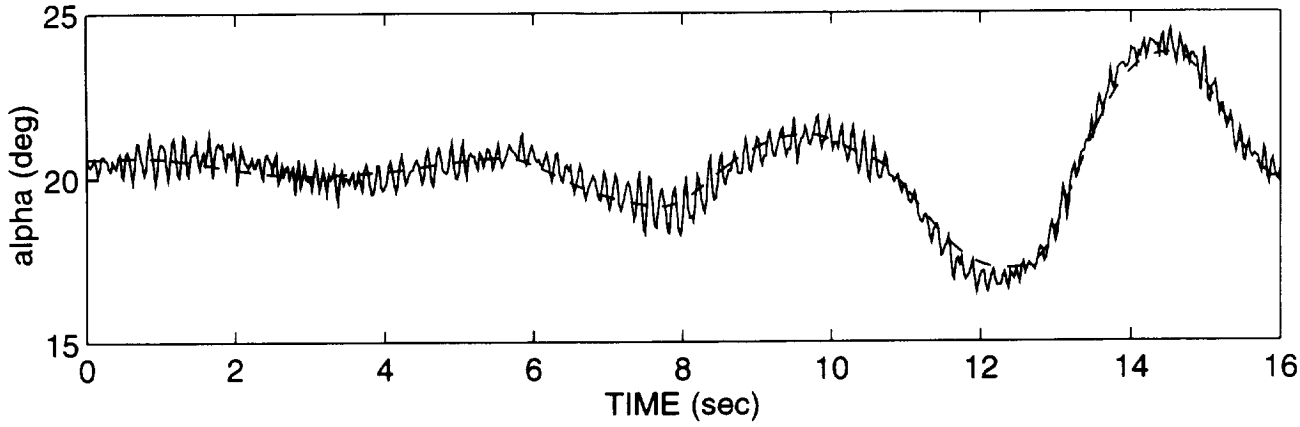

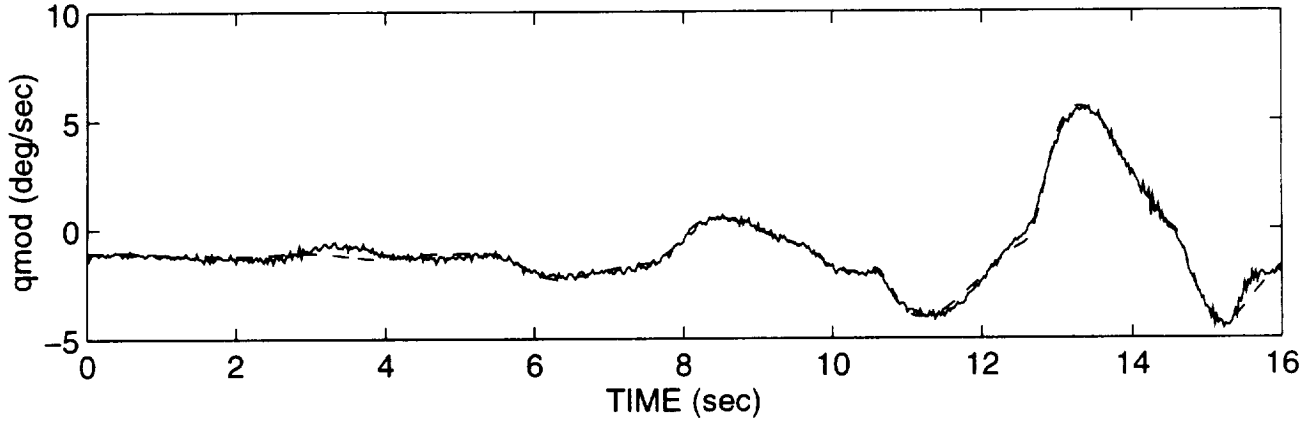

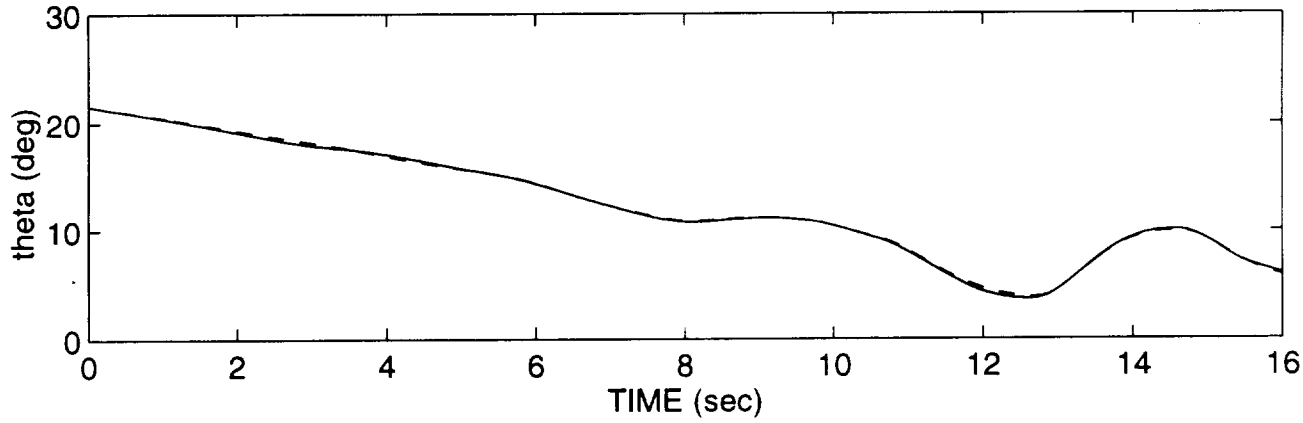

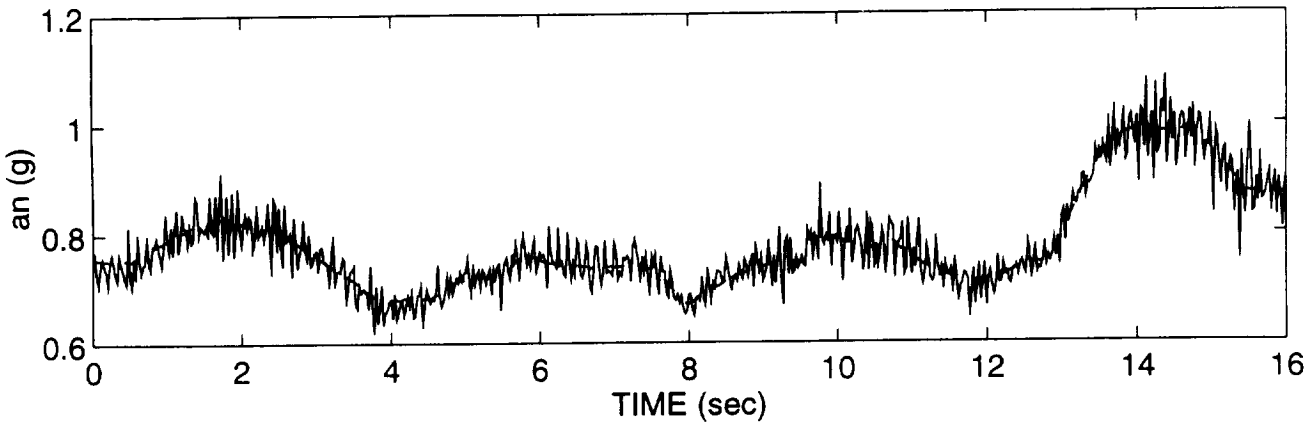
1.2
1
0.8
0.6
an (g)
0
2
4
6
8
10
12
14
16
TIME (sec)

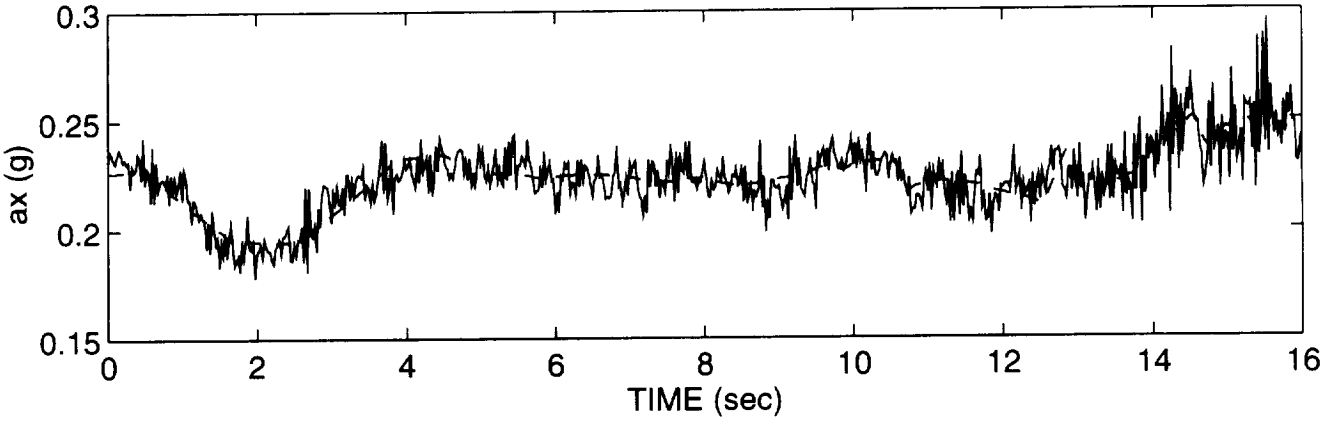
0.3
0.25
0.2
0.15
ax (g)
0
2
4
6
8
10
12
14
16
TIME (sec)

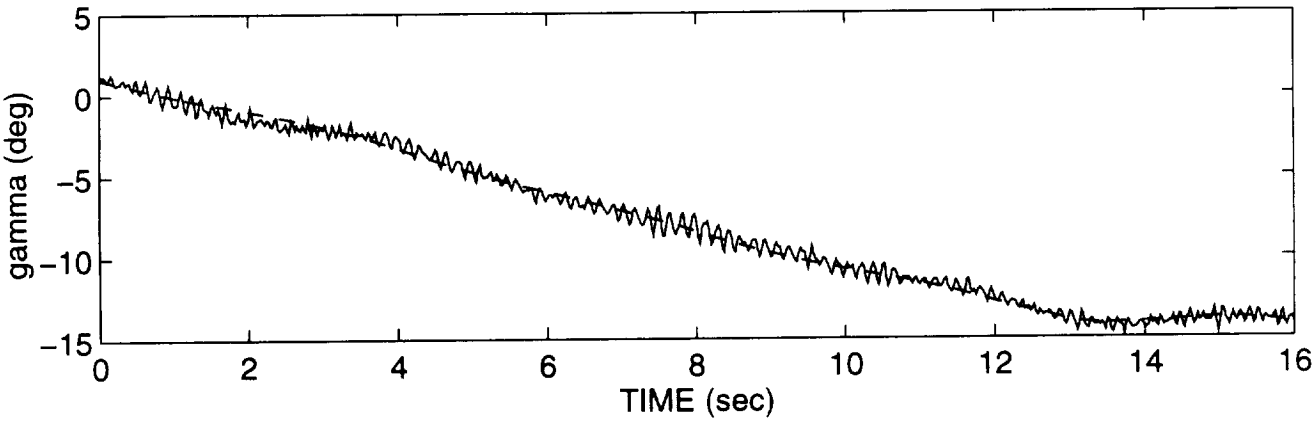
5
0
−5
−10
−15
gamma (deg)
0
2
4
6
8
10
12
14
16
TIME (sec)

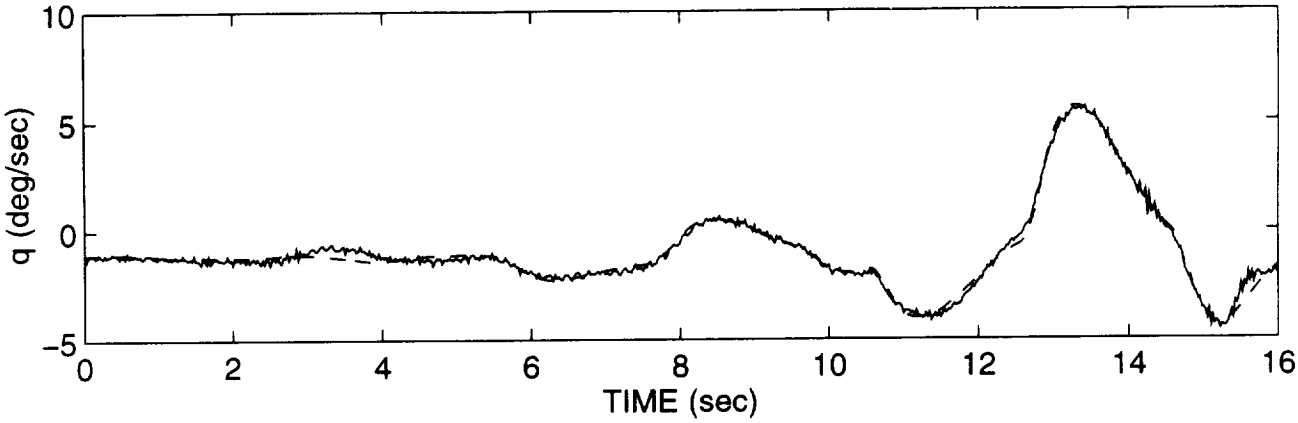
10
5
0
−5
q (deg/sec)
0
2
4
6
8
10
12
14
16
TIME (sec)

LONGITUDINAL SINGLE SURFACE MULTIPLE DOUBLET FOR ALPHA OF 30 DEGREES

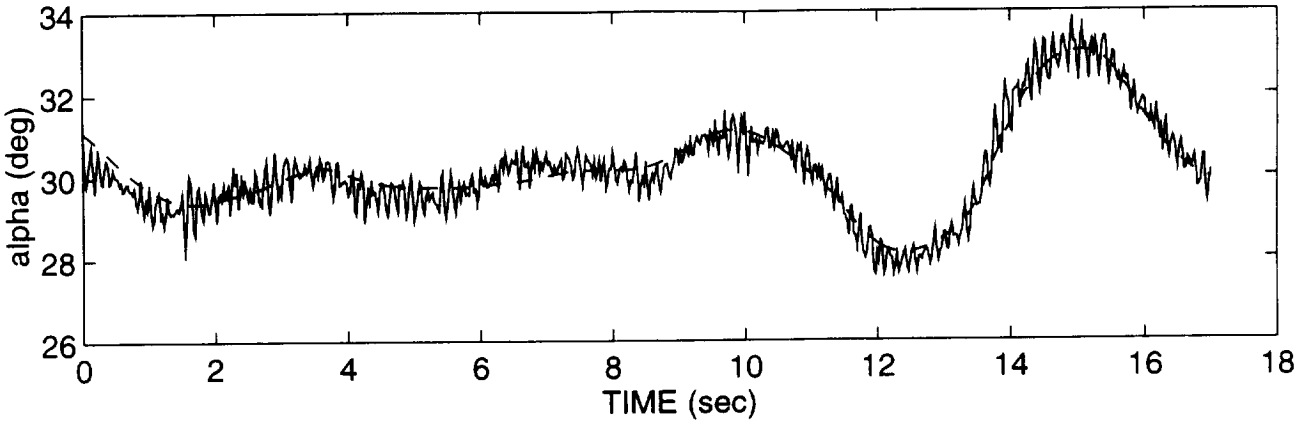

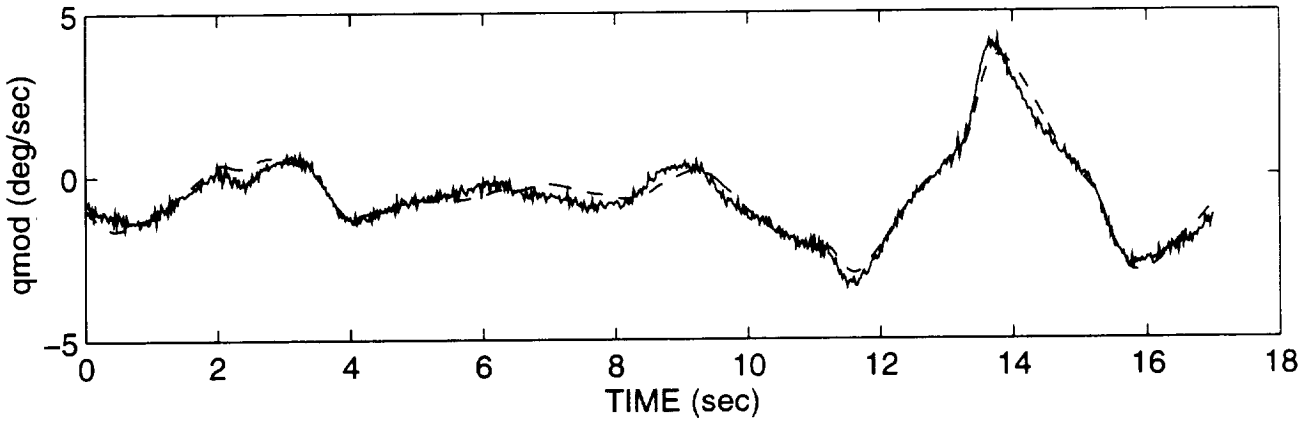

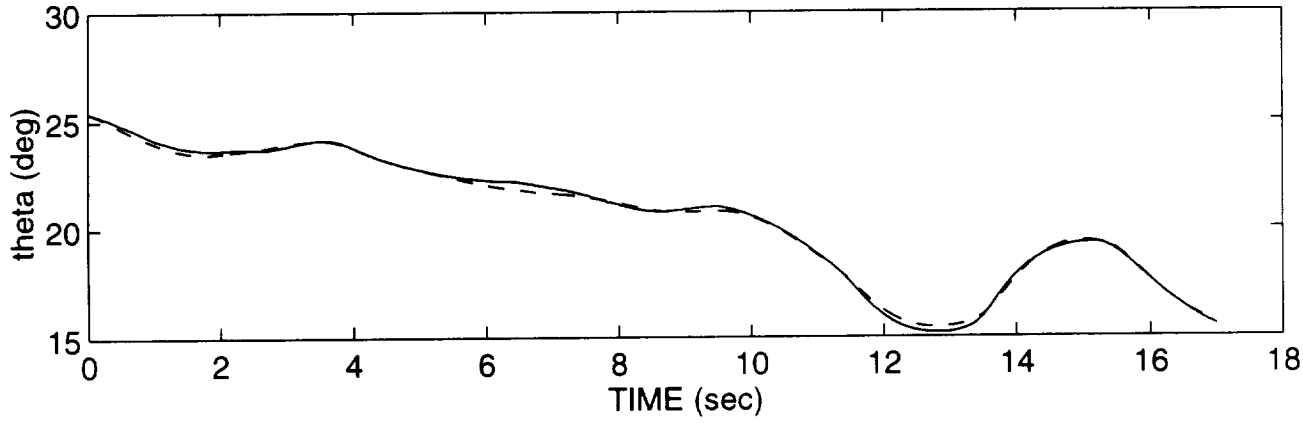

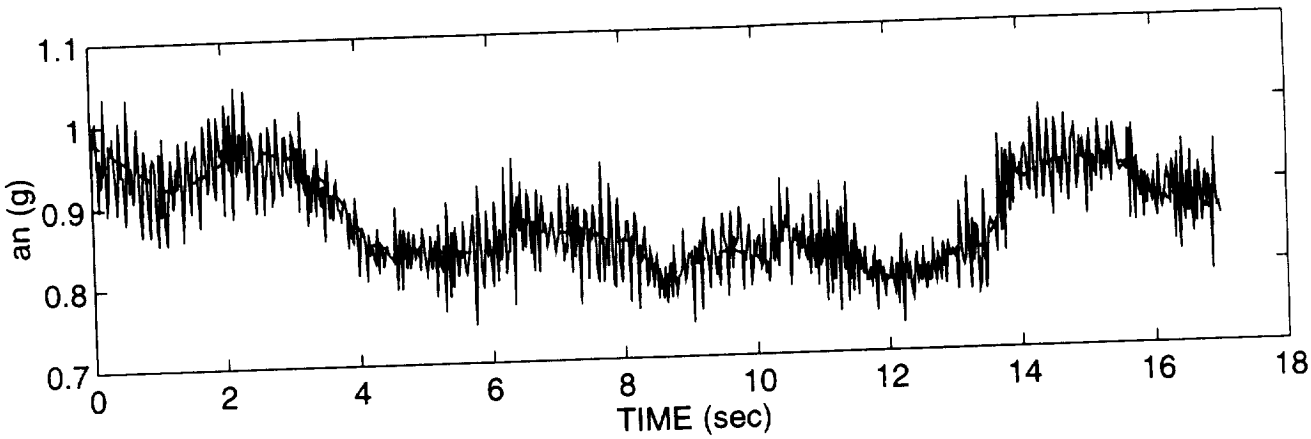
1.1
1
0.9
0.8
0.7
an (g)
0
2
4
6
8
10
12
14
16
18
TIME (sec)

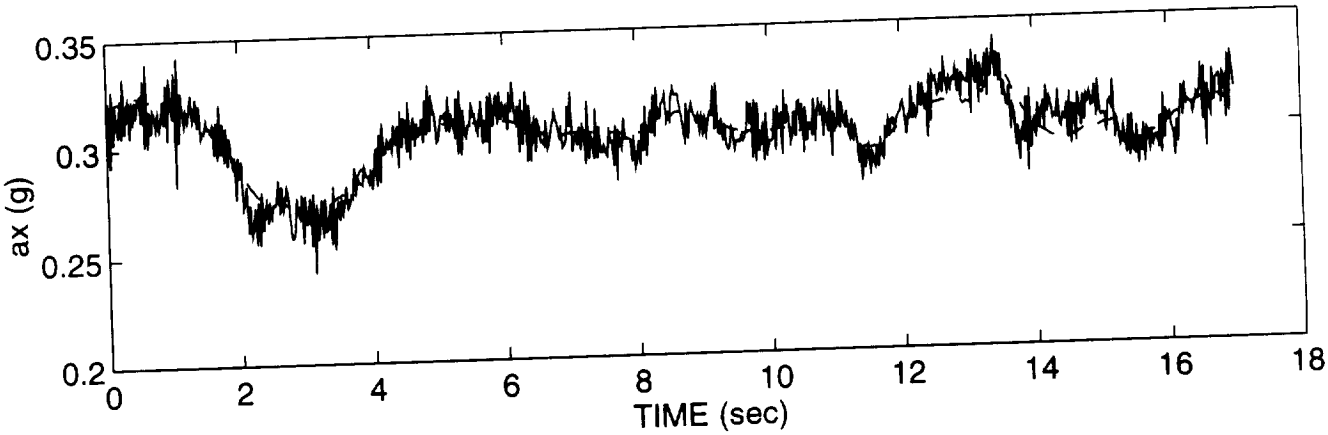
0.35
0.3
0.25
0.2
ax (g)
0
2
4
6
8
10
12
14
16
18
TIME (sec)

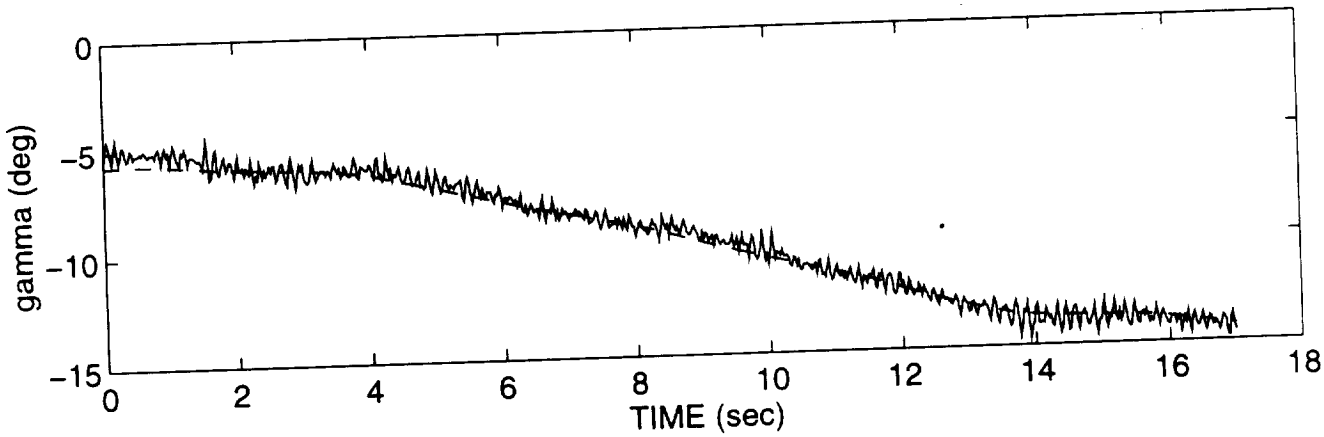
0
−5
−10
−15
gamma (deg)
0
2
4
6
8
10
12
14
16
18
TIME (sec)

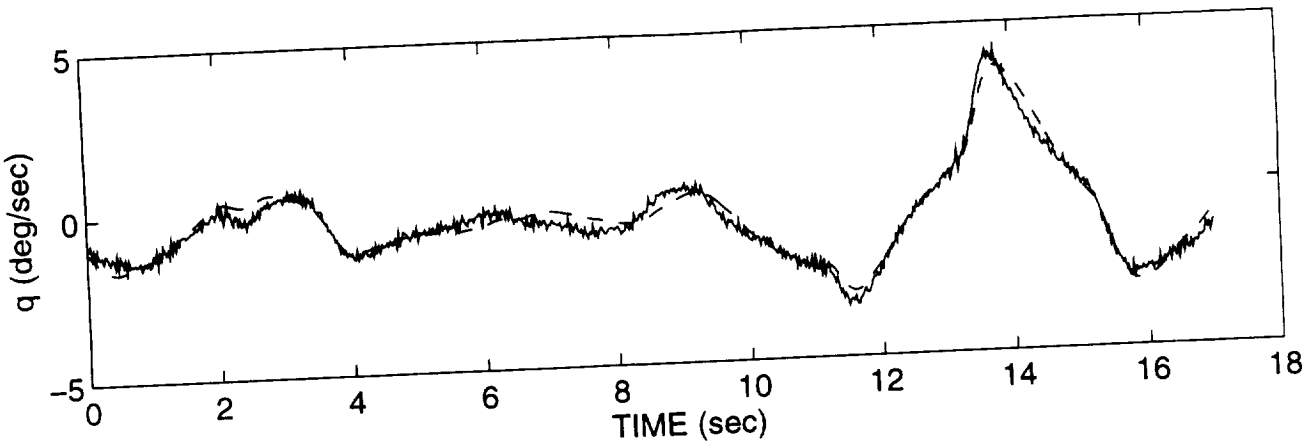
5
0
−5
q (deg/sec)
0
2
4
6
8
10
12
14
16
18
TIME (sec)

LONGITUDINAL SINGLE SURFACE MULTIPLE DOUBLET FOR ALPHA OF 40 DEGREES

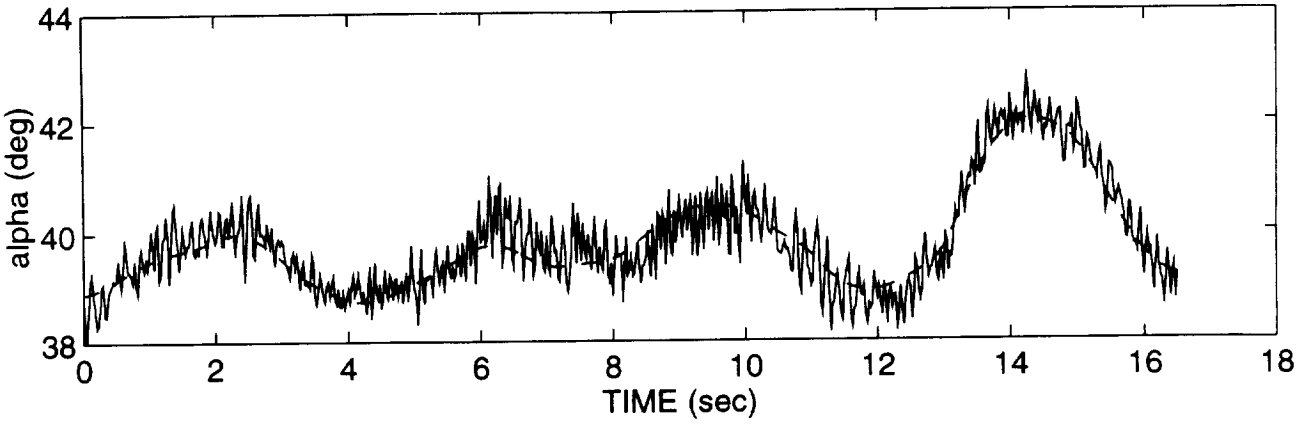

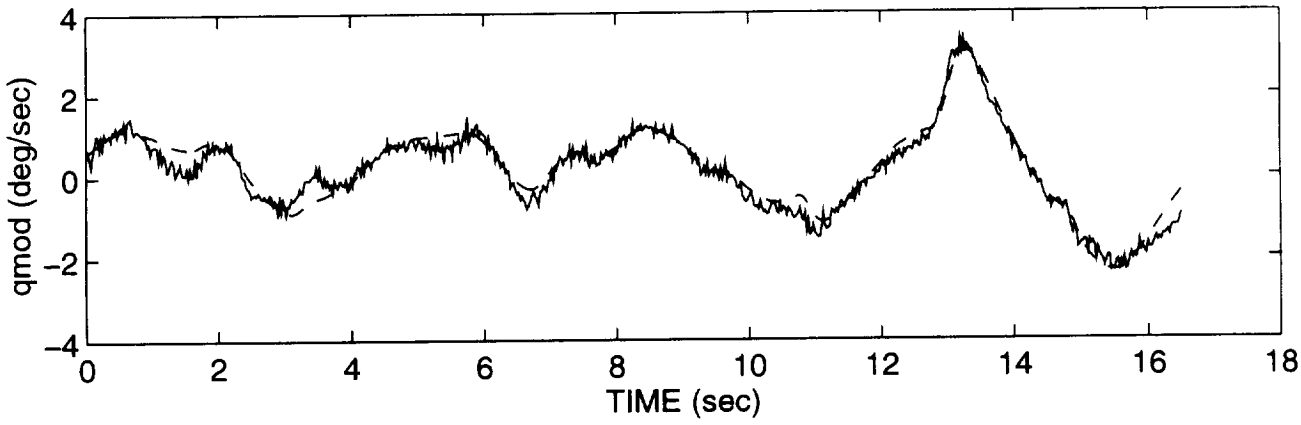

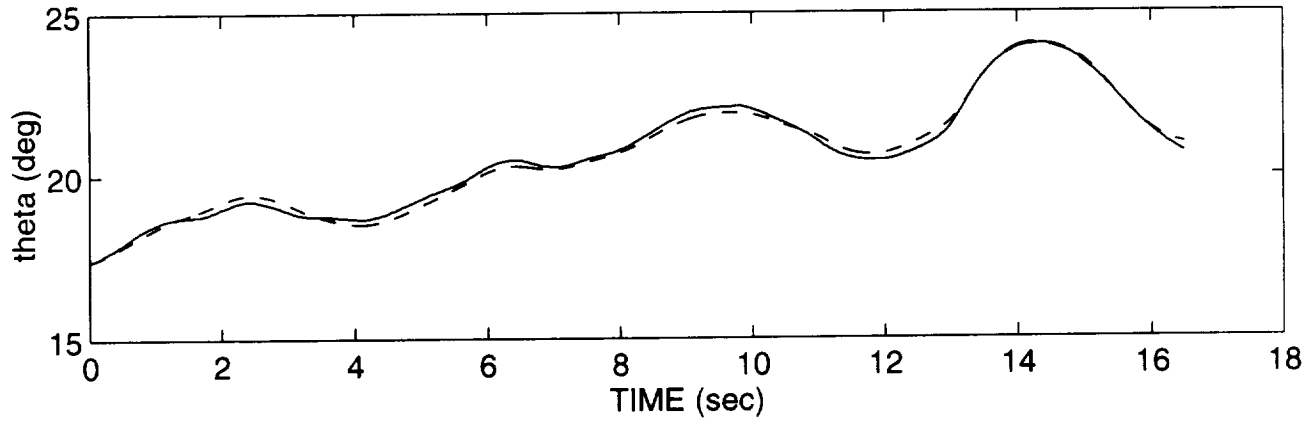

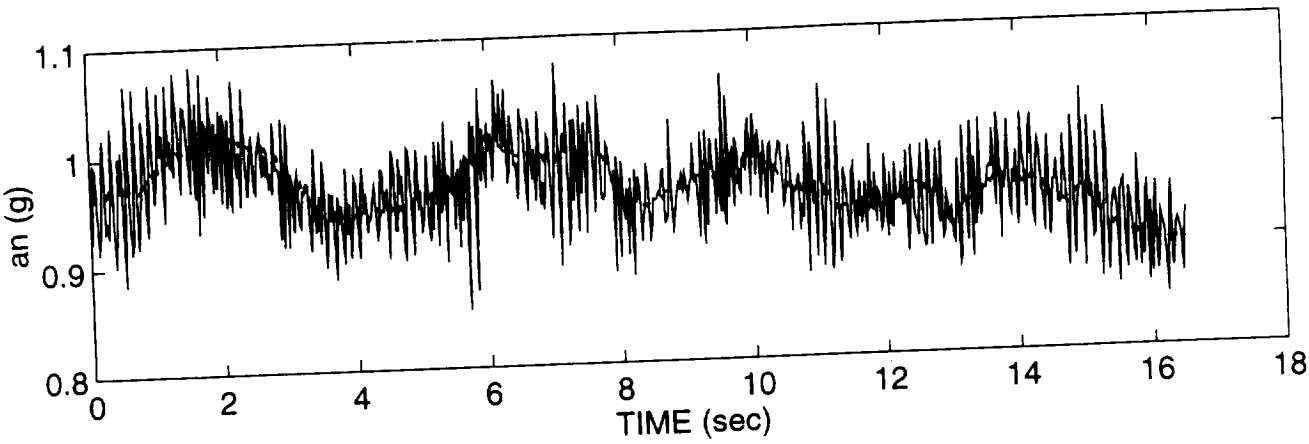
1.1
1
0.9
0.8
an (g)
0
2
4
6
8
10
12
14
16
18
TIME (sec)

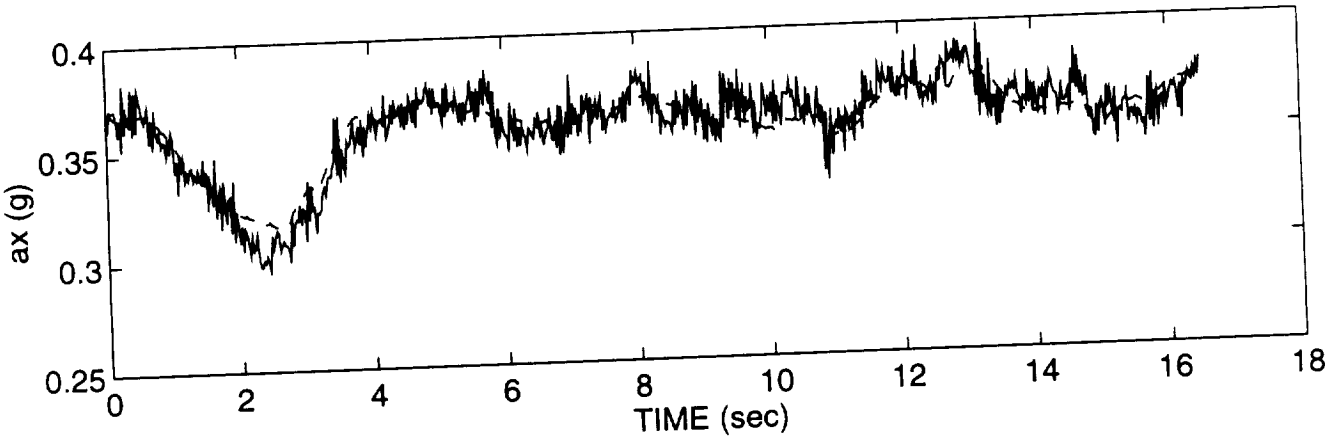
0.4
0.35
0.3
0.25
ax (g)
0
2
4
6
8
10
12
14
16
18
TIME (sec)

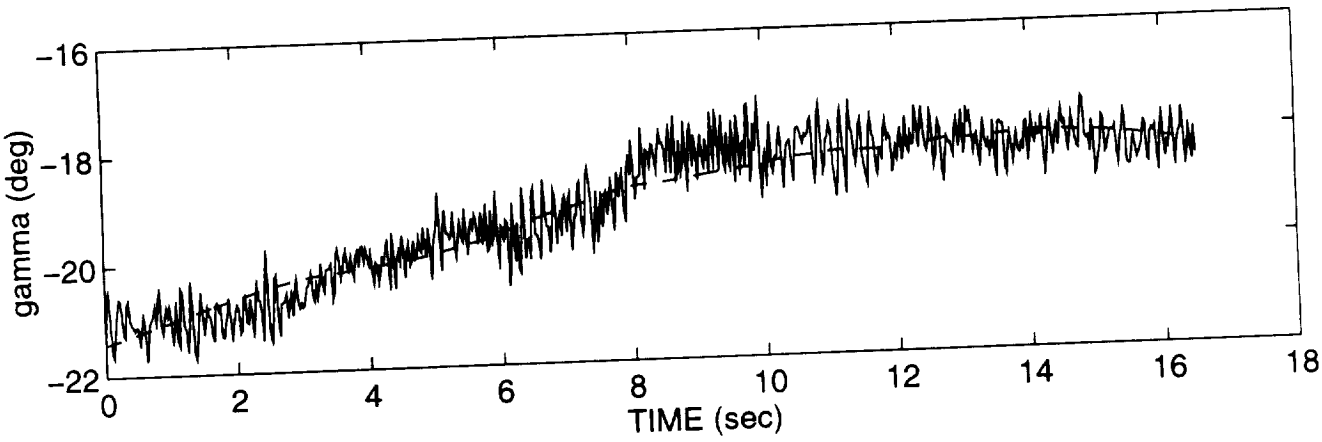
-16
-18
-20
-22
gamma (deg)
0
2
4
6
8
10
12
14
16
18
TIME (sec)

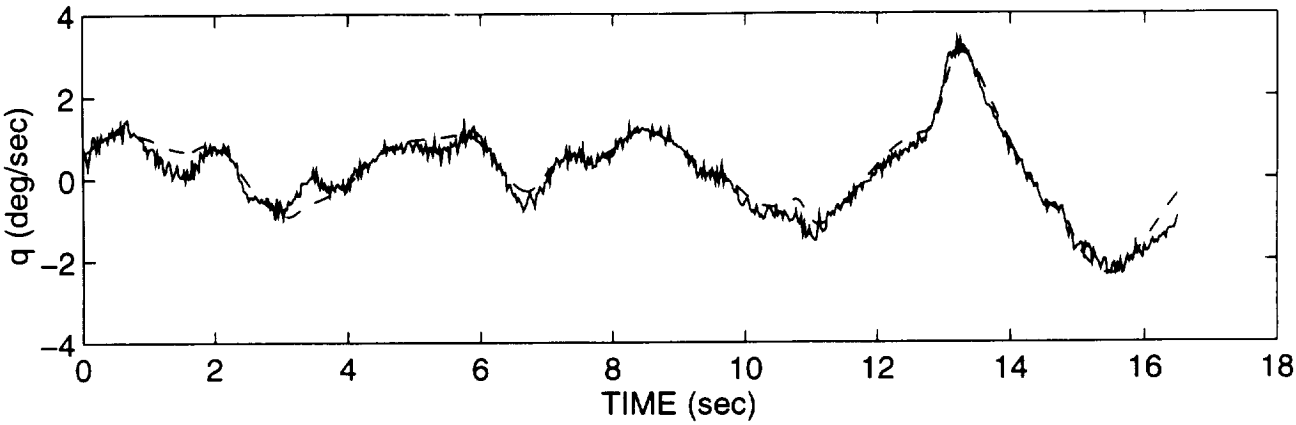
4
2
0
−2
−4
q (deg/sec)
0
2
4
6
8
10
12
14
16
18
TIME (sec)

LONGITUDINAL SINGLE SURFACE MULTIPLE DOUBLET FOR ALPHA OF 50 DEGREES

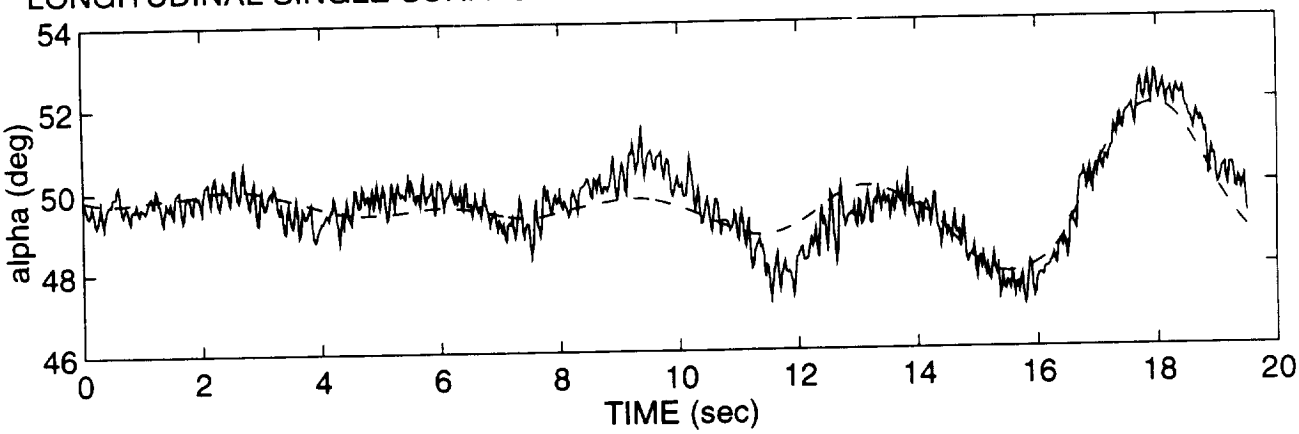

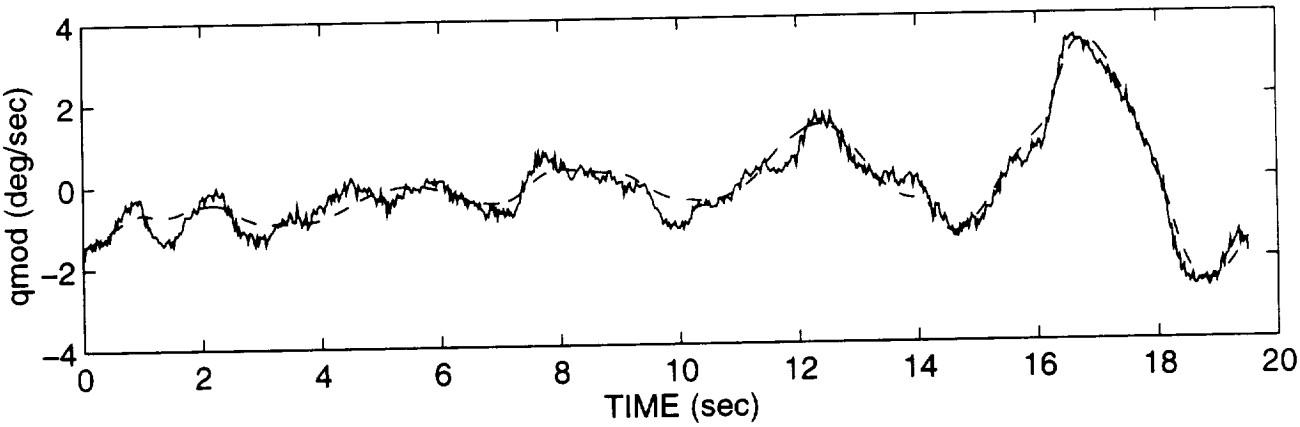

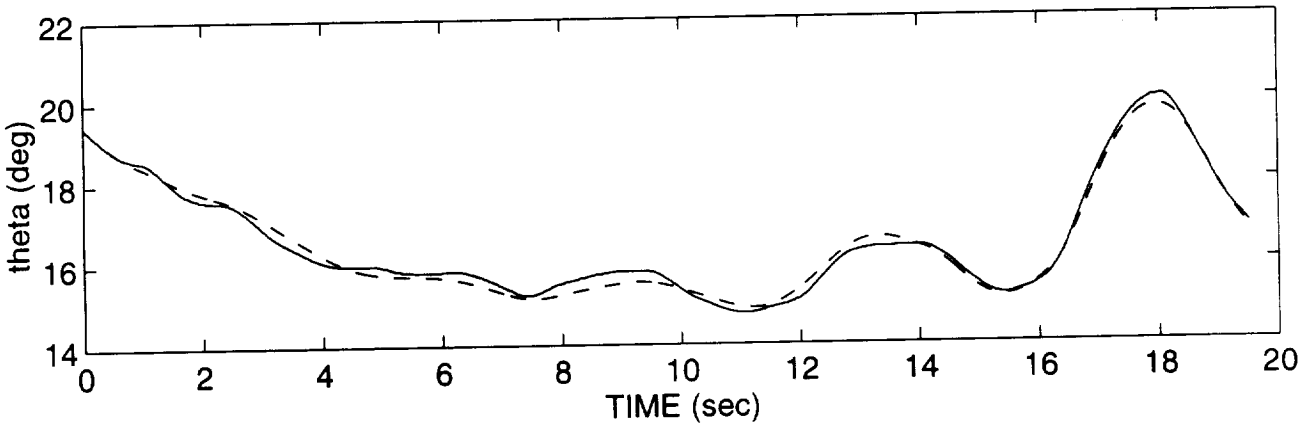

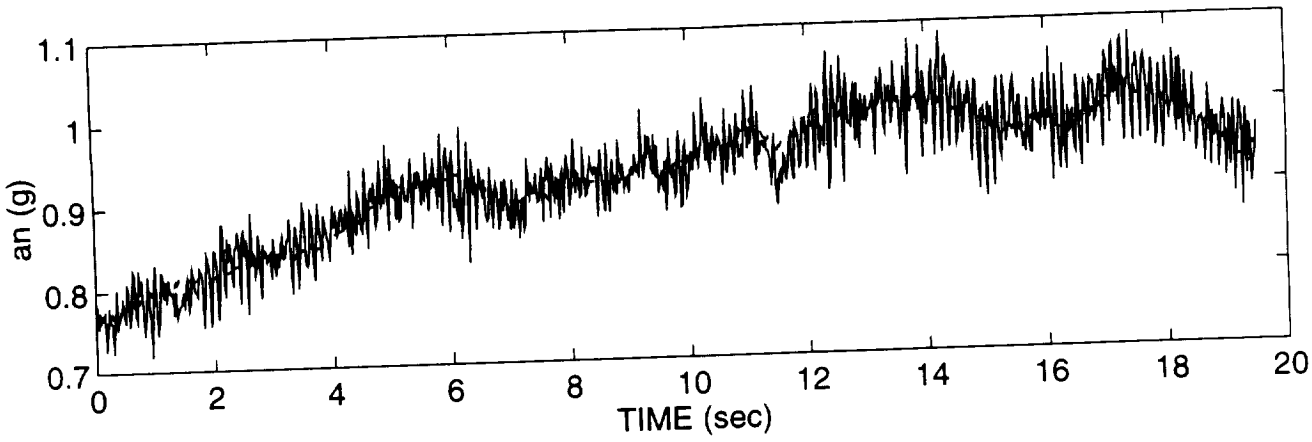
1.1
1
0.9
0.8
0.7
an (g)
0
2
4
6
8
10
12
14
16
18
20
TIME (sec)

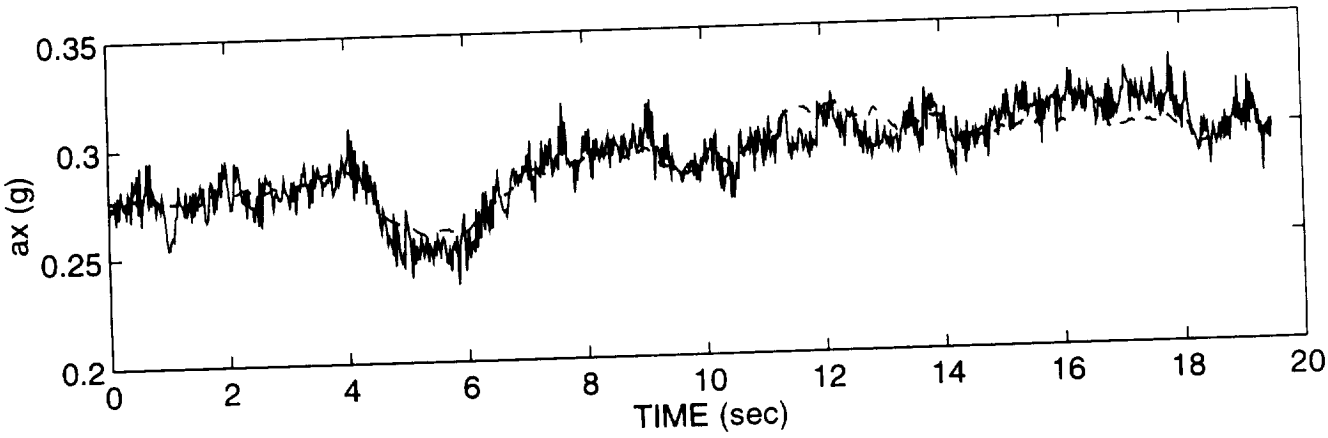
0.35
0.3
0.25
0.2
ax (g)
0
2
4
6
8
10
12
14
16
18
20
TIME (sec)

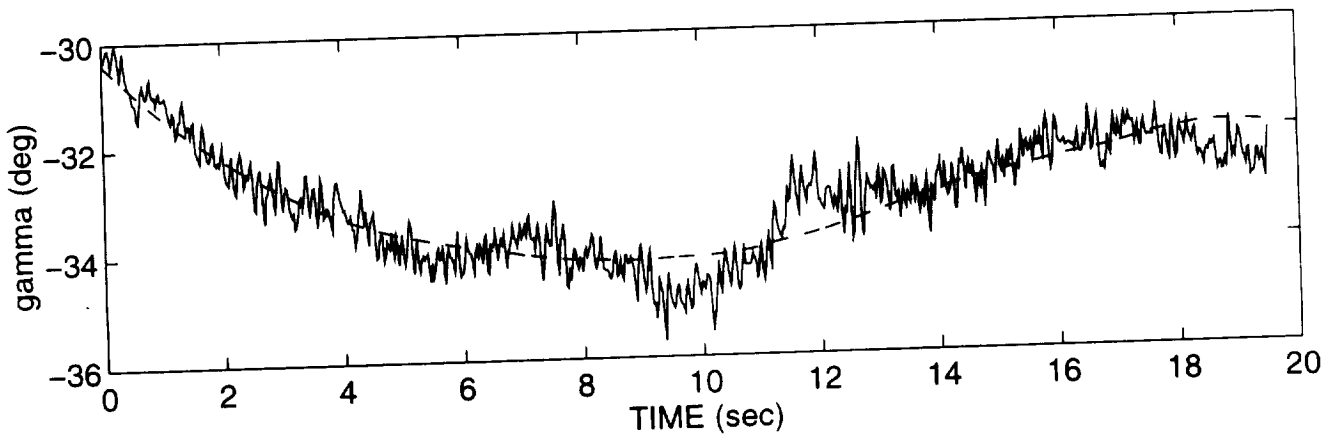
−30
−32
−34
−36
gamma (deg)
0
2
4
6
8
10
12
14
16
18
20
TIME (sec)

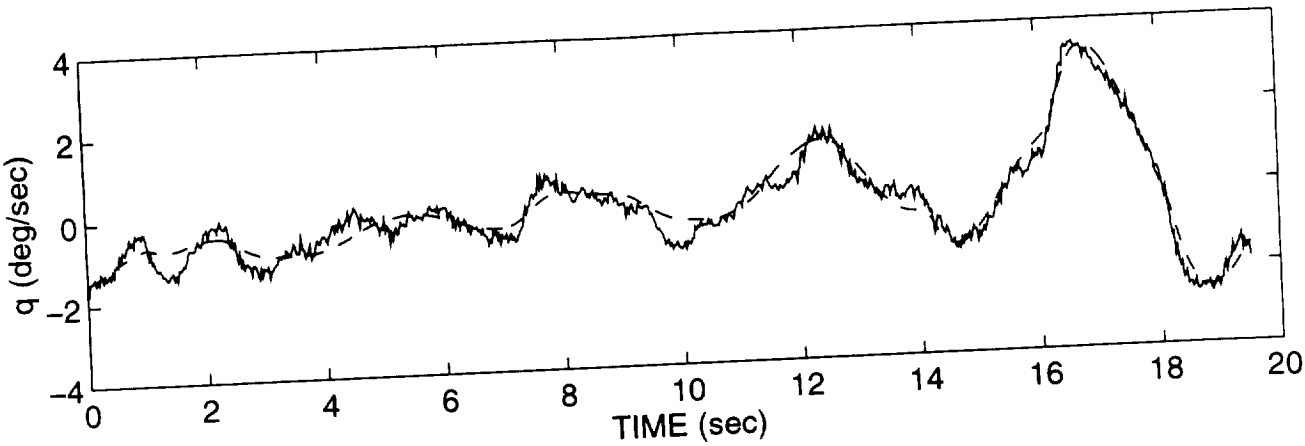
4
2
0
−2
−4
q (deg/sec)
0
2
4
6
8
10
12
14
16
18
20
TIME (sec)

LONGITUDINAL SINGLE SURFACE MULTIPLE DOUBLET FOR ALPHA OF 60 DEGREES

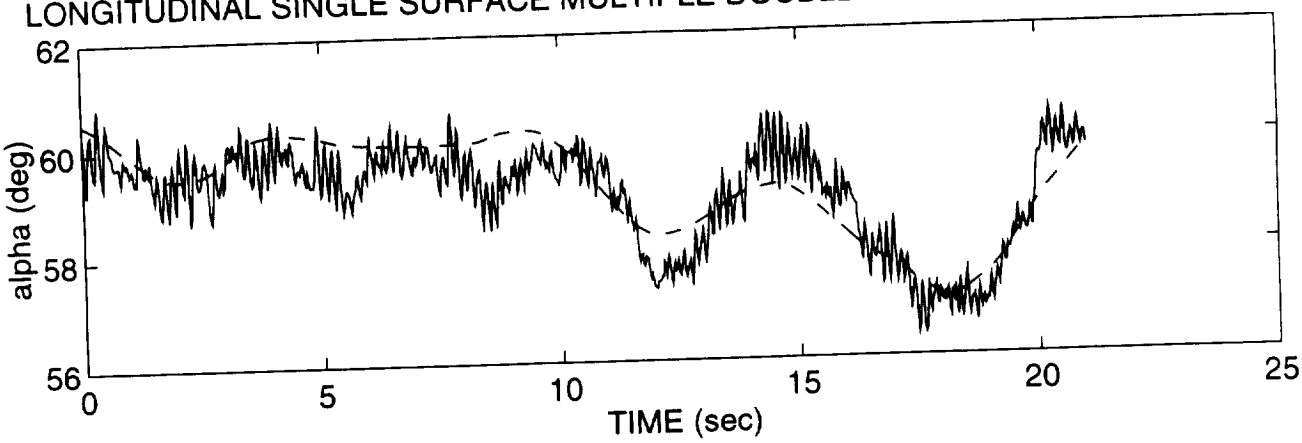

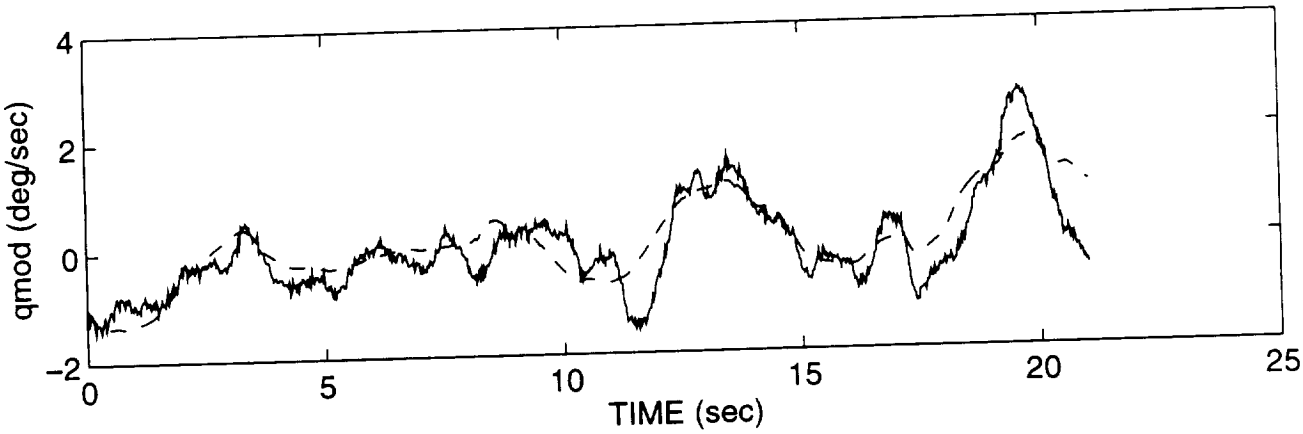

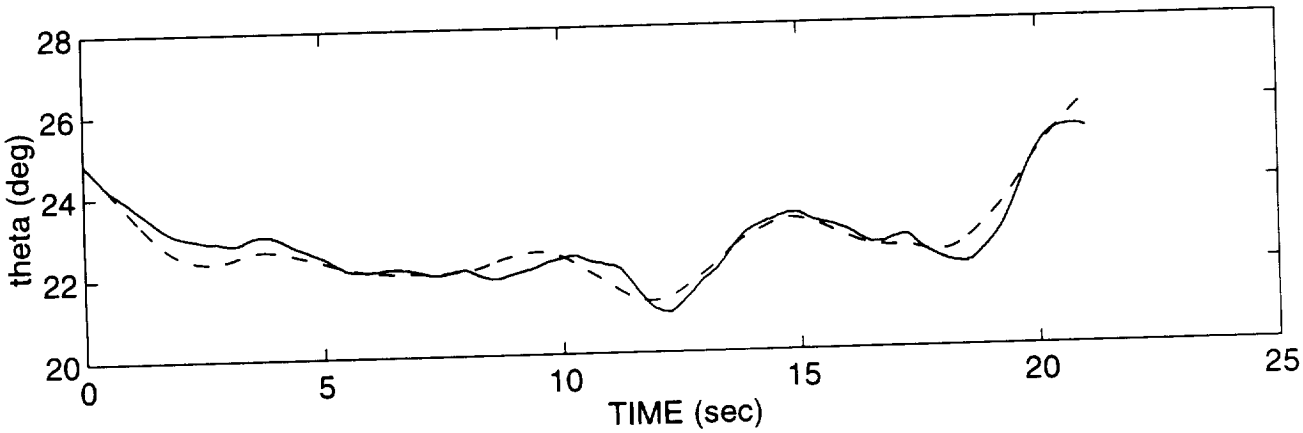

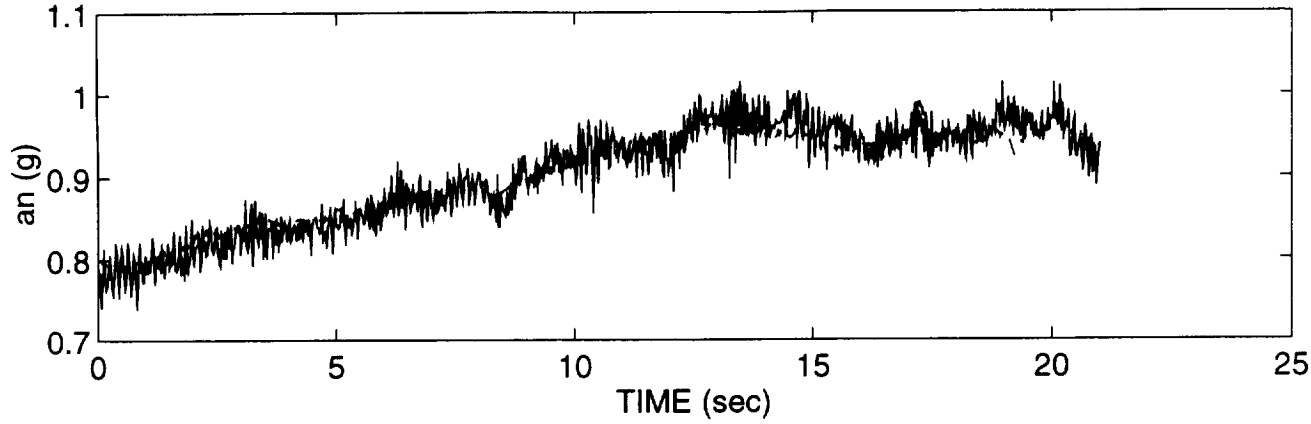
1.1
1
0.9
0.8
0.7
an (g)
0
5
10
15
20
25
TIME (sec)

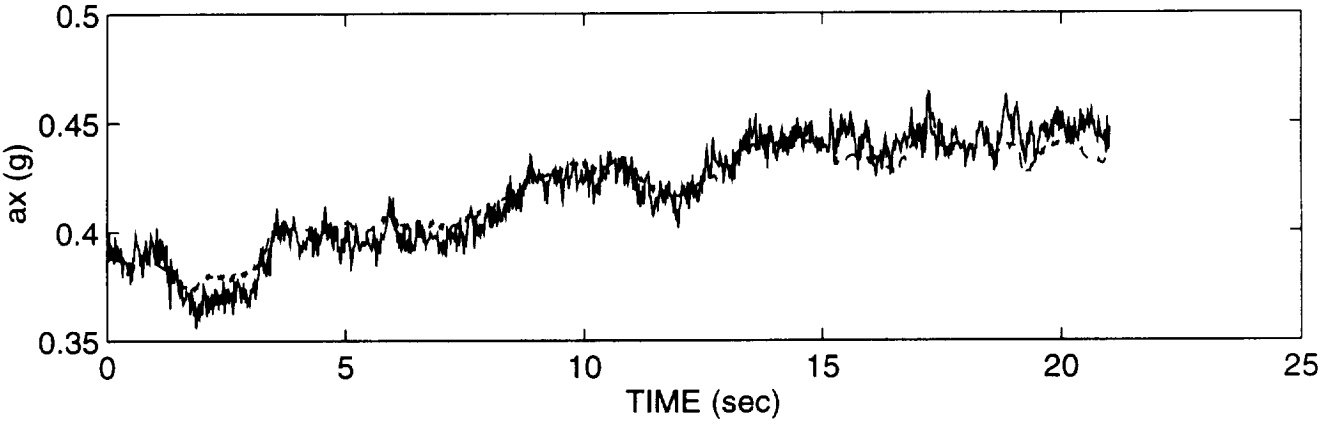
0.5
0.45
0.4
0.35
ax (g)
0
5
10
15
20
25
TIME (sec)

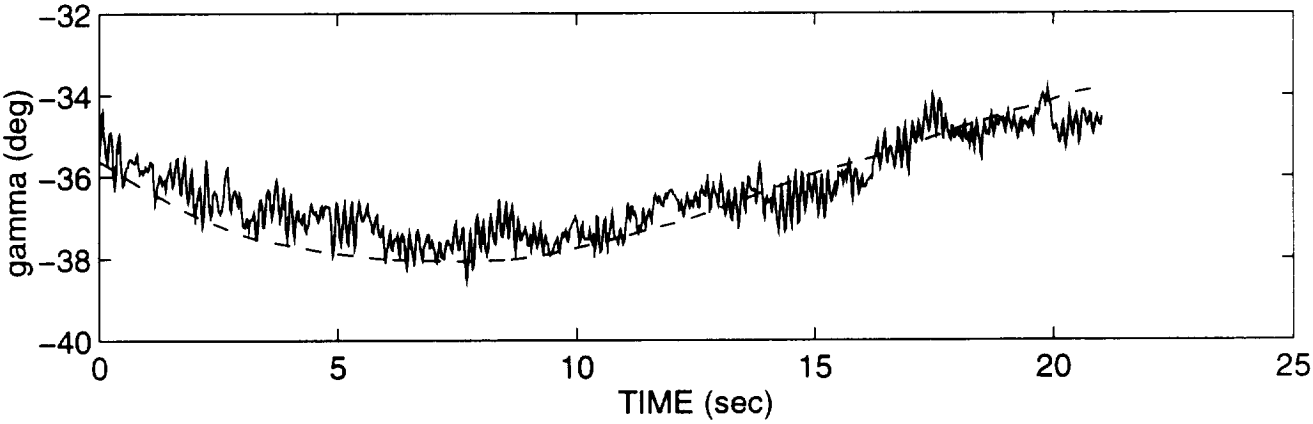
−32
−34
−36
−38
−40
gamma (deg)
0
5
10
15
20
25
TIME (sec)

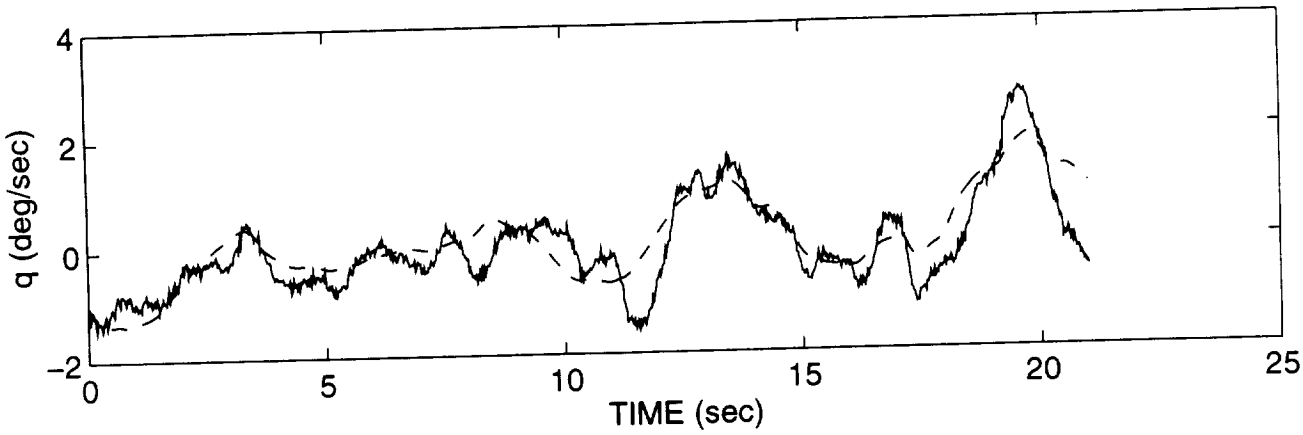
4
2
0
−2
q (deg/sec)
0
5
10
15
20
25
TIME (sec)

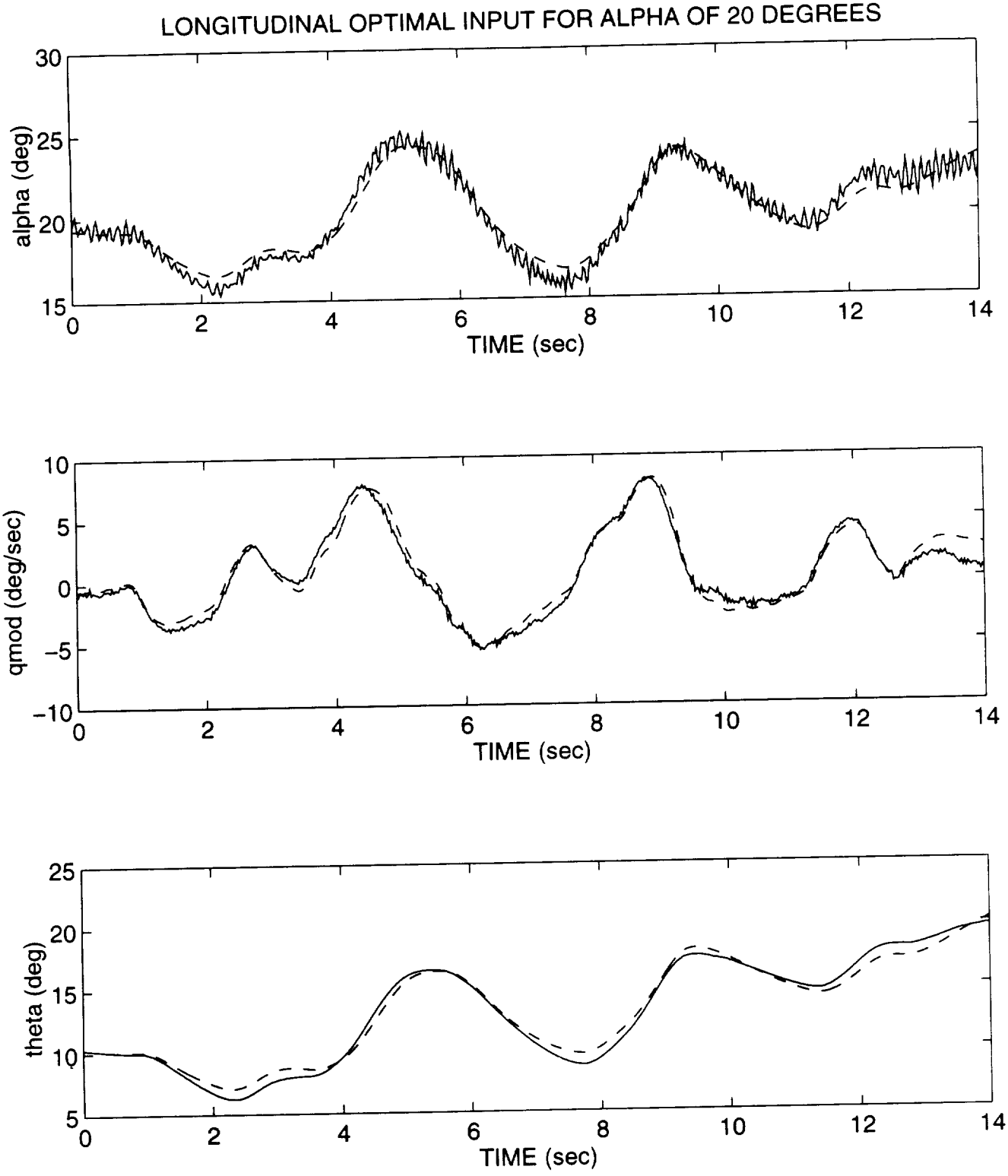
LONGITUDINAL OPTIMAL INPUT FOR ALPHA OF 20 DEGREES
alpha (deg)
30
25
20
15
0
2
4
6
8
10
12
14
TIME (sec)
qmod (deg/sec)
10
5
0
−5
−10
0
2
4
6
8
10
12
14
TIME (sec)
theta (deg)
25
20
15
10
5
0
2
4
6
8
10
12
14
TIME (sec)

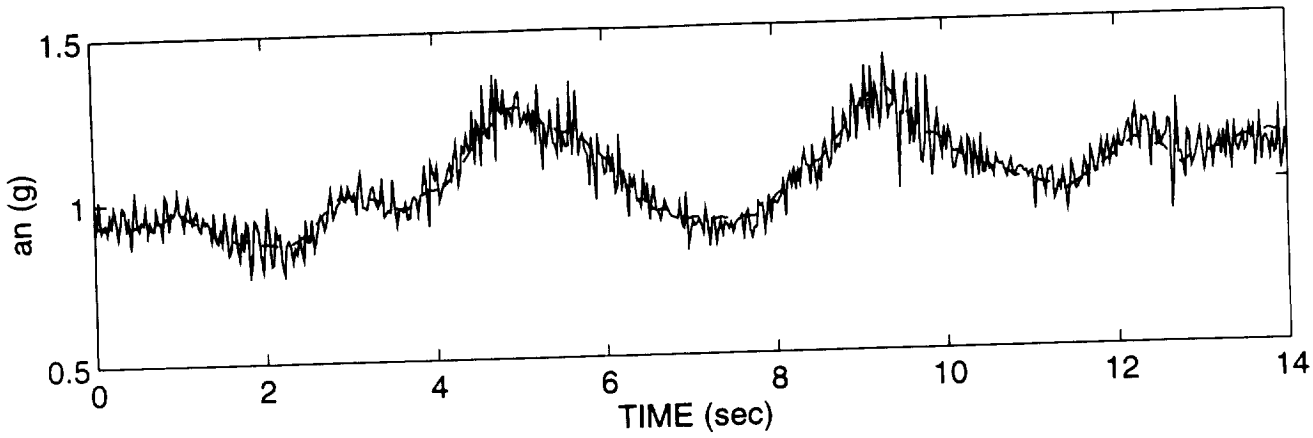
1.5
1
0.5
an (g)
0
2
4
6
8
10
12
14
TIME (sec)

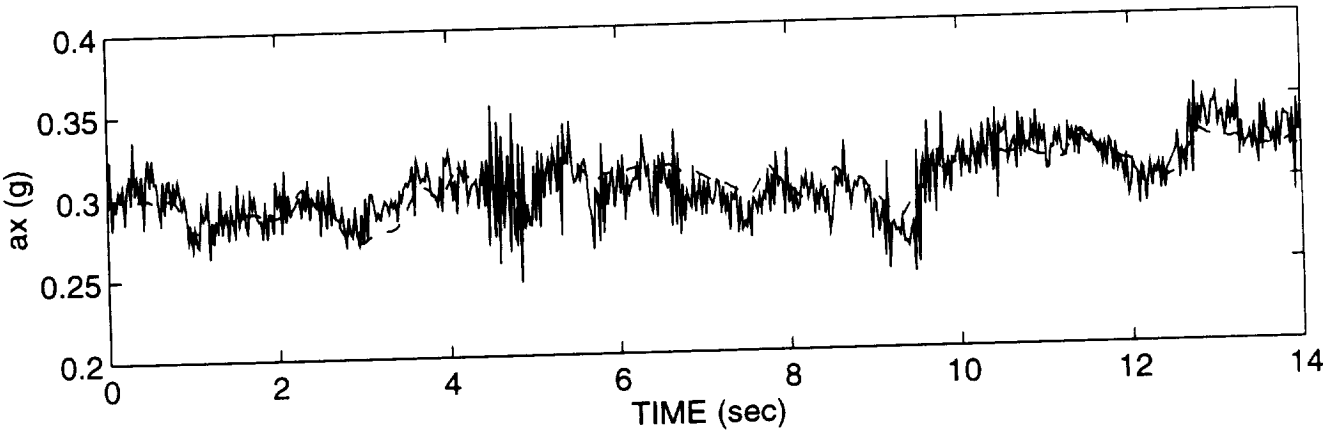
0.4
0.35
0.3
0.25
0.2
ax (g)
0
2
4
6
8
10
12
14
TIME (sec)

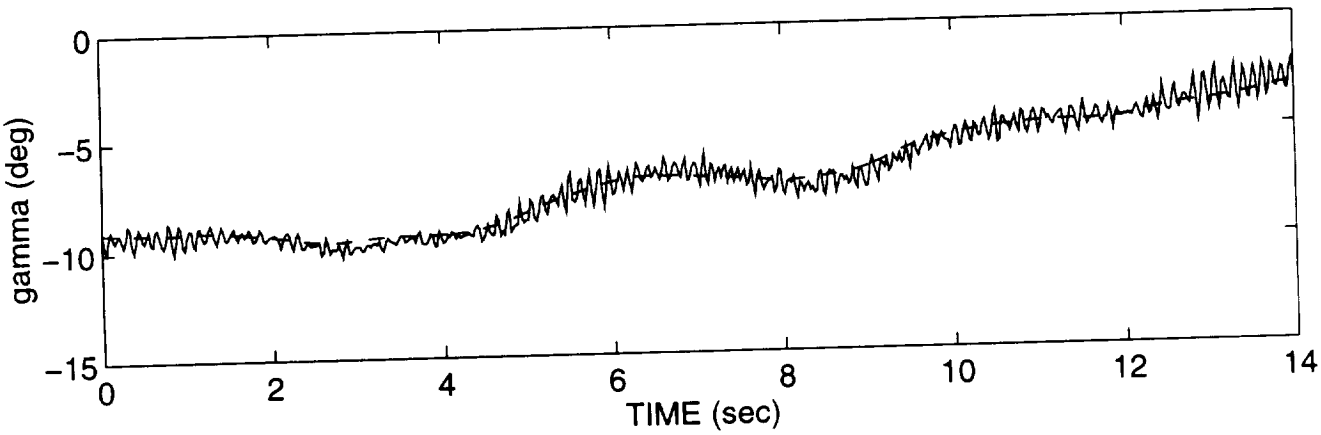
0
−5
−10
−15
gamma (deg)
0
2
4
6
8
10
12
14
TIME (sec)

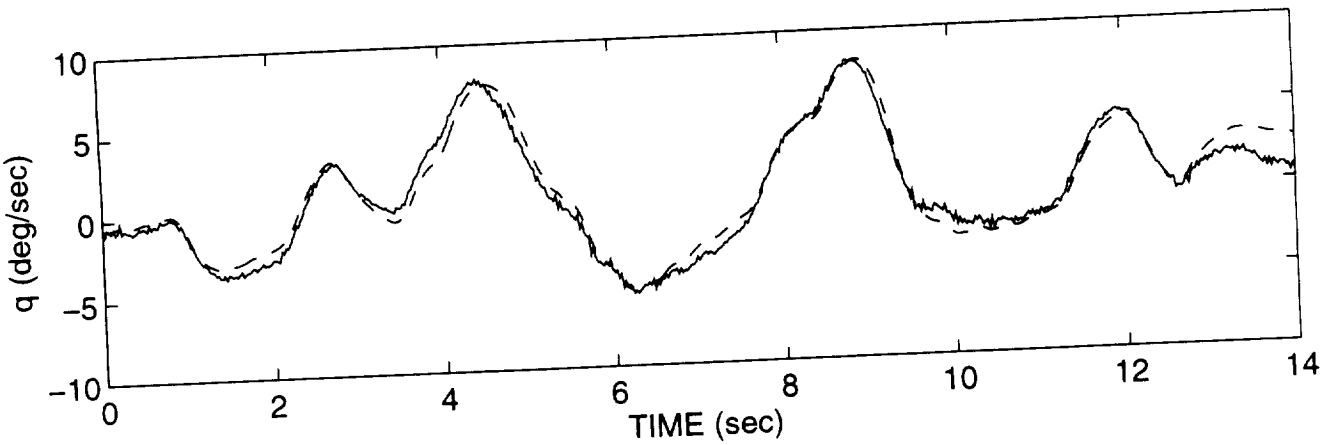
10
5
0
−5
−10
q (deg/sec)
0
2
4
6
8
10
12
14
TIME (sec)

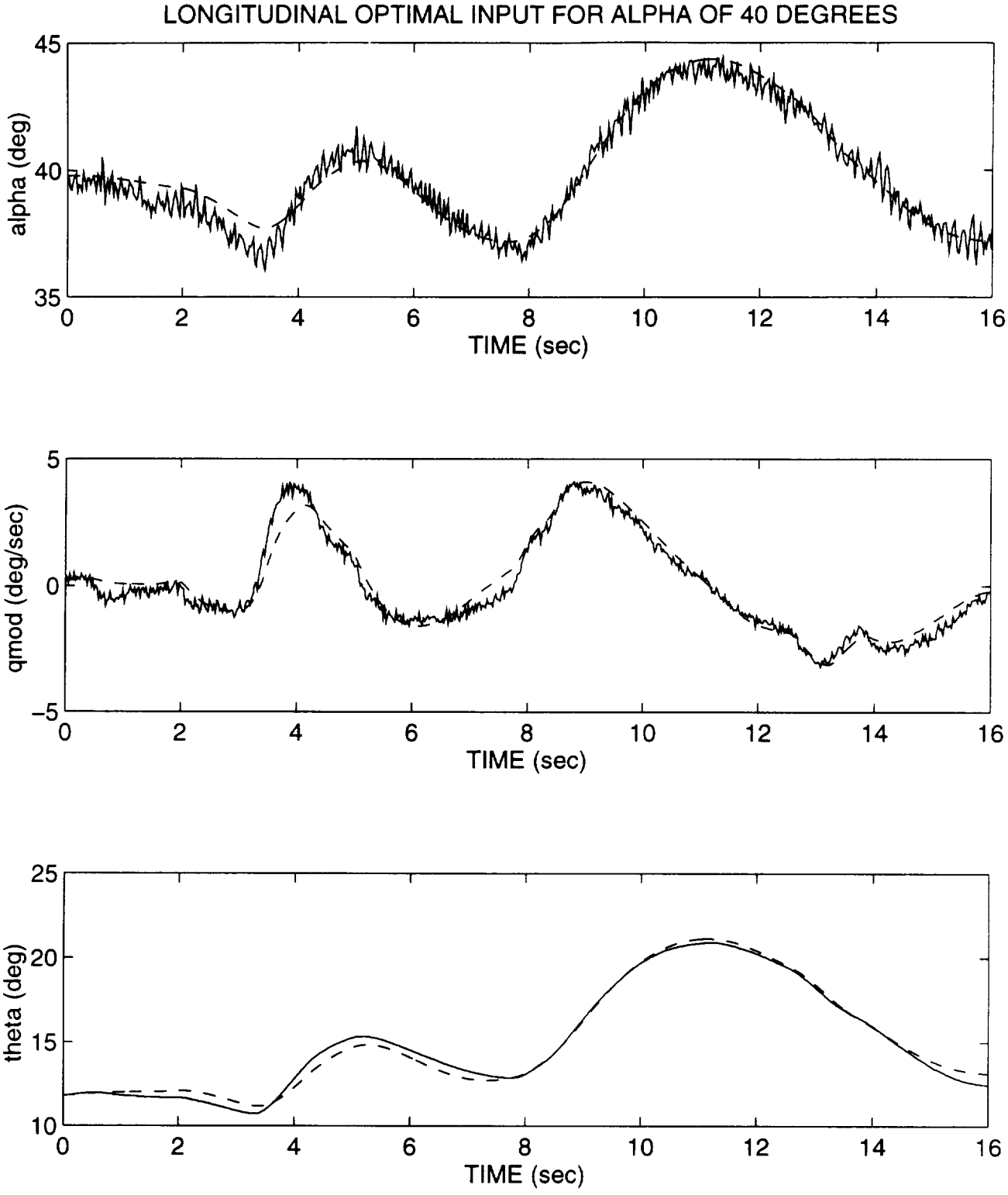
LONGITUDINAL OPTIMAL INPUT FOR ALPHA OF 40 DEGREES
alpha (deg)
45
40
35
0
2
4
6
8
10
12
14
16
TIME (sec)
qmod (deg/sec)
5
0
−5
0
2
4
6
8
10
12
14
16
TIME (sec)
theta (deg)
25
20
15
10
0
2
4
6
8
10
12
14
16
TIME (sec)

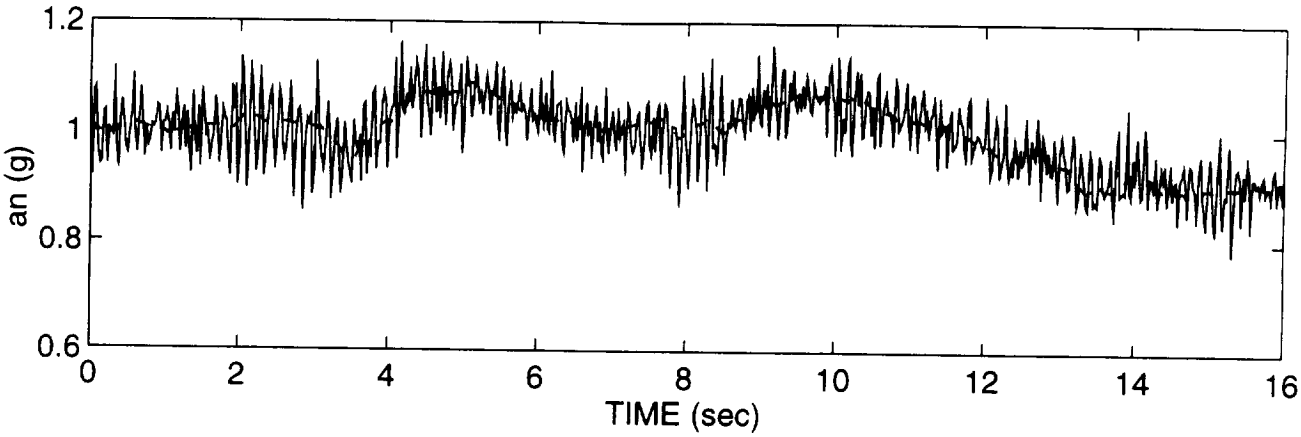
1.2
1
0.8
0.6
an (g)
0
2
4
6
8
10
12
14
16
TIME (sec)

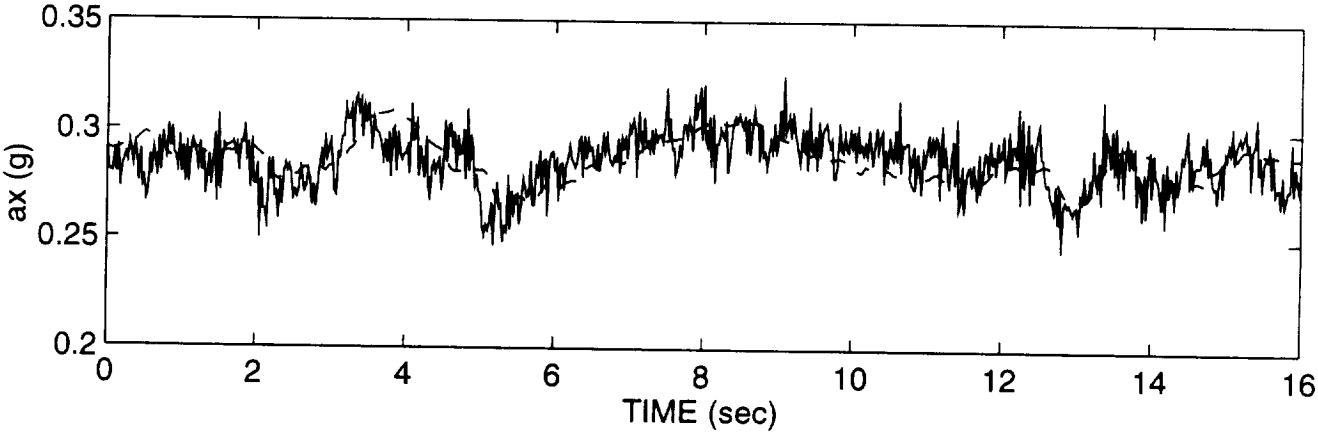
0.35
0.3
0.25
0.2
ax (g)
0
2
4
6
8
10
12
14
16
TIME (sec)

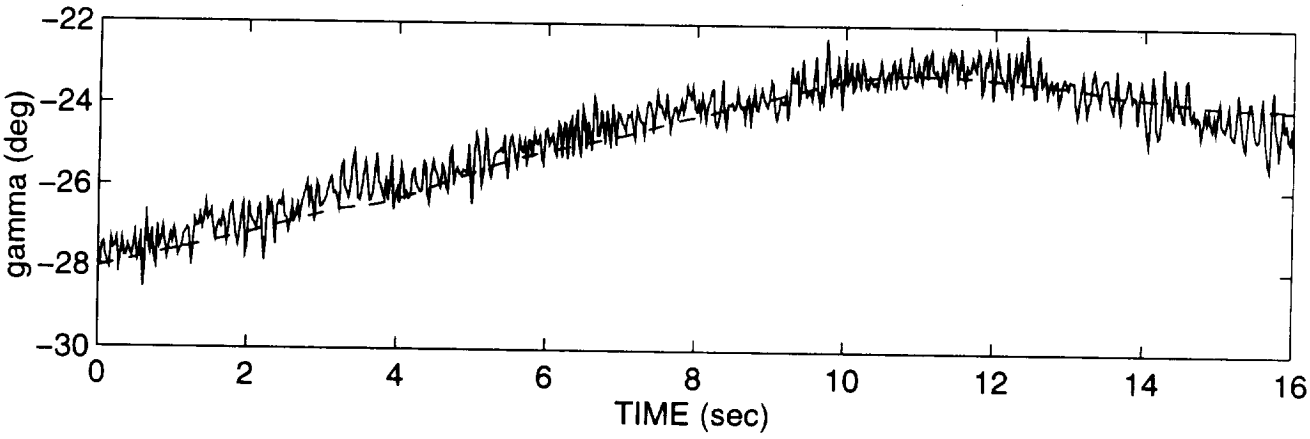
-22
-24
-26
-28
-30
gamma (deg)
0
2
4
6
8
10
12
14
16
TIME (sec)

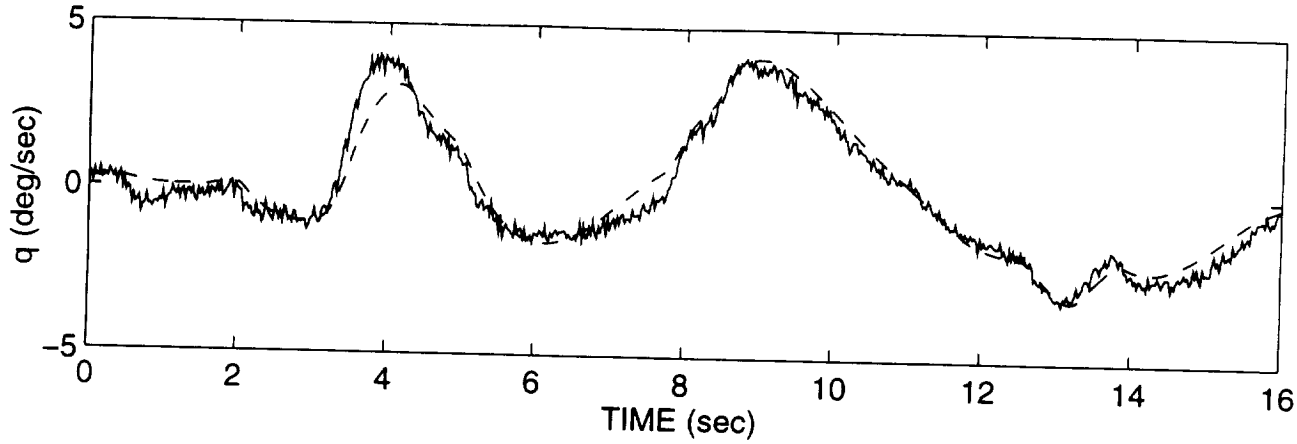
5
0
-5
q (deg/sec)
0
2
4
6
8
10
12
14
16
TIME (sec)

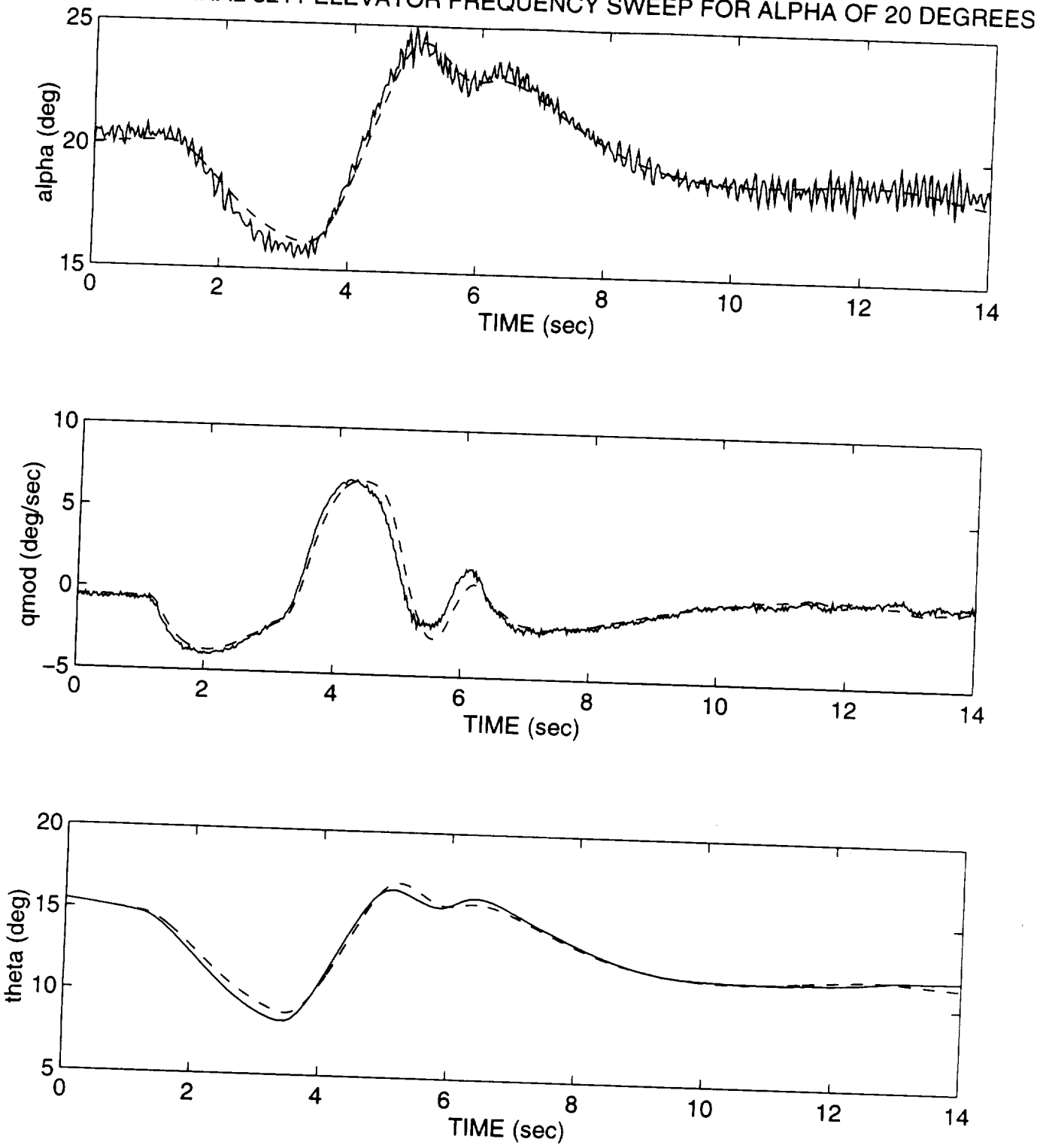
LONGITUDINAL 3211 ELEVATOR FREQUENCY SWEEP FOR ALPHA OF 20 DEGREES
alpha (deg)
25
20
15
0
2
4
6
8
10
12
14
TIME (sec)
qmod (deg/sec)
10
5
0
-5
0
2
4
6
8
10
12
14
TIME (sec)
theta (deg)
20
15
10
5
0
2
4
6
8
10
12
14
TIME (sec)

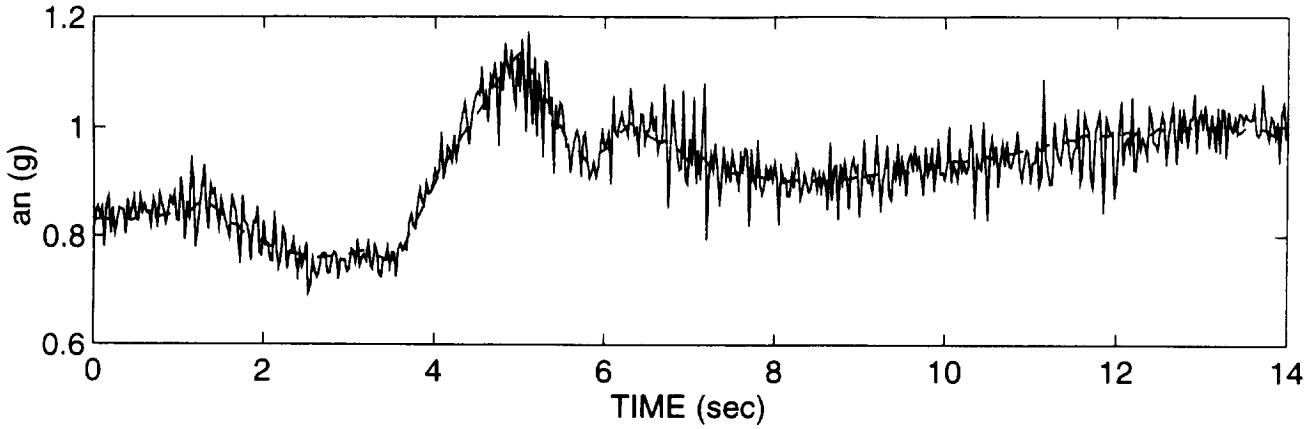
1.2
1
0.8
0.6
an (g)
0
2
4
6
8
10
12
14
TIME (sec)

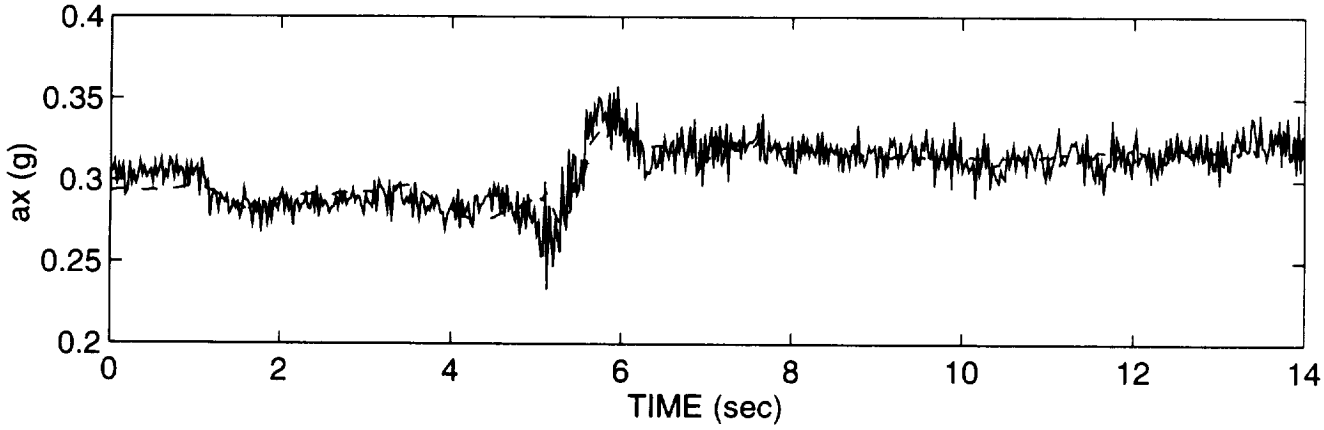
0.4
0.35
0.3
0.25
0.2
ax (g)
0
2
4
6
8
10
12
14
TIME (sec)

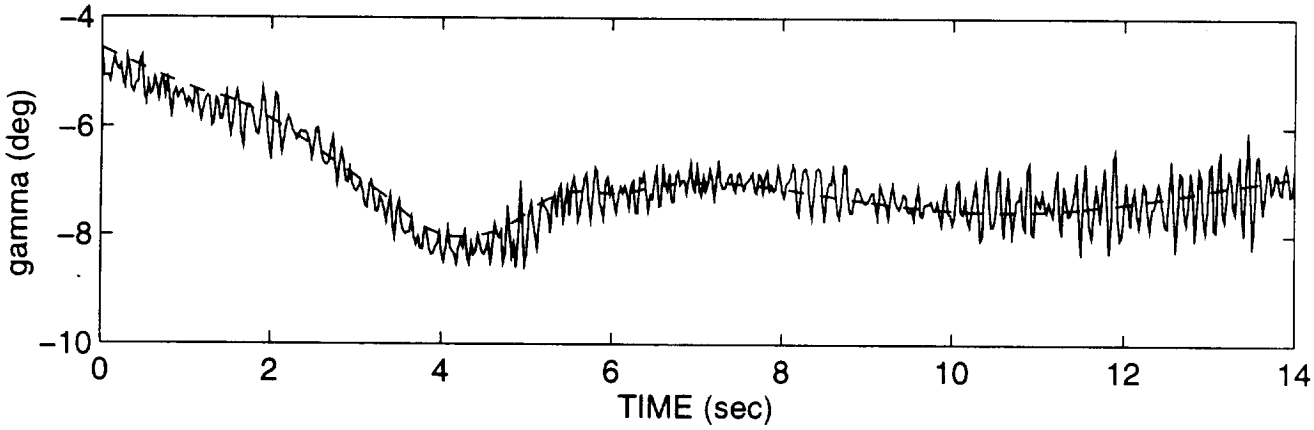
−4
−6
−8
−10
gamma (deg)
0
2
4
6
8
10
12
14
TIME (sec)

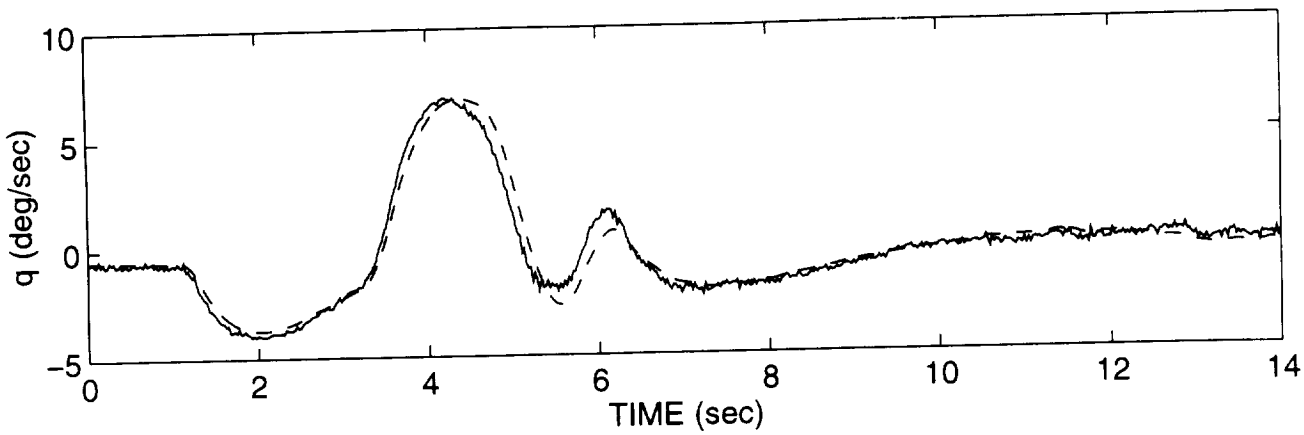
10
5
0
−5
q (deg/sec)
0
2
4
6
8
10
12
14
TIME (sec)

LONGITUDINAL PILOT 1" PITCH STICK STEPS FOR ALPHA OF 20 DEGREES

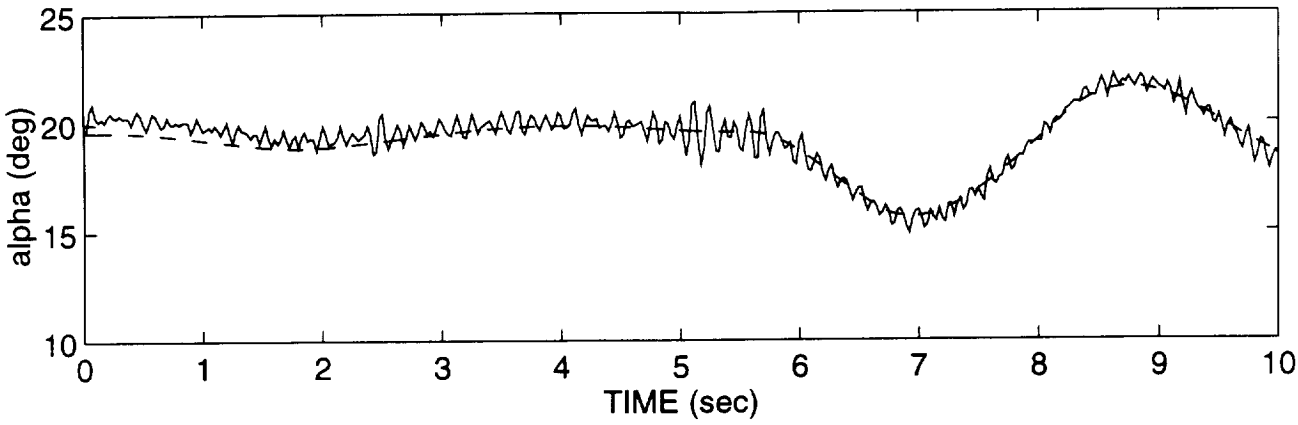

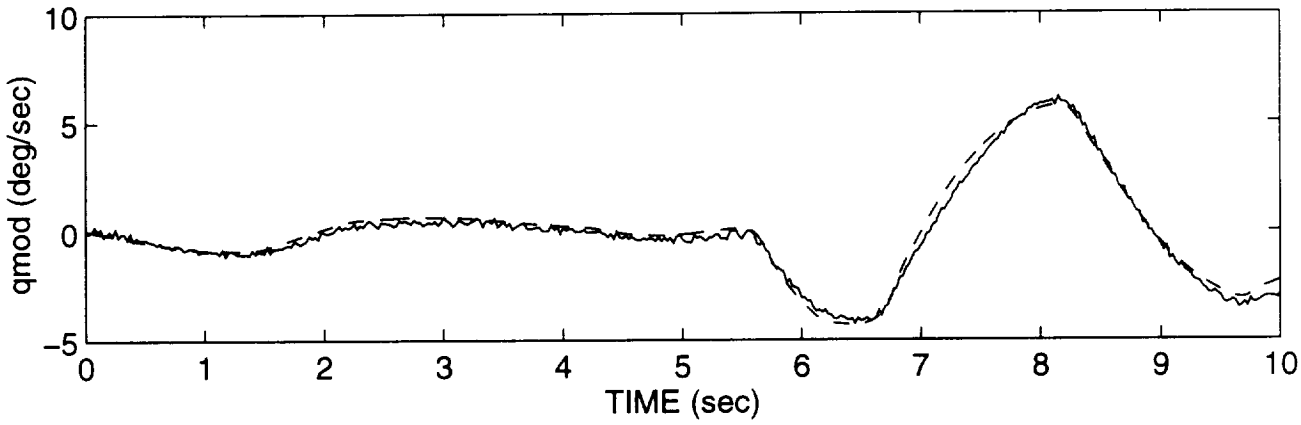

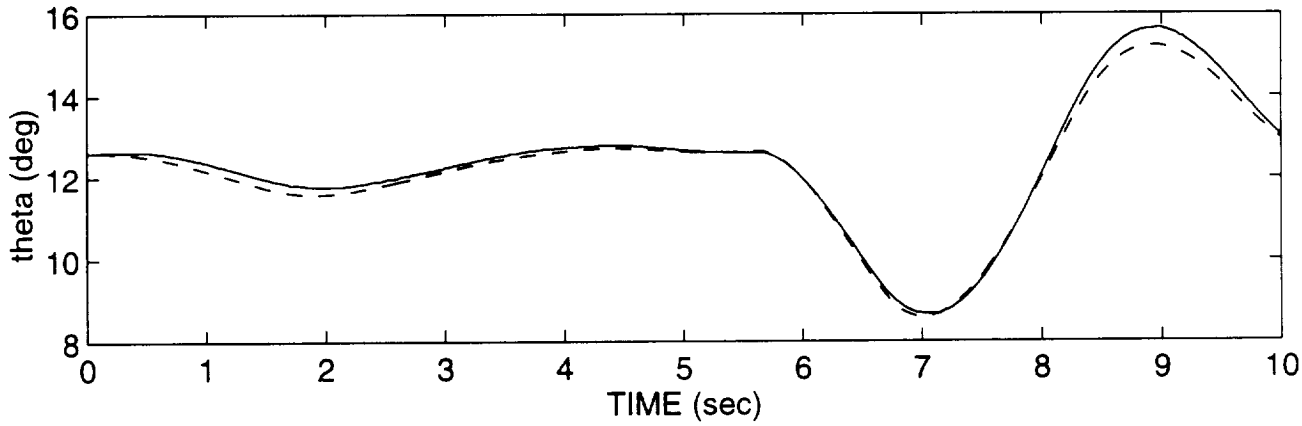

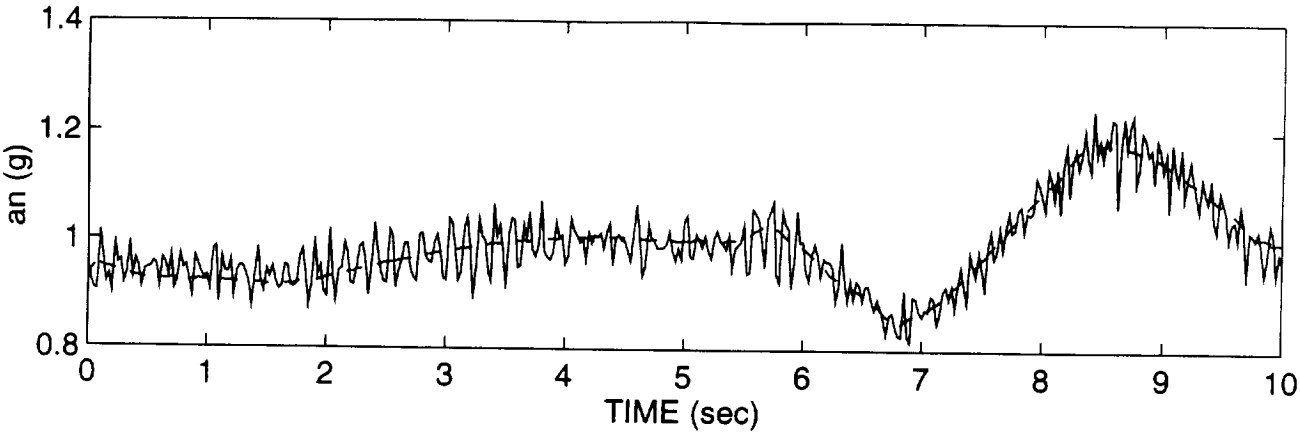
1.4
1.2
1
0.8
an (g)
0
1
2
3
4
5
6
7
8
9
10
TIME (sec)

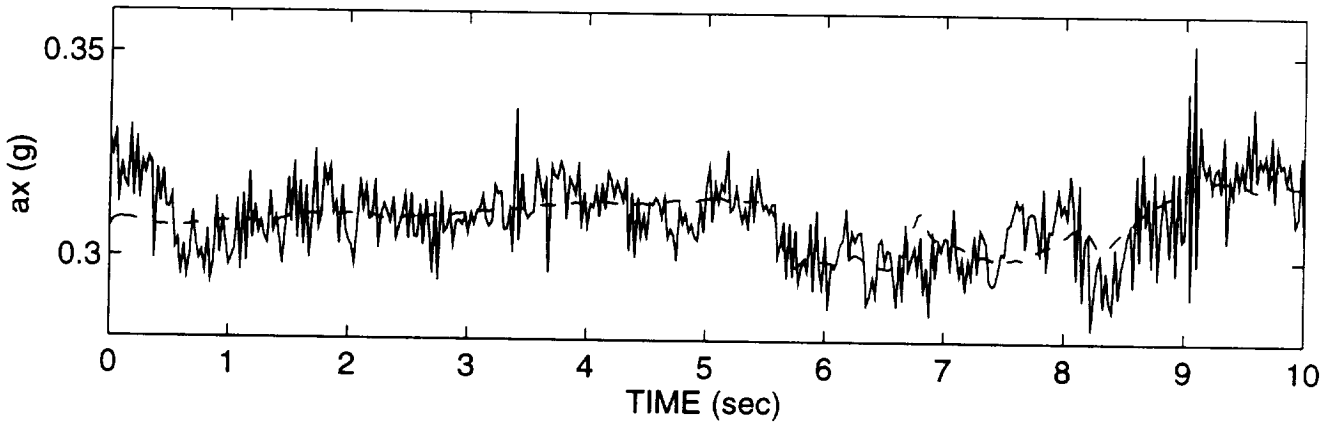
0.35
0.3
ax (g)
0
1
2
3
4
5
6
7
8
9
10
TIME (sec)

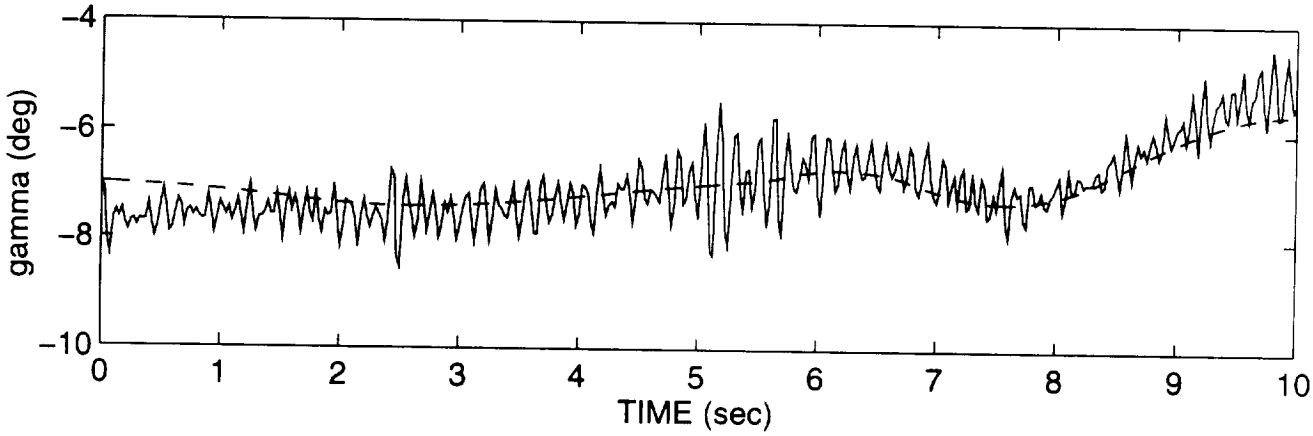
−4
−6
−8
−10
gamma (deg)
0
1
2
3
4
5
6
7
8
9
10
TIME (sec)

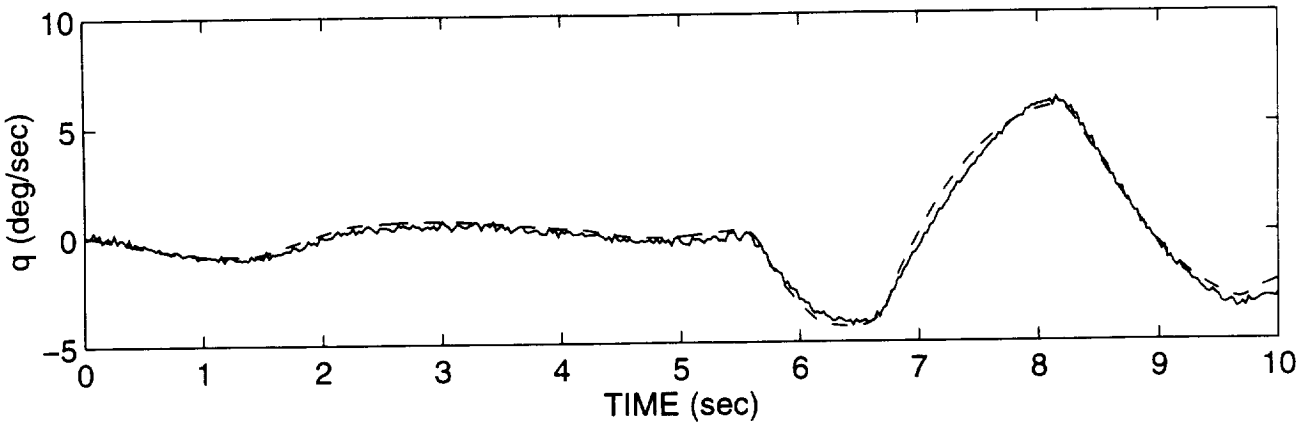
10
5
0
−5
q (deg/sec)
0
1
2
3
4
5
6
7
8
9
10
TIME (sec)

LONGITUDINAL PILOT 1" PITCH STICK STEPS FOR ALPHA OF 30 DEGREES

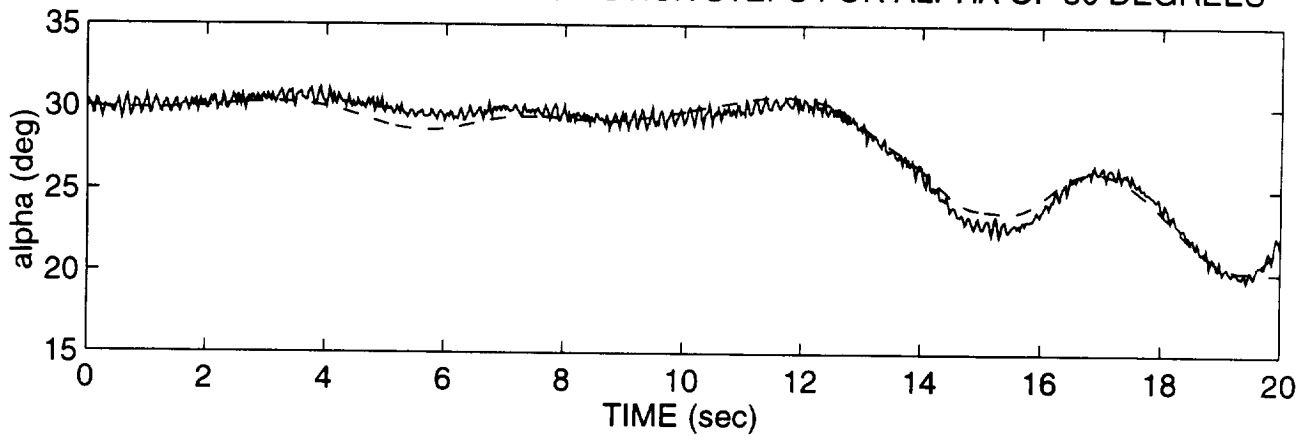

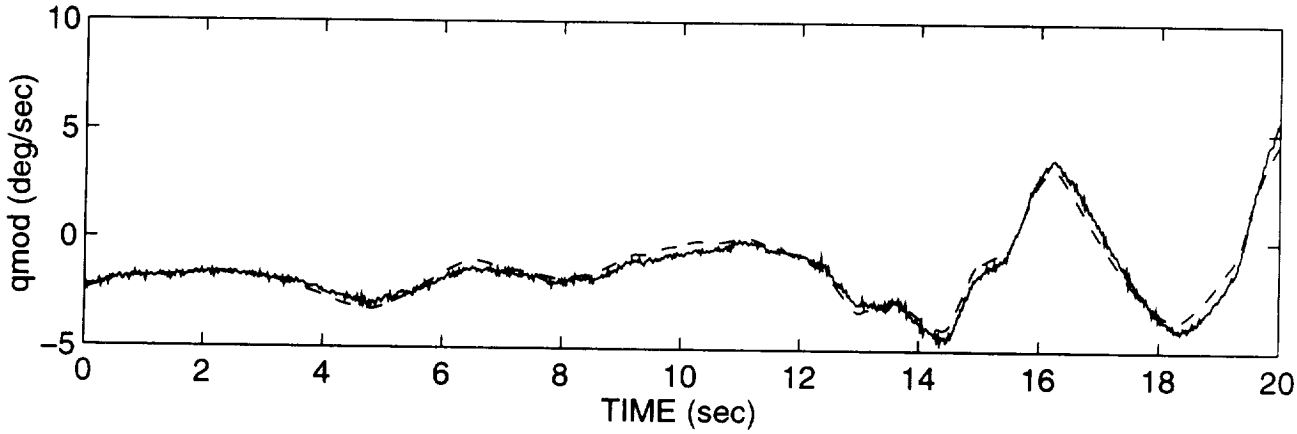

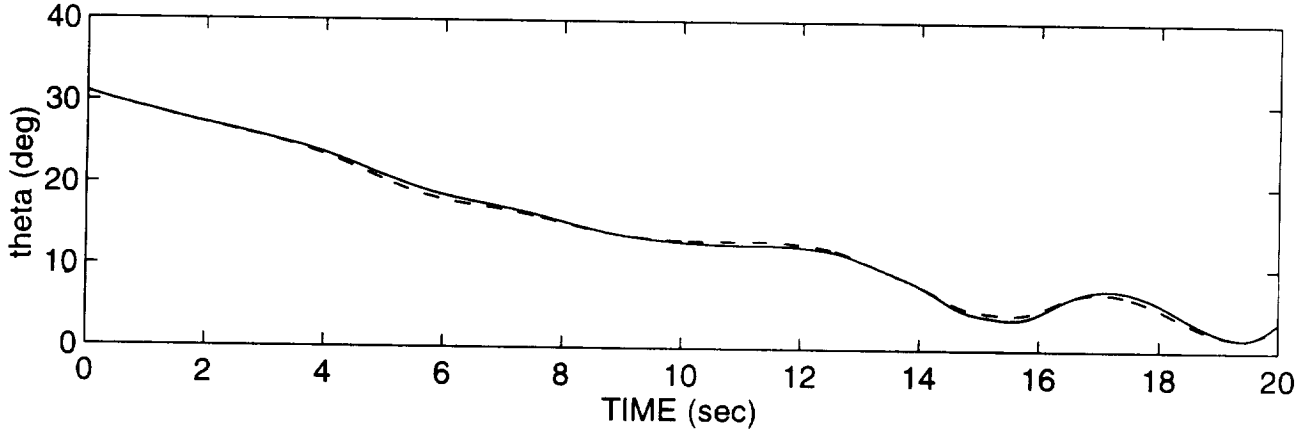

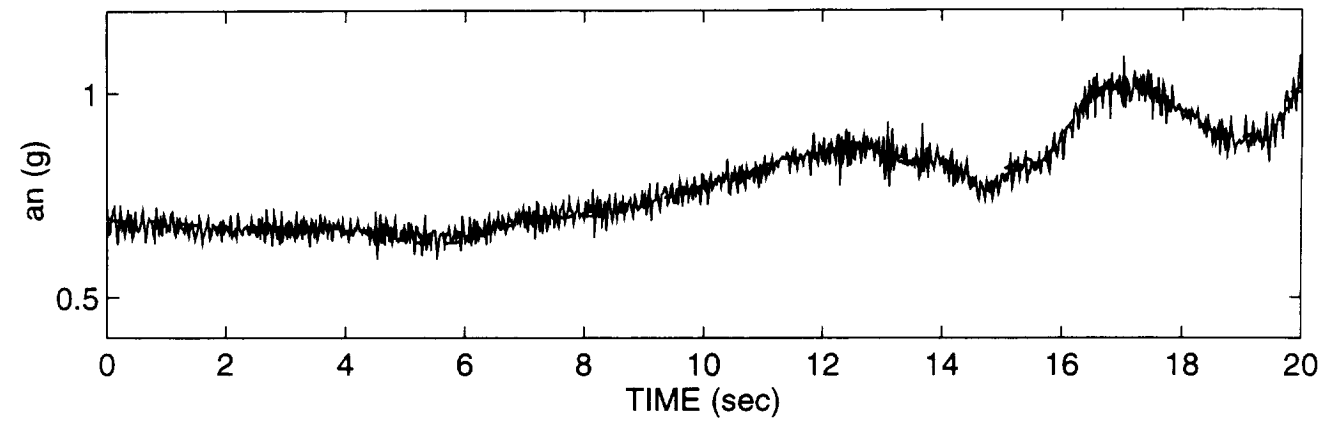
an (g)
1
0.5
0
2
4
6
8
10
12
14
16
18
20
TIME (sec)

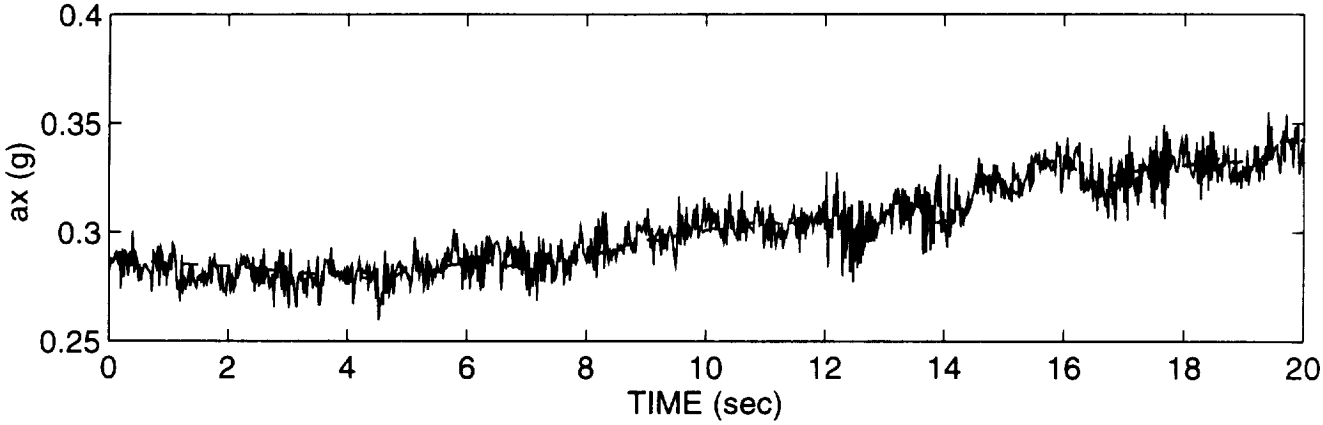
ax (g)
0.4
0.35
0.3
0.25
0
2
4
6
8
10
12
14
16
18
20
TIME (sec)

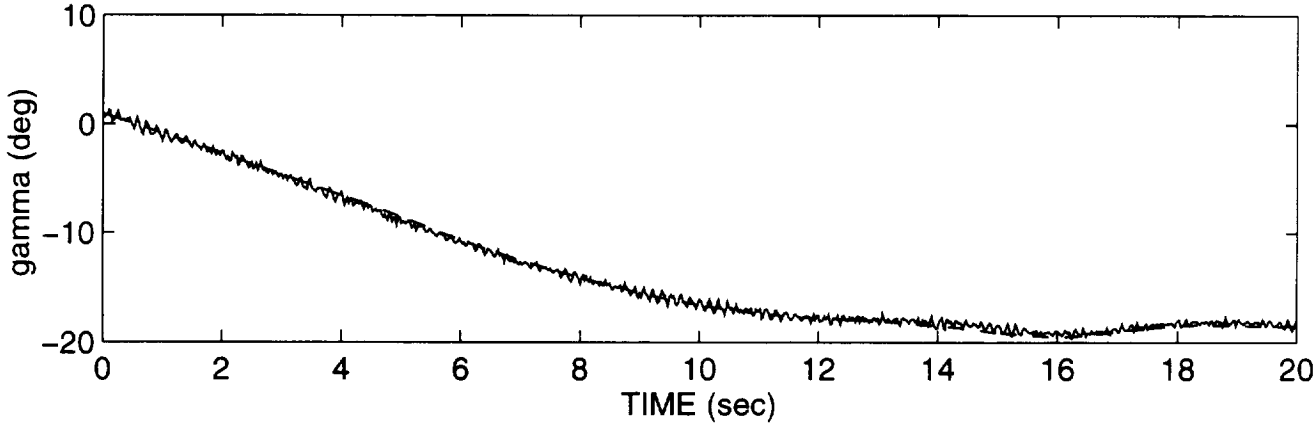
gamma (deg)
10
0
−10
−20
0
2
4
6
8
10
12
14
16
18
20
TIME (sec)

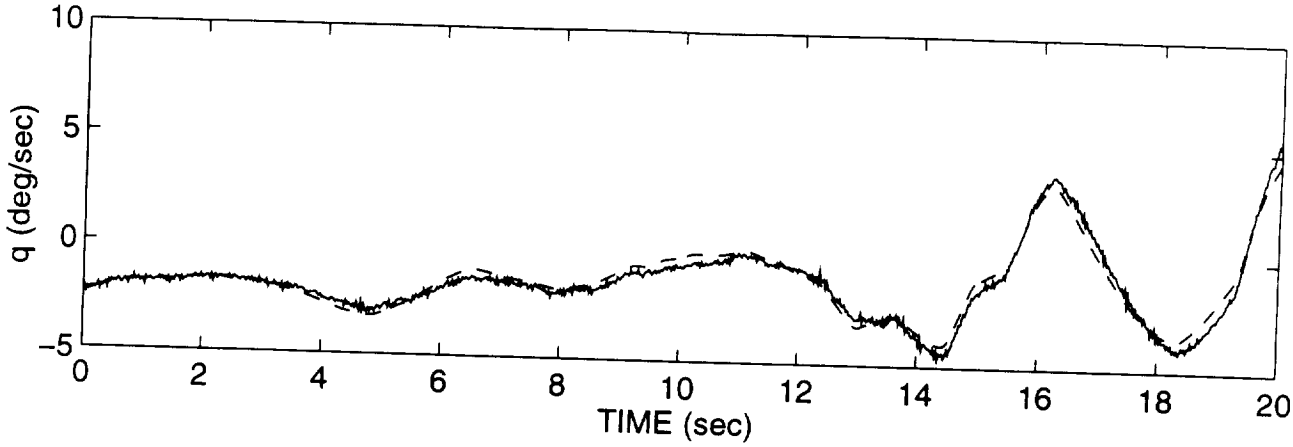
10
5
0
−5
q (deg/sec)
0
2
4
6
8
10
12
14
16
18
20
TIME (sec)

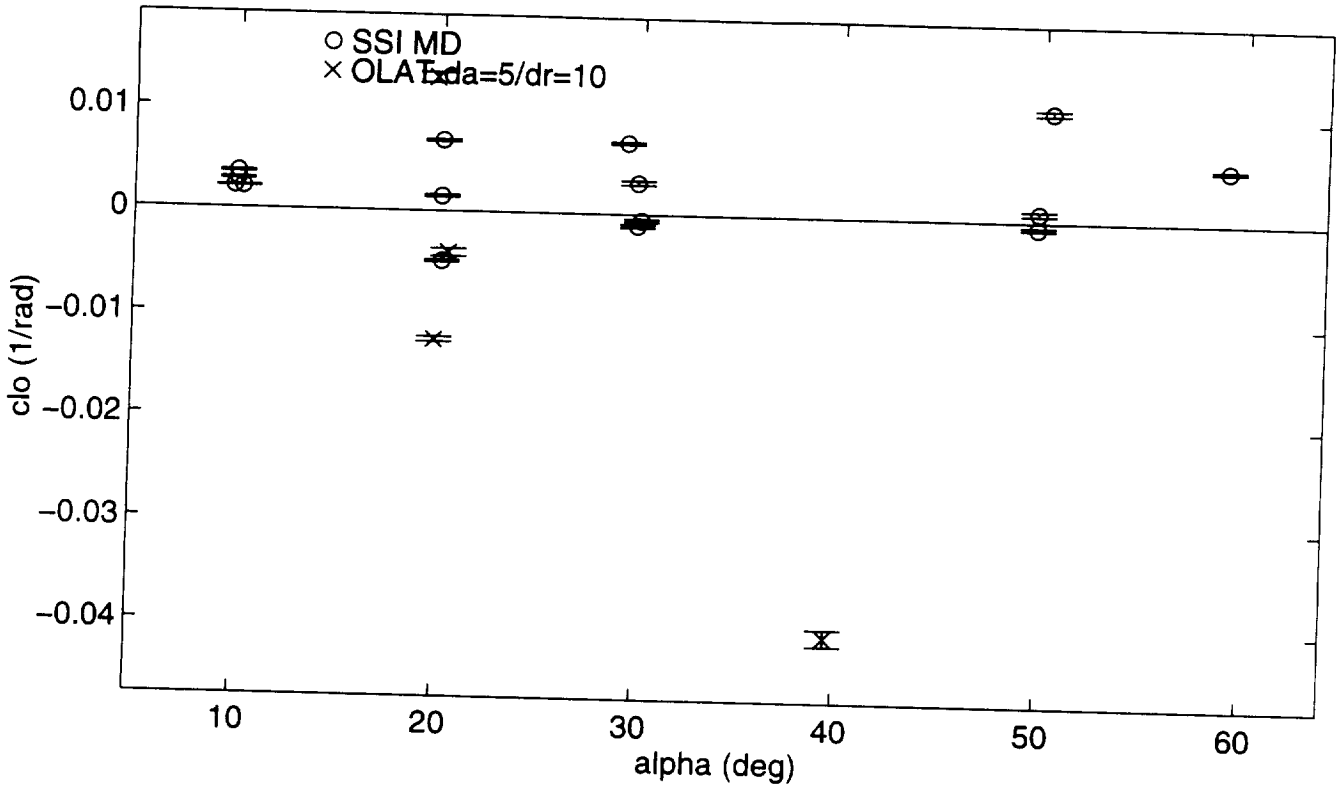
SSI MD
OLAT da=5/dr=10
clo (1/rad)
0.01
0
−0.01
−0.02
−0.03
−0.04
10
20
30
40
50
60
alpha (deg)

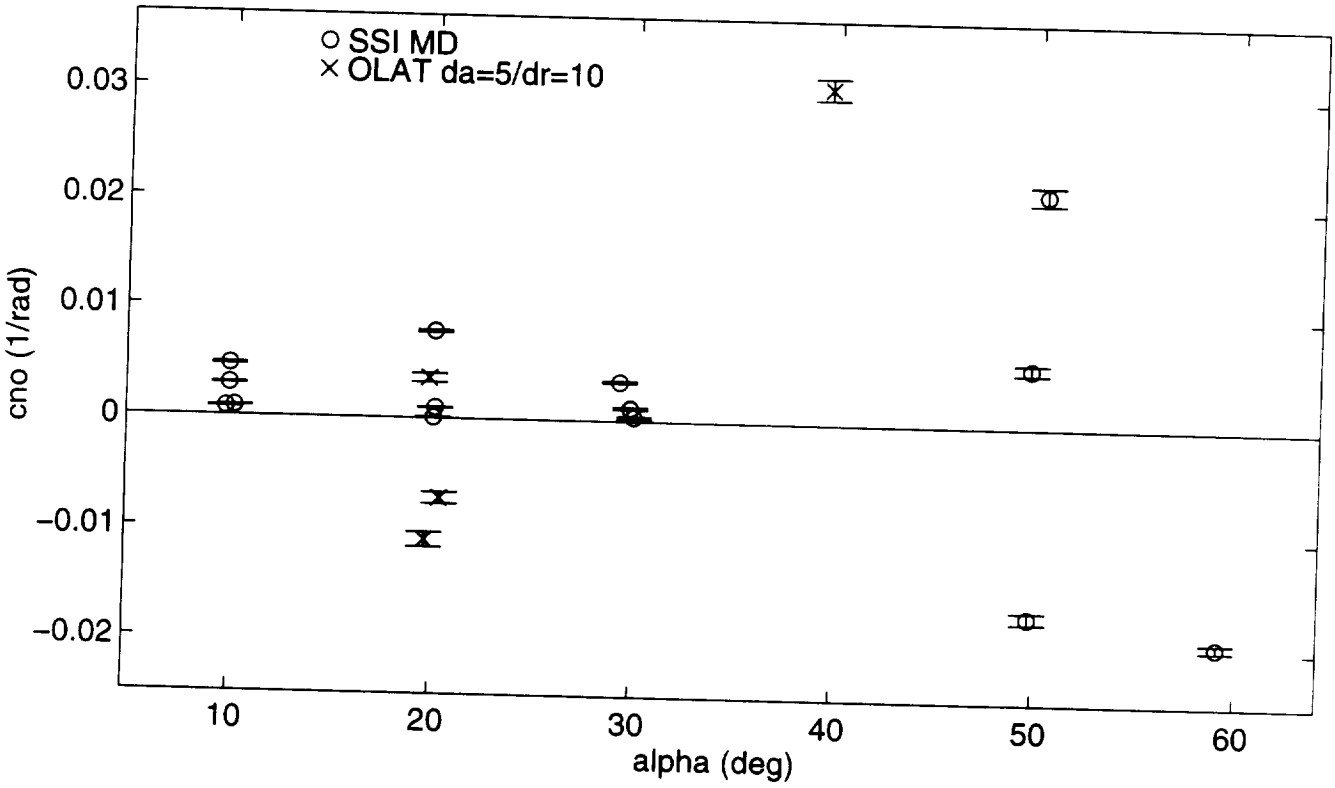
SSI MD
OLAT da=5/dr=10
cno (1/rad)
0.03
0.02
0.01
0
−0.01
−0.02
10
20
30
40
50
60
alpha (deg)

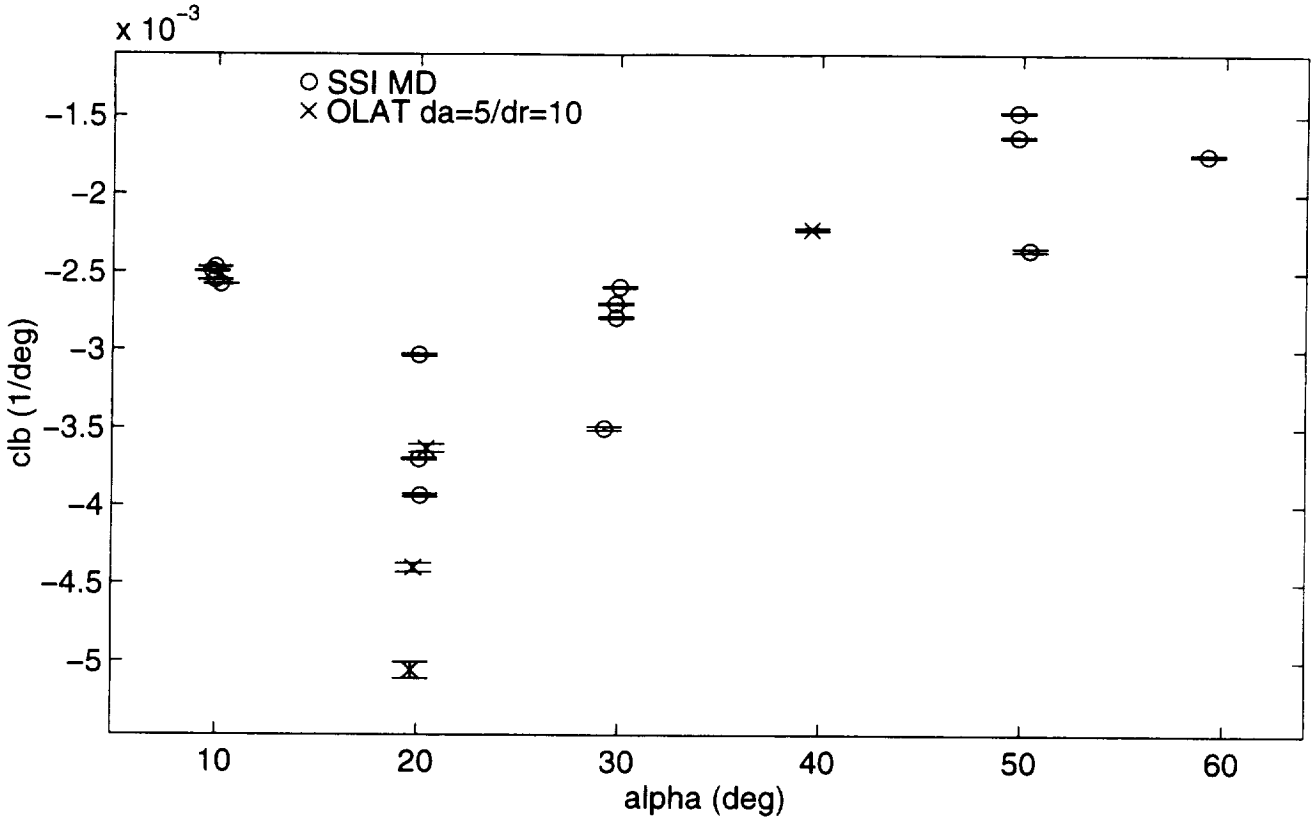
x 10^-3
SSI MD
OLAT da=5/dr=10
-1.5
-2
-2.5
-3
-3.5
-4
-4.5
-5
clb (1/deg)
10
20
30
40
50
60
alpha (deg)

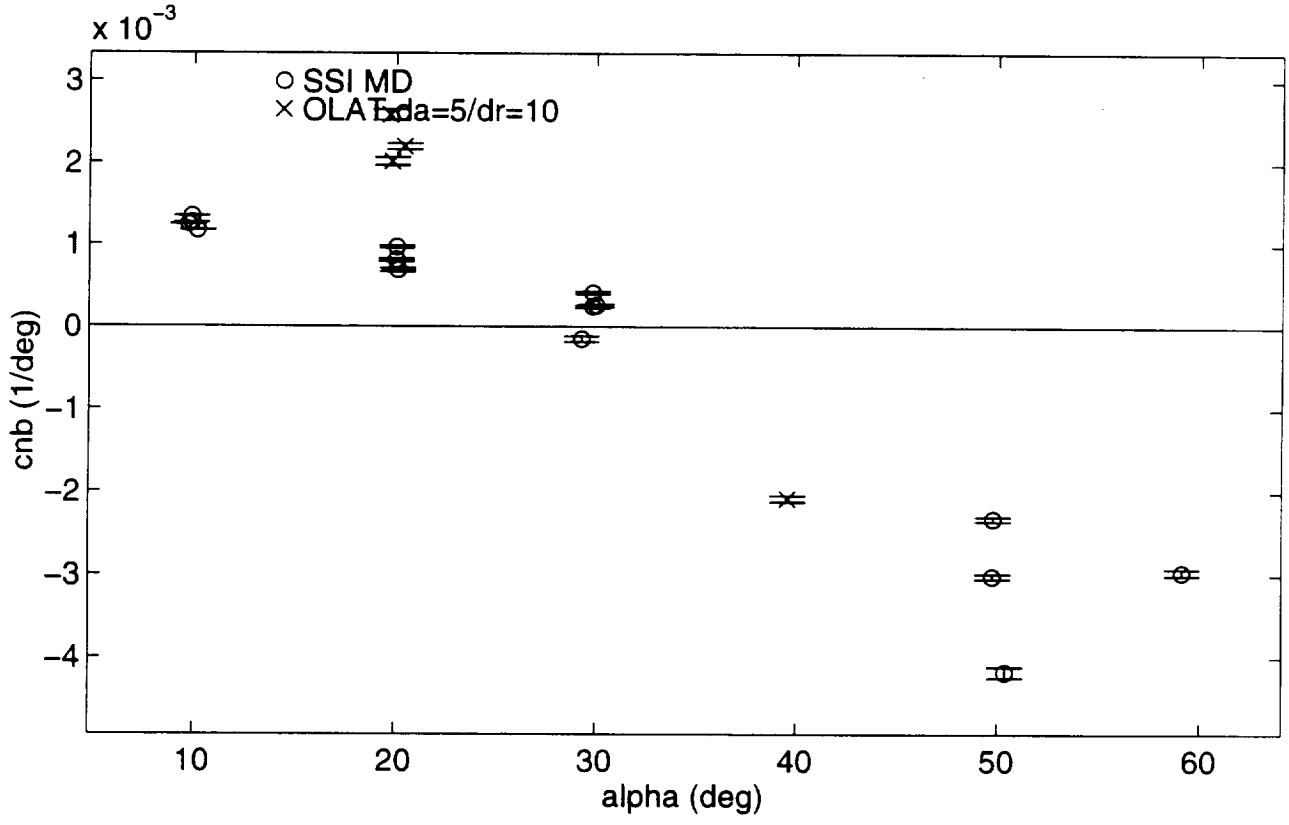
x 10^-3
SSI MD
OLAT da=5/dr=10
3
2
1
0
-1
-2
-3
-4
cnb (1/deg)
10
20
30
40
50
60
alpha (deg)

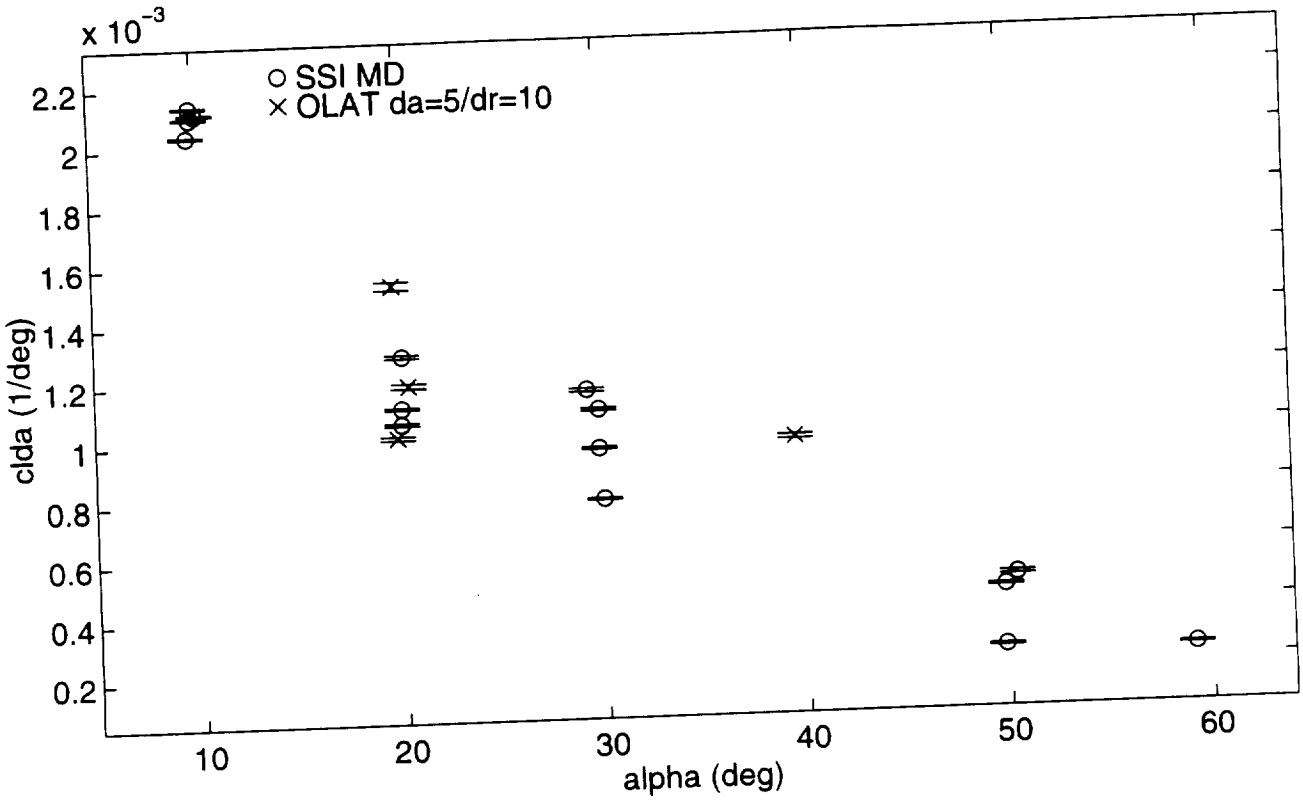
x 10^-3
SSI MD
OLAT da=5/dr=10
clda (1/deg)
alpha (deg)

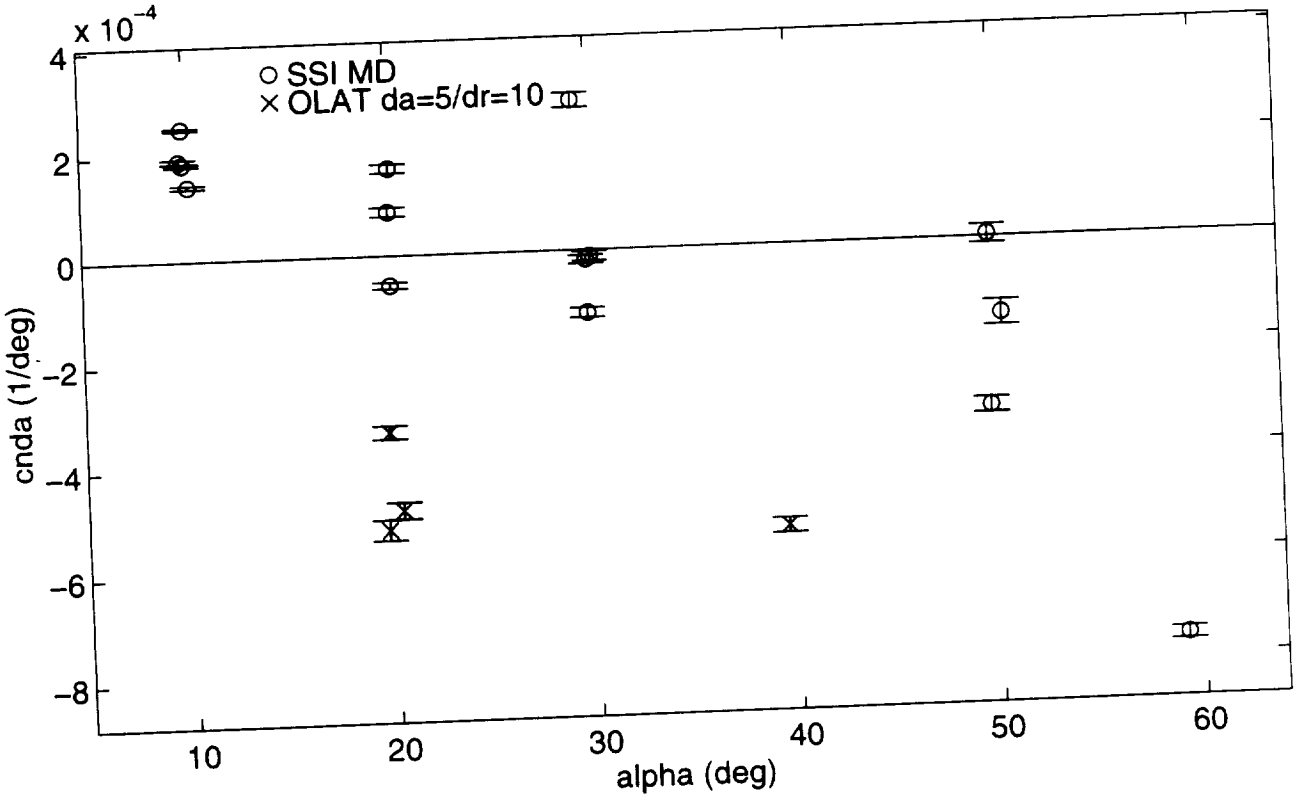
x 10^-4
SSI MD
OLAT da=5/dr=10
cnda (1/deg)
alpha (deg)

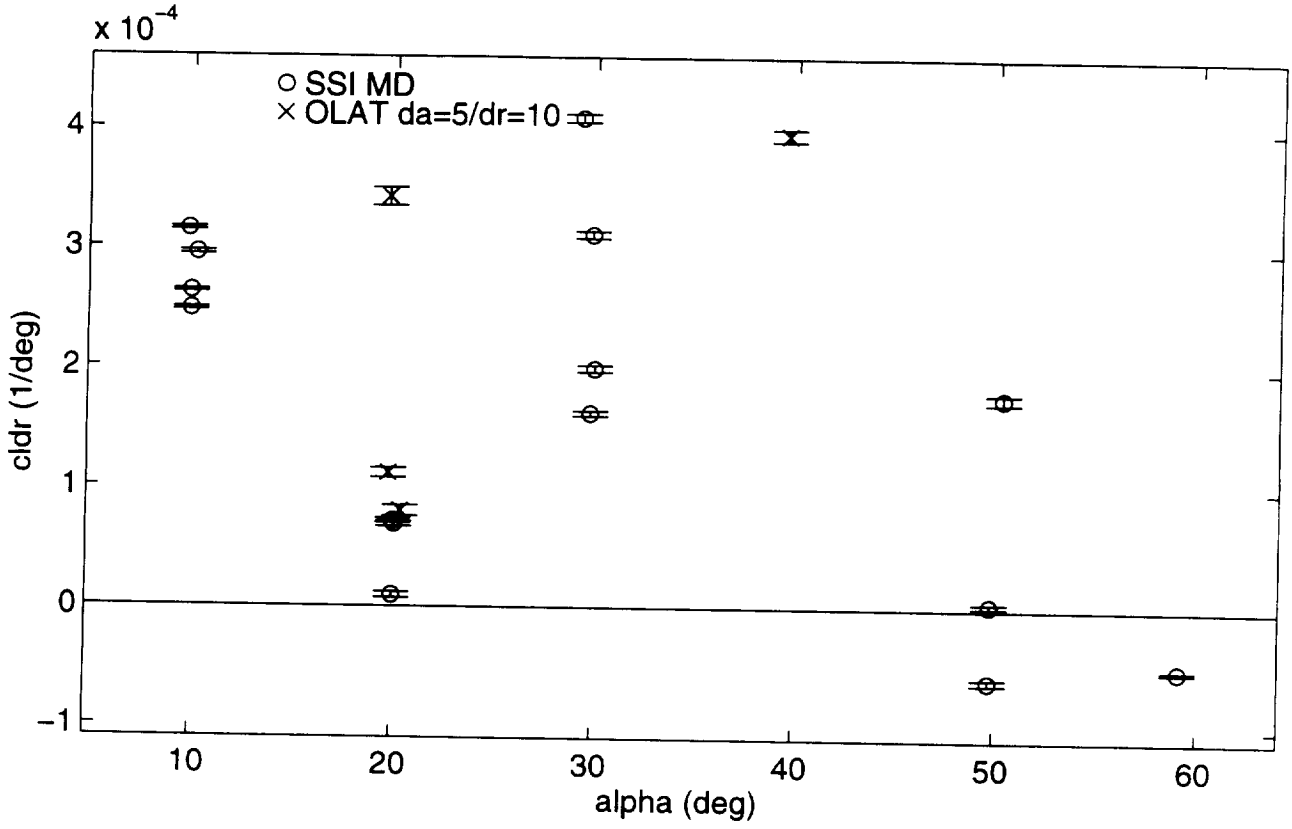
x 10^-4
SSI MD
OLAT da=5/dr=10
cldr (1/deg)
alpha (deg)
4
3
2
1
0
-1
10
20
30
40
50
60

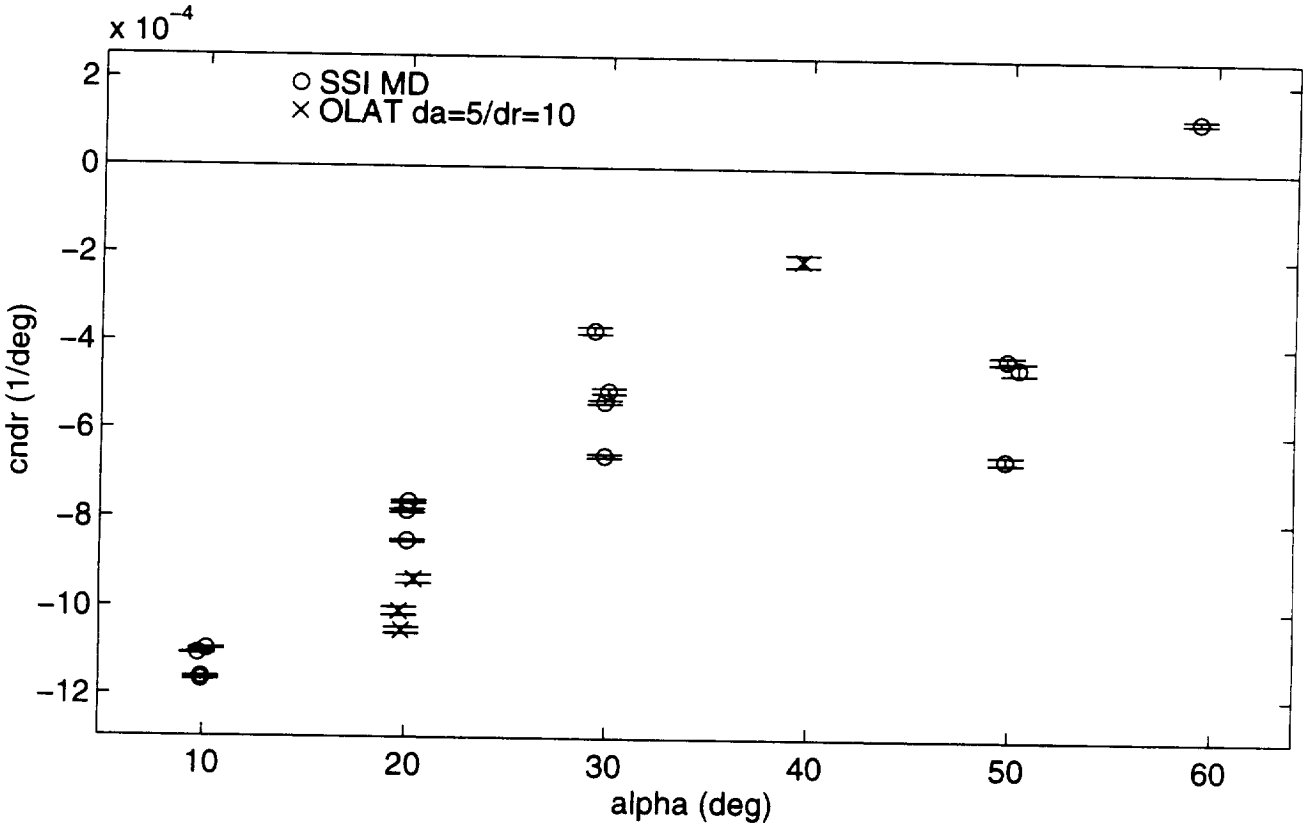
x 10^-4
SSI MD
OLAT da=5/dr=10
cndr (1/deg)
alpha (deg)
2
0
-2
-4
-6
-8
-10
-12
10
20
30
40
50
60

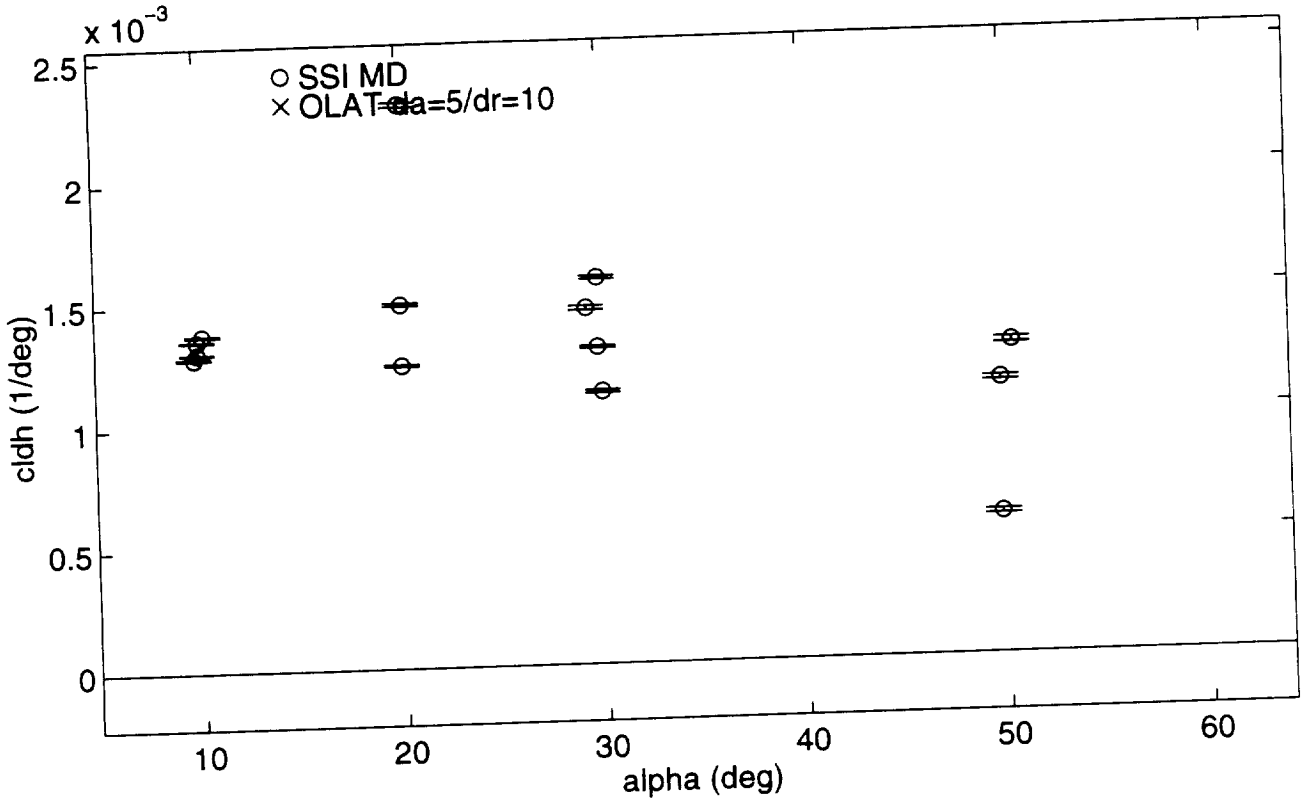
x 10^-3
SSI MD
OLAT da=5/dr=10
cldh (1/deg)
alpha (deg)

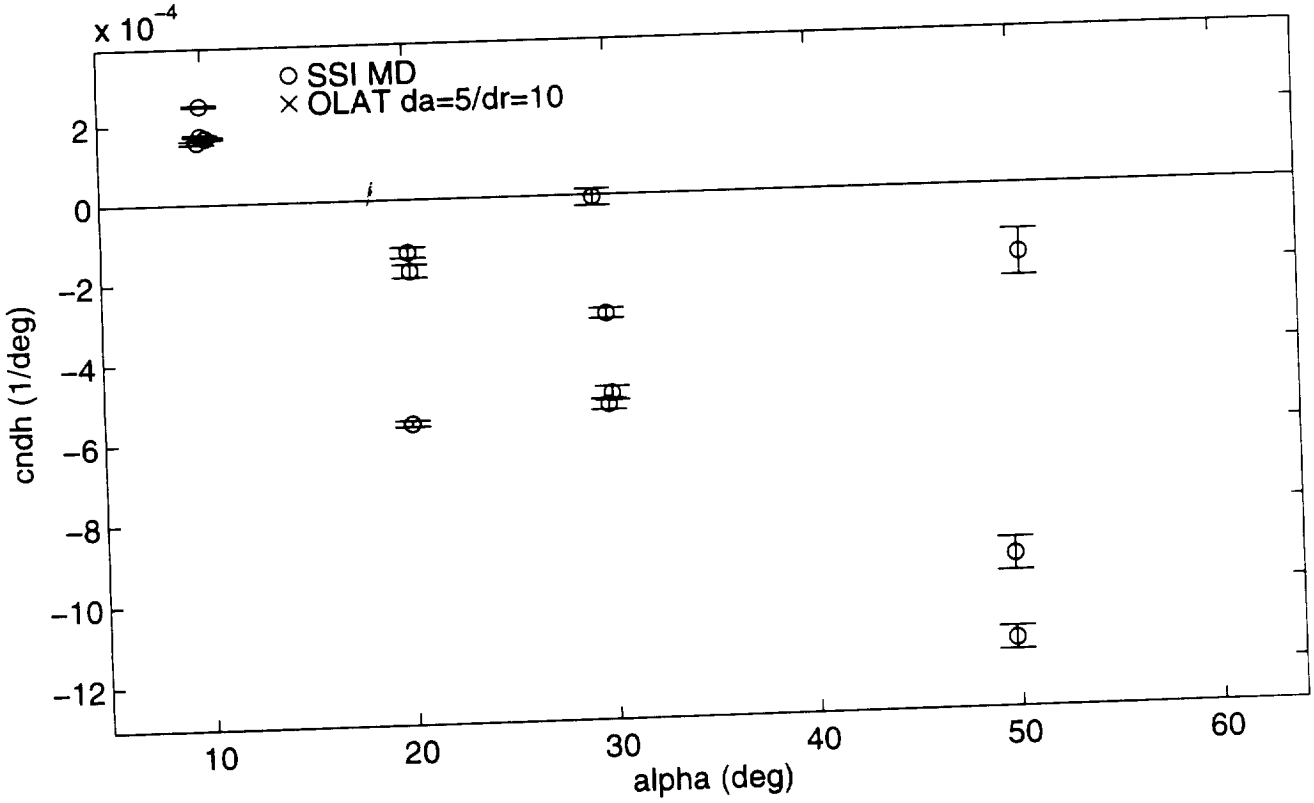
x 10^-4
SSI MD
OLAT da=5/dr=10
cndh (1/deg)
alpha (deg)

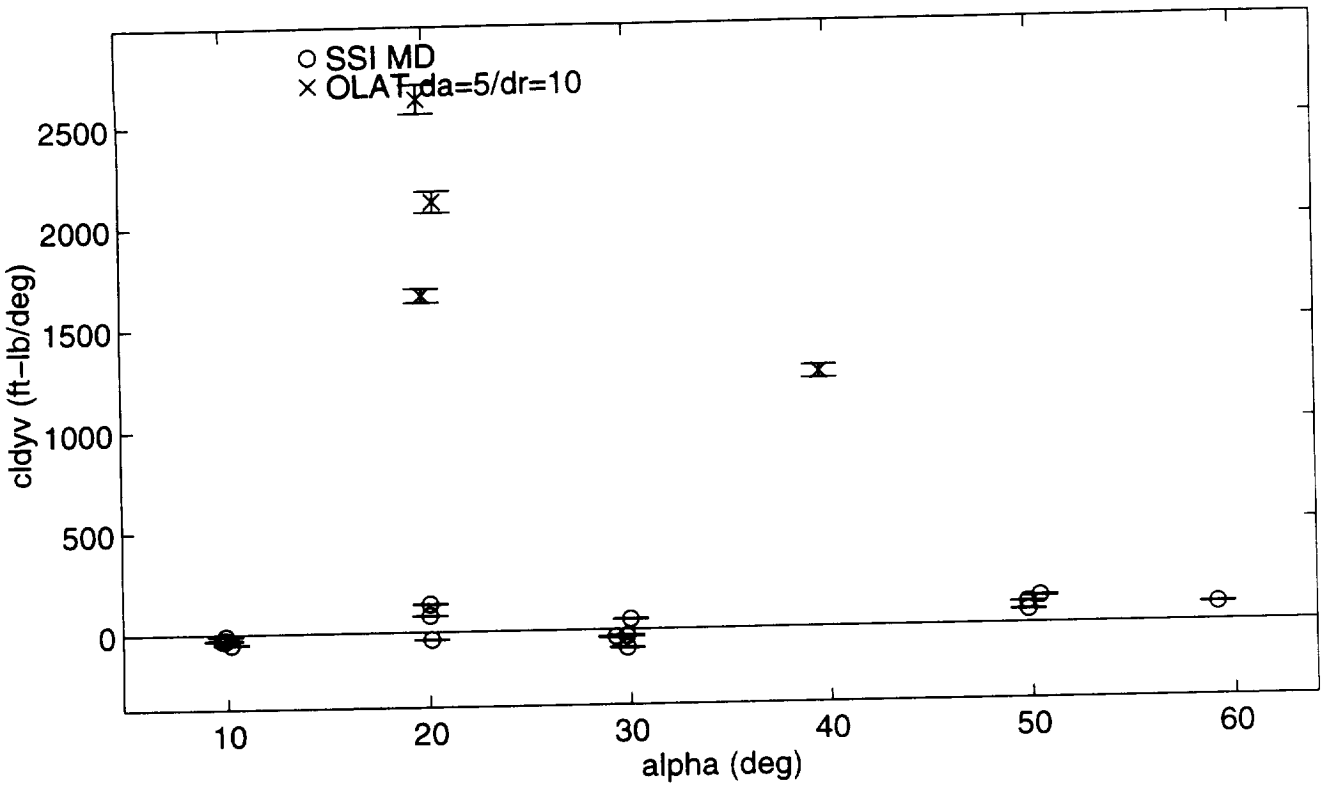
SSI MD
OLAT da=5/dr=10
cldyv (ft-lb/deg)
2500
2000
1500
1000
500
0
10
20
30
40
50
60
alpha (deg)

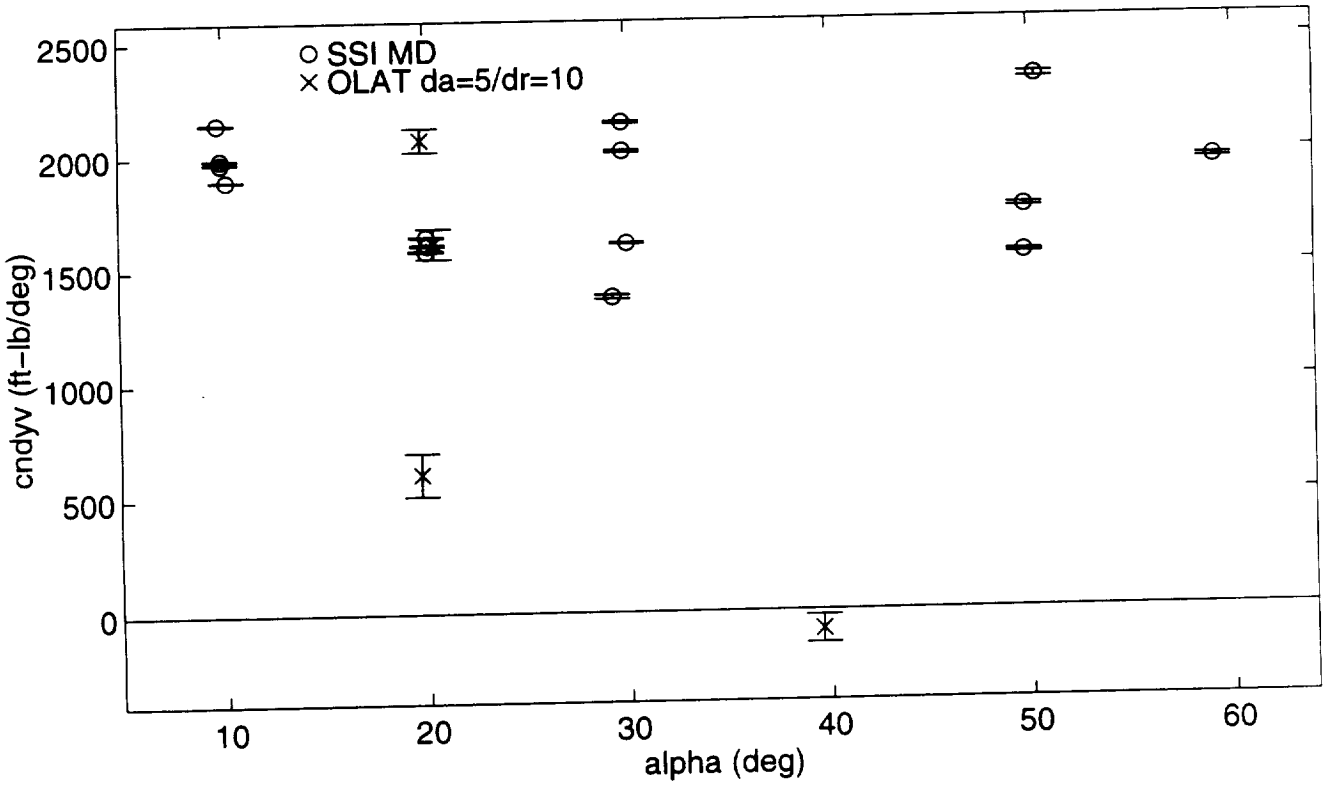
SSI MD
OLAT da=5/dr=10
cndyv (ft-lb/deg)
2500
2000
1500
1000
500
0
10
20
30
40
50
60
alpha (deg)

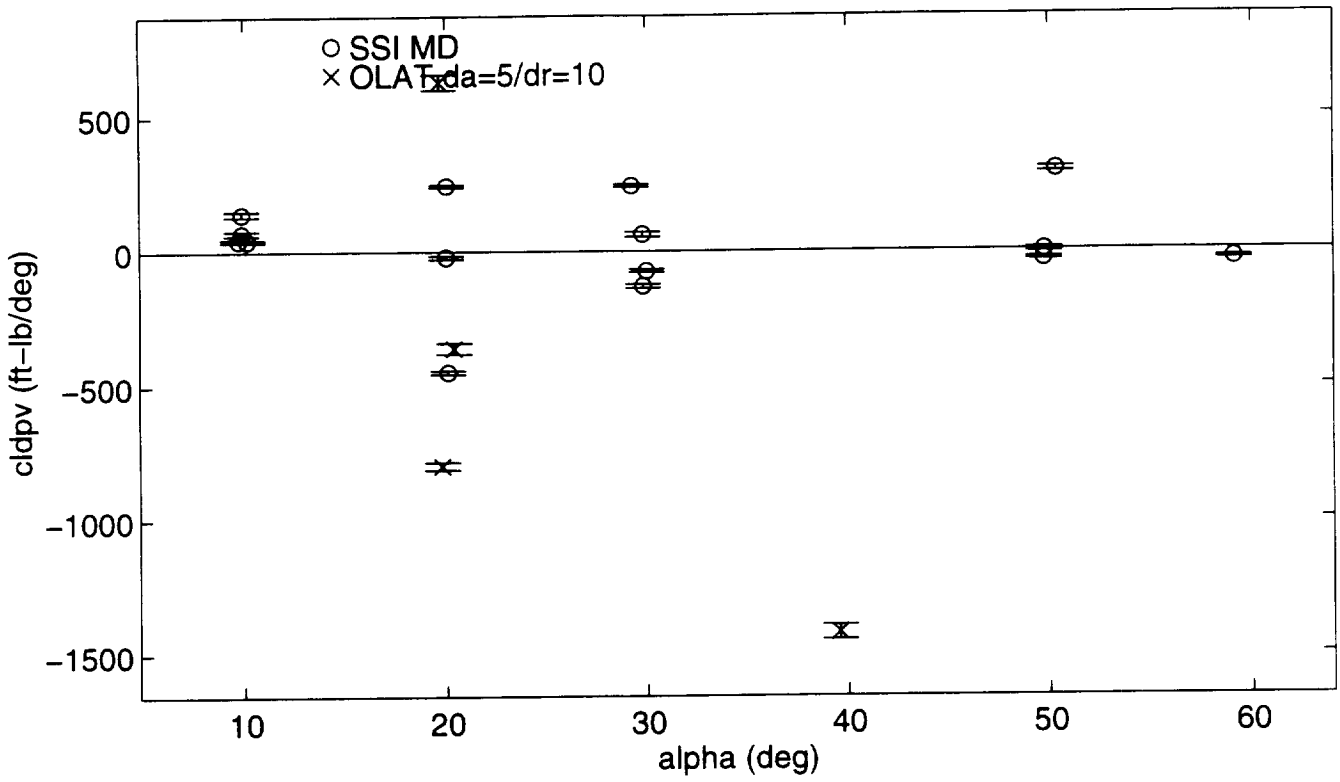
SSI MD
OLAT da=5/dr=10
500
0
−500
−1000
−1500
cldpv (ft−lb/deg)
10
20
30
40
50
60
alpha (deg)

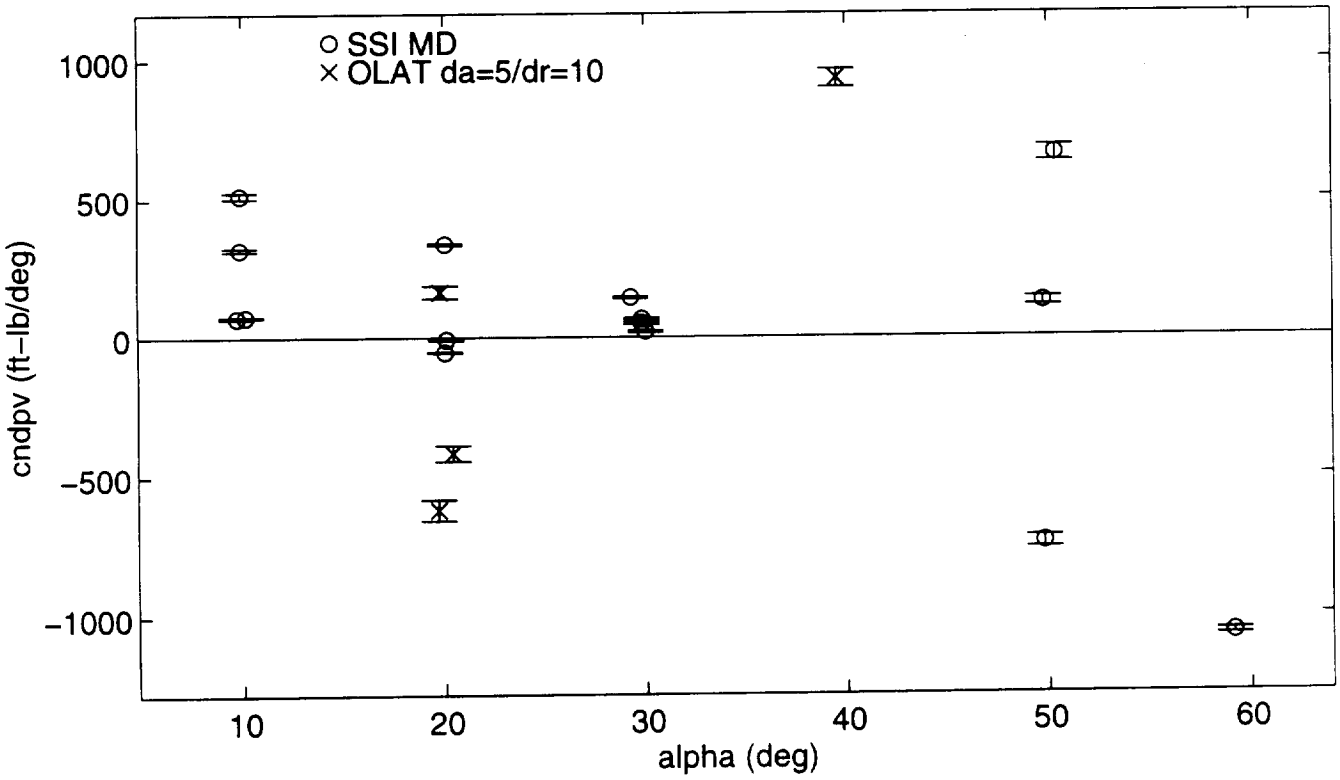
SSI MD
OLAT da=5/dr=10
1000
500
0
−500
−1000
cndpv (ft−lb/deg)
10
20
30
40
50
60
alpha (deg)

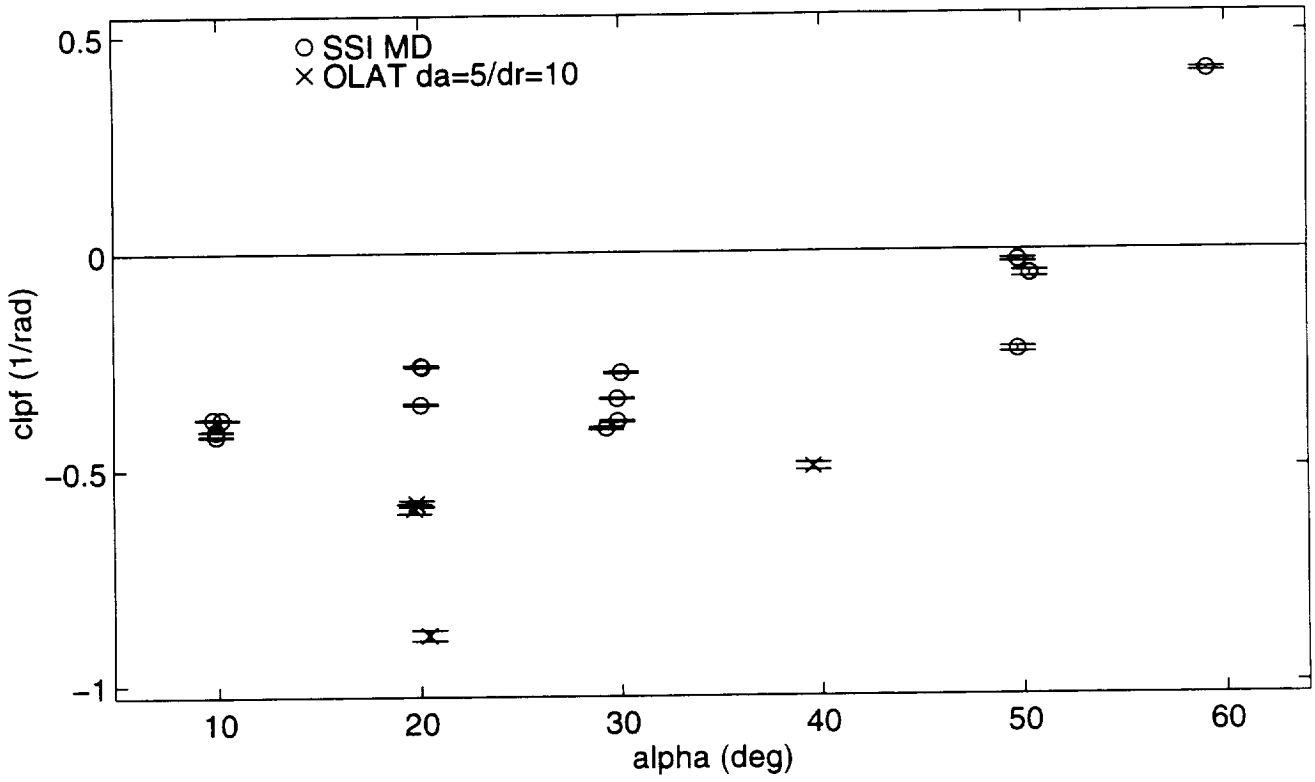
○ SSI MD
× OLAT da=5/dr=10
clpf (1/rad)
0.5
0
−0.5
−1
10
20
30
40
50
60
alpha (deg)

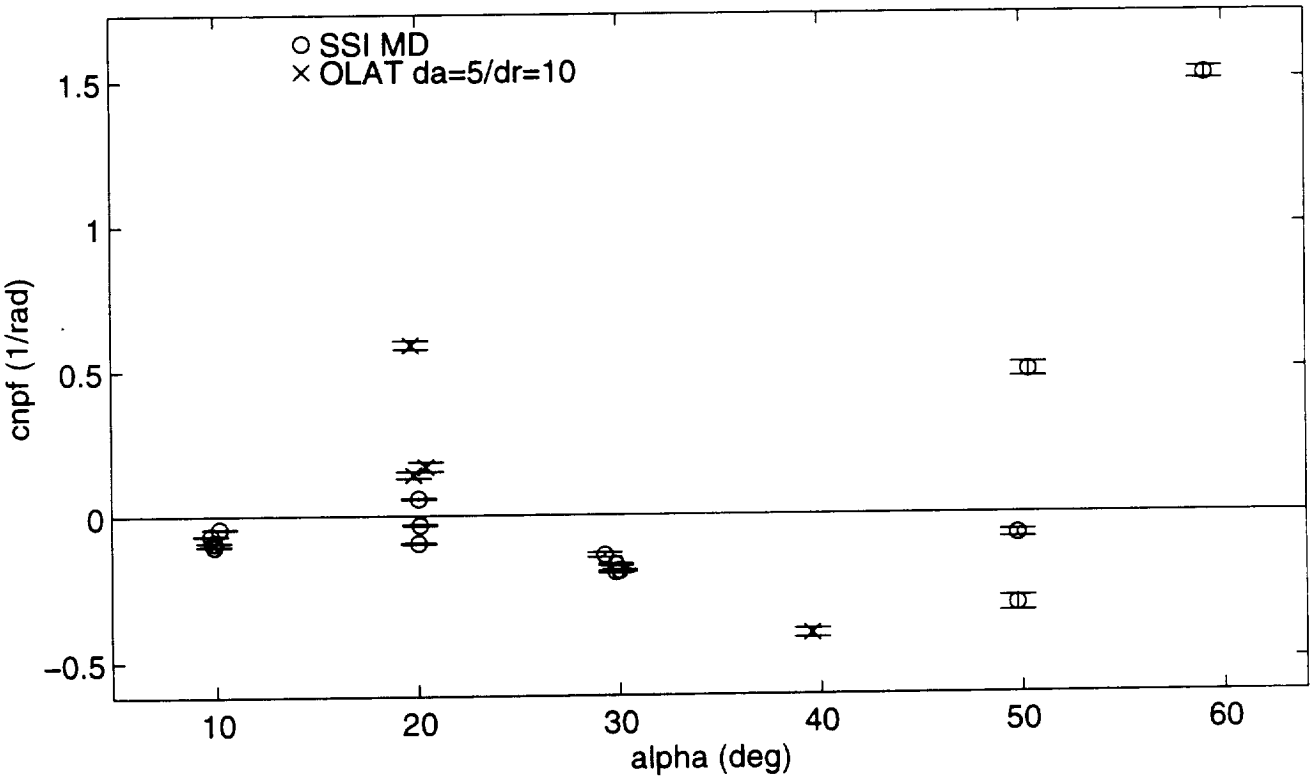
○ SSI MD
× OLAT da=5/dr=10
cnpf (1/rad)
1.5
1
0.5
0
−0.5
10
20
30
40
50
60
alpha (deg)

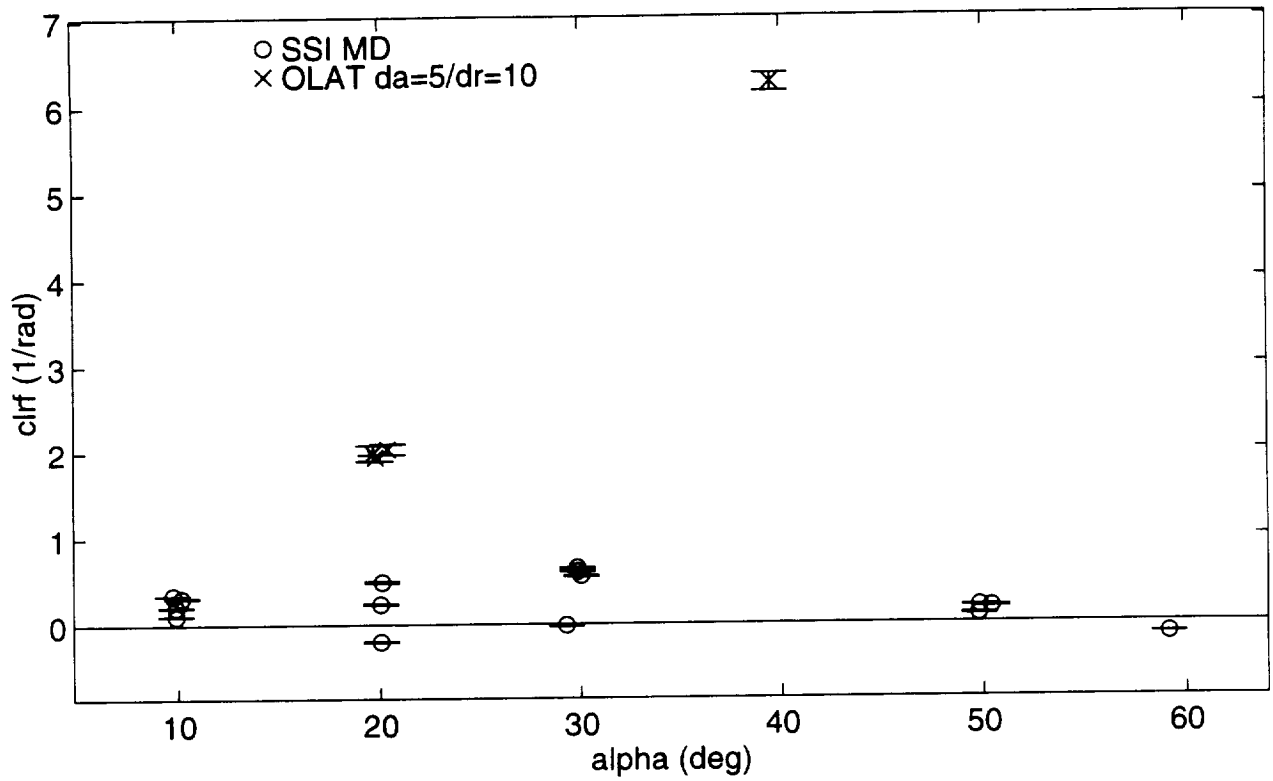
SSI MD
OLAT da=5/dr=10
clrf (1/rad)
alpha (deg)
7
6
5
4
3
2
1
0
10
20
30
40
50
60

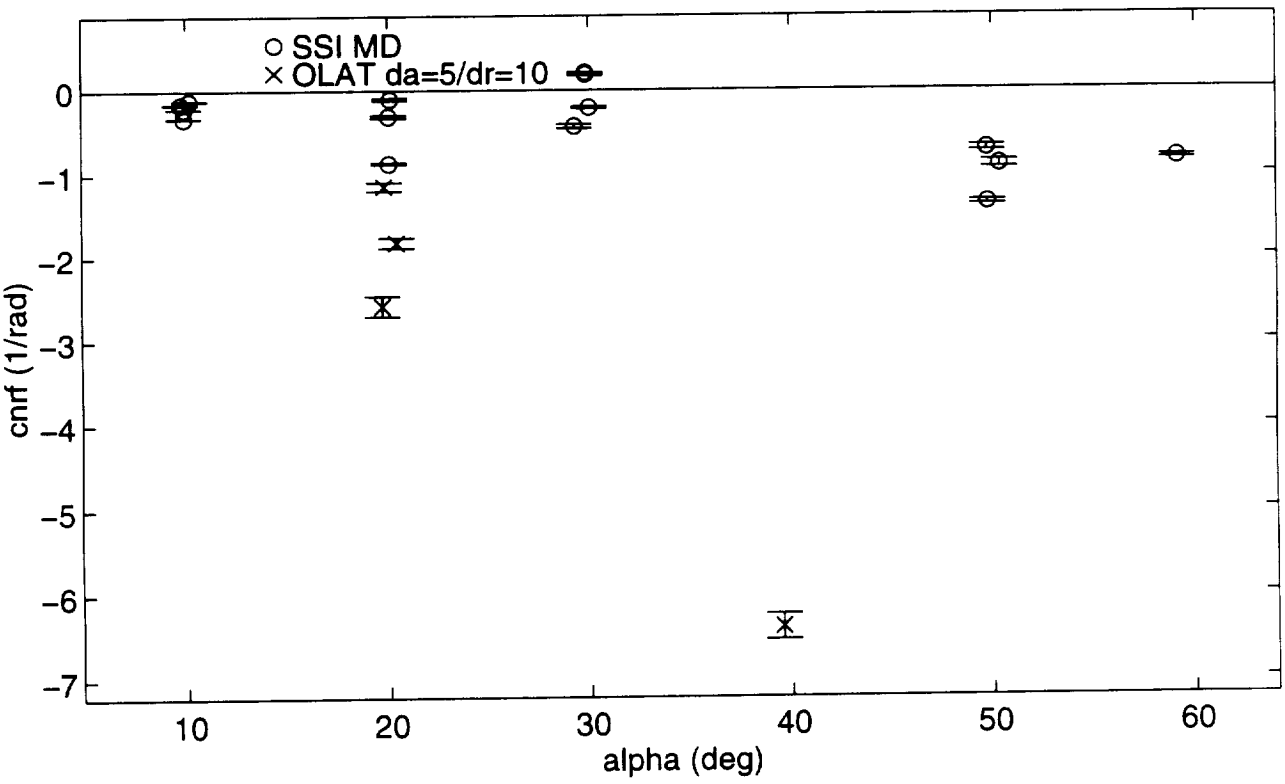
SSI MD
OLAT da=5/dr=10
cnrf (1/rad)
alpha (deg)
0
−1
−2
−3
−4
−5
−6
−7
10
20
30
40
50
60

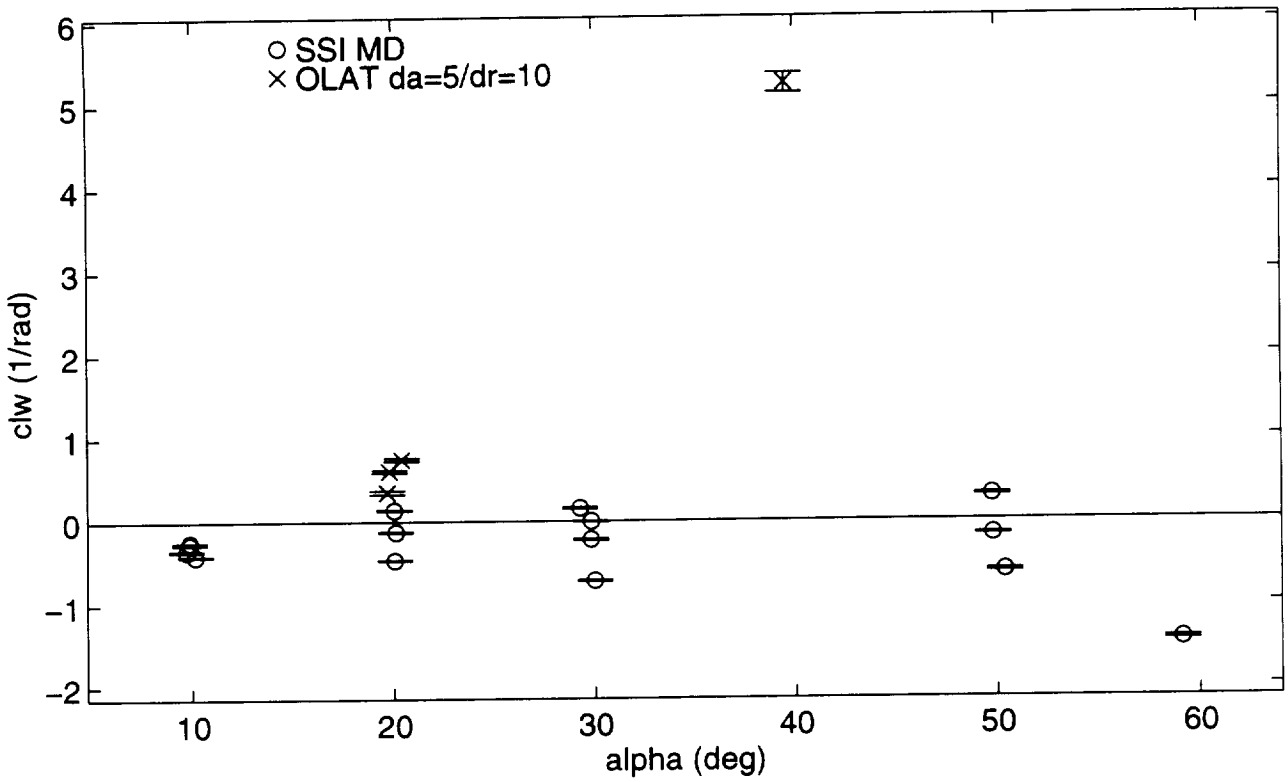
o SSI MD
× OLAT da=5/dr=10
clw (1/rad)
alpha (deg)
6
5
4
3
2
1
0
−1
−2
10
20
30
40
50
60

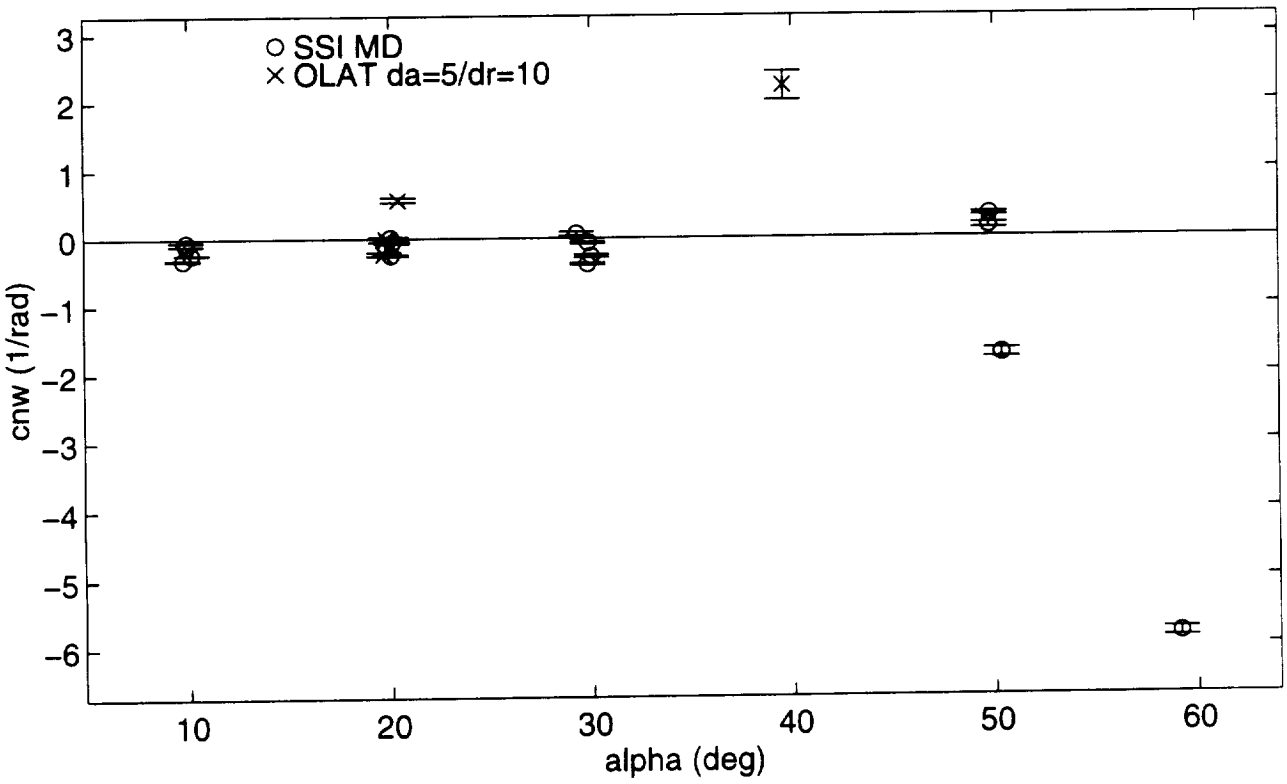
o SSI MD
× OLAT da=5/dr=10
cnw (1/rad)
alpha (deg)
3
2
1
0
−1
−2
−3
−4
−5
−6
10
20
30
40
50
60

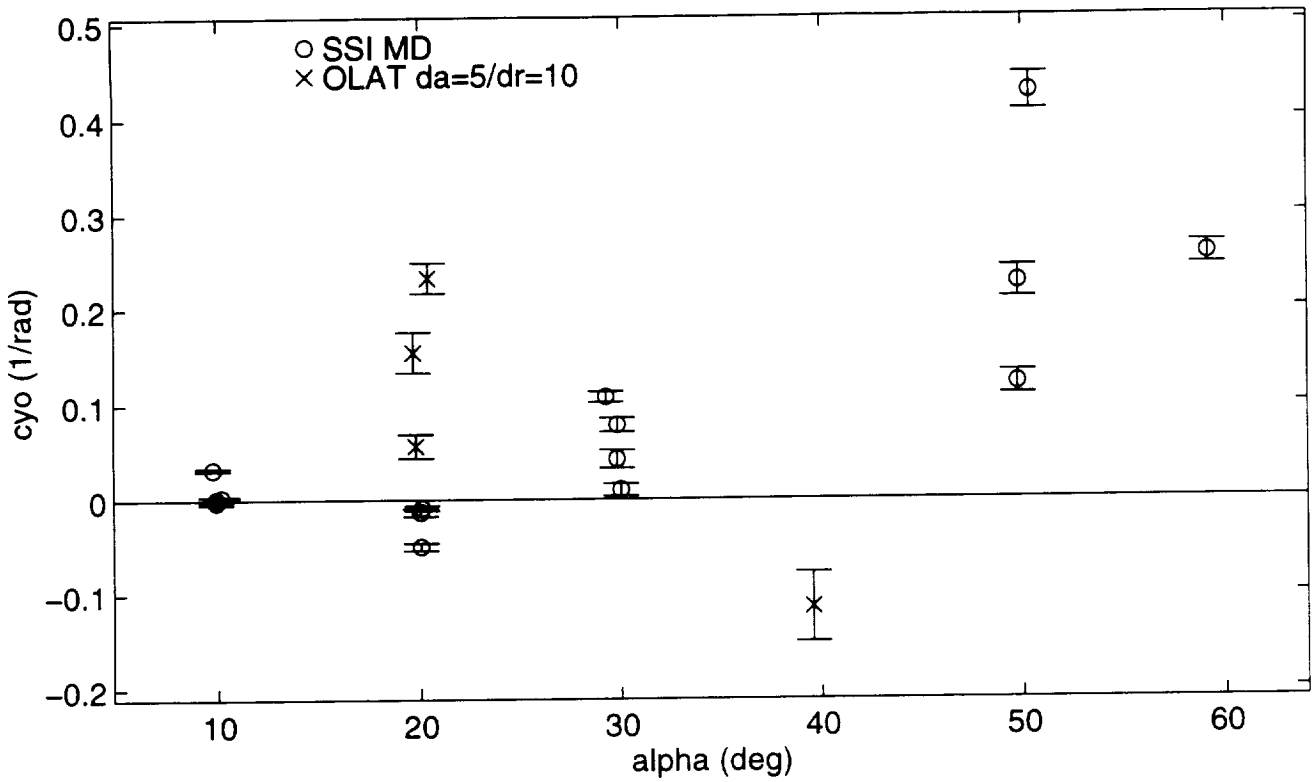
SSI MD
OLAT da=5/dr=10
cyo (1/rad)
alpha (deg)
0.5
0.4
0.3
0.2
0.1
0
−0.1
−0.2
10
20
30
40
50
60

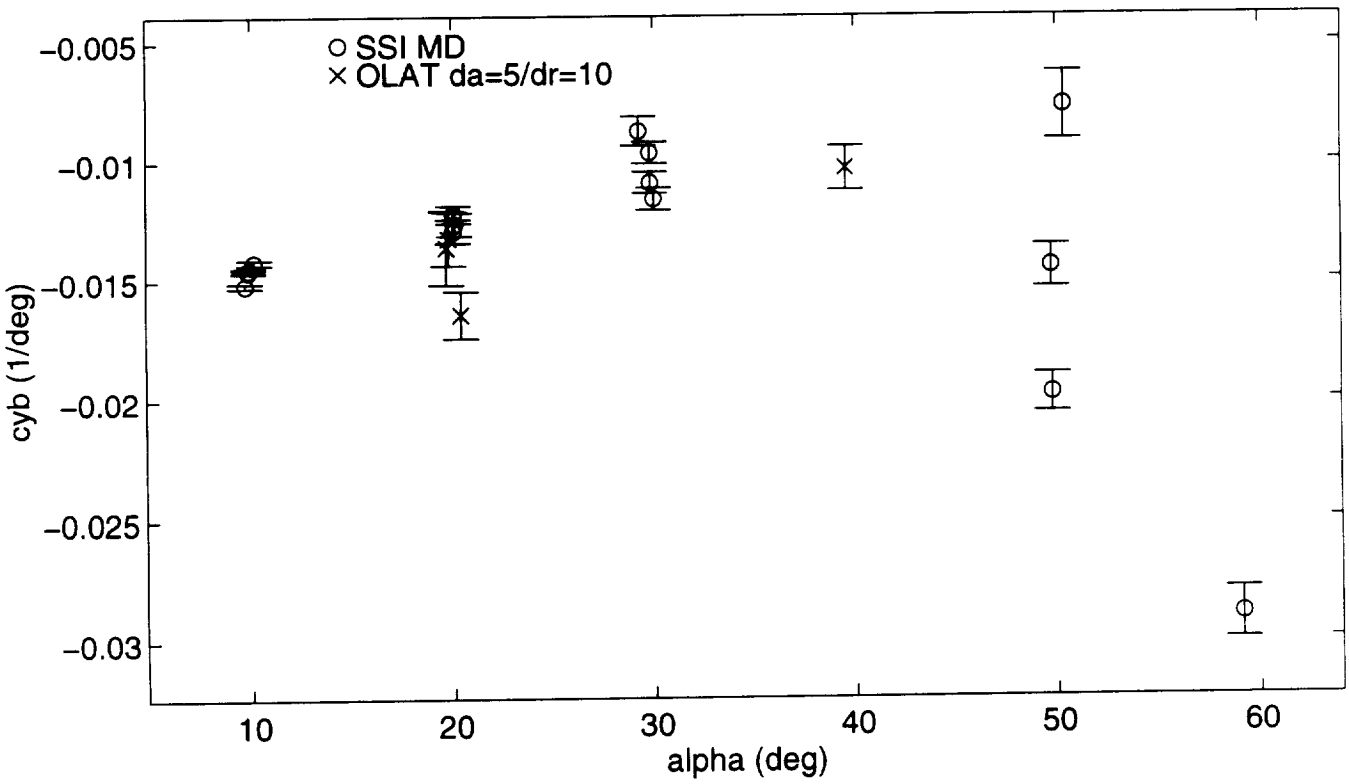
SSI MD
OLAT da=5/dr=10
cyb (1/deg)
alpha (deg)
−0.005
−0.01
−0.015
−0.02
−0.025
−0.03
10
20
30
40
50
60

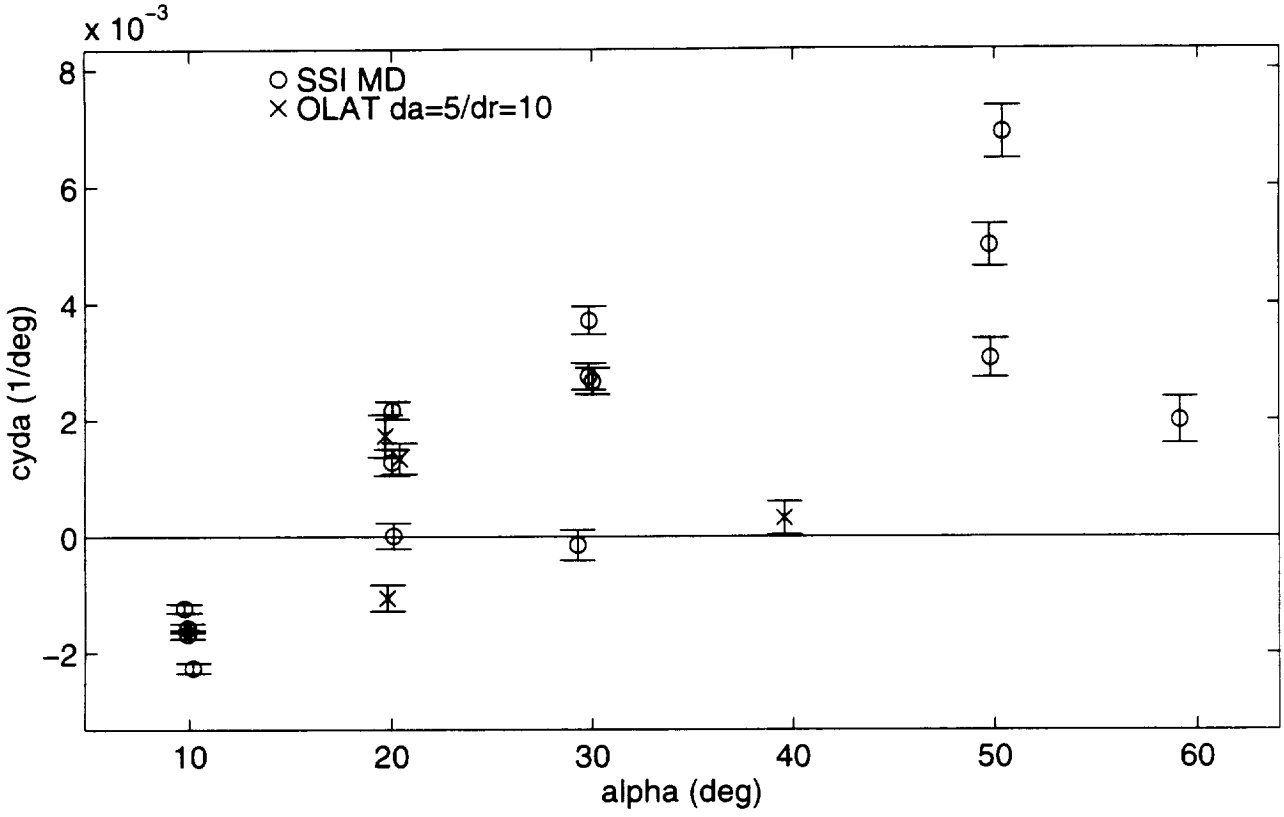
x 10^-3
SSI MD
OLAT da=5/dr=10
cyda (1/deg)
alpha (deg)

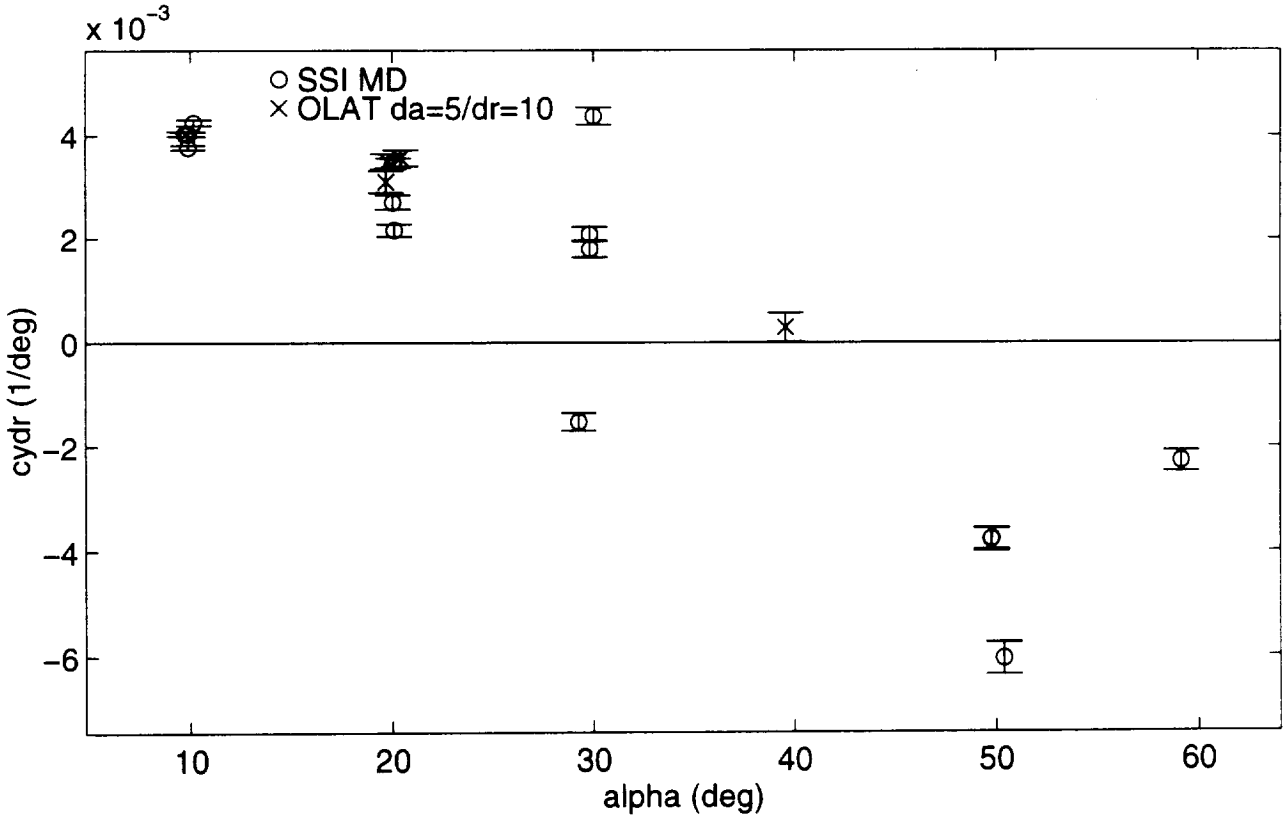
x 10^-3
SSI MD
OLAT da=5/dr=10
cydr (1/deg)
alpha (deg)

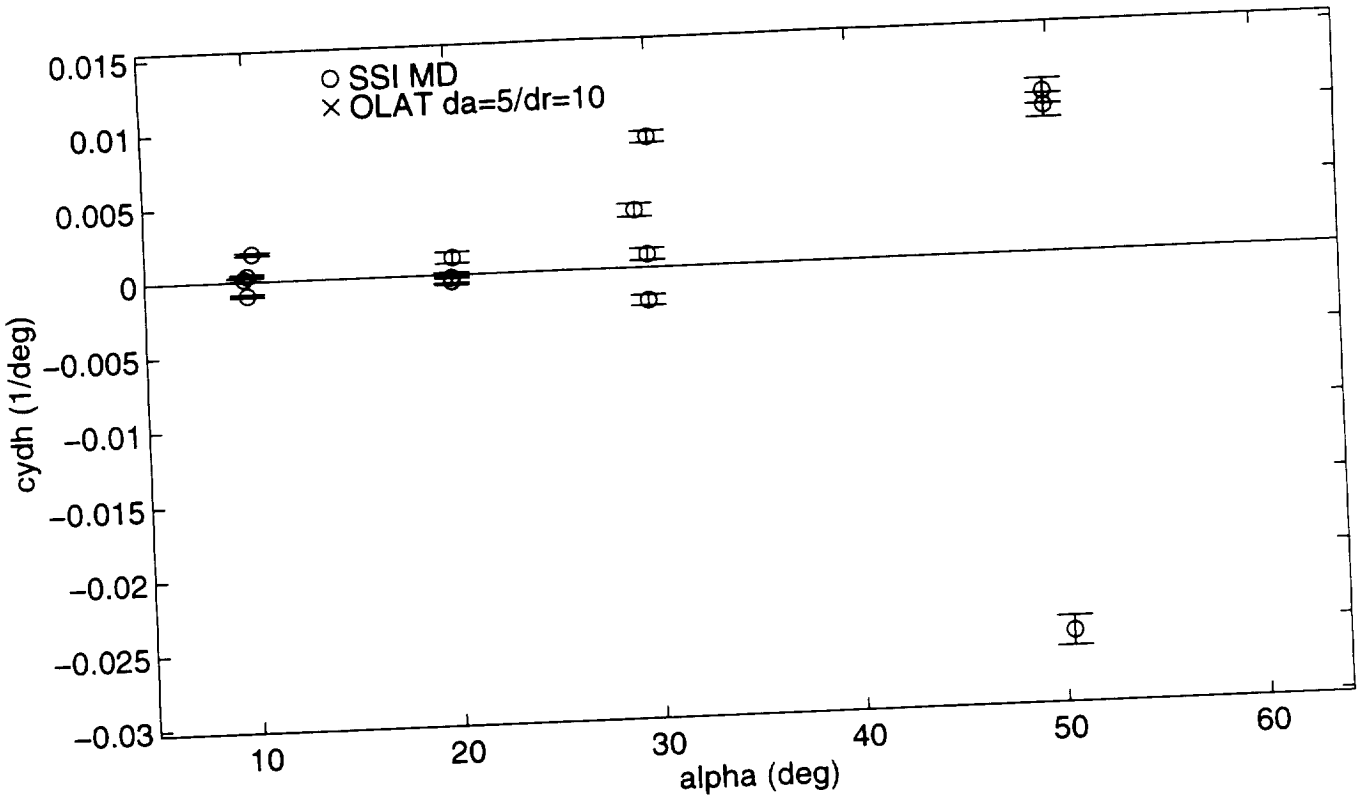
SSI MD
OLAT da=5/dr=10
cydh (1/deg)
alpha (deg)
0.015
0.01
0.005
0
-0.005
-0.01
-0.015
-0.02
-0.025
-0.03
10
20
30
40
50
60

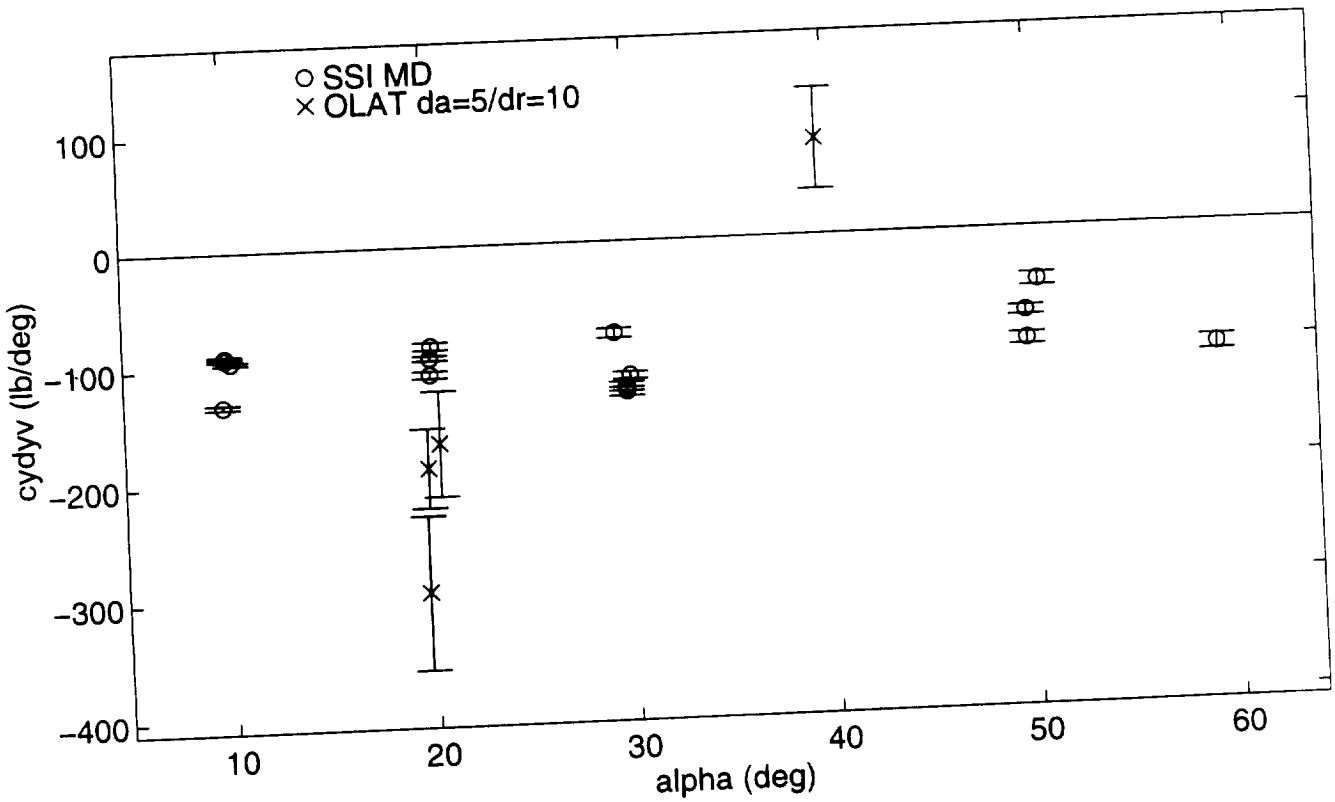
SSI MD
OLAT da=5/dr=10
cydyv (lb/deg)
alpha (deg)
100
0
-100
-200
-300
-400
10
20
30
40
50
60

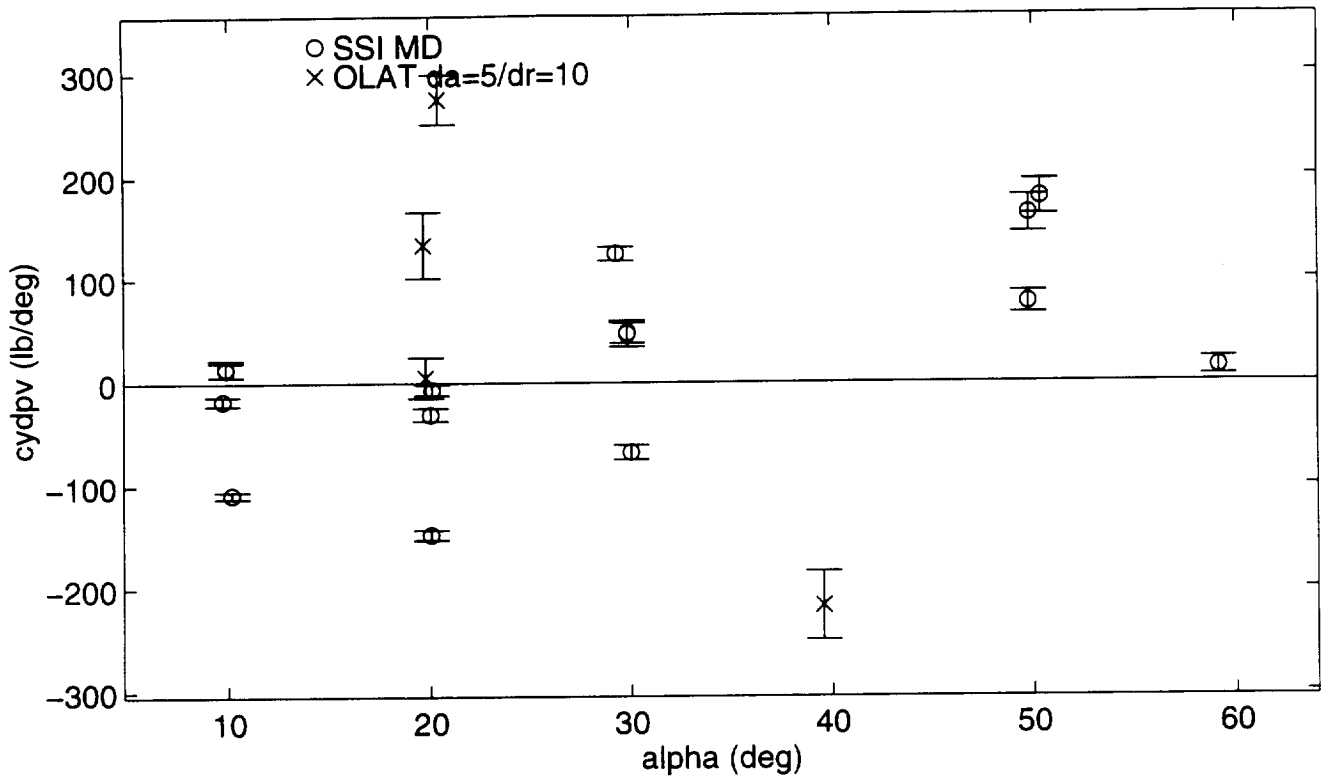
SSI MD
OLAT da=5/dr=10
cydpv (lb/deg)
alpha (deg)
300
200
100
0
−100
−200
−300
10
20
30
40
50
60

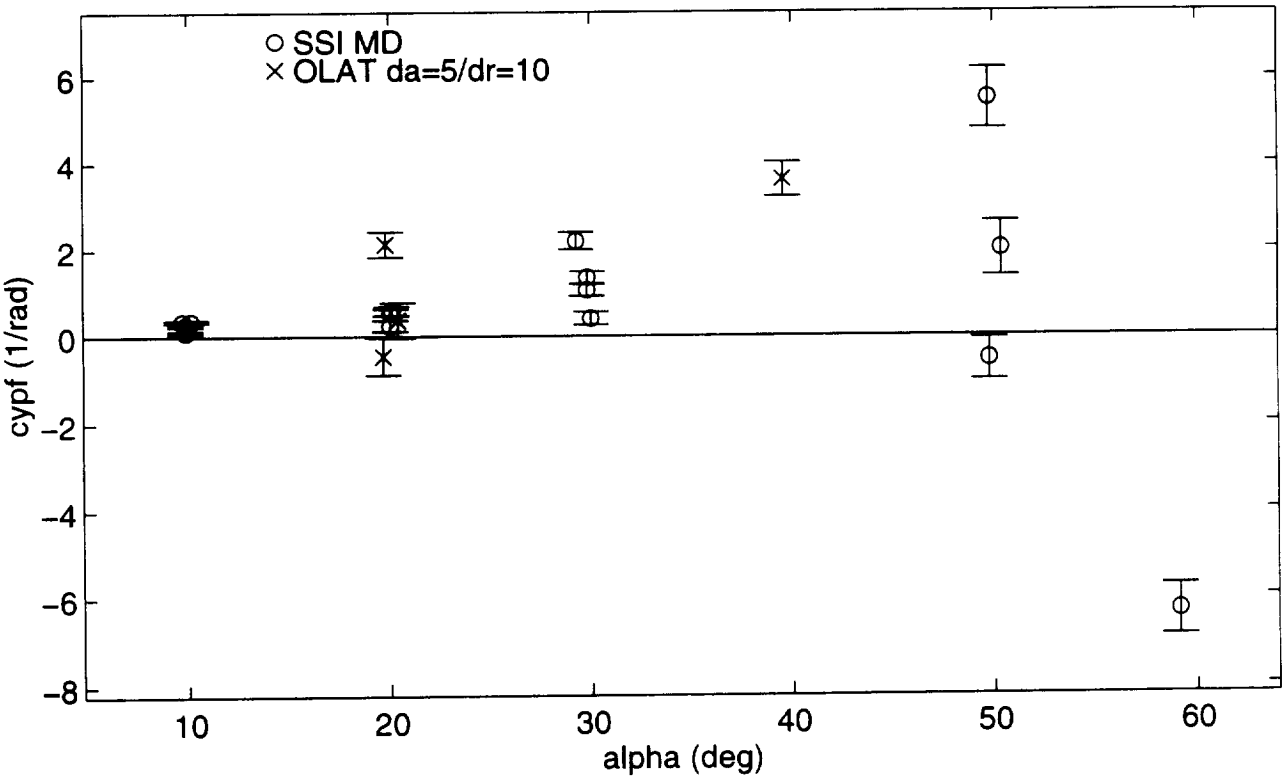
SSI MD
OLAT da=5/dr=10
cypf (1/rad)
alpha (deg)
6
4
2
0
−2
−4
−6
−8
10
20
30
40
50
60

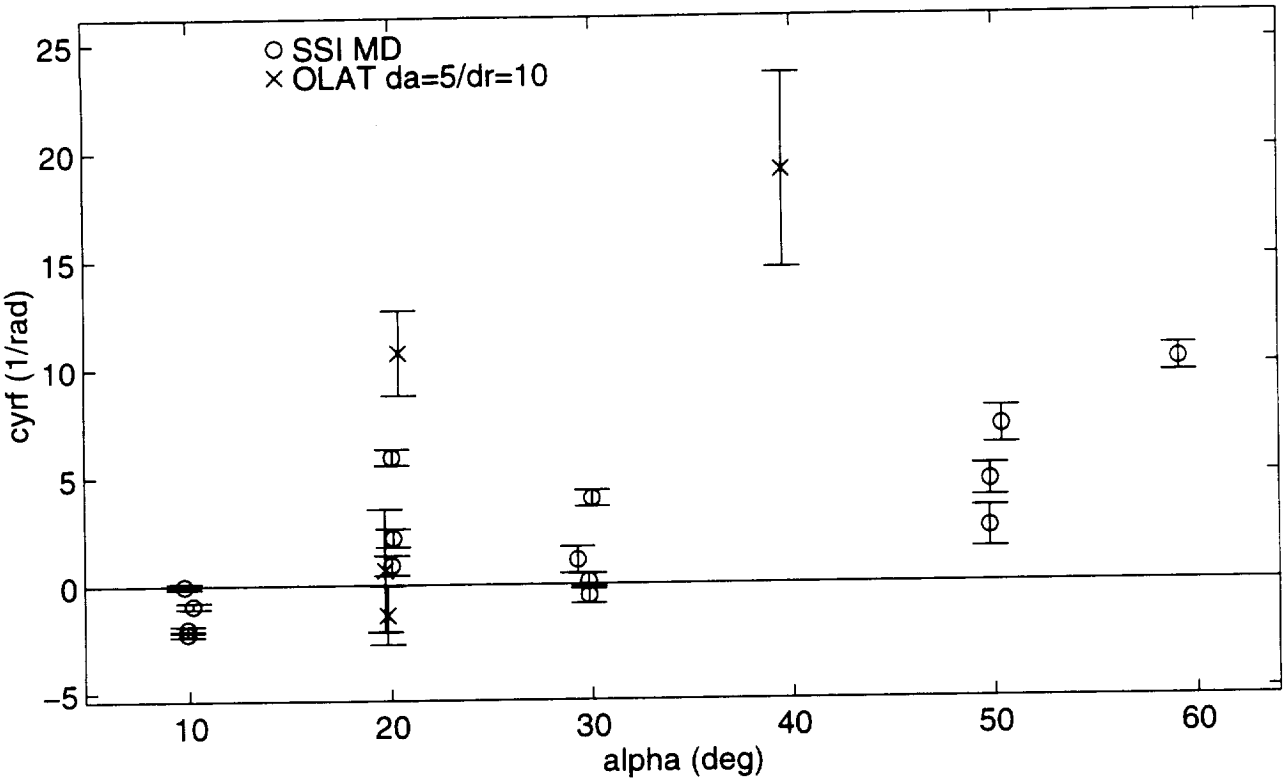
SSI MD
OLAT da=5/dr=10
cyrf (1/rad)
alpha (deg)
25
20
15
10
5
0
−5
10
20
30
40
50
60

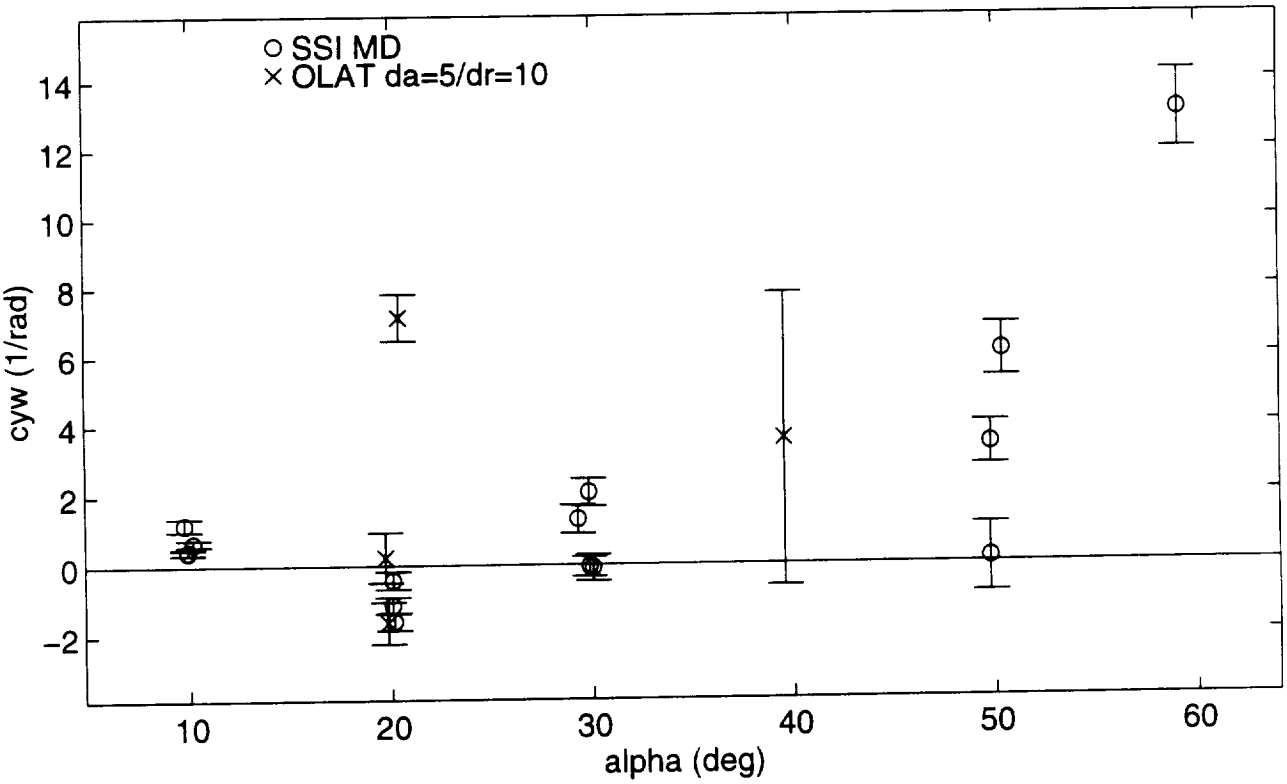
SSI MD
OLAT da=5/dr=10
cyw (1/rad)
alpha (deg)
14
12
10
8
6
4
2
0
−2
10
20
30
40
50
60

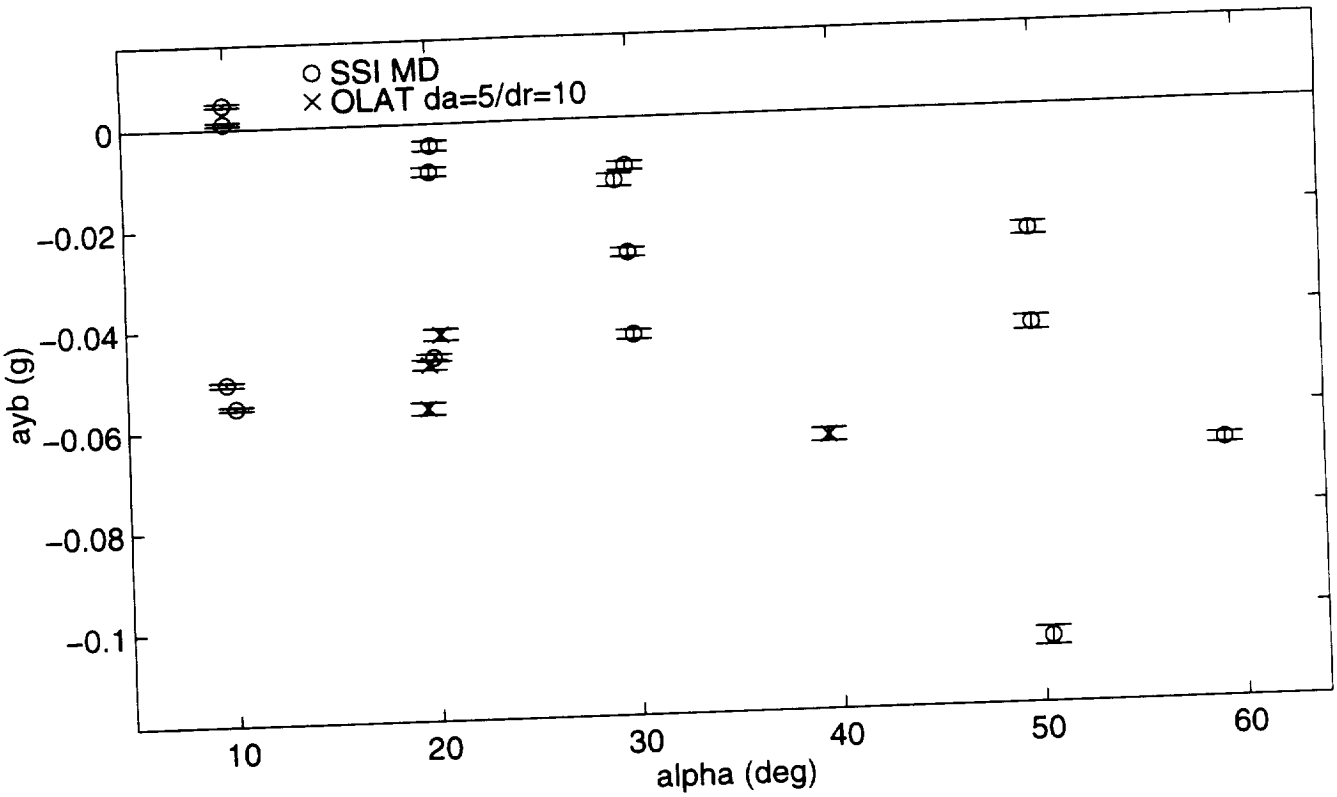
SSI MD
OLAT da=5/dr=10
0
-0.02
-0.04
-0.06
-0.08
-0.1
ayb (g)
10
20
30
40
50
60
alpha (deg)

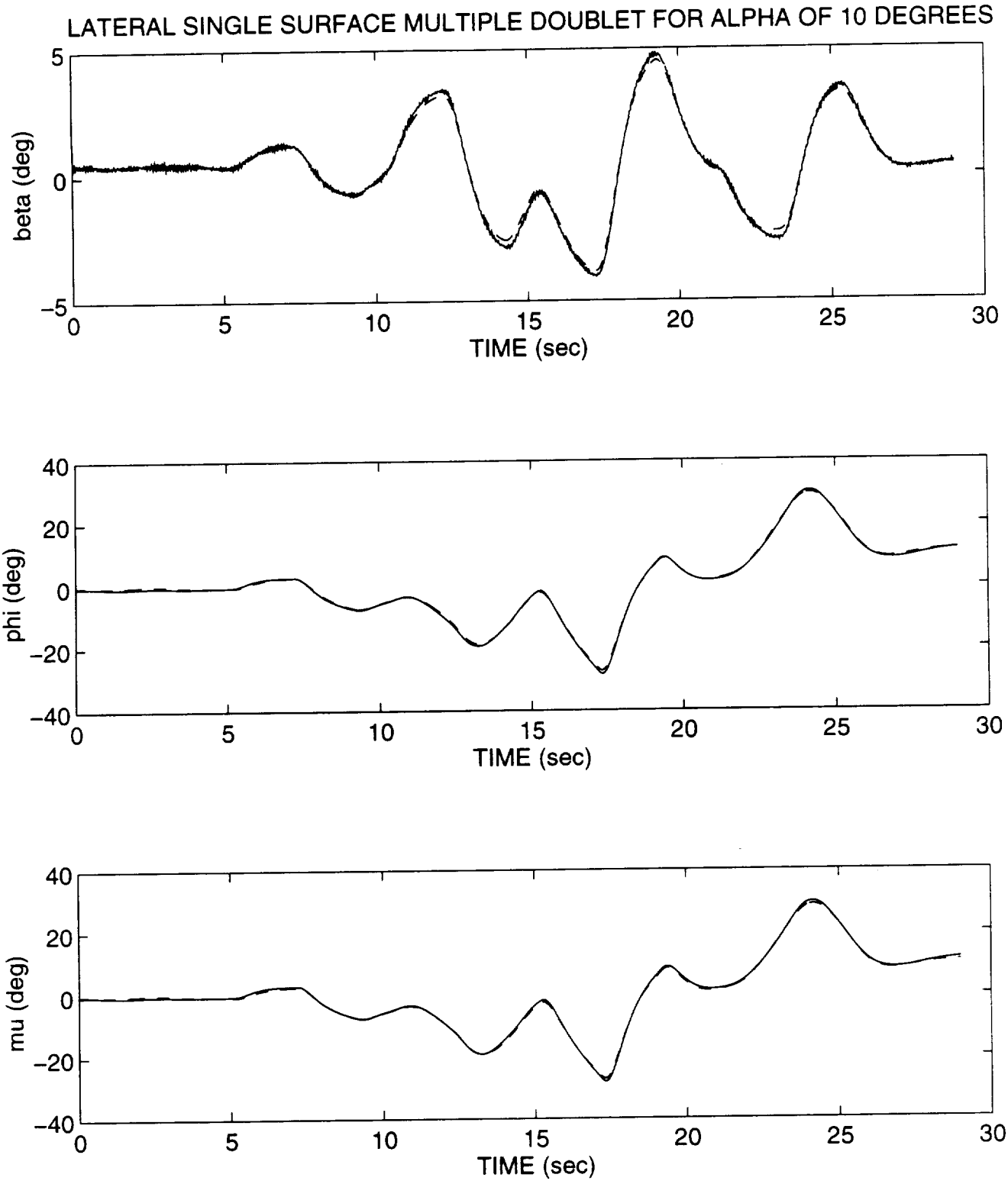
LATERAL SINGLE SURFACE MULTIPLE DOUBLET FOR ALPHA OF 10 DEGREES
beta (deg)
5
0
-5
0
5
10
15
20
25
30
TIME (sec)
phi (deg)
40
20
0
-20
-40
0
5
10
15
20
25
30
TIME (sec)
mu (deg)
40
20
0
-20
-40
0
5
10
15
20
25
30
TIME (sec)

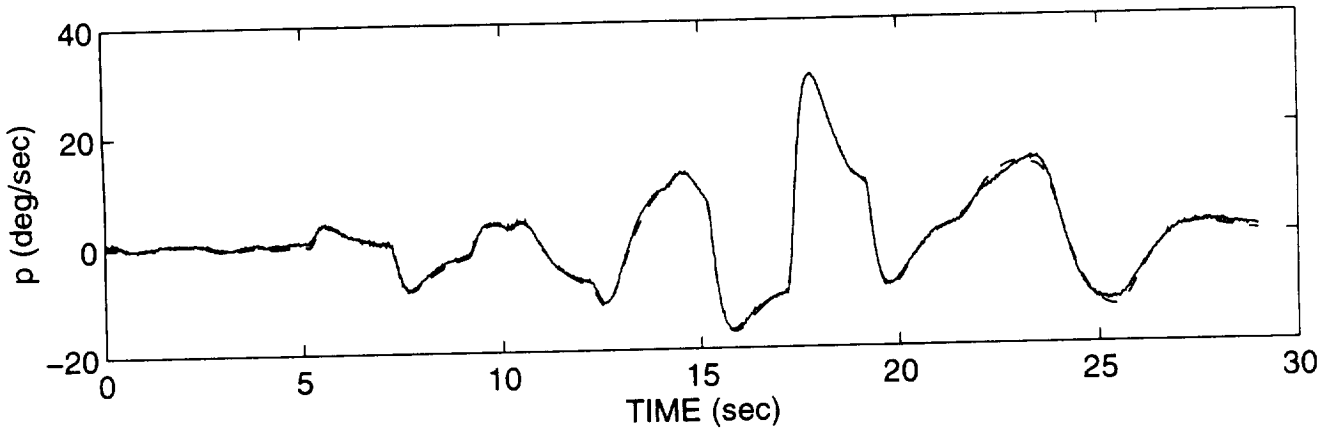
40
20
0
−20
p (deg/sec)
0
5
10
15
20
25
30
TIME (sec)

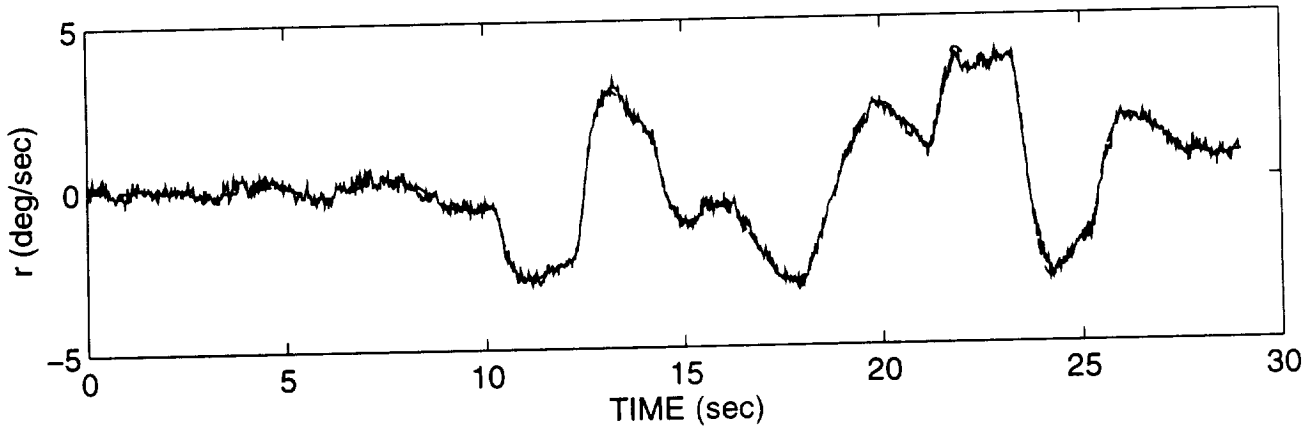
5
0
−5
r (deg/sec)
0
5
10
15
20
25
30
TIME (sec)

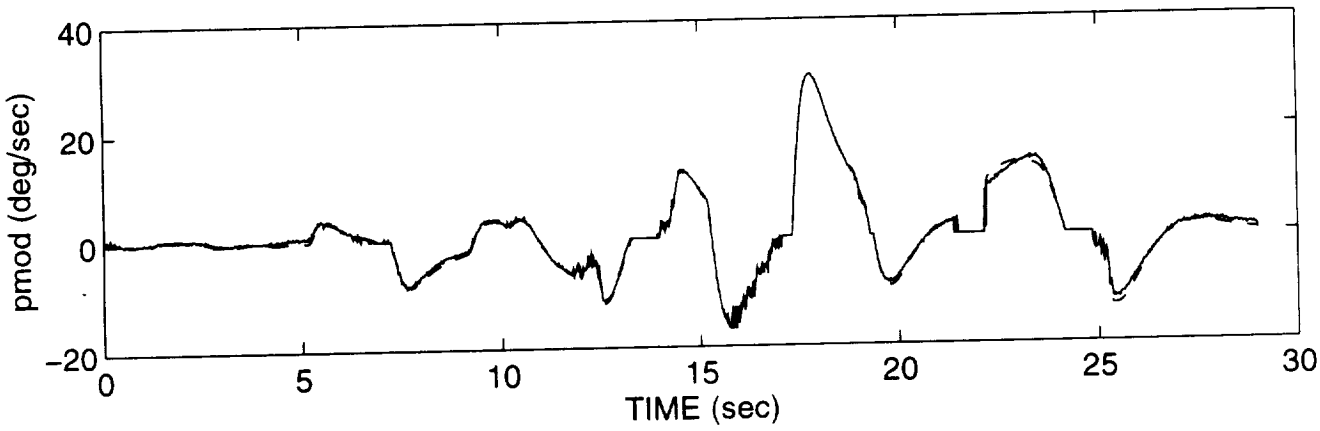
40
20
0
−20
pmod (deg/sec)
0
5
10
15
20
25
30
TIME (sec)

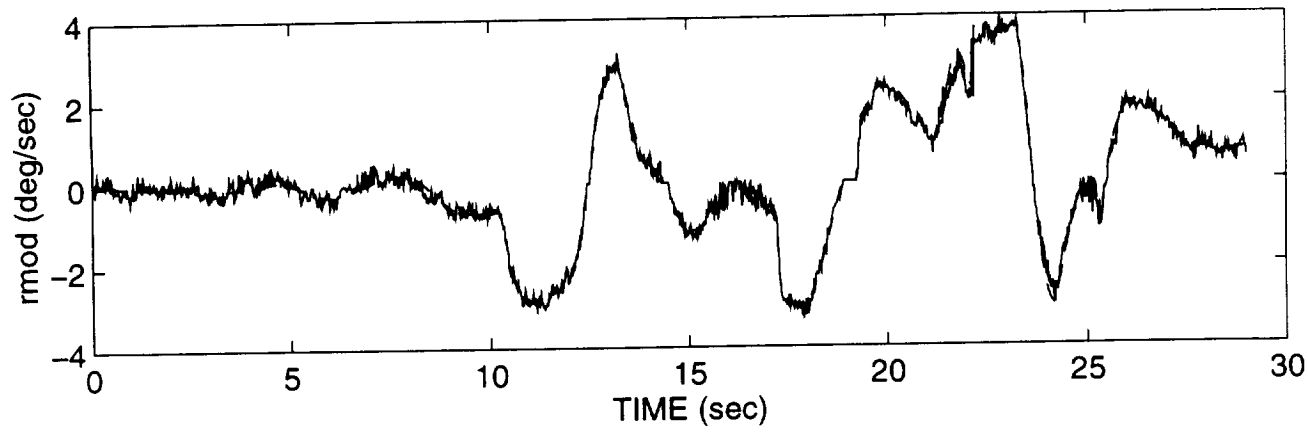
rmod (deg/sec)
4
2
0
−2
−4
0
5
10
15
20
25
30
TIME (sec)

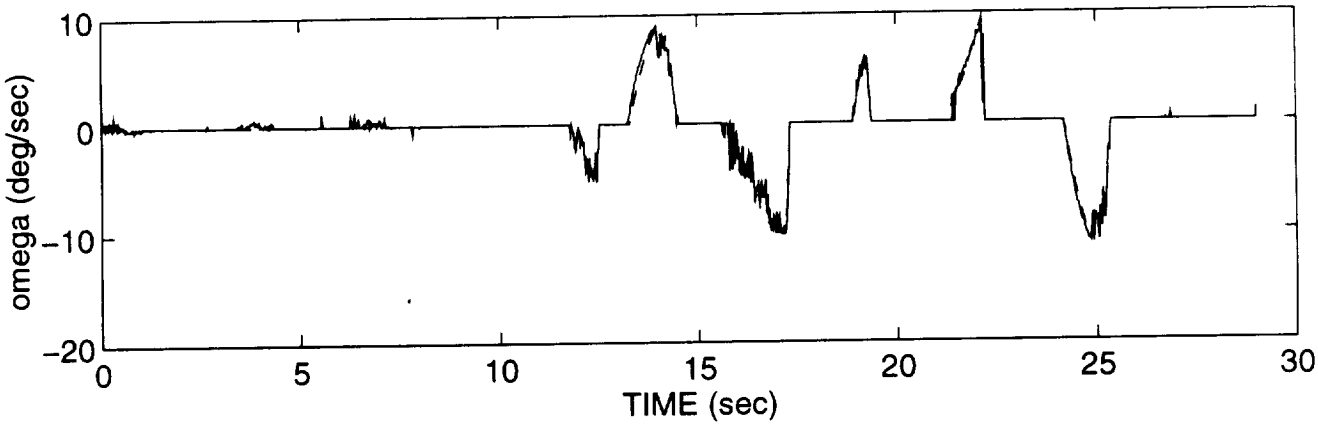
omega (deg/sec)
10
0
−10
−20
0
5
10
15
20
25
30
TIME (sec)

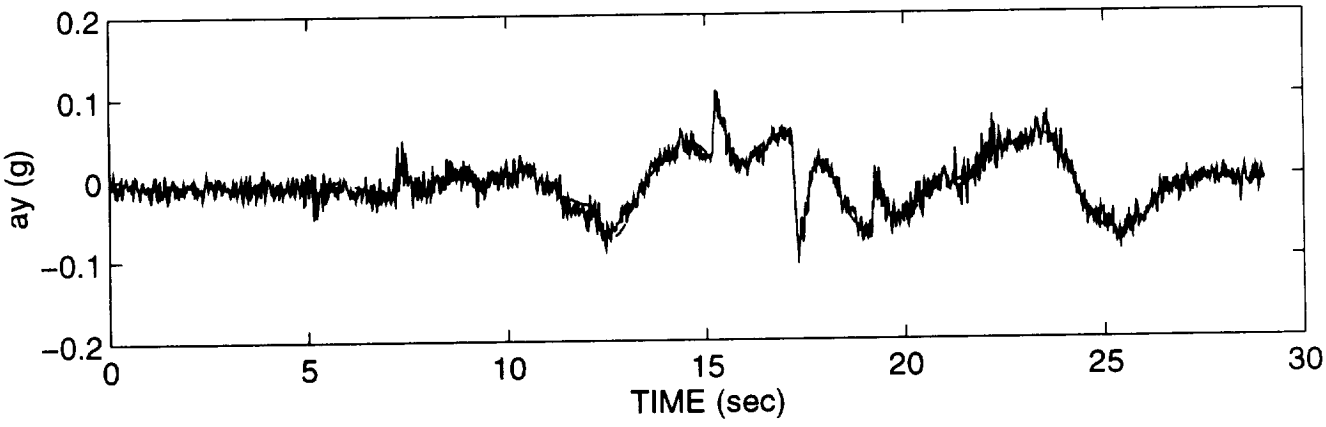
ay (g)
0.2
0.1
0
−0.1
−0.2
0
5
10
15
20
25
30
TIME (sec)

LATERAL SINGLE SURFACE MULTIPLE DOUBLET FOR ALPHA OF 20 DEGREES

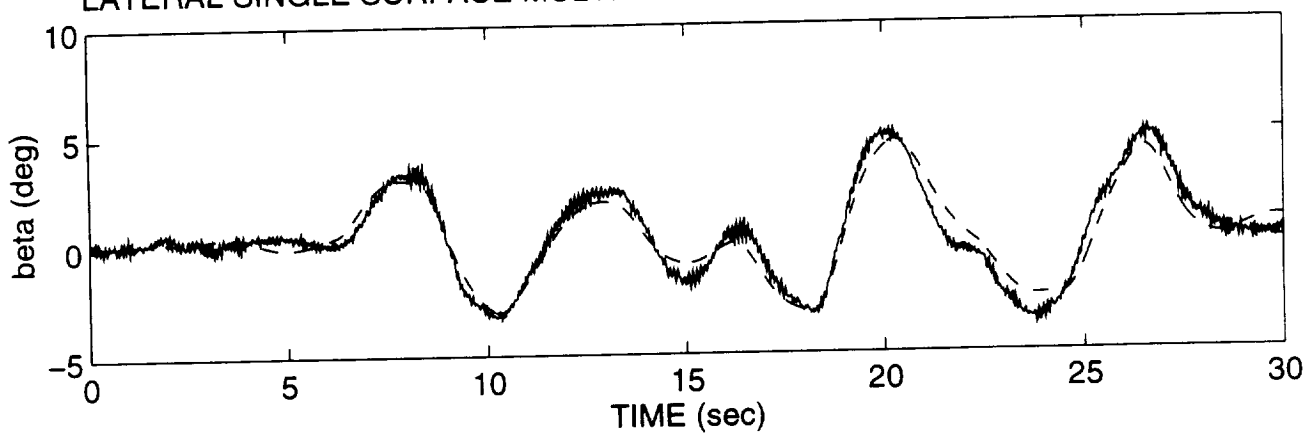

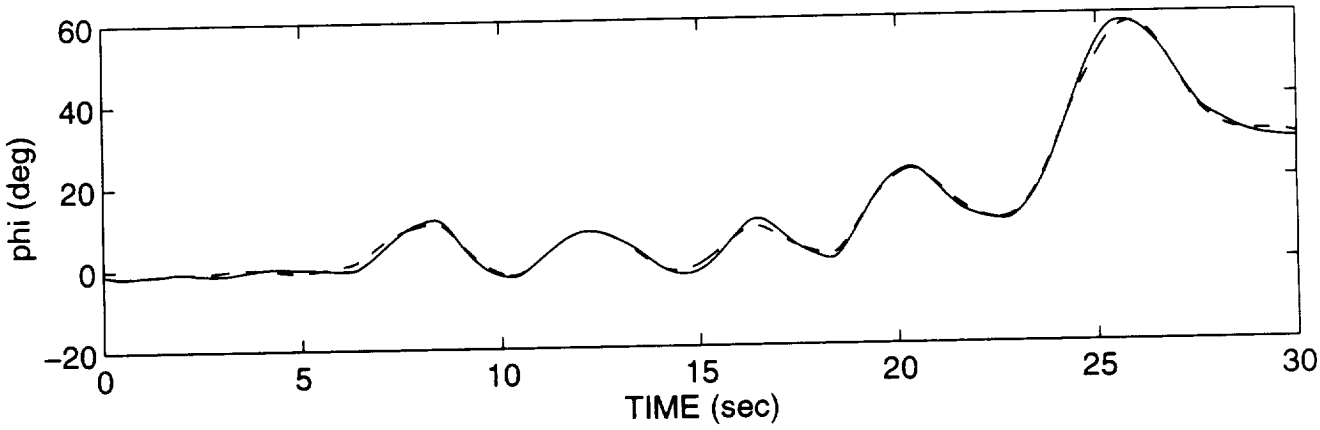

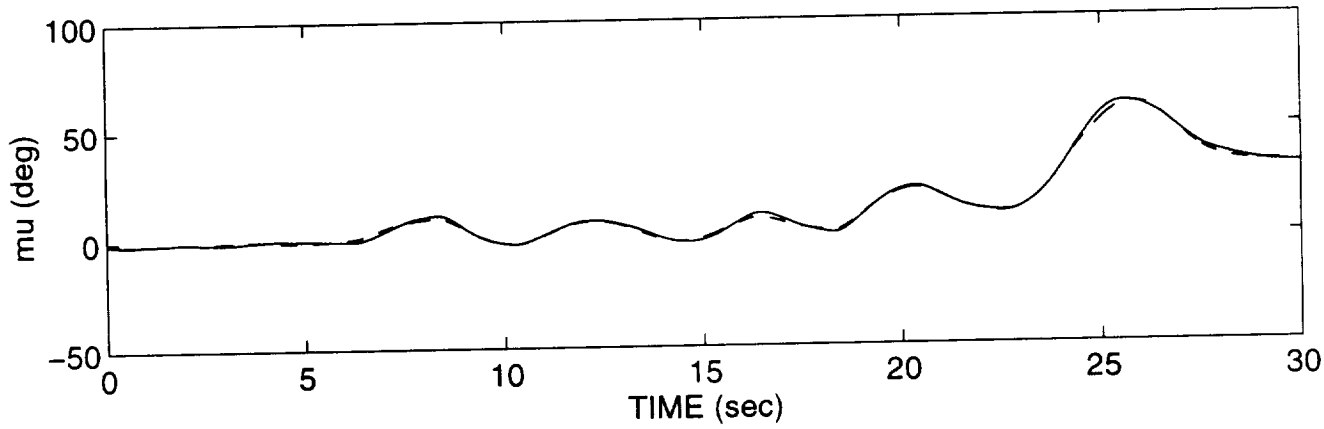

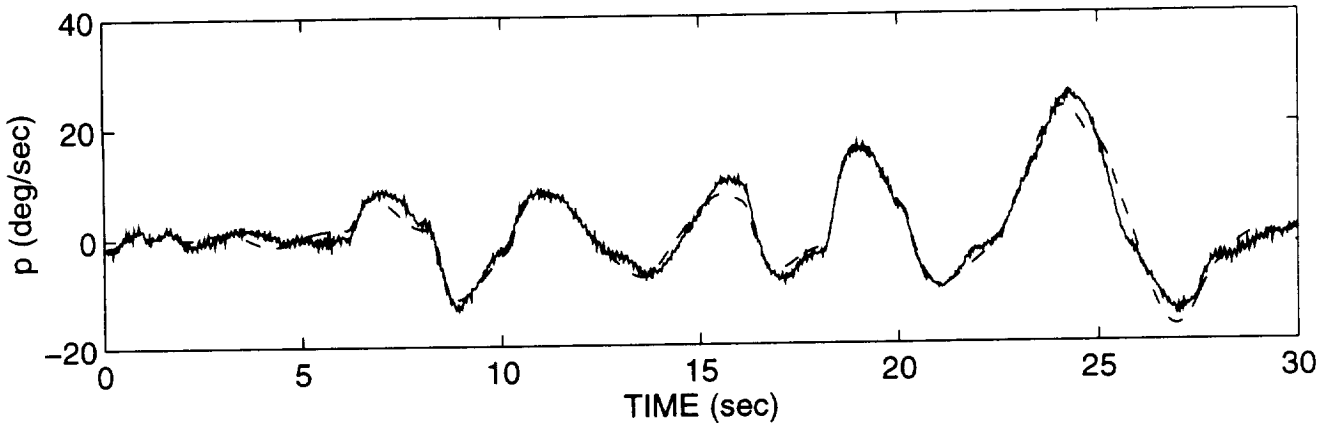
40
20
0
−20
p (deg/sec)
0
5
10
15
20
25
30
TIME (sec)

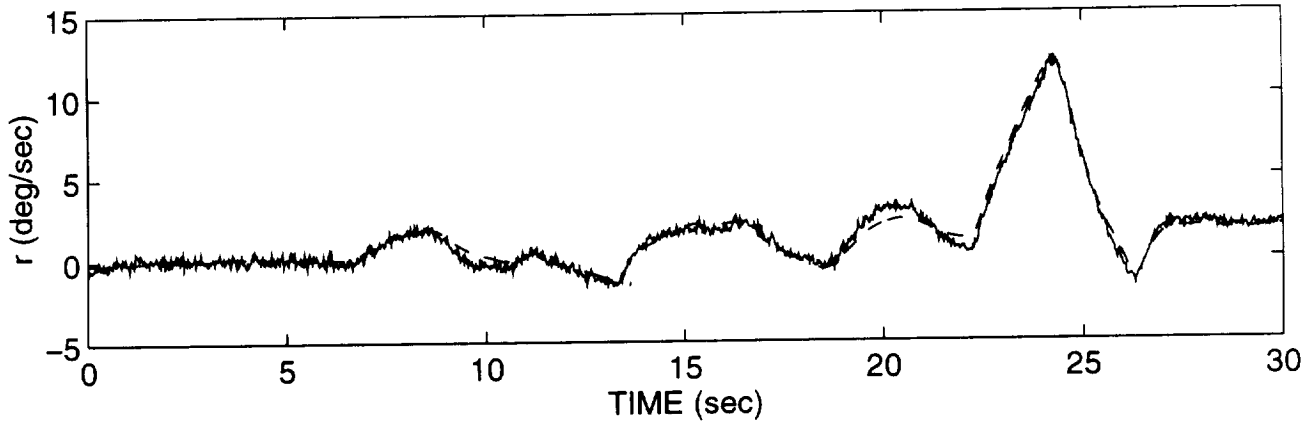
15
10
5
0
−5
r (deg/sec)
0
5
10
15
20
25
30
TIME (sec)

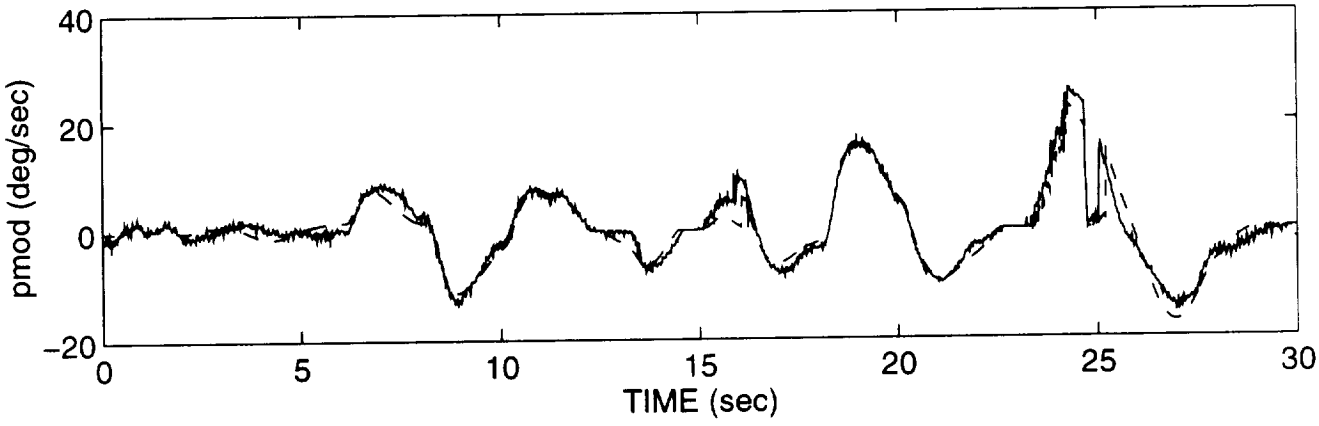
40
20
0
−20
pmod (deg/sec)
0
5
10
15
20
25
30
TIME (sec)

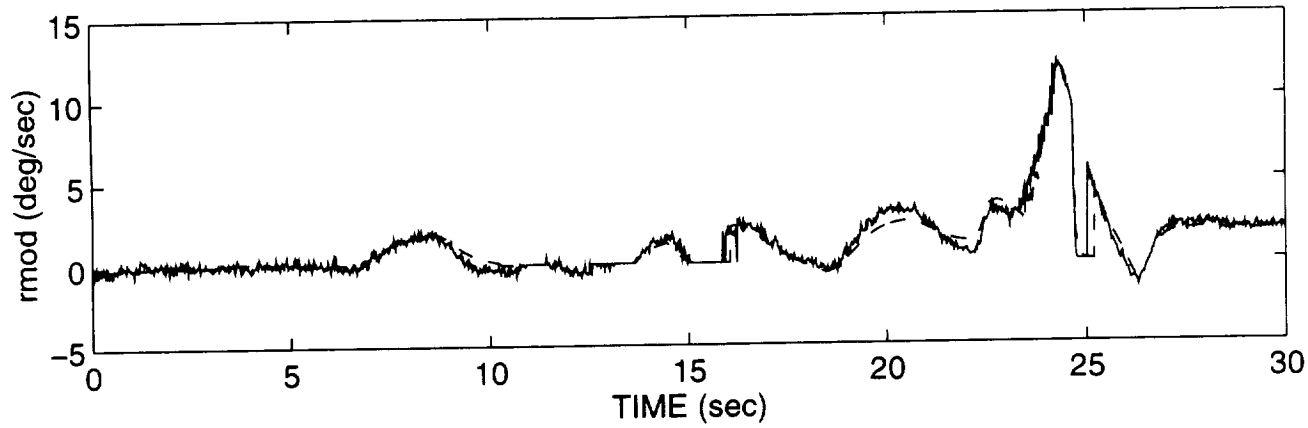
rmod (deg/sec)
15
10
5
0
−5
0
5
10
15
20
25
30
TIME (sec)

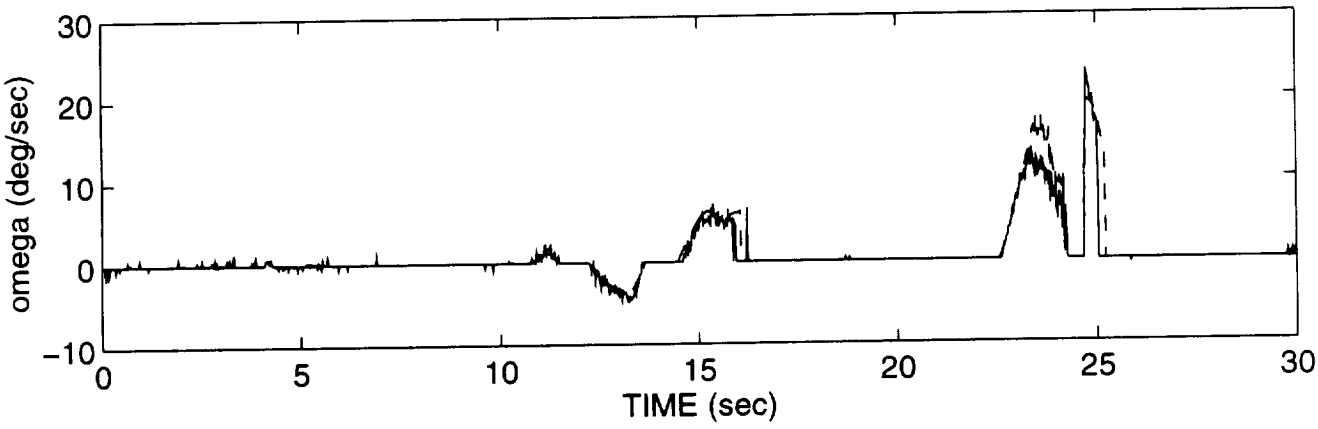
omega (deg/sec)
30
20
10
0
−10
0
5
10
15
20
25
30
TIME (sec)

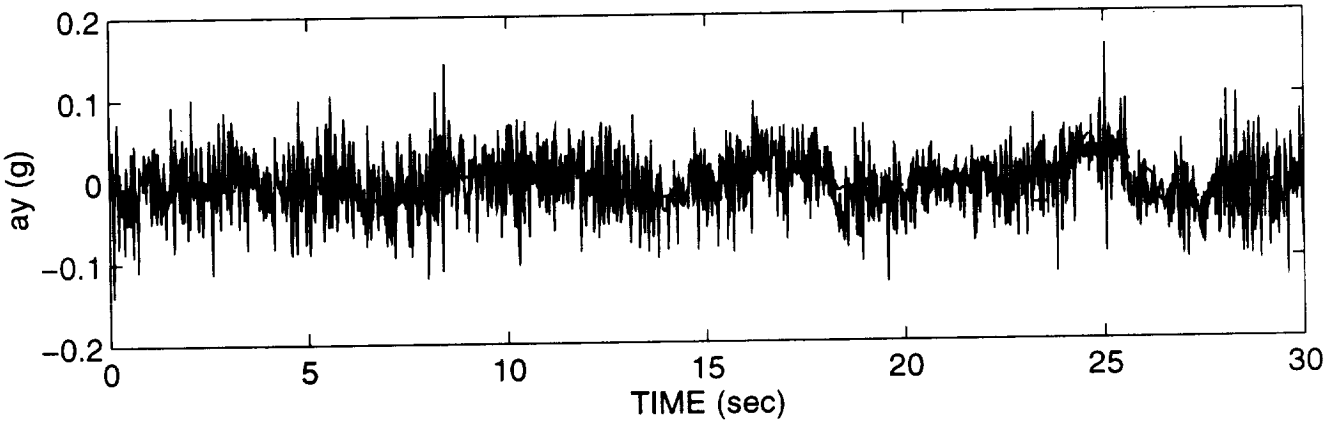
ay (g)
0.2
0.1
0
−0.1
−0.2
0
5
10
15
20
25
30
TIME (sec)

LATERAL SINGLE SURFACE MULTIPLE DOUBLET FOR ALPHA OF 30 DEGREES

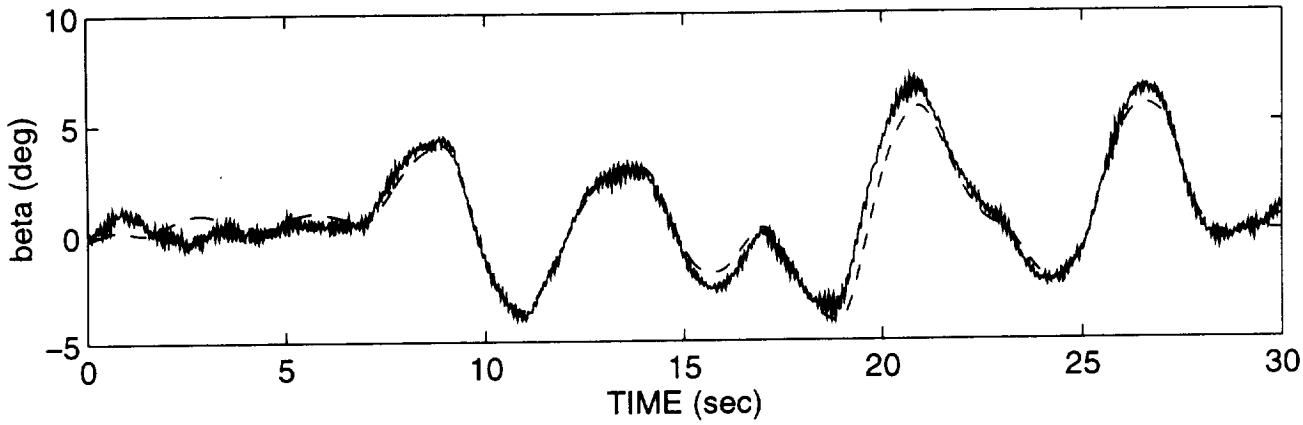

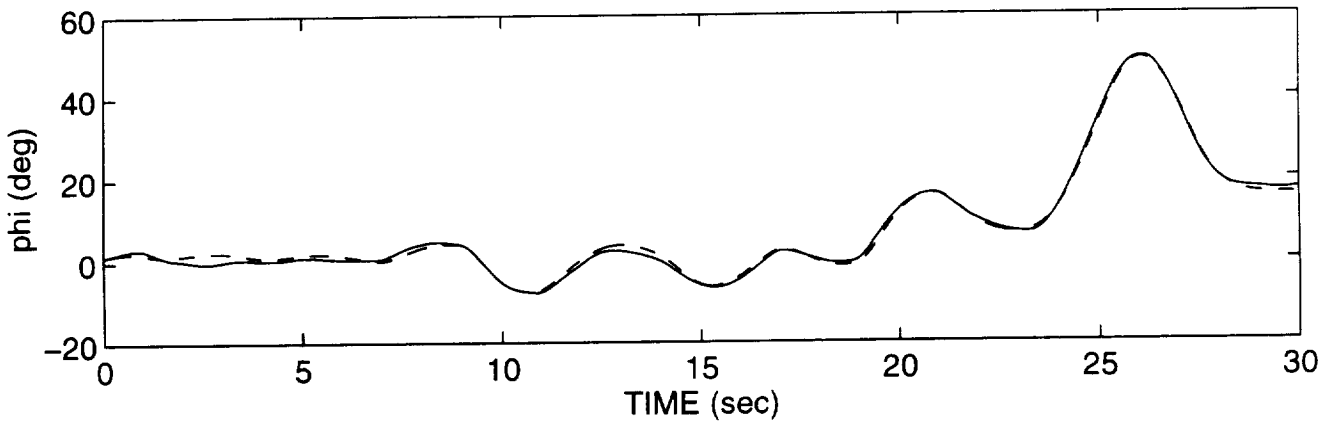

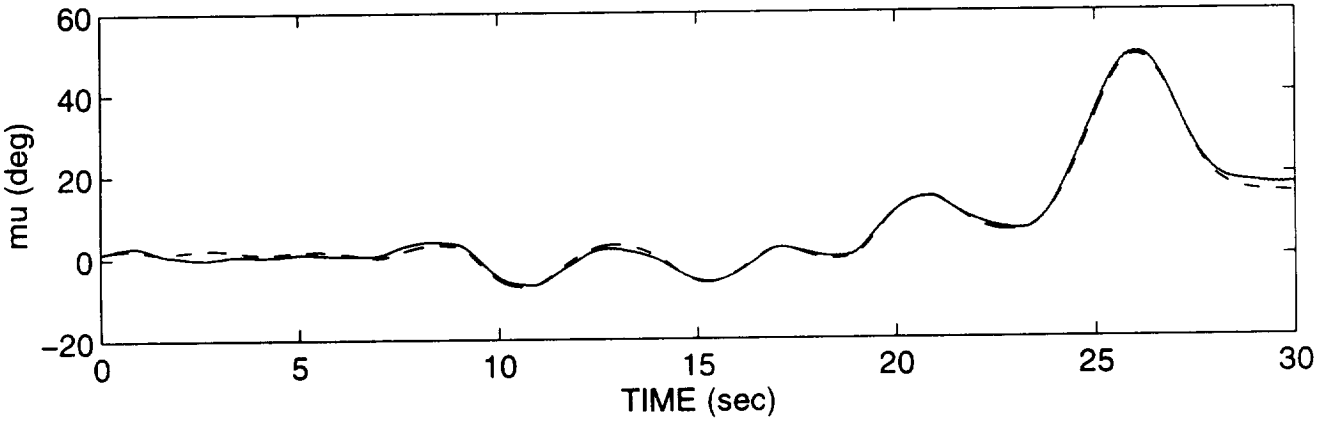

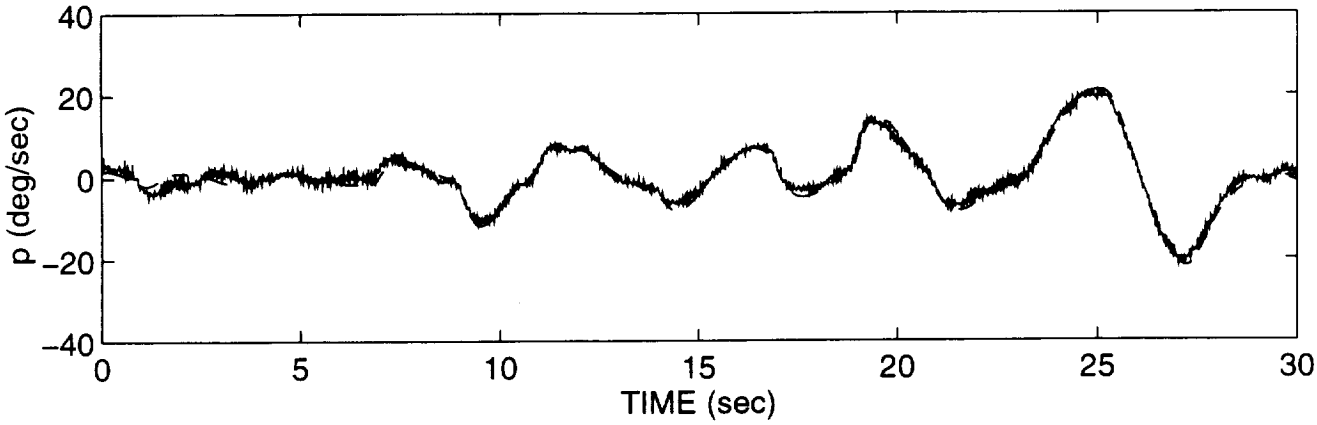
40
20
0
−20
−40
p (deg/sec)
0
5
10
15
20
25
30
TIME (sec)

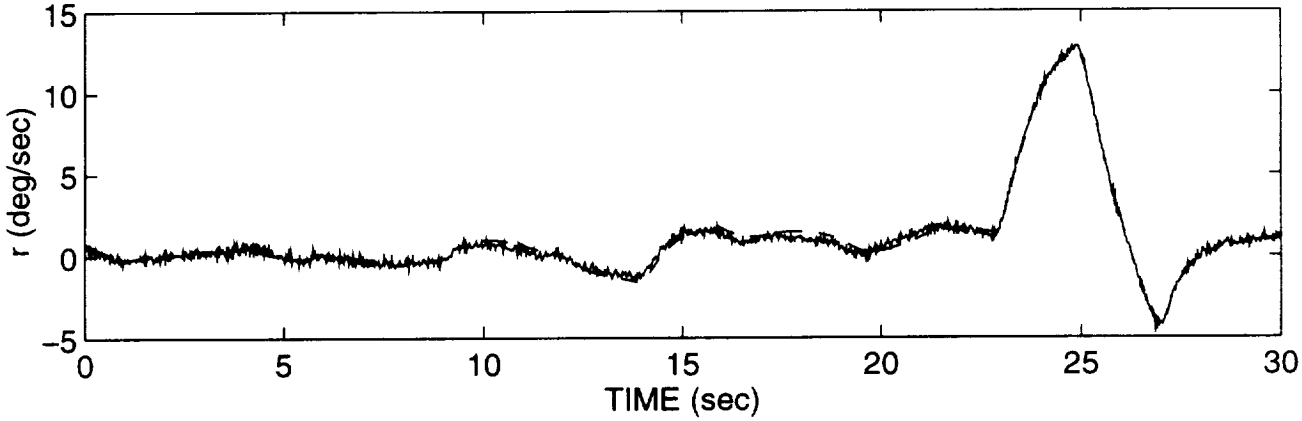
15
10
5
0
−5
r (deg/sec)
0
5
10
15
20
25
30
TIME (sec)

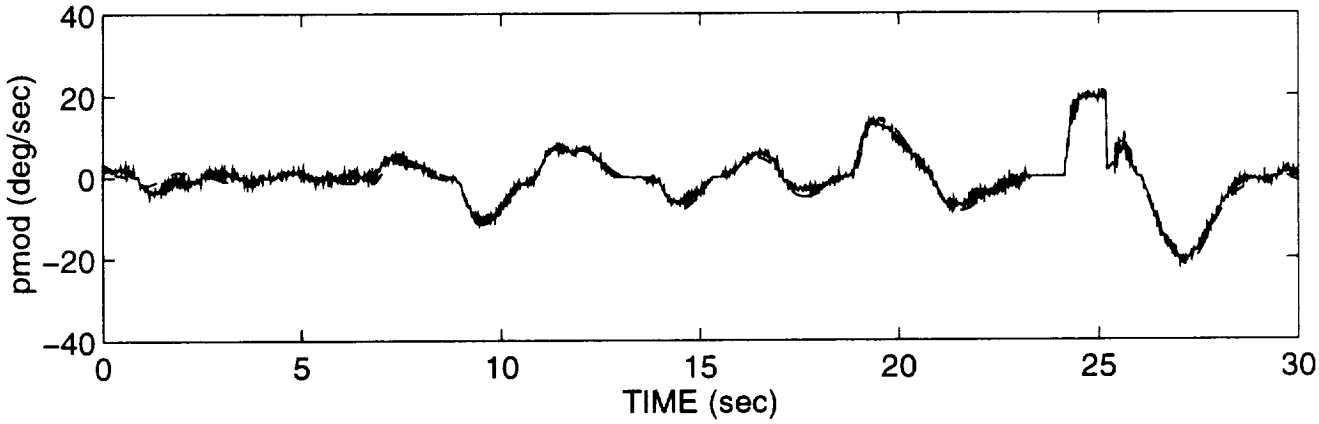
40
20
0
−20
−40
pmod (deg/sec)
0
5
10
15
20
25
30
TIME (sec)

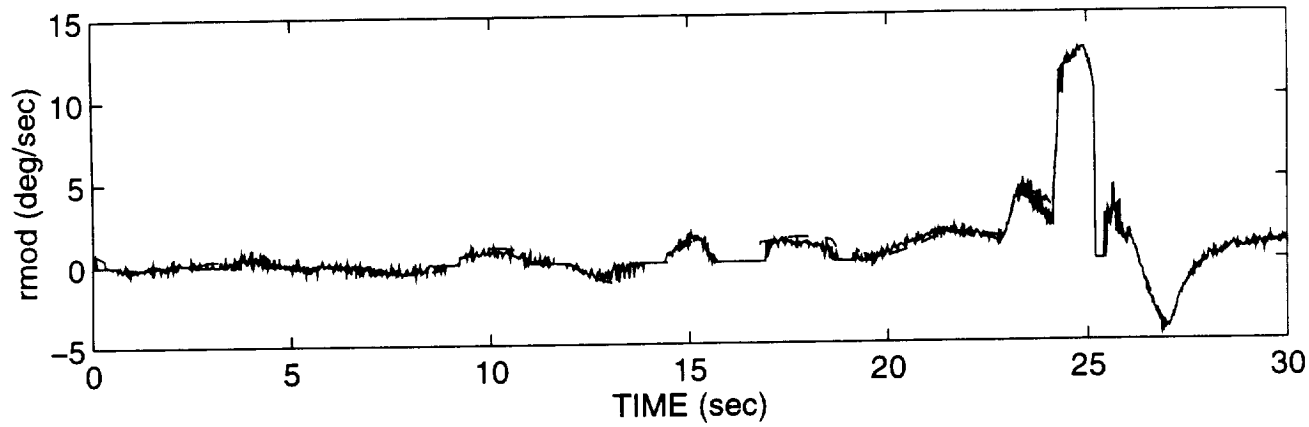
15
10
5
0
−5
rmod (deg/sec)
0
5
10
15
20
25
30
TIME (sec)

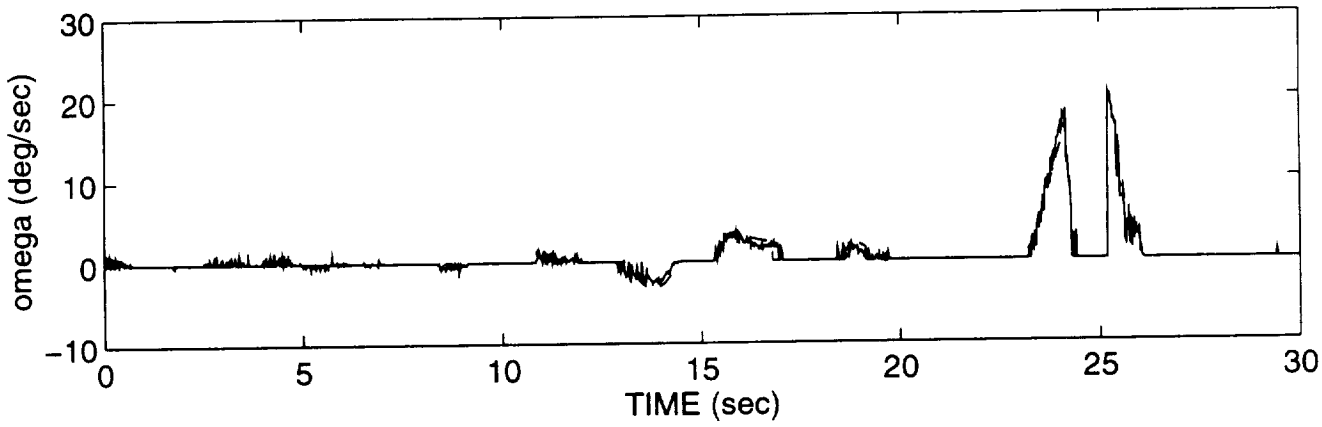
30
20
10
0
−10
omega (deg/sec)
0
5
10
15
20
25
30
TIME (sec)

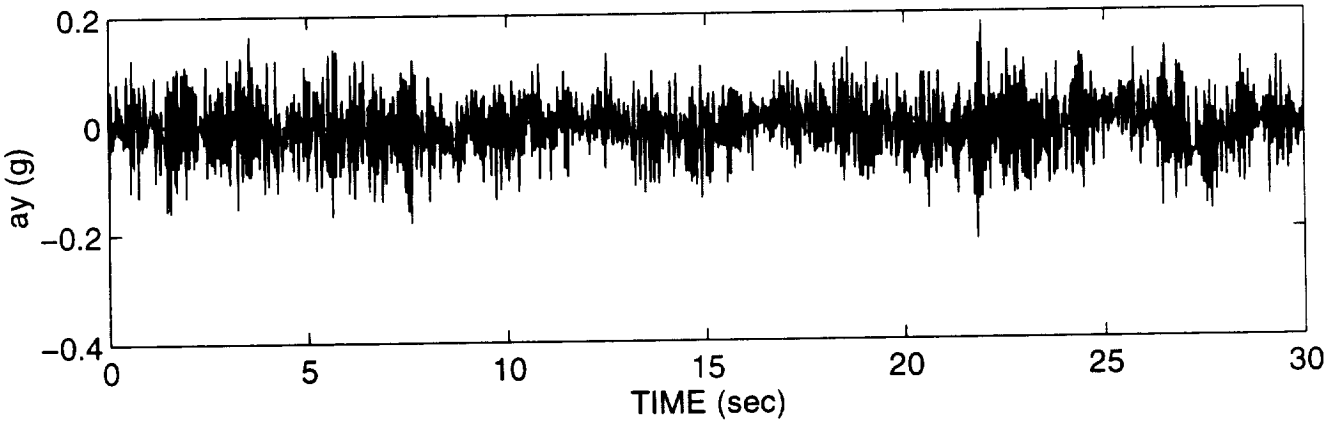
0.2
0
−0.2
−0.4
ay (g)
0
5
10
15
20
25
30
TIME (sec)

LATERAL SINGLE SURFACE MULTIPLE DOUBLET FOR ALPHA OF 50 DEGREES

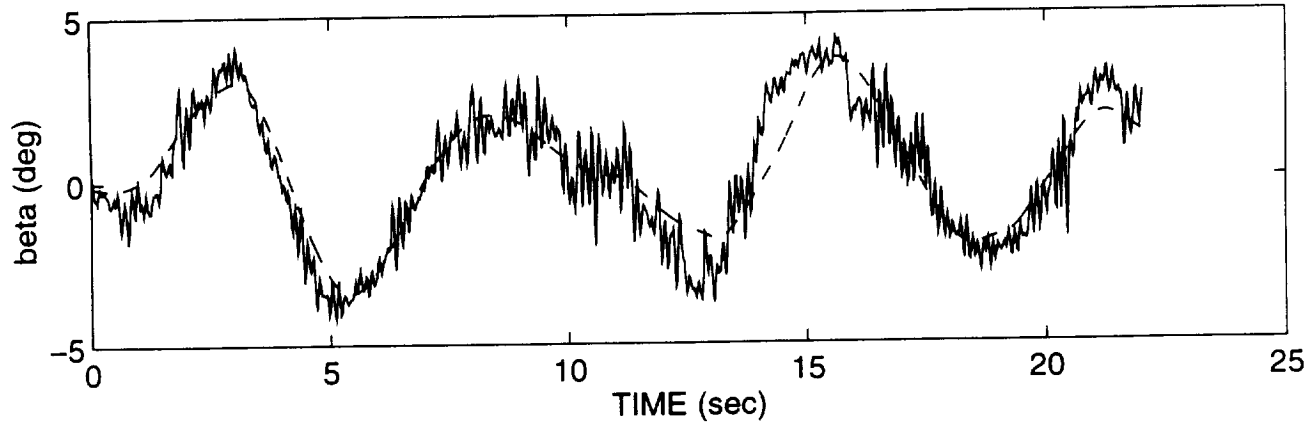

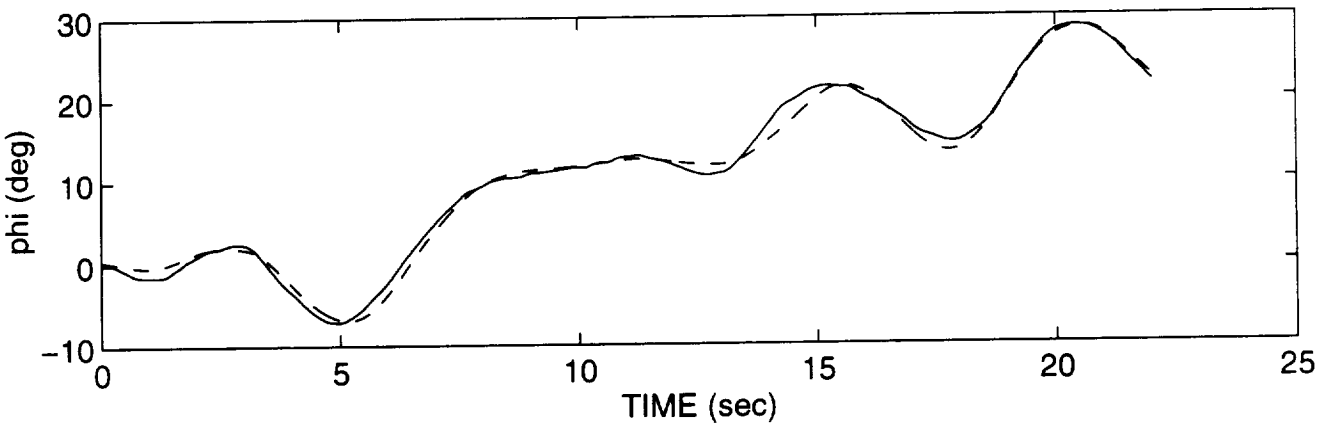

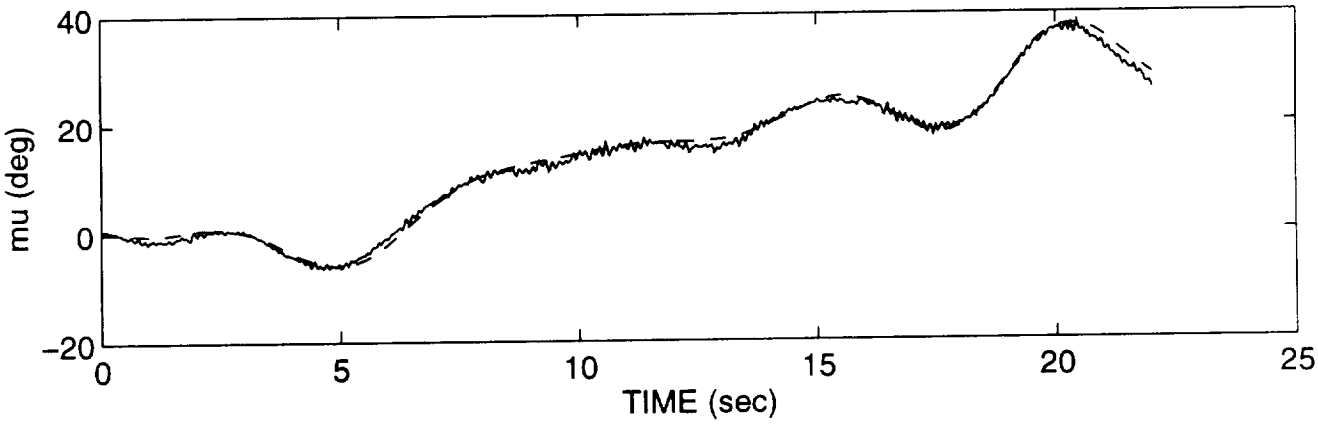

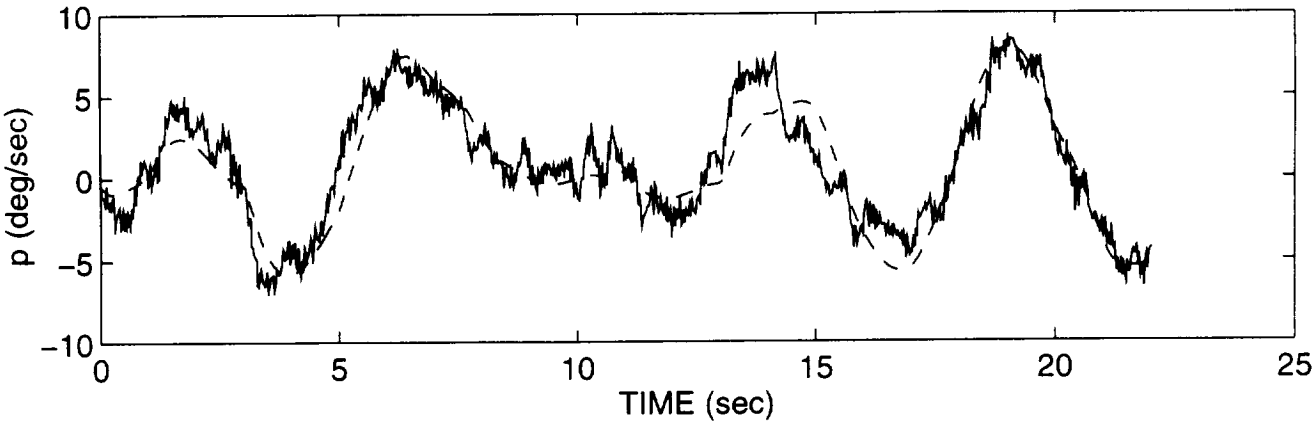
p (deg/sec)
10
5
0
−5
−10
0
5
10
15
20
25
TIME (sec)

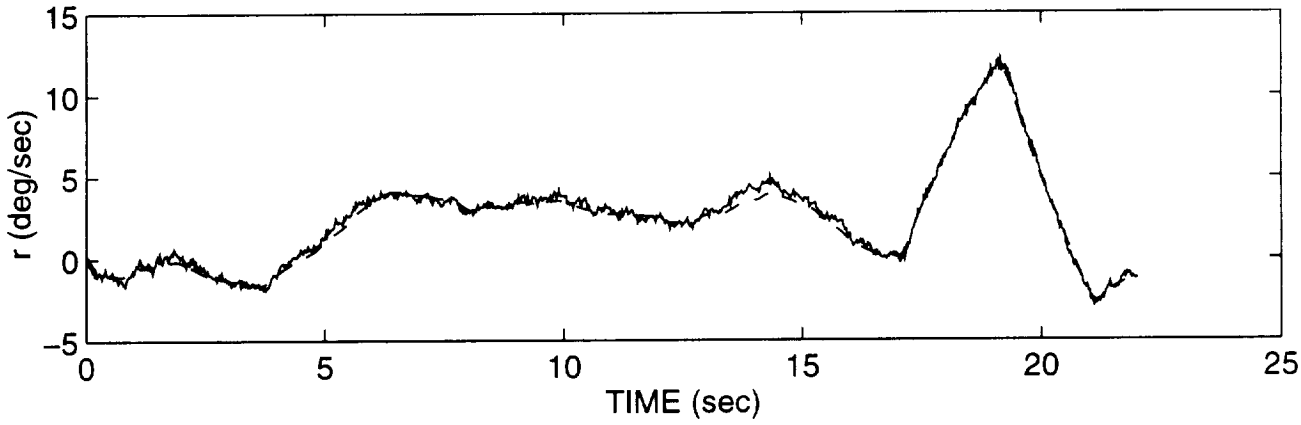
r (deg/sec)
15
10
5
0
−5
0
5
10
15
20
25
TIME (sec)

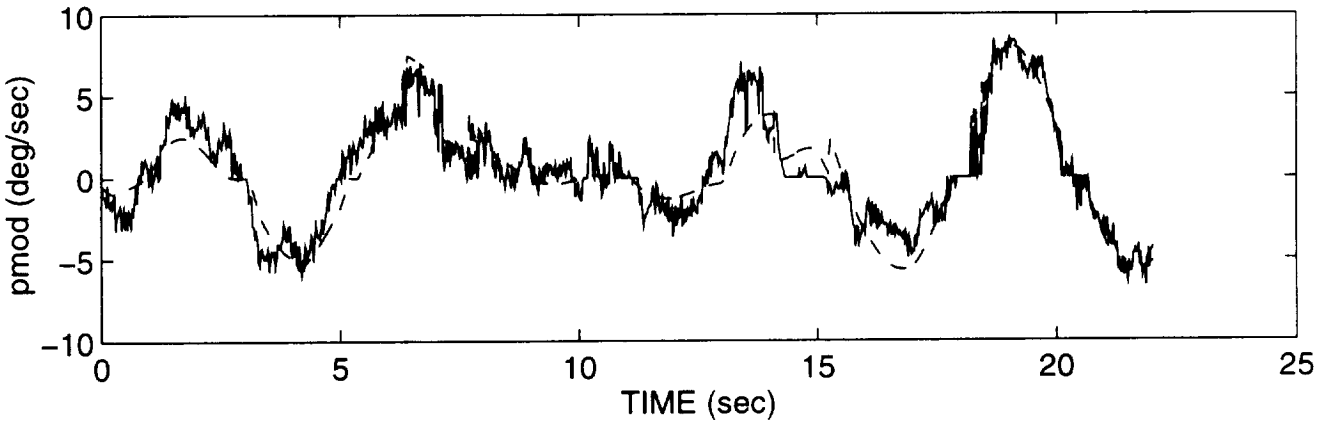
pmod (deg/sec)
10
5
0
−5
−10
0
5
10
15
20
25
TIME (sec)

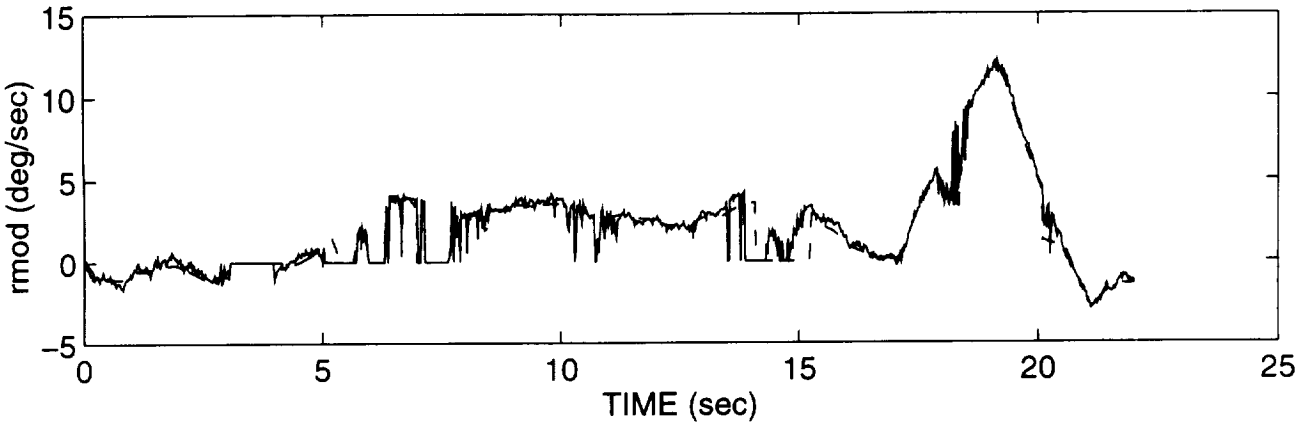
15
10
5
0
−5
rmod (deg/sec)
0
5
10
15
20
25
TIME (sec)

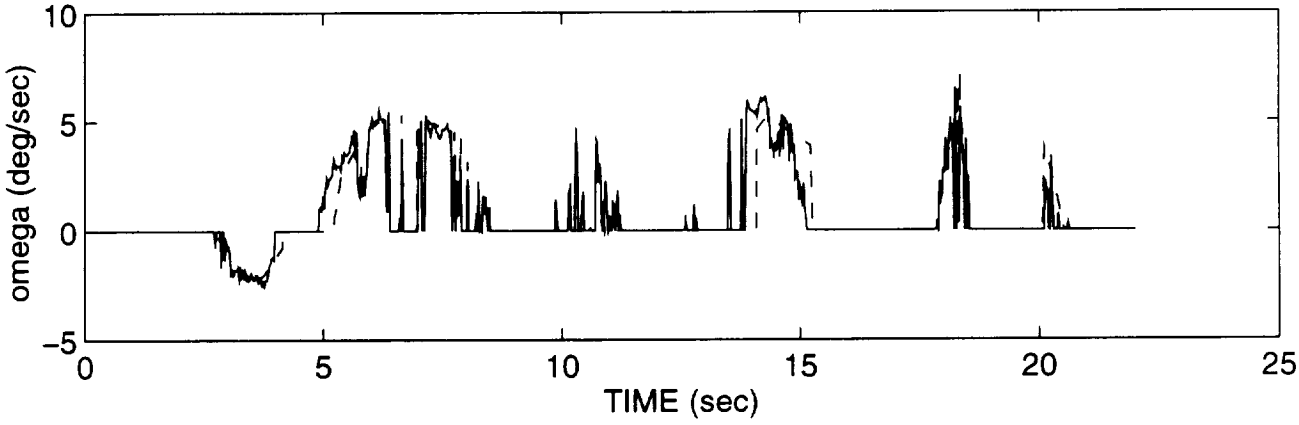
10
5
0
−5
omega (deg/sec)
0
5
10
15
20
25
TIME (sec)

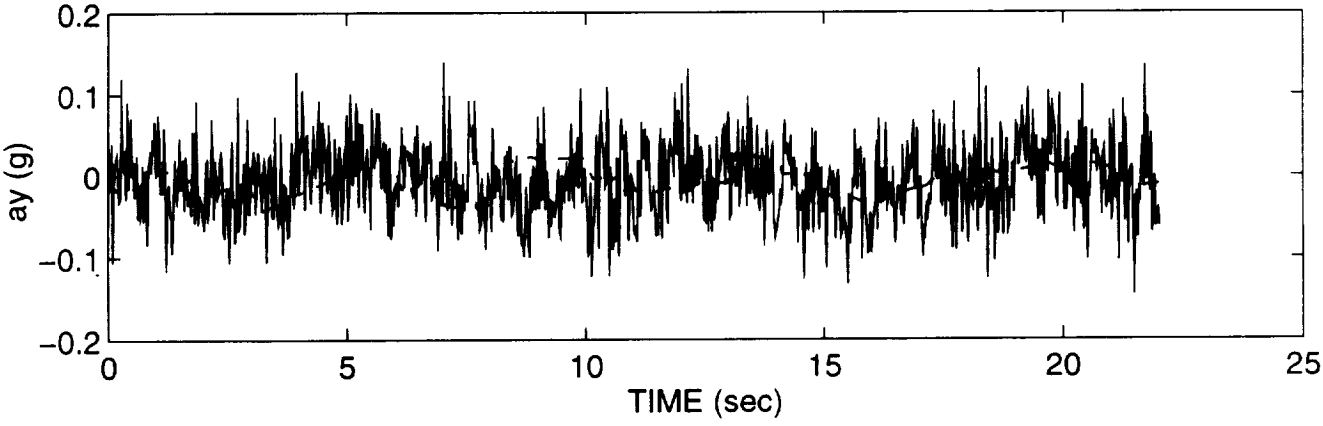
0.2
0.1
0
−0.1
−0.2
ay (g)
0
5
10
15
20
25
TIME (sec)

LATERAL SINGLE SURFACE MULTIPLE DOUBLET FOR ALPHA OF 60 DEGREES

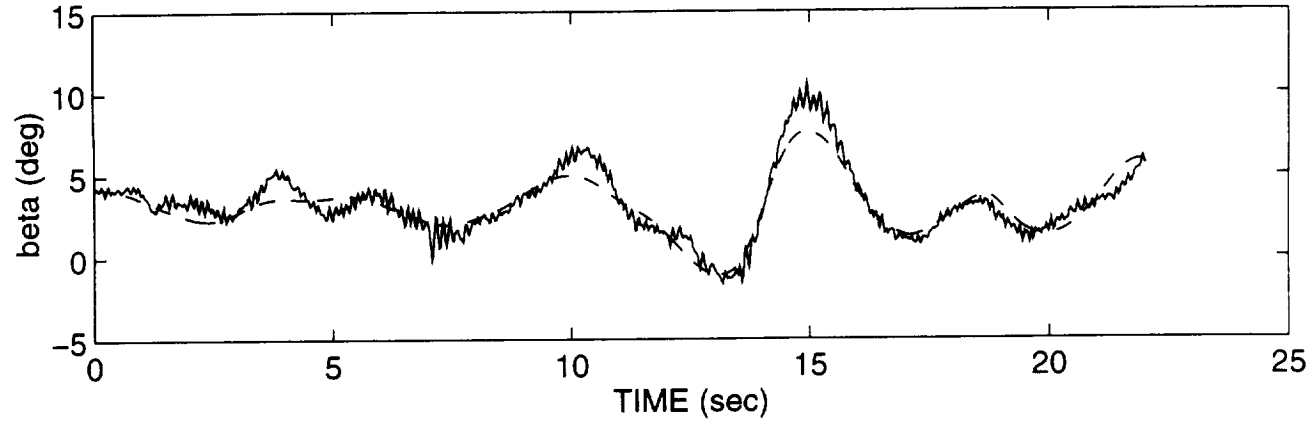

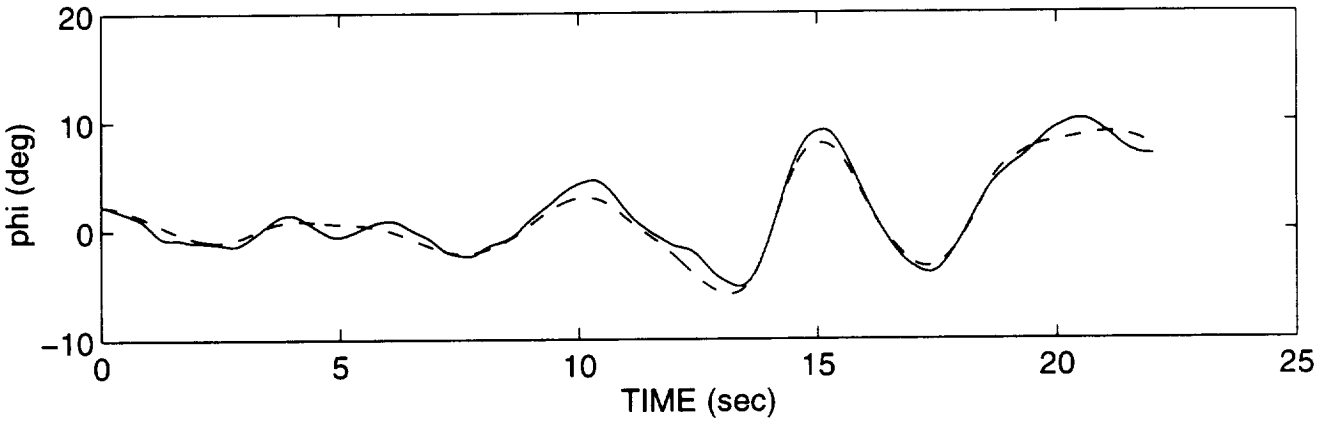

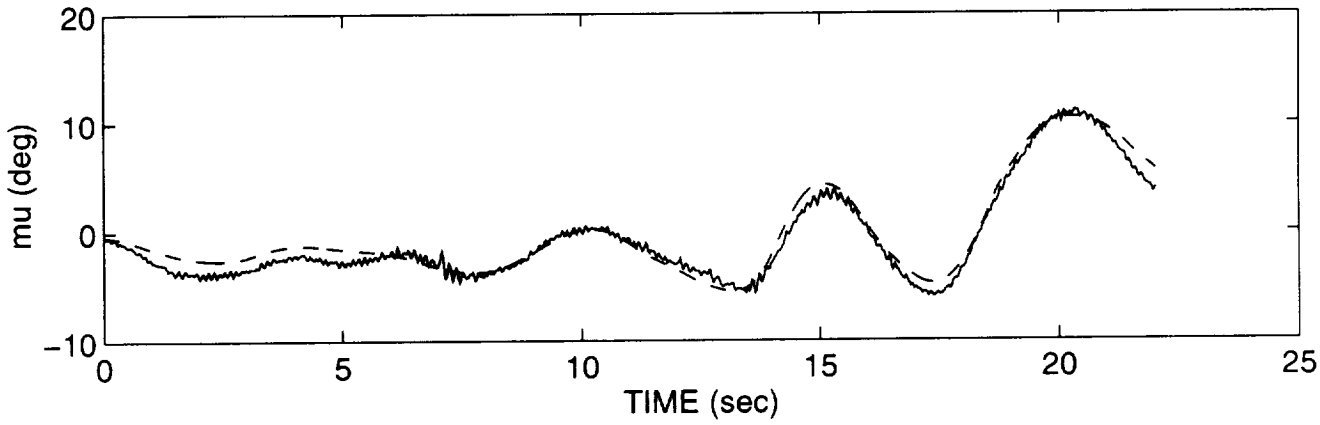

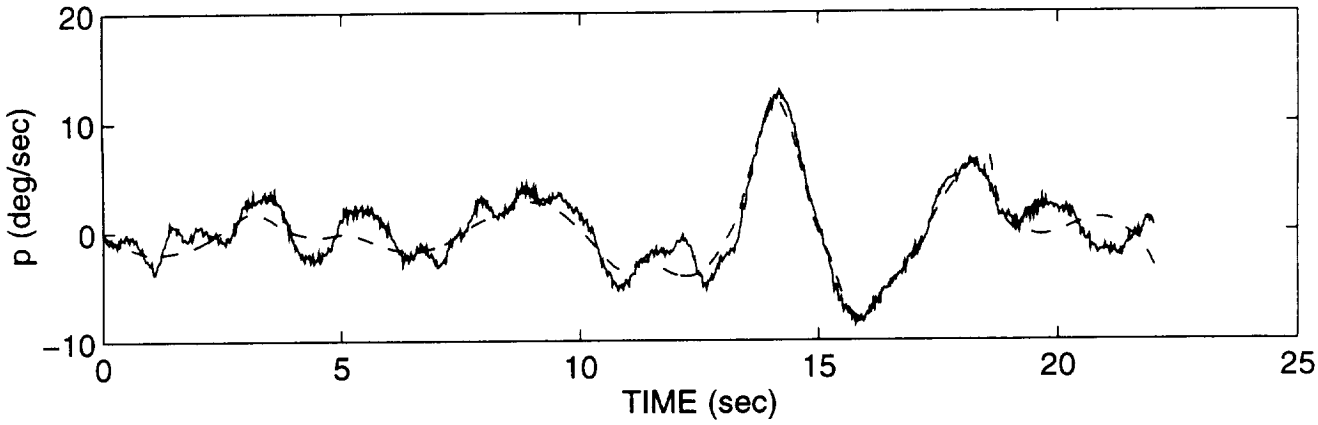
20
10
0
−10
p (deg/sec)
0
5
10
15
20
25
TIME (sec)

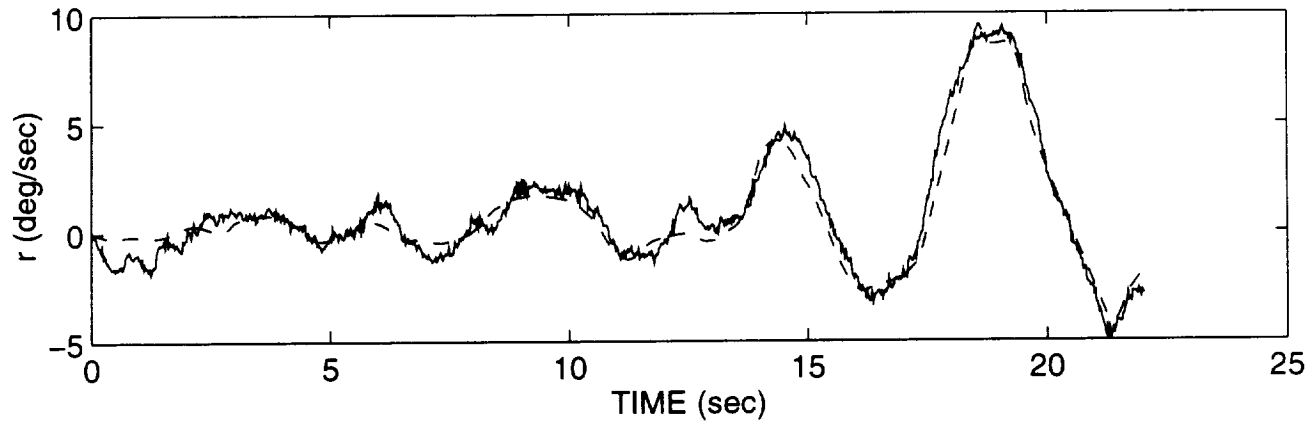
10
5
0
−5
r (deg/sec)
0
5
10
15
20
25
TIME (sec)

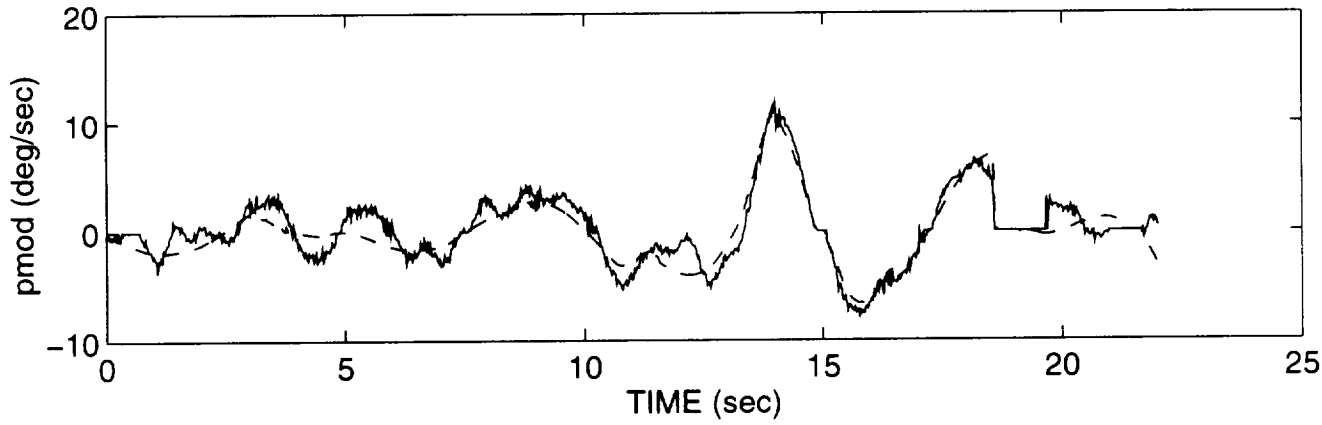
20
10
0
−10
pmod (deg/sec)
0
5
10
15
20
25
TIME (sec)

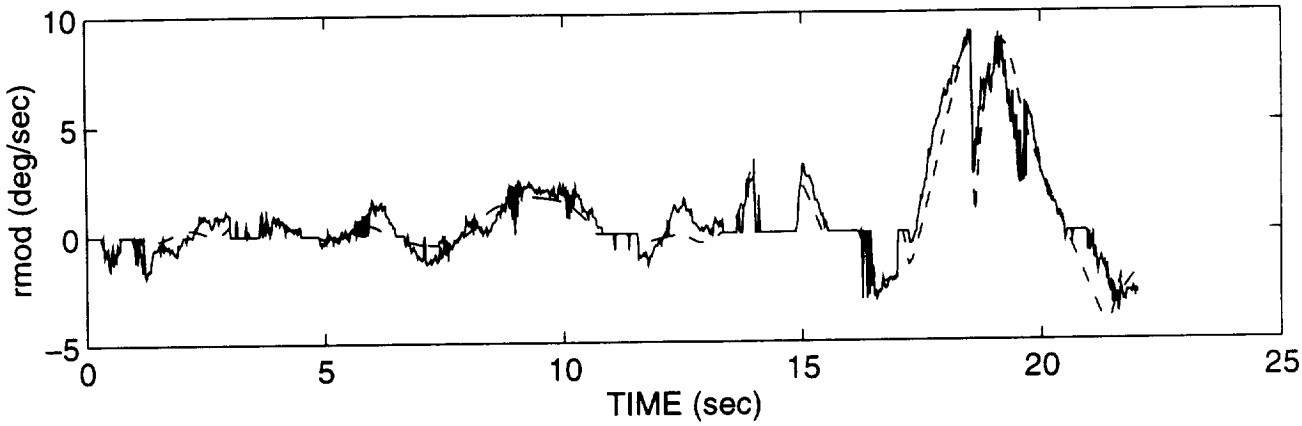
rmod (deg/sec)
10
5
0
−5
0
5
10
15
20
25
TIME (sec)

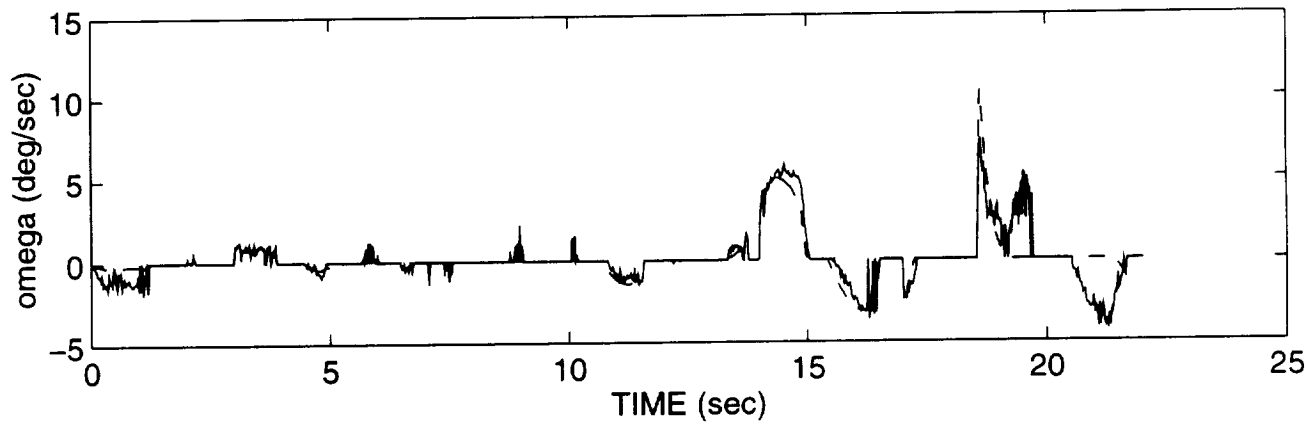
omega (deg/sec)
15
10
5
0
−5
0
5
10
15
20
25
TIME (sec)

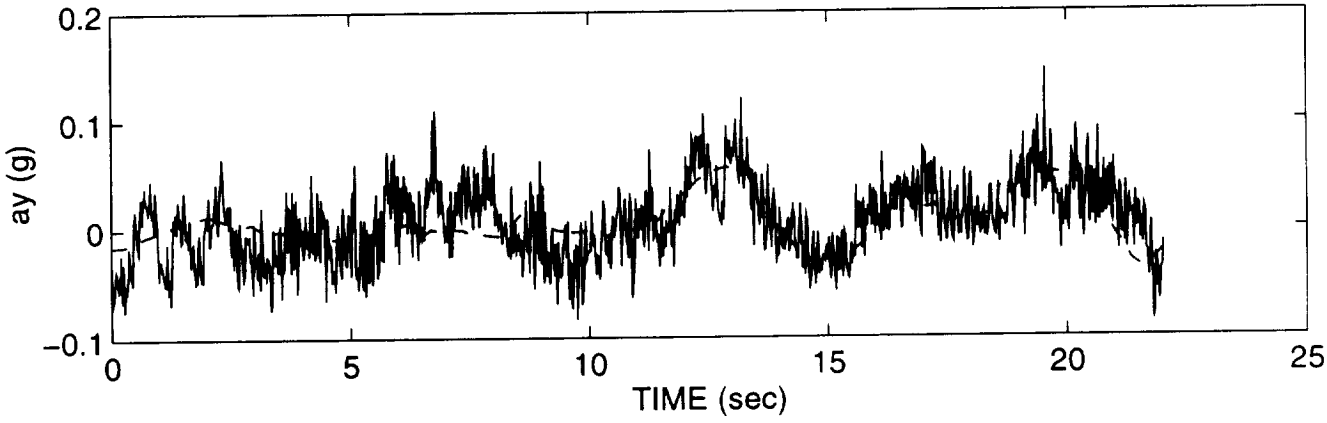
ay (g)
0.2
0.1
0
−0.1
0
5
10
15
20
25
TIME (sec)

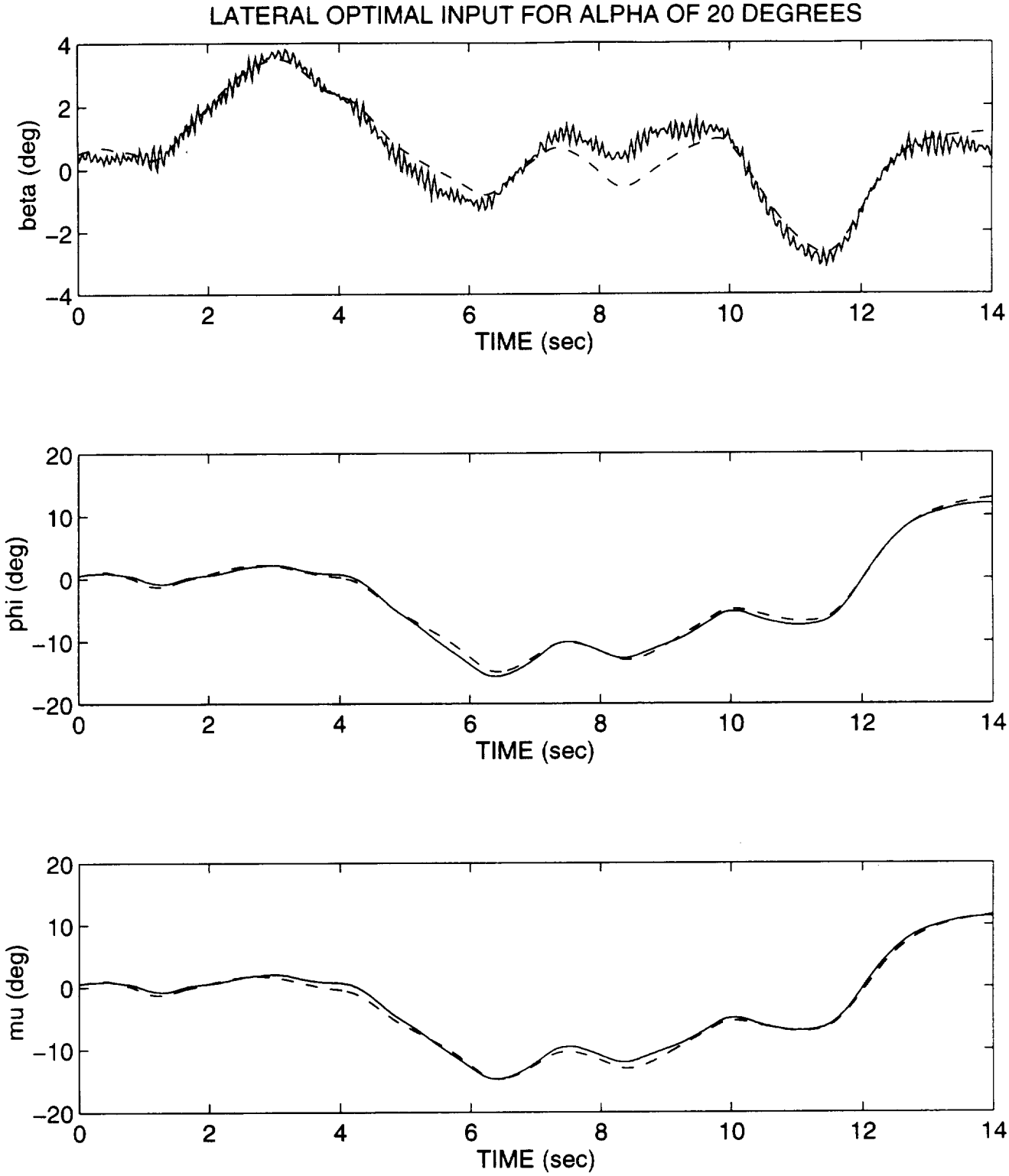
LATERAL OPTIMAL INPUT FOR ALPHA OF 20 DEGREES
beta (deg)
4
2
0
−2
−4
0
2
4
6
8
10
12
14
TIME (sec)
phi (deg)
20
10
0
−10
−20
0
2
4
6
8
10
12
14
TIME (sec)
mu (deg)
20
10
0
−10
−20
0
2
4
6
8
10
12
14
TIME (sec)

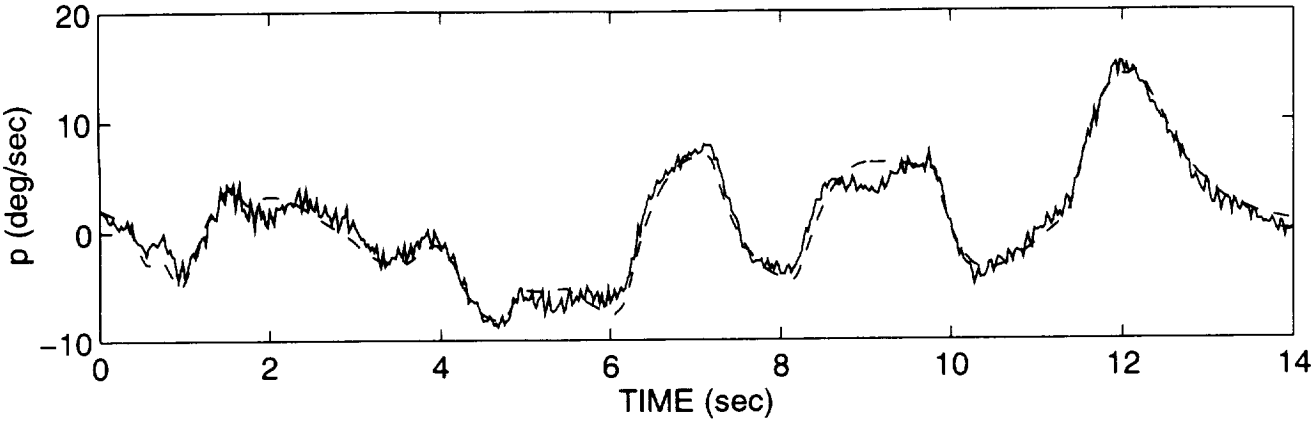
20
10
0
−10
p (deg/sec)
0
2
4
6
8
10
12
14
TIME (sec)

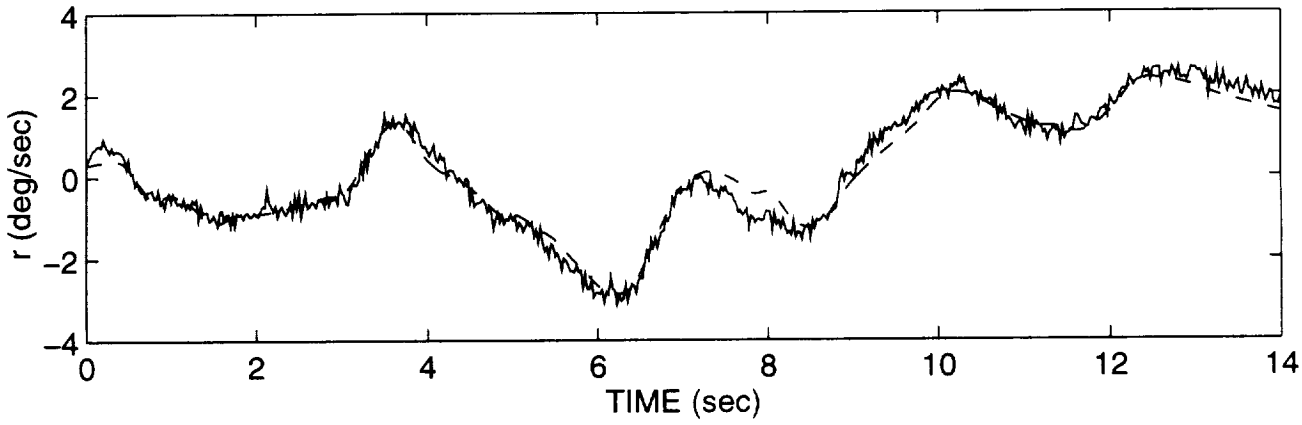
4
2
0
−2
−4
r (deg/sec)
0
2
4
6
8
10
12
14
TIME (sec)

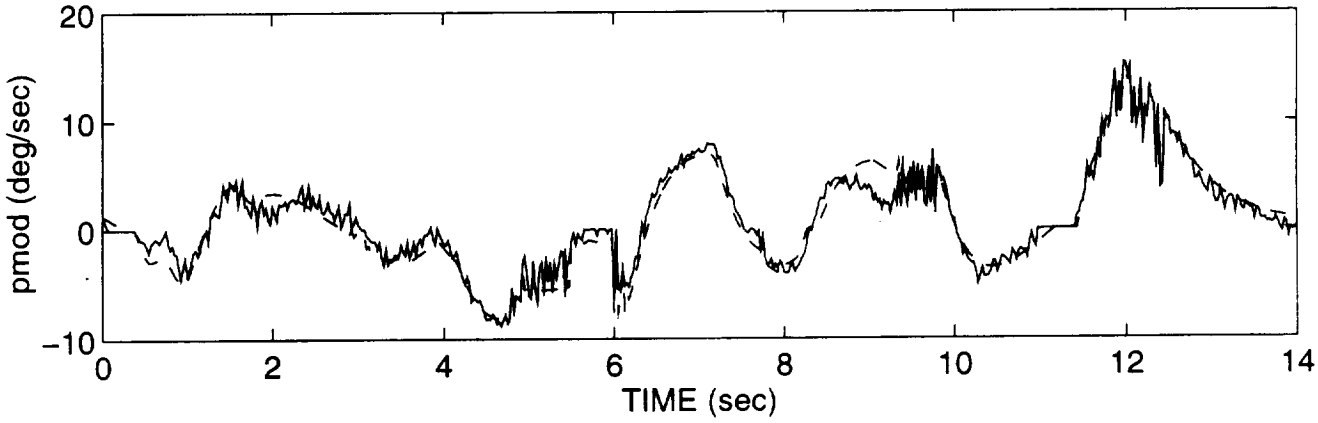
20
10
0
−10
pmod (deg/sec)
0
2
4
6
8
10
12
14
TIME (sec)

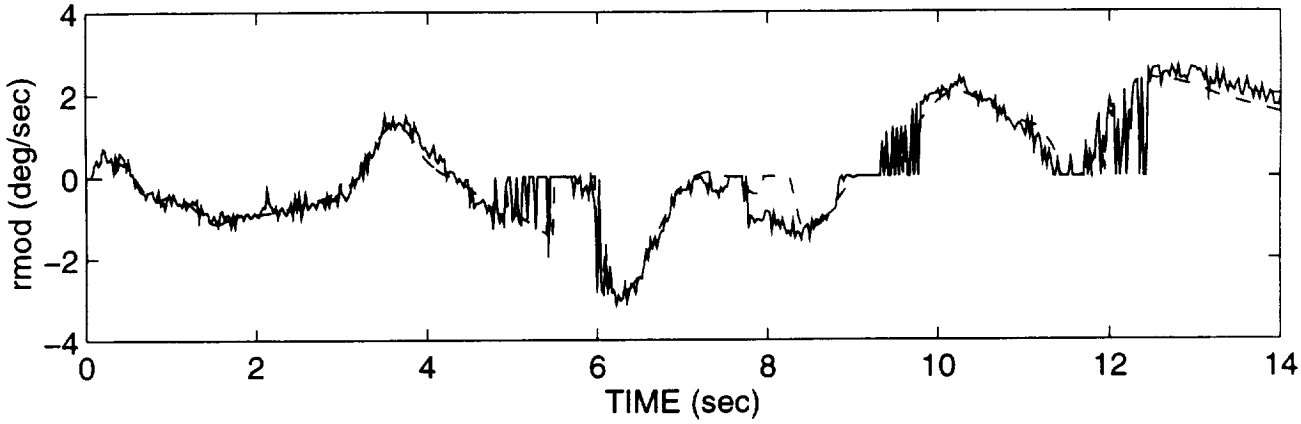
rmod (deg/sec)
4
2
0
−2
−4
0
2
4
6
8
10
12
14
TIME (sec)

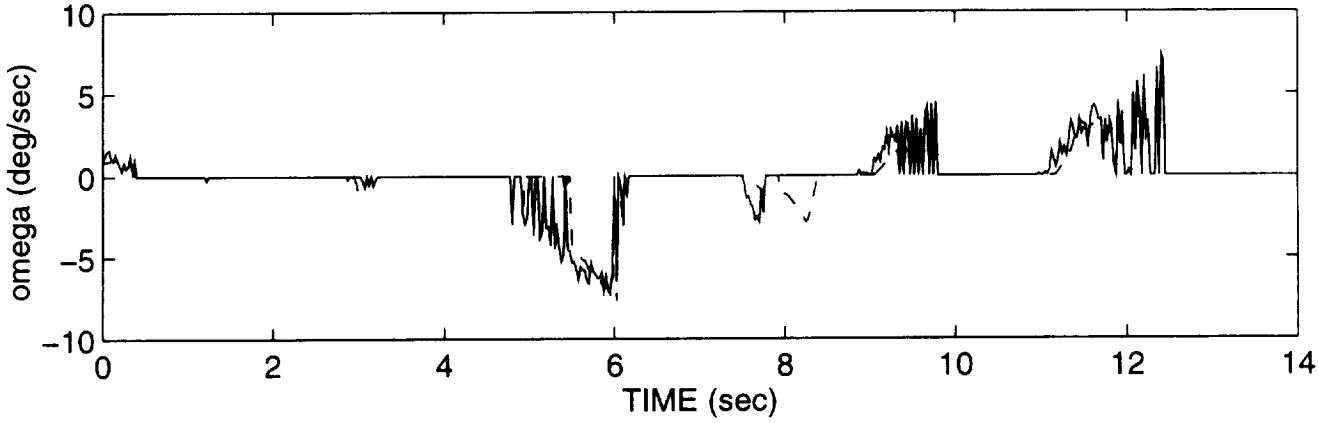
omega (deg/sec)
10
5
0
−5
−10
0
2
4
6
8
10
12
14
TIME (sec)

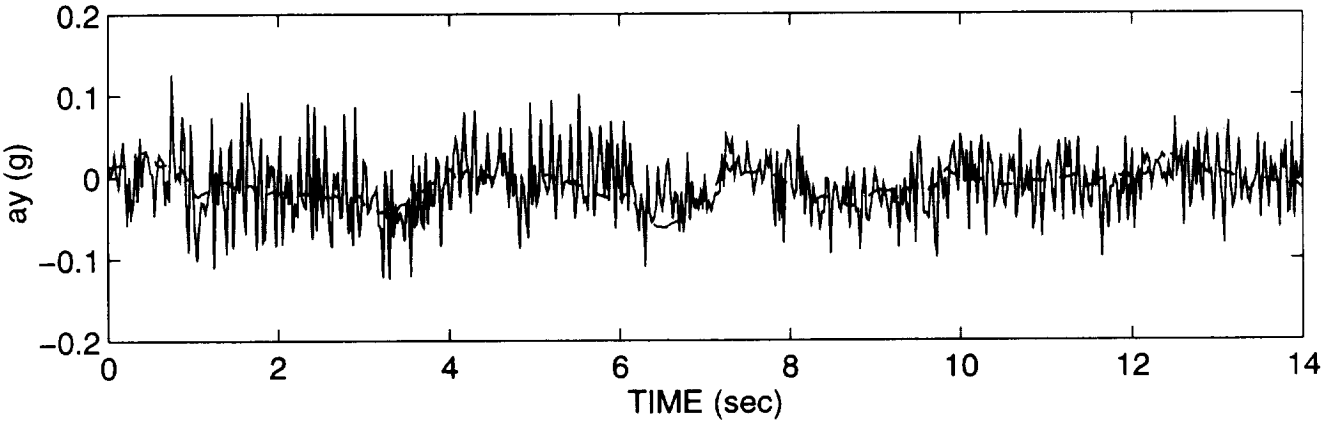
ay (g)
0.2
0.1
0
−0.1
−0.2
0
2
4
6
8
10
12
14
TIME (sec)

LATERAL OPTIMAL INPUT FOR ALPHA OF 40 DEGREES

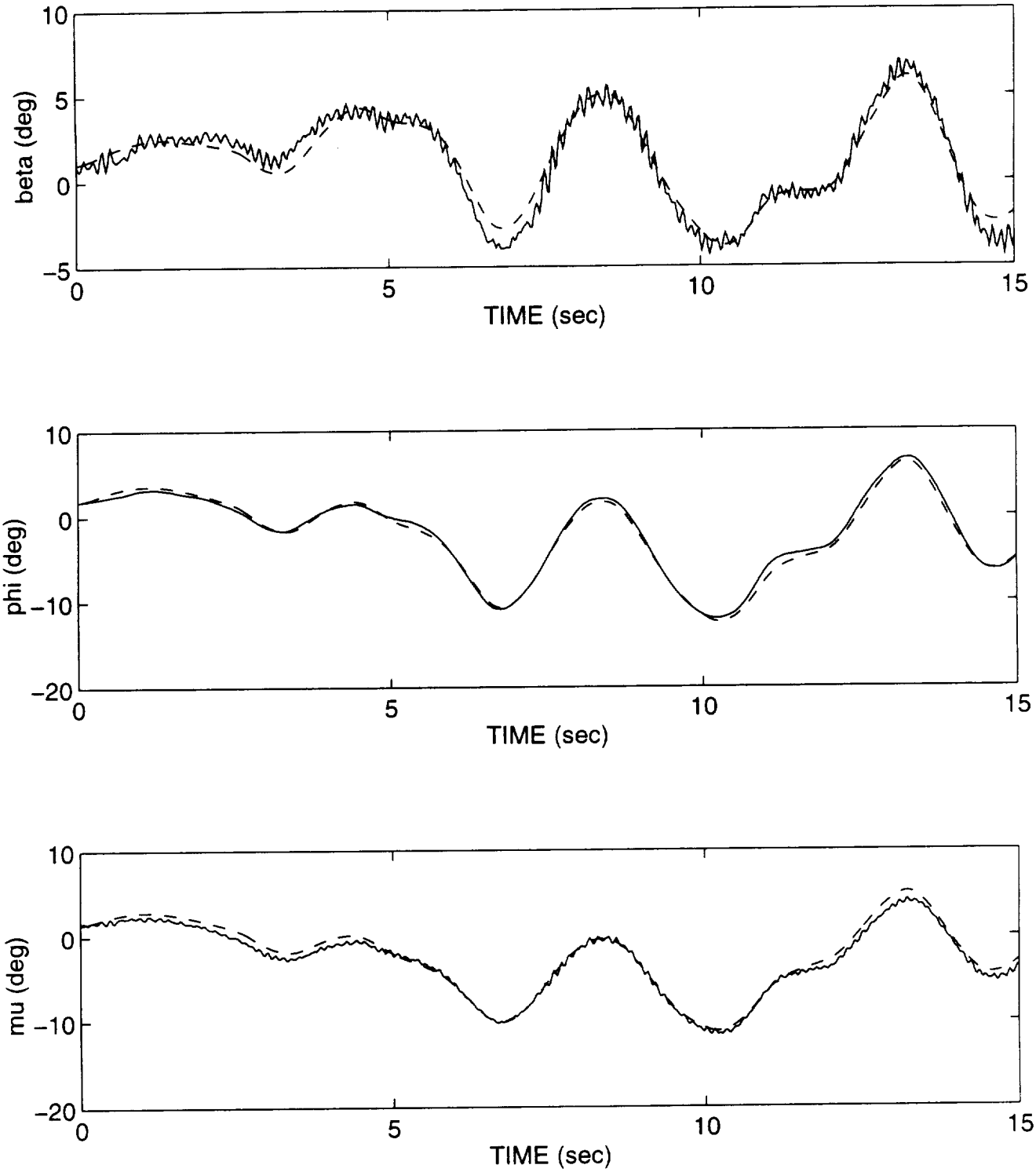

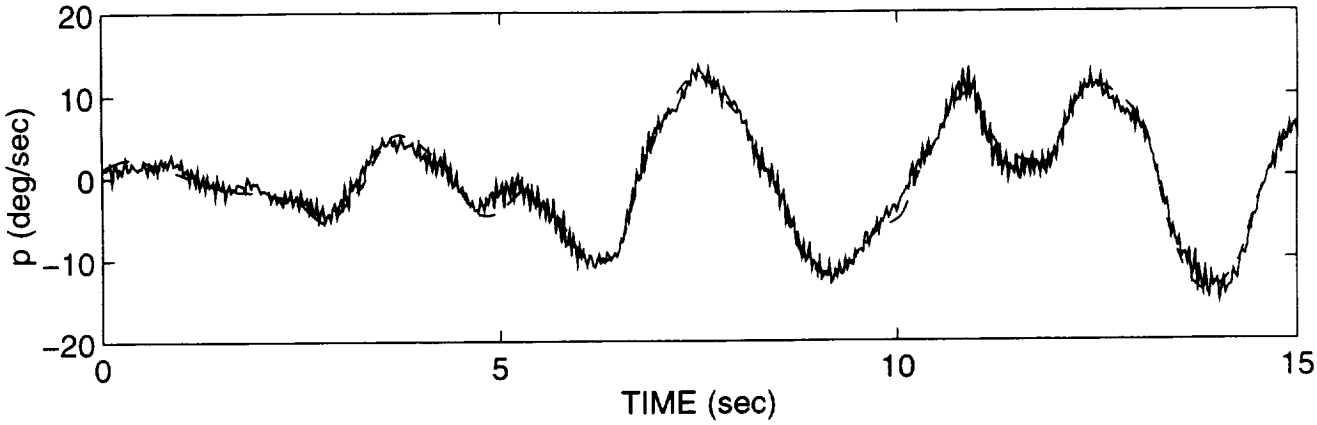
20
10
0
−10
−20
p (deg/sec)
0
5
10
15
TIME (sec)

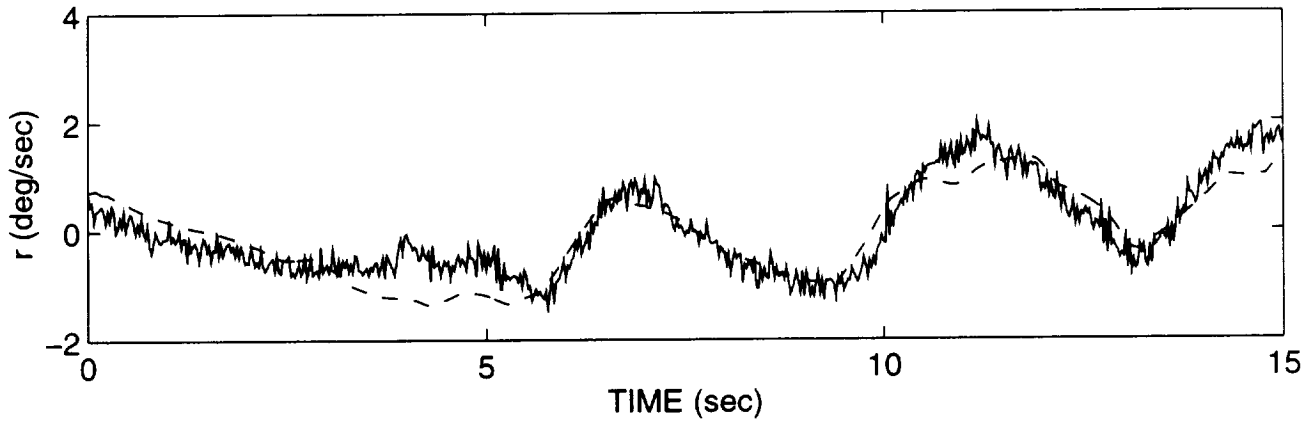
4
2
0
−2
r (deg/sec)
0
5
10
15
TIME (sec)

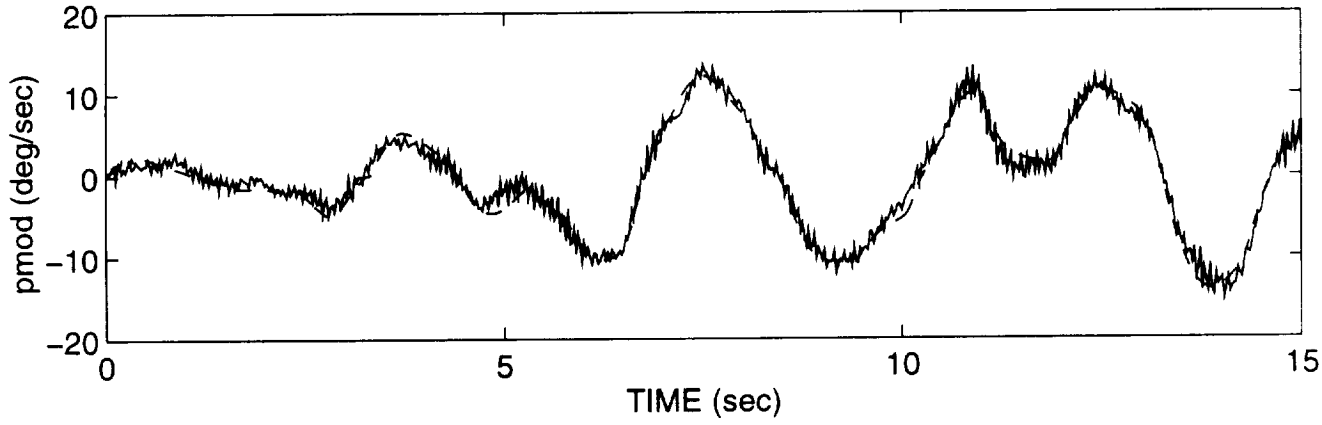
20
10
0
−10
−20
pmod (deg/sec)
0
5
10
15
TIME (sec)

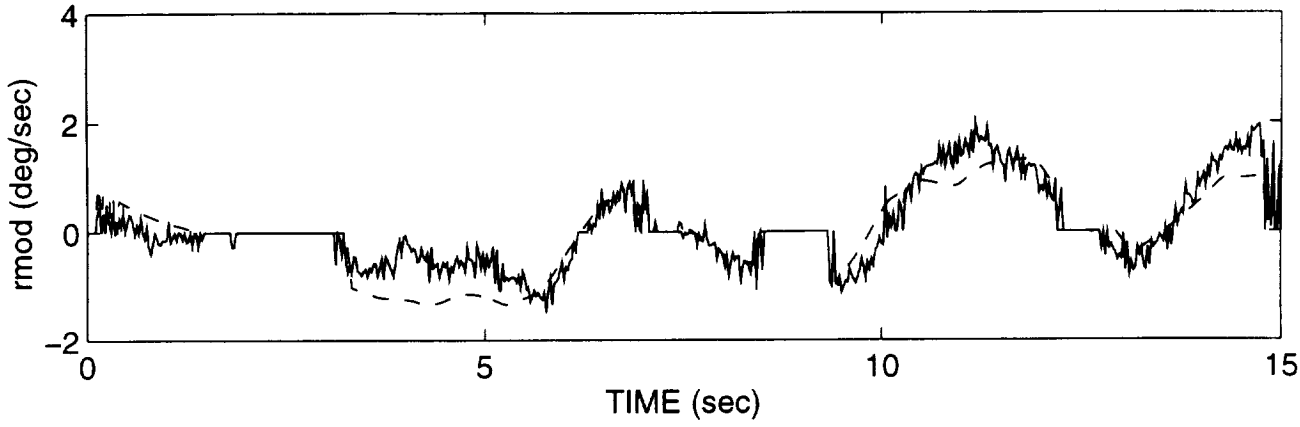
rmod (deg/sec)
4
2
0
−2
0
5
10
15
TIME (sec)

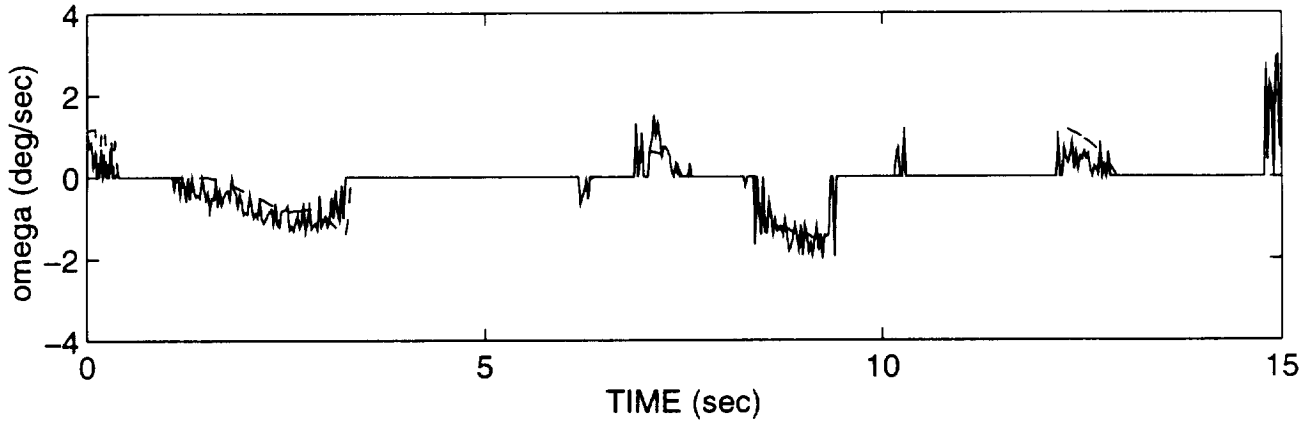
omega (deg/sec)
4
2
0
−2
−4
0
5
10
15
TIME (sec)

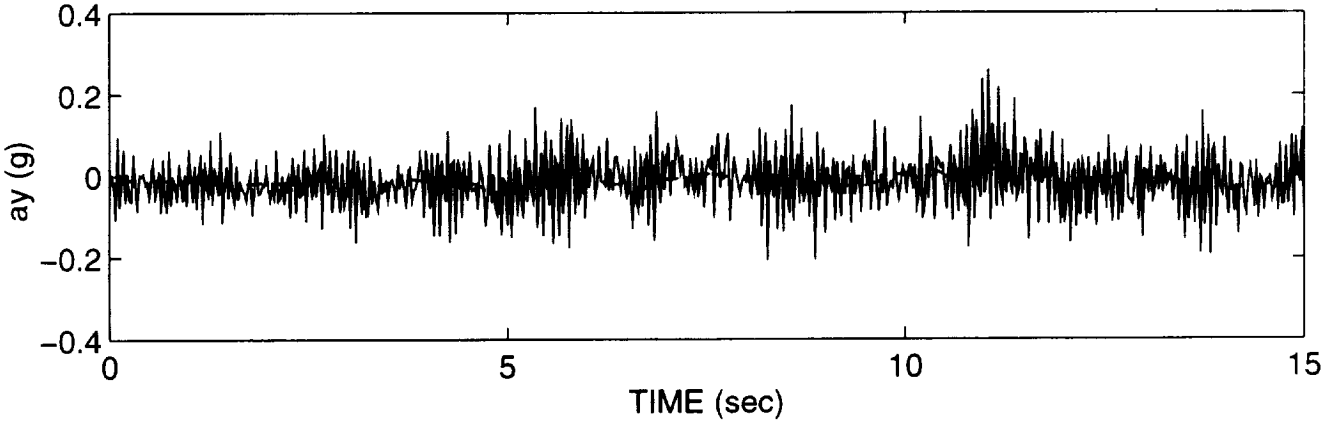
ay (g)
0.4
0.2
0
−0.2
−0.4
0
5
10
15
TIME (sec)